Max-Planck-Institut für extraterrestrische Physik

Unification of radio-loud AGN: the X-ray perspective

Elisa Ferrero

August 2004

Max-Planck-Institut für extraterrestrische Physik

Unification of radio-loud AGN: the X-ray perspective

DISSERTATION

der Fakultät für Physik der Ludwig-Maximilians-Universität München
zur Erlangung des Grades
Doktor der Naturwissenschaften
Dr. rer. nat.

vorgelegt von

ELISA FERRERO
aus Torino, Italien

München, den 31. August 2004

1. Gutachter: Prof. Dr. Gregor Morfill
2. Gutachter: Dr. Hans Böhringer
Tag der mündlichen Prüfung: 14. Januar 2005

Aknowledgement

I would like to especially express my gratitude to Dr. Wolfgang Brinkmann who constantly guided and supervised every phase of this work and who introduced me to astrophysical research.
I am grateful to Dr. Wolfgang Voges for performing the cross-correlations with the ROSAT catalogs and I also wish to thank Dr. Hans Böhringer for providing his cluster catalogs with useful X-ray data employed in this thesis. It is a pleasure to thank Dr. I. Papadakis at the University of Crete who made possible the Skinakas observations described in Appendix A.
My PhD work was carried out in the framework of the graduate program of the International Max-Planck Research School on Astrophysics to which I am therefore greatly indebted. I am also grateful to Prof. Dr. G. Morfill who welcomed me in his theory group and who provided financial support for the last months of my stay at MPE.
Finally, I would like to thank my family for the unconditional and uninterrupted support they give me, each of them by his own means and in his own way. A final thank goes to Mustapha who helped me to keep my feet firmly on the ground.

Abstract

In this thesis we address the subject of the unification of radio-loud Active Galactic Nuclei (AGN) (FRI/FRII galaxies, BL Lac objects and quasars) with a statistical and multiwavelength approach, paying particular attention to the X-ray band which carries precious information on the innermost regions of AGN. A large sample of 2260 AGN of different kinds was created by cross-correlating the ROSAT catalogs with various radio surveys and, for each source, data were collected in the radio, optical and soft X-ray bands. 1682 objects are formally classified as radio-loud and are analyzed in this thesis.

The main purpose of this thesis is to test the unified scheme for radio-loud AGN by investigating if the correlations between luminosities at different frequencies are consistent with the basic assumption that BL Lac objects and radio-loud quasars are relativistically beamed counterparts of FRI and FRII radio galaxies, respectively. Although this is the key hypothesis of the unification scheme for radio-loud AGN, these questions have not been carefully analyzed so far.

The results of this thesis are in general agreement with the relativistic beaming scenario, however, some complications have been highlighted. Tight relationships between the nuclear emission in the three wavebands considered are confirmed for all classes and we were able to better constrain the parameters of the correlations due to the larger number of objects compared to previous investigations. However, for FRI galaxies and BL Lac objects, more than one emission component is required, at least in the X-ray band, to explain in a relativistic beaming scenario the different parameters observed for the correlations. One component can easily be associated with the jet, whereas the other remains so far unknown.

A possible problematic aspect of the unified scheme is that, among the FRI galaxies, the counterparts of Low-energy-peaked BL Lacs have not been found.

Absorption with $N_{\rm H} \gtrsim 10^{22}$ cm^{-2} is present in FRII galaxies and plays, together with relativistic beaming, a major role in the unification with radio-loud quasars. Allowing for absorption, only one emission component is required at all frequencies to account for the observed correlations in both classes.

Flat-spectrum quasars (FSRQ) appear to be more beamed than steep-spectrum quasars (SSRQ) only at radio frequencies, but not in the optical and X-ray bands. This might imply that quasars are disk-dominated in the X-ray and optical band, and jet-dominated at radio frequencies. On the other hand, FRI galaxies and BL Lacs appear to be globally jet-dominated.

A parameter which might account for the FRI/BL Lac - FRII/quasar dichotomy is the accretion rate. At low, sub-Eddington values jets are weak but the emission from them dominates that from the disk and these sources are classified as FRI galaxies or BL Lacs, depending on the viewing angle. At values close to the Eddington limit the disk emission is comparable to that from the jet, which is also more powerful due to the higher accretion rate, and either a FRII galaxy or a radio-loud quasar is produced in this case.

Contents

Chapter 1

Introduction

Although the space and ground-based observatories of the new generation, such as, for example, XMM, Chandra, HST, VLT, etc., are providing us with high quality data which allow accurate and detailed studies of Active Galactic Nuclei (AGN), usually only the most luminous or nearby or peculiar objects are observed. Therefore, in spite of the precious information on the physics of these objects contained in such data, the conclusions that can be drawn from their analyses might not convey a faithful view of the typical properties of AGN. The best method to study these general features has proved to be the statistical analysis of large samples of AGN. This is the approach chosen for this work in order to tackle the problem of the unification of radio-loud AGN.
For a better understanding of the nature and the inter-relationships between different classes of AGN it is indispensable to use multiwavelength data. Only with the analysis and the comparison of the properties of AGN at different frequencies it is possible to clarify which emission mechanisms are operating in these objects and how the various classes are related to each other. The X-ray emission, in particular, is produced from the innermost regions, very close to the black hole at the center of every AGN and, therefore, it is potentially the richest carrier of information about the physics of their powerful engines.
A large amount of data exist for a great number of AGN, both in the literature and in the archives available to the astrophysical community, as a result of many investigations of different samples of objects observed in various wavebands, each one created according to particular requirements. This work attempts to construct a very large, multiwavelength sample of AGN exploiting this huge data reservoir, especially in the X-ray band. The final aim is to build a functional database that can also be used for future studies beyond the scope of this work. The sample that we present (shown in Table 1 at the end of this thesis) contains 2260 sources for which information is available in the radio, optical and soft X-ray bands. The collected data constitute a good basis for the study of radio-loud AGN, which are the subject of this thesis. Nonetheless, as outlined in Chapter 9, the sample should be updated with new data, when they become available, and extended to other wavebands, including spectral information, absorption and variability properties, etc.

The unified scheme is a model which interprets the different observational properties of the various classes of AGN in terms of orientation effects. The main test which gives support to this scheme comes from the comparison of the luminosity functions of the different classes (Urry & Padovani 1995). However, more independent tests are needed to further corroborate the unification scenario. Furthermore, the statistical significance of these tests is somewhat limited by the small sizes of the samples used and by the employment of data in only one waveband at a time. Therefore, samples combining both large sizes and multi-wavelength information are desirable to test the validity of the unified scheme. This work aims at contributing to this through the study of a sample fulfilling both requirements.

For quite some time it is known that the emission from AGN at different wavelengths is tightly correlated and this has allowed to recognize the radiation mechanisms in these sources. However, only few studies investigated if the correlations observed are consistent with the hypothesis of the unified scheme claiming that, in the case of the radio-loud population, BL Lac objects and quasars are beamed and unabsorbed versions of FRI and FRII galaxies, respectively, oriented at small angle to the line of sight. However, relativistic beaming together with obscuration by dust and gas constitute the basis of any unification scheme and this point deserves a careful examination. Our sample is best suited for this analysis which is the main topic of this thesis. However, the potential of our database is not exhausted by such a study as stated above.

The structure of the thesis is the following: Chapter 2 describes the observational properties and the classification of AGN; Chapter 3 discusses the unified scheme; Chapter 4 illustrates the spectral energy distributions of AGN and the emission mechanisms in the various wavebands; in Chapter 5 the sample is presented and the statistical techniques employed in the subsequent analysis are described; in Chapter 6, 7 and 8 we show and discuss the results for the radio-loud AGN, comparing the properties of FRI and FRII galaxies, FRI galaxies and BL Lac objects, and FRII galaxies and radio-loud quasars, respectively; in Chapter 9 we give the conclusions and the prospects of this work.

Chapter 2

Active Galactic Nuclei: observational properties

The term Active Galactic Nucleus (commonly abbreviated as AGN) denotes a large variety of extragalactic objects. The objects of this class can have very different emission properties, however, they all share a striking characteristic which distinguishes them from all the other galaxies in the Universe: the emission from the nucleus largely outshines that of the whole galaxy. Various subclasses forming the AGN population, e.g. radio galaxies, quasars or Seyfert galaxies, have been known for quite a long time but only in relatively recent years attempts have been made to unify them in a coherent picture (see Chapter 3). According to this unified view all AGN subclasses share a common mechanism of energy production, the accretion of matter onto a supermassive black hole in their center. Their different observational properties arise, to a large degree, from their intrinsically anisotropic geometry and radiation pattern, from absorption as well as from relativistic effects.
In this chapter we will briefly summarize the historical background concerning the discovery and the study of AGN, then we will describe the observational properties common to all AGN subclasses and, finally, we will treat in detail the properties of each subclass and the related AGN taxonomy.

2.1 Historical background

Astronomers have been aware of the existence of AGN since the beginning of the 20th century, even though they could not recognize them as such. At that time their extragalactic nature was unknown, as it was for galaxies in general which were called *nebulae*. The starting date of the observational study of AGN may be set in 1908 thanks to the work of E. A. Fath on *spiral nebulae*. These objects showed absorption lines in their optical spectra and, since the same lines had also been observed in star clusters, their emission was interpreted analogously in terms of the integrated light from a large number of stars, too distant to be resolved individually. However, one nebula, NGC 1068, revealed some high-ionization emission lines in its optical spectrum. Later, in 1943, Carl Seyfert discovered that these "emission line" objects constituted a small fraction of the galaxies in general. He also argued that they showed emission lines wider than the absorption lines in normal galaxies, with a wide range of ionization, originating in a small, bright nucleus of stellar appearance in the host galaxy. The discovery of these AGN traditionally dates back to this work and they were thus called *Seyfert galaxies* ever since (Seyfert 1943).

Radio galaxies have been known since the mid-1950s when the *Third Cambridge Catalog (3C)* was created. Cygnus A was the first detected radio source outside the solar system, however, its optical identification with an elliptical galaxy had to wait until 1954 (Baade & Minkowski 1954) followed by the identification of other strong radio sources soon after. In 1962 a lunar occultation of the radio source 3C 273 allowed an accurate determination of its radio position and consequently the identification of its optical counterpart. This turned out to be of stellar-like appearance, but its optical spectrum contained several strong emission lines unlike stellar spectra where only absorption lines are detected. For this reason 3C 273 and similar objects were called *quasars* which stands for *quasi-stellar radio sources (QSR)*. It was only in 1963 that quasars' spectra were interpreted in terms of cosmological redshift by Maarten Schmidt and that these objects were recognized to be extragalactic, at extremely large distances from our Galaxy (Schmidt 1963). Later on, with the discovery of many stellar-like objects, which lacked strong radio emission, it was understood that this is not a general feature of quasars, but only for $\sim 10-15\%$ of them. The new objects were named *Quasi-Stellar Objects* (*QSO*), a term which became frequently used for radio-quiet[1] quasars only, whereas the term *quasar* is reserved for the radio-loud quasars. The term *quasar* is also used to indicate both classes in general when we do not need to specify their radio properties. The terms *radio-loud* and *radio-quiet quasars* are used when an explicit distinction is necessary.
With the advent of the Einstein Observatory in 1980 it was realized that a general feature of quasars is their X-ray emission and that this waveband carries useful information on the energy production mechanisms, on the circumnuclear matter and on the internal structure of AGN.

A final remark is necessary on *BL Lac objects*, the most peculiar members of the AGN class. BL Lacertae (or BL Lac) was at first believed to be a variable star in the constellation of Lacerta due to its stellar appearance. In 1968 its radio counterpart was found (MacLeod & Andrew 1968, Schmidt 1968) and in 1969 the optical continuum was found to be featureless without either emission or absorption lines (Visvanathan 1969). Together with its variability and high degree of polarization, this established the unusual nature of BL Lac. In 1974 Adams identified a faint nebulosity around it with color and brightness distribution consistent with that of an elliptical galaxy, thus proving its extragalactic nature. When similar sources were discovered afterwards they inherited the name *BL Lac objects* from it.

2.2 General properties of AGN

The separately discovered types of AGN actually share some remarkable properties which eventually led to grouping them together into a common class. In the following we list these general properties and discuss them briefly.

[1] For a quantitative definition of radio-loudness see §2.3.

The first remarkable property of all AGN is the emission of radiation over the entire electromagnetic spectrum with bolometric luminosities $L \gtrsim 10^{44}$ erg s^{-1}, sometimes reaching $L \sim 10^{47} - 10^{48}$ erg s^{-1}. In comparison, normal galaxies have $L \lesssim 10^{42}$ erg s^{-1} and the bulk of their luminosity is emitted in the visible band, essentially produced by stars.

The second remarkable property is the high variability of their emission observed at all frequencies, on time scales ranging from years down to hours. Such short time scales imply that the region from which the luminosity is emitted is very compact. If R is the linear dimension of this region and $\Delta t_{\rm var}$ is some characteristic variability timescale, a simple light travel time argument demands that $R \lesssim c\Delta t_{\rm var}$ for the variability to be observed (where c is the speed of light). From the measured $\Delta t_{\rm var}$ in AGN it is usually found that $R \lesssim 0.1$ pc, i.e. the emission region is contained well within the nucleus of the galaxy (a fact that justifies the name of AGN).

The spectra of AGN over the whole electromagnetic band are essentially of non-thermal origin (however, see also Chapter 4 on the SED of AGN), contrary to normal galaxies where the spectrum is given by the integration of the stars' thermal spectra. In a given waveband the AGN spectra can usually be well described by a power law with flux density of the form $f(\nu) \propto \nu^{-\alpha}$ (erg s^{-1} cm^{-2} Hz^{-1}) where α is called the *spectral index*. An equivalent parameterization of the spectrum of an AGN, preferred at high energies, is given by $N(E) \propto E^{-\Gamma}$, where E is the energy, $N(E)$ is the number of photons s^{-1} cm^{-2} keV^{-1} and Γ is called the *photon index*. The spectral index is related to the photon index by $\Gamma = \alpha+1$.

Together with the non-thermal continuum, the optical spectrum of an AGN usually shows strong emission lines. Both permitted and forbidden narrow emission lines are observed, whereas only permitted broad emission lines have been seen. The widths of the emission lines yield information on the velocity properties of the emitting material. Interpreting the line widths in terms of Doppler broadening, velocity dispersions of the order of $\sigma \sim 300 - 400$ km s^{-1} are found in the case of narrow lines and an order of magnitude higher, i.e. $\sigma \sim 3000 - 4000$ km s^{-1}, for the broad lines.

Some AGN also reveal strong radio emission in the form of spectacular jets and extended lobes (see Fig. 2.2). These radio structures can reach distances from the center of the AGN of the order of ~ 100 kpc up to ~ 1 Mpc, well beyond the optical extension of the host galaxy. However, the majority of AGN seem to be radio-quiet.

All properties listed above are indicators of powerful physical mechanisms acting at the centers of active galaxies producing such highly energetic phenomena in a very compact region. Clearly, nuclear processes in the cores of stars cannot account for the enormous AGN energy output and in §2.4 the current model for the central engine of an AGN will be discussed.

The fraction of galaxies which show these peculiar properties is only $\sim 1\%$ of the total population, however, they are outstanding and intriguing objects providing insight into yet unexplored physical processes. As extremely luminous and distant objects they are also unique probes of the Universe at early stages and thus useful cosmological tools. A

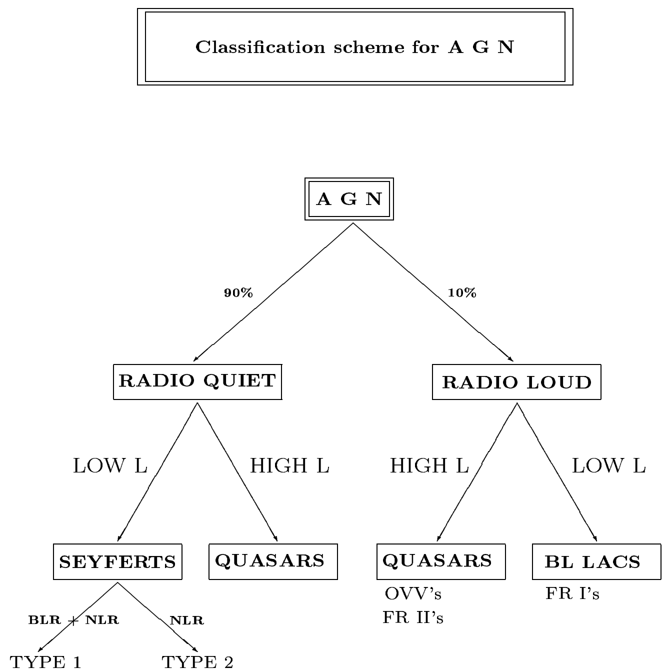

Figure 2.1: *The AGN taxonomy. See text for the explanation of the various classes.*

key question regarding the galaxy evolution is: does every galaxy pass through an activity phase or can only a small fraction of galaxies become active, for example due to special environmental conditions?

In the following section we will give a more detailed classification scheme for the AGN, based on their observed radio and optical properties. This scheme will be useful to understand the AGN terminology and it has helped to uncover some order behind the various manifestations of the AGN phenomenon and eventually to develop a unification scheme, which relates the observed properties to both geometrical and physical causes (see Chapter 3).

2.3 Classification of AGN

Fig. 2.1 gives the principal classification of AGN based on radio emission and optical spectral properties. It must be noticed that the X-ray properties of the objects are normally not taken into account for this classification scheme.

The first rough division is made according to the parameter called *radio-loudness*, defined as:

$$R_{\rm L} = \log\left(\frac{f_{\rm 5GHz}}{f_{\rm B}}\right) \tag{2.1}$$

where $f_{5\mathrm{GHz}}$ is the radio flux at 5 GHz and f_{B} is the optical flux in the B band, centered on the wavelength $\lambda = 4400\mathring{A}$. If an AGN has $R_{\mathrm{L}} \gtrsim 1$ it is conventionally said to be *radio-loud*, whereas if it has $R_{\mathrm{L}} \lesssim 1$ it is said to be *radio-quiet* (Kellermann et al. 1989). The radio-loud objects represent a small percentage ($\sim 10 - 15\%$) of all AGN.
However, it must be pointed out that the sharp separation into these two classes has been questioned following the results of the FIRST survey (Brinkmann et al. 2000, White et al. 2000). The AGN could instead follow a continuous distribution in radio-loudness, rather than being sharply divided into two populations. However, it has been argued recently that the lack of a bimodality in radio loudness as inferred from FIRST data could be due to an intrinsic insensitivity of the survey to the extended emission (Laor 2003).
It has been thought for some time that the physical basis for the radio-loud classification was that, whenever the host galaxy could be imaged, radio-quiet AGN were found to reside in spiral galaxies, whereas radio-loud AGN were usually housed by ellipticals. However, HST observations recently allowed the accurate measurement of the AGN host galaxies' luminosity profiles (for $z \lesssim 0.5$), unambiguously revealing that both radio-loud and radio-quiet quasars with nuclear $M_V < -23.5$ inhabit massive ellipticals with negligible disc components (Dunlop et al. 2003). The current picture thus appears to be that above a given optical nuclear luminosity threshold AGN can only reside in massive ellipticals regardless of their radio power. At lower optical nuclear luminosities spiral host galaxies become more common within the radio-quiet population, whereas radio-loud AGN are always hosted in ellipticals.

The second basic classification, independent from the previous one and valid for both radio-loud and radio-quiet AGN, is made according to the optical spectra. AGN with a bright continuum and both broad and narrow emission lines are called *type 1 AGN*, those with a weak continuum and only narrow emission lines are called *type 2 AGN*. Some AGN, BL Lacs and flat-spectrum quasars (FSRQ), show very unusual spectra and peculiar properties, such as featureless spectra, strong variability on very short time scales (i.e. hours), strong and variable polarization. These objects are collectively called *blazars*. BL Lacs, however, lack the strong emission lines observed in FSRQ, suggesting a fundamental difference between the two classes in spite of their similar peculiar properties. As we will see in Chapter 3 it is currently believed that the separation into type 1, type 2 and blazars is due, at least partly, to orientation and obscuration effects.

Keeping in mind the classification criteria above, we now discuss the various subclasses of AGN and their main properties.

2.3.1 Radio-quiet AGN

Type 2 objects: The radio-quiet type 2 AGN are the *Seyfert 2 galaxies*, hosted in nearby spiral galaxies, showing only narrow emission lines with $FWHM \lesssim 1000$ km s^{-1}. They are mostly seen at small cosmic distances because of their low luminosities. This subclass also includes the *Narrow Emission Line Galaxies (NELG)* (Mushotzky 1982) also called Narrow Line X-ray Galaxies (NLXG). They have optical spectra similar to the Seyfert 2 with narrow emission lines only (a part from a broad wing in the Hα line in some cases) but their hard X-ray emission is stronger, more typical to that of the Seyfert 1 (see below).

At first they were thought to constitute a separate class, but nowadays they are usually considered as intermediate Seyferts (i.e. Sy 1.8, 1.9 or 2; Osterbrock 1989).

Type 1 objects: The lower-luminosity radio-quiet type 1 AGN are called *Seyfert 1 galaxies*. They are similar to the Seyfert 2, but with broad emission lines in their optical spectra ($FWHM \gtrsim 1000$) in addition to the narrow lines. At higher luminosities we find the *radio-quiet quasars* or *QSO*. Unlike the Seyfert 1 galaxies these objects are usually very distant and it is very difficult to image the host galaxy around them. However, apart from their pointlike appearance they are undistinguishable from the Seyfert 1[2].

Other classes: An interesting subgroup of radio-quiet quasars (not shown in Fig. 2.1) are the so called *Broad Absorption Line Quasars (BAL QSO)*. These are objects showing broad P-Cygni-like features in their optical-UV spectra with deep, wide absorption troughs on the blue side of the corresponding emission lines indicating outflow velocities of $v \sim 0.1-0.2c$. They constitute $\sim 10-15\%$ of the optically selected quasars and they are almost exclusively radio-quiet. The BAL phenomenon is believed to be caused by orientation effects, with the line of sight passing through a high column density ($N_{\rm H} \gtrsim 10^{23}$ cm^{-2}) absorber flowing outwards with high velocity (Weymann et al. 1991, Hamann et al. 1993). According to a recent model (Elvis 2000), which is still under debate, all radio-quiet quasars possess high-velocity outflows rising vertically (possibly due to disk instabilities) at some radius of the accretion disk and then bending outwards. Only when they are seen through the outflow they show BAL properties.
The *Low Ionization Nuclear Emission Line Regions (LINERs)* are the least luminous AGN known. They are considered as transition objects with a weak non-thermal AGN-like continuum component together with a starburst component. They have low ionization emission lines ($[OI]/[OIII] > 1/3$ and $[OII]/[OIII] > 1$) with somewhat narrower widths ($\sim 200-400$ km s^{-1}) than those of the narrow lines in Seyfert 1. Some of them show weak broad emission lines.
Narrow Line Seyfert 1 Galaxies (NLSy1) are a very interesting subgroup of Seyfert 1 galaxies, having widths of the Balmer lines between $\sim 500-2000$ km s^{-1}, narrower than typical broad lines, FeII multiplet emission and $[OIII]/H\beta < 3$. They are extremely variable in X-rays and have the steepest soft and hard X-ray spectra (for an extensive review see, for example, Boller 2000).

2.3.2 Radio-loud AGN

Type 2 objects: The radio-loud type 2 AGN are the classical radio galaxies, which in this context will be more precisely called *Narrow Line Radio Galaxies (NLRG)*. According to their radio properties, they are further divided into *Fanaroff-Riley type 1 (FRI)* and *Fanaroff-Riley type 2 (FRII)* (Fanaroff & Riley 1974). The FRII have radio morphologies characterized by powerful edge-brightened double lobes with prominent hot spots and tend to be found in poor environments; the FRI have radio emission peaking near the nucleus, have rather diffuse edge-darkened lobes and frequently inhabit rich environments. An example for each class is shown in Fig. 2.2.
A subgroup of the FRII radio galaxies have low excitation optical spectra with [OIII] lines

[2] An object is classified as QSO if its absolute optical magnitude is $M_{\rm V} \lesssim -23$.

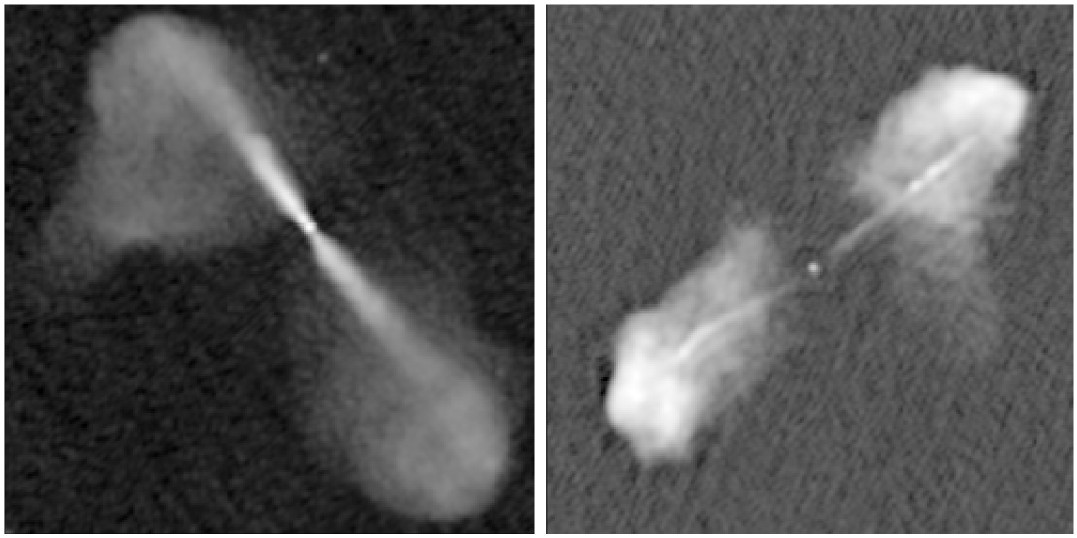

Figure 2.2: *The radio galaxies 3C 296 (left panel) and 3C 438 (right panel), examples of a FRI and of a FRII radio source, respectively.*

very weak compared to the hydrogen lines ($[OIII]/H\alpha < 0.2$ and $EW_{[OIII]} < 3\mathring{A}$, Hardcastle & Worrall 1999). They can either be called *Weak Line Radio Galaxies (WLRG)* or *Low Excitation Radio Galaxies (LERG)* (Laing et al. 1994). In spite of their FRII radio morphology they have optical spectra resembling those of FRI galaxies and this will have some implications on the unified scheme (see § 3.3.1).

Type 1 objects: The radio-loud type 1 AGN are called *Broad Line Radio Galaxies (BLRG)* at low luminosity and *radio-loud quasars* at high luminosity[3]. The latter are further separated into *Steep-Spectrum Radio Quasars (SSRQ)* with radio spectral index $\alpha_{\rm r} \gtrsim 0.5$ and *Flat-Spectrum Radio Quasars (FSRQ)* with $\alpha_{\rm r} \lesssim 0.5$. The SSRQ are basically more luminous BLRG and both classes (as observed so far) display exclusively FRII radio morphologies. FSRQ on the other hand appear compact in the radio band with no extended lobes. They have broad emission lines in their optical spectra and can thus be classified as type 1 objects, but their continuum spectrum has the peculiar properties of blazars (see below).

Blazars: They include the FSRQ, also grouped with type 1 objects as described above, and the *BL Lacertae (BL Lac)* objects. It must be remarked that the optical spectra of BL Lacs and FSRQ differ greatly. In fact, whereas FSRQ show strong broad emission lines, BL Lacs have only weak (typical $EW < 5\mathring{A}$) or no emission lines in their optical spectra. Therefore grouping them together in a common optical spectral class might be confusing. The reason why they are commonly put together in the blazar class is that, in spite of the dissimilarity of their optical spectra, they share the same peculiar continuum properties (e.g. strong variability and polarization properties). As we will see in Chapter 3, the unification scheme interprets both FSRQ and BL Lacs as AGN observed at a small

[3]An object is classified as a quasar if its absolute optical magnitude is $M_{\rm V} \lesssim -23$.

viewing angle so that the continuum emission is dominated by the jet. However, the lack of emission lines in BL Lacs indicates that they are not just lower-luminosity versions of FSRQ but that fundamental differences exist between the two classes.
Further objects such as *Optically Violently Variable Quasars (OVV)*, *Highly Polarized Quasars (HPQ)* and *Core Dominated Quasars (CDQ)* turned out to be different empirical definitions of the same kind of objects and are now included in the FSRQ class.

Other classes: A peculiar subclass of radio-loud AGN is formed by the so-called *GHz-Peaked Spectrum (GPS)* sources and the *Compact Steep-Spectrum (CSS)* sources (for a review see O'Dea 1998). They constitute a non-negligible fraction of the cm-wavelength selected radio sources ($\sim$ 10% and $\sim$ 30%, respectively) and they are characterized by strong radio power ($\gtrsim 10^{25}$ W Hz^{-1} at 1.4 GHz) originating from a very compact region ($R \lesssim 1$ kpc and $R \lesssim 20$ kpc, respectively). Their most puzzling property is a convex radio spectrum peaking around few GHz for the GPS and below $\sim$ 500 MHz for the CSS. The convex shape is commonly interpreted in terms of synchrotron self-absorption and the GPS/CSS sources are supposed to be young progenitors of the classical radio galaxies and radio-loud quasars. An alternative hypothesis is that they are frustrated sources confined by a very dense gas.

Given the properties above, we will describe in the next paragraph the standard interpretation for the central engine powering the AGN and we will introduce the unified scheme.

2.4 Current interpretation

Any model for the AGN must be able to explain the peculiar properties discussed in the previous paragraphs. The fundamental question is: what kind of source is capable to produce such a large amount of energy from such a compact region?

Initially, astronomers tried to explain the AGN energy source in terms of very massive stars evolving into super-supernovae (Hoyle & Fowler 1962), populations of massive O stars, and collections of supernovae. All these scenarios failed to account for the high emission efficiency implied by the AGN luminosity. In fact, any spherical object held together by gravitational forces must radiate below a well defined luminosity limit dependent on its mass, called the *Eddington luminosity*. Beyond the Eddington limit the radiation pressure would be larger than the gravitational force and the object would be disrupted. The Eddington limit is obtained imposing the equilibrium between the gravitational force acting on the protons (neglecting the small contribution from the electrons) and the radiation pressure acting on the electrons (assuming that the interaction between the radiation and the protons is negligible). This yields:

$$L \lesssim L_{\rm E} = \frac{4\pi c G m_{\rm H} M}{\sigma_{\rm T}} = 1.26 \times 10^{38} \frac{M}{M_\odot} \tag{2.2}$$

where $\sigma_{\rm T}$ is the Thomson cross section. For a typical AGN luminosity of $10^{12} L_\odot$ this implies a lower limit for the mass of the star of $M \gtrsim 3 \times 10^7 M_\odot$. If we write for the AGN luminosity:

$$L = \epsilon M c^2 \Delta t^{-1} \tag{2.3}$$

where ϵ is the efficiency of the energy production mechanism, $\Delta t \sim 10^8$ yrs is the typical lifetime of an AGN and we take $L \approx L_{\rm E}$, substituting Eq. (2.2) into Eq. (2.3) we get $\epsilon \approx 0.4$, independent of the AGN mass. This value largely exceeds that for thermonuclear processes in stars and demands other mechanisms for the energy production.

In 1963 Hoyle & Fowler proposed that the energy source in AGN was of gravitational origin from the collapse of very massive objects in analogy to what happens in the early stages of star formation. Later on this idea was developed into the so called *black hole-accretion disk paradigm* which was already working well for the X-ray binaries in our Galaxy. According to this model the core of an AGN is a supermassive black hole ($M_{\rm BH} \sim 10^6 - 10^9 M_\odot$) onto which matter is accreted by its strong gravitational force. If this matter possesses angular momentum it cannot fall directly towards the black hole but rotates around it on nearly Keplerian orbits at different radii forming an accretion disk. As a consequence of losing angular momentum due to viscosity it slowly spirals in and finally falls into the black hole. The liberated gravitational energy is mostly emitted in the form of radiation and supplies the kinetic power of the jets. How the gravitational energy is transformed into kinetic and radiative energy is still poorly understood. However from general relativity it is known that the efficiency of such a mechanism can be $\sim 10\%$ in the case of a Schwarzschild black hole and as high as $\sim 40\%$ in the case of a maximally rotating Kerr black hole. Therefore, it can easily account for the large amount of energy emitted from an AGN.

There have been suggestions that the energy source of AGN could be of gravitational origin but without the need for supermassive black holes. The central engine could be a cluster of compact objects, i.e. neutron stars or neutron stars and stellar-mass black holes. However, the small dimensions of the source would force the system to collapse anyway into a supermassive black hole. Due to the large masses required by the Eddington limit argument and the extreme compactness of the emitting regions inferred from the variability timescales, it seems very difficult to avoid the formation of supermassive black holes in the nuclei of active galaxies independently of the initial configuration we start from (Rees 1984). The black hole-accretion disk paradigm is thus the currently best accepted interpretation of the AGN phenomenon. Furthermore, there is mounting evidence for the existence of supermassive black holes at the center of many normal galaxies (Kormendy & Gebhardt 2001, Richstone 2002 and Schödel et al. 2002 for the Galactic center) providing experimental support for this scenario.

In this chapter we have discussed the observational properties and classification of AGN and we have described the black hole-accretion disk paradigm which explains the extreme properties of AGN. This model identifies the source of energy of AGN, but cannot account as such for the observed diversity described in §2.3 and their broad spectral energy distribution (see Chapter 4). The *unified scheme* (see Chapter 3), based on the black hole-accretion disk paradigm, attempts to explain the various AGN manifestations by adding some other structural elements. In Chapter 4 we will treat in more detail the emission properties in different wavebands, i.e. the spectral energy distribution of AGN, in the framework of the unified scheme.

Chapter 3

Unification of AGN

In Chapter 2 we have seen that the black hole-accretion disk paradigm is the favored interpretation of the AGN phenomenon, capable to account for the high luminosity and compactness. However, various different types of AGN have been defined (described in Chapter 2) according to their distinct observational properties. Since the discovery of AGN evidence has been accumulating that their emission is not isotropic and the reasons for the anisotropy have been mainly attributed to obscuration by dust or gas and relativistic beaming. As a consequence the belief grew that the large variety of AGN types resulted from a family of intrinsically similar objects seen with different orientations with respect to the observer's line of sight. Some classes of AGN were recognized to be intrinsically similar once obscuration and relativistic beaming effects were removed. The models describing this scenario became known as the *unified schemes*.

In the following we will first discuss the evidence for anisotropic emission in AGN and then the various steps undertaken towards the currently best accepted version of the unified scheme. We will concentrate mainly on the unified schemes for radio-loud AGN which constitute the principal subject of our work. A brief review of the tests which support the unified scheme and of the remaining unsolved problems will be given at the end of the chapter. For the radio-quiet population we will limit ourselves to describe the basic elements of their unification and refer to the literature for a more extensive treatment.

3.1 Sources of anisotropy

Obscuration (provided that the absorber has anisotropic geometry) by intervening gas or dust and relativistic beaming will result in enhanced emission along a preferential direction and in a different appearance of the object depending on the viewing angle. In the next paragraph we discuss in more detail these two points and their supporting evidence.

3.1.1 Obscuration

Direct evidence for obscuration comes from spectropolarimetric studies of type 2 AGN. Their optical/UV spectra observed in polarized light show broad emission lines as strong as those observed in type 1 AGN. The first object for which scattered broad emission lines have been seen is the Seyfert 2 galaxy NGC 1068 (Antonucci & Miller 1985). Later, a hidden Broad Line Region (BLR) was revealed as well in the radio galaxy 3C 234 (Antonucci 1984) where it was also found that the plane of polarization is perpendicular to the radio jet axis, suggesting that the absorber's axis must coincide with that of the jet. The polarization is mostly wavelength independent, favoring an electron scattering origin, but in other sources scattering by dust seems to be also present (Miller et al. 1991). An important remark is that all radio galaxies in which a hidden BLR has been detected are so far FRII and not FRI galaxies.

If type 2 AGN are obscured they should shine brightly in the infra-red band, where the optical depth is much lower than in the optical case. This in fact has been observed in a few NLRG (see for example Antonucci & Barvainis 1990) together with broad Paschen lines in some cases, indicating the presence of a hidden BLR (Hill et al. 1996).

Optical images of some type 2 objects reveal a conical or biconical structure of the extended Narrow Line Region (NLR), for example the HST image of NGC 1068 in the light of [OIII] (Wilson et al. 1993). The suggestion is that the emission from the nuclear source is emerging through a torus-like absorber, photo-ionizing the gas in the NLR which will shine in a conical shape with apex at the obscured nucleus.

Soft X-ray observations of type 2 objects showed that they are systematically less luminous than the type 1 objects and that their spectra are consistent with being absorbed by high column densities of gas (Mulchaey et al. 1992).

3.1.2 Relativistic beaming

If a source of radiation moves with relativistic velocities towards the observer a series of relativistic effects will take place. The radiation will be collimated in the direction of motion into a cone with opening angle $\theta \sim 1/\Gamma$ where Γ is the bulk Lorentz factor and the intensity of the radiation will be amplified by Doppler boosting in the direction of motion. The time intervals measured in the observer's frame will be shorter than in the rest frame of the source and consequently the measured frequencies will be higher. These effects are all direct consequences of the Lorentz transformations of special relativity and they are known as *relativistic beaming*. The parameter which quantifies the relativistic beaming is the *Doppler factor*:

$$\delta = \frac{1}{\Gamma(1-\beta\ cos\theta)} \tag{3.1}$$

where θ is the angle between the line of sight of the observer and the direction of motion of the source. Time intervals and frequencies will transform as:

$$\Delta t = \delta^{-1}\Delta t' \tag{3.2}$$

$$\nu = \delta\nu' \tag{3.3}$$

where primed quantities refer to the rest frame of the source.

The specific intensity, flux density (of the form $f(\nu) \propto \nu^{-\alpha}$) and the total flux transform as:

$$I(\nu) = \delta^3 I'(\nu') \qquad (\text{erg s}^{-1}\text{ cm}^{-1}\text{ Hz}^{-1}\text{ sr}^{-1}) \tag{3.4}$$

$$f(\nu) = \delta^{3+\alpha} f'(\nu') \qquad (\text{erg s}^{-1}\text{ cm}^{-1}\text{ Hz}^{-1}) \tag{3.5}$$

$$f = \delta^4 f' \qquad (\text{erg s}^{-1}\text{ cm}^{-1}) \tag{3.6}$$

The monochromatic luminosity and the total luminosity transform as in Eq. (3.5) and (3.6), respectively. These formulae are valid for a point source (i.e. a blob in a radio jet), whereas for a continuous jet the exponent of δ in Eq. (3.5) and (3.6) becomes equal to $2 + \alpha$ and 3 respectively.

Relativistic beaming affects the isotropy of the radiation if the emitting material has relativistic bulk velocities and it has thus been proposed as one of the probable reasons of the aspect dependence of AGN. The main evidence for relativistic beaming relies on the detection (in blazars) of superluminal motion, on observations of jets' asymmetries, on the "Compton catastrophe" argument, on brightness temperature calculations and on observations of extremely rapidly variable gamma-ray sources.

Superluminal motion: In many blazars single radio components (i.e. blobs) have been seen moving at apparent velocities greater than c. This has been interpreted as an effect of relativistic beaming in the following way. When a source is moving at a velocity close to c along a direction which forms a small angle with the observer's line of sight it "runs after" the photons it emits. This reduces the time intervals between the emission of two photons as measured in the observer's frame and the source appears to move faster than it actually does. The apparent speed is given by:

$$\beta_{\text{app}} = \frac{\beta \sin\theta}{1 - \beta\cos\theta} \tag{3.7}$$

and β_{app} reaches a maximum for $\cos\theta = \beta$. It must be kept in mind, however, that an apparent superluminal speed might also be obtained by subsequent illumination of different jet regions without the need for actual motion of matter.

Jet asymmetries: Radio jets in AGN are often one-sided, which means that the brightness of the jets on both sides of the radio core is significantly different. The one-sidedness usually holds at pc and kpc scales, implying that relativistic velocities are maintained over large distances from the core. If jets are really moving at relativistic speeds one-sidedness is expected. Further supporting evidence that jets are affected by relativistic beaming comes from frequently detected depolarization asymmetries in the radio lobes of a single source. The radiation coming from the lobe connected with the bright jet is usually less depolarized than that coming from the opposite lobe. This finds a natural explanation if we assume that the bright jet is moving towards us and the invisible counter-jet is moving away from us and that the radio source is embedded in a hot gaseous halo. Then the lobe with the jet is closer to us and its radiation has to pass through a smaller amount of depolarizing material than that from the opposite, more distant lobe. It seems thus that jet one-sidedness can more likely be attributed to relativistic beaming than to an intrinsic origin.

Gamma-ray variability: In many cases the emission from blazars is dominated by gamma-rays which typically show very short variability timescales of the order of days or less. This constrains the emitting region to be very compact and, consequently, the density of gamma-ray photons to be very high. In these conditions the optical depth for pair production via interaction of gamma-ray photons with X-ray photons is larger than unity and would prevent gamma-rays from escaping the emission region. However, the fact that we observe gamma-ray photons means that the actual optical depth must be less than unity. This paradox is easily solved if we take into account relativistic beaming which has the effect of both reducing the intrinsic variability time scale (see Eq. (3.2)) and boosting the gamma-ray luminosity. As a consequence, in the restframe of the source the upper limit on its dimensions ($R \lesssim c\Delta t_{\rm var}$) will be larger and both the gamma-ray luminosity and optical depth will be lower.

Compton catastrophe: As we will see in Chapter 4 radio emission from AGN is believed to be produced by accelerated electrons in a magnetic field via the synchrotron process. The X-ray emission can then be generated through inverse Compton scattering of low-frequency photons off relativistic electrons. If the photons are the synchrotron ones scattered by the same electron population (Synchrotron Self-Compton scenario) it is possible to predict the amount of X-ray emission from the energy density of radio synchrotron photons, assuming energy equipartition between the magnetic fields and the particles. In some radio-loud AGN the predicted X-ray flux strongly exceeds the observed flux (*Compton catastrophe*). The easiest explanation is that the radio flux is intrinsically weaker than observed, but enhanced by relativistic beaming.

Brightness temperature: The same inconsistency between predictions and observations is found when calculating the brightness temperature from radio measurements. The energy density of the magnetic fields must be larger than the energy density of the photons. If the opposite is true the inverse Compton scattering would rapidly prevail and the energy of the electrons would decrease rapidly, eventually quenching the synchrotron emission.
The energy density of the magnetic fields is:

$$u_{\rm B} = \frac{B^2}{8\pi} \tag{3.8}$$

The energy density of the photons is given by:

$$u_{\rm ph} = \Delta\Omega c I(\nu) \tag{3.9}$$

where $I(\nu)$ is the specific intensity which is taken to follow a black body law. At radio frequencies, this reduces to the Rayleigh-Jeans formula:

$$I(\nu) = \frac{8\pi\nu^2}{c^3} k_{\rm B} T \tag{3.10}$$

where T is the brightness temperature. The condition that $u_{\rm ph} < u_{\rm B}$ translates into an upper limit for the brightness temperature of the source of $T_{\rm B} \lesssim 10^{11}$ K. In numerous blazars we still see synchrotron radiation with $T_{\rm B}$ greater than this value. The problem is overcome by taking into account relativistic beaming. The condition $u_{\rm ph} < u_{\rm B}$ is satisfied in the rest frame of the source, but $u_{\rm ph}$ is boosted by relativistic beaming in the observer's frame, causing the apparent violation of the upper limit on the brightness temperature.

3.2 First attempts of unification

As we have seen in the previous paragraphs quite reliable evidence exists that the radiation we receive from AGN is emitted anisotropically, either due to relativistic beaming or to obscuration or both. The consequent idea is that intrinsically similar AGN appear different depending on the viewing angle, giving rise to the different classes of objects we see.

A first attempt of unification was made by Scheuer & Readhead (1979). These authors put forward the hypothesis that flat-spectrum radio-loud quasars were the beamed counterparts of radio-quiet quasars. They calculated the expected relative numbers of FSRQ and radio-quiet quasars from a population of randomly oriented sources. Comparing them with those actually observed they concluded that the bulk Lorentz factor required to match the observations was $\Gamma \sim 5$. This simple unification scheme failed mainly for two reasons. The first was that the predicted luminosity distribution function was a simple power law, not consistent with the observations. The second reason was that at that time, prior to VLA, the FSRQ appeared as compact radio sources with no trace of extended emission. When this was finally detected by VLA it was much stronger than the weak (but not absent) extended radio emission of radio-quiet quasars. However, according to the proposed scheme the extended radio emission of both the beamed and parent populations are expected to be unbeamed and, therefore, comparable.

Lobe-dominated SSRQ, on the other hand, have extended radio luminosities in accordance with those of FSRQ and it was first suggested by Perley et al. (1979) that the former could constitute the parent population of the latter. Orr & Browne (1982) developed this idea further into a unifying relativistic beaming model. However, even this model was not satisfactory, because the linear sizes of SSRQ were systematically smaller than the deprojected linear sizes of FSRQ, whereas they were expected to match. Another problem was that even lobe-dominated quasars had one-sided jets on large scales, as if they too were observed at a small viewing angle sufficient for relativistic beaming to play a role.

FRII radio galaxies also have extended radio emission comparable to those of FSRQ and SSRQ and Barthel (1989) tried to include them into a unified scheme as the parent population of both SSRQ and FSRQ, in a progression from larger to smaller viewing angles. This was now consistent with observations, however, FRII radio galaxies lack the broad emission lines in the optical/UV spectra which are found in quasars. A gas/dust torus was then invoked (the supporting evidence is discussed above), coaxial with the radio jet, obscuring the broad line region at large (i.e. in FRII galaxies), but not at small,

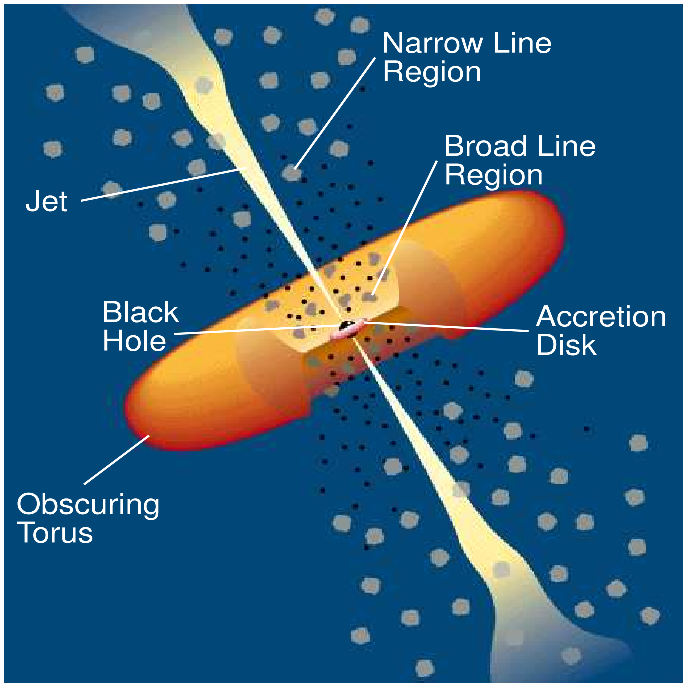

Figure 3.1: *Scheme of an AGN from Urry & Padovani (1995).*

viewing angles.

Barthel's model was leaving out many AGN classes, such as FRI radio galaxies, BLRG, BL Lacs and of course the whole radio-quiet population, but it formed the basis for further developments and improvements. In the following chapter we will discuss the currently accepted version of the unified scheme for radio-loud and radio-quiet objects and related problems.

3.3 Current unification schemes

3.3.1 Radio-loud AGN

The components of the unification scheme for the radio-loud AGN are shown in Fig. 3.1 and an exhaustive review is given, for example, by Urry & Padovani (1995).

A supermassive black hole ($M_{\rm BH} \sim 10^6 - 10^9 M_\odot$) is located at the center of an AGN. An accretion disk of matter falling onto the black hole is surrounding it and, for a black hole of mass $M_{\rm BH} \sim 10^8 M_\odot$ with a Schwarzschild radius[1] of $R_{\rm S} \sim 3 \times 10^{13}$ cm, it extends from $\sim 3 - 100 R_{\rm S}$. The accretion disk emits UV up to soft X-ray radiation and perhaps hard X-ray radiation in the innermost region from a hot corona above the disk. Within

[1]The Schwarzschild radius is defined as:

$$R_{\rm S} = \frac{2GM_{\rm BH}}{c^2} \tag{3.11}$$

a radius of $\sim 2 - 20 \times 10^{16}$ cm several gas clouds form the Broad Line Region (BLR) emitting broad emission lines in the UV/optical band with typical widths of the order of several thousands km s^{-1}. Surrounding the BLR is a dusty torus with inner radius of the order of $\sim 10^{17}$ cm. Outside the torus we find the Narrow Line Region (NLR) made of gas clouds producing the narrow emission lines with widths of the order of several hundred km s^{-1}. It extends from $\sim 10^{18} - 10^{20}$ cm. Two radio jets flow from the black hole in opposite directions feeding the radio lobes (not shown in the figure). The radio jets can extend up to $0.1 - 1$ Mpc, well outside the size of the optical galaxy.

Given this structure, the separation of AGN into type 1, type 2 objects and blazars is just a matter of viewing angle. If the viewing angle is large the observer's line of sight will intercept the dusty torus and both the optical continuum from the central region and the BLR will be hidden. In this case the object will be classified as type 2 or NLRG. At intermediate angles the line of sight will be affected by absorption in the dusty torus but it will avoid the radio jet; both NLR and BLR plus optical continuum will be observed, but relativistic beaming effects will not be relevant. In this case the object will be classified as type 1, as BLRG or as SSRQ. When the line of sight intercepts the radio jet which is then viewed along its axis, relativistic beaming strongly amplifies the luminosity and produces strong variability, polarization, superluminal motion and all the other effects described for the blazar class.

As already predicted in Barthel's model, FRII radio galaxies are considered as the parent population of BLRG, SSRQ and FSRQ in order of decreasing angle with the line of sight. The FRII lack the broad emission lines because they are obscured by the dusty torus.
Similarly, for the low-luminosity radio-loud objects, the FRI radio galaxies are believed to be the misaligned parent objects of BL Lacs. BL Lacs have featureless spectra, with no or weak emission lines, so obscuration of a BLR by a dusty torus, like in the FRII case, does not need to be invoked in this case, neither is there observational evidence for it. It has been proposed that the FRI/BL Lacs intrinsically lack a BLR, maybe because of a weaker ionizing continuum (Chiaberge et al. 1999). The intermediate-angle equivalents of the BLRG are missing in this case. A possible complication of this model is that a fraction of BL Lacs show a radio morphology of FRII type in contrast to the commonly observed FRI morphology. It could well be that the parent AGN of some BL Lacs are FRII radio galaxies and possible candidates are the WLRG, which have line properties more consistent with those of BL Lacs.
The parameters governing the physical division into low-power and high-power objects (i.e. FRI/BL Lacs vs. FRII/SSRQ/FSRQ) are still unknown.

The unification scheme for radio-loud AGN has been tested by calculating the predicted luminosity functions for the beamed sources, starting from a randomly oriented population of objects with an intrinsic power law luminosity function to which relativistic beaming is applied (Urry & Padovani 1995). The obtained beamed luminosity function is a broken power law steepening at higher luminosities. Taking the FRI and FRII galaxies as the unbeamed objects, it is possible to compare their predicted luminosity, boosting their observed luminosity function with the observed ones of BL Lacs and quasars, respectively.

In this process the bulk Lorentz factor Γ and the fraction f of intrinsic luminosity of the jet are free parameters and adjusted to match the observed luminosity functions. A range of values $\Gamma \sim 5 - 40$ is required for the high-luminosity objects and $\Gamma \sim 5 - 32$ for the low-luminosity objects.
The predictions seem to agree quite well with the observations thus supporting the proposed unification model. Further support comes from the comparison of the angle-independent properties of the beamed and the parent AGN. They generally seem to be consistent with each other in agreement with the predictions of the unified scheme. Some of these properties are the extended radio emission, the narrow emission line luminosities, the infra-red emission and the host galaxy types.

3.3.2 Radio-quiet AGN

We will just outline the unified scheme for radio-quiet AGN, since we are mainly interested in the radio-loud population. A complete review of the classical unified scheme for radio-quiet AGN can be found in Antonucci (1993).

The same angle dependence as for the radio-loud AGN is thought to explain the division into type 2 and type 1, but in this case relativistic beaming is not invoked. In fact, strong relativistic jets are absent in radio-quiet objects and, therefore, no radio-quiet equivalent of the blazars are expected. Unification relies instead on obscuration alone and objects with type 2 spectra are seen through the absorber whereas type 1 objects are seen at lines of sight free from absorption. At intermediate angles broad wings can appear in the narrow lines, becoming progressively stronger as the angle decreases, leading to intermediate classifications such as Seyfert 1.2, 1.5, 1.8, 1.9 (Osterbrock 1989). It could also be the case for the existence of both obscured Sy1-like Seyfert 2 galaxies and unobscured intrinsic Seyfert 2 type galaxies (Tran 2001). The role of BAL QSO is still uncertain.

3.4 Comments

The unification schemes proposed so far seem to be capable to explain the most general properties of AGN. Little doubt is left that orientation plays a major role in determining the appearance of an AGN, so that some kind of unification scheme is certainly needed. The schemes are still rather simple and it is not surprising that a large variety of observational data remains to be explained. With further work and improved data it will perhaps be possible to develop more complex models and tackle finer details. However, it is improbable that the whole picture will be modified dramatically.
Nonetheless, there are some very basic questions which the current unified schemes cannot answer. The unified schemes explain the type 2/type 1/blazars separation, but nothing is said about the distinction between radio-loud and radio-quiet AGN. There are many ideas and hypotheses, such as different environments or different spins of the black holes, but this dichotomy is essentially unexplained. Related to this is also the question of how jets are formed. Quite uncertain is as well the role of evolution of AGN, which must be of fundamental importance for objects which have the highest redshifts in the Universe.

Finally, some objects have not yet found a place within the AGN unification scheme, such as the BAL QSO or the GPS/CSS sources in the radio-loud class.

Chapter 4

The Spectral Energy Distribution of AGN

AGN are powerful emitters in every energy band of the electromagnetic spectrum, from radio frequencies up to gamma-ray energies. A correct understanding of the AGN physics and a reliable estimate of the total emitted power strongly depend on a detailed knowledge of the emission properties in every region of the spectrum and therefore on the quality of the observations available in each band. Some wavebands are better studied than others, like the radio, the optical and the X-rays, whereas some are inaccessible by our instruments, like the extreme UV beyond the Lyman limit of 912 $\mathring{A}$, due to the high opacity of the interstellar medium in our Galaxy. Understandably, we have a better knowledge of the multiwavelength properties of the brightest AGN, i.e. blazars. In the following paragraphs I will give an overview of these properties as they are presently known, starting with a general description of the spectral energy distribution of AGN and I will then discuss the emission mechanisms in each band. The last two paragraphs will concentrate on the emission and absorption lines observed in AGN.

4.1 The shape of the SED

The usual way to illustrate the multiwavelength energy output of AGN is through the so called Spectral Energy Distribution (SED). This is a broad band spectrum covering the whole range of frequencies, from radio to gamma-rays, generally represented in a $\log\nu$-$\log\nu f_\nu$ (or $\log\nu \mathrm{L}_\nu$) plot. Such a plot has the advantage of approximately showing the energy emitted per unit logarithmic frequency interval (or per decade of frequency), which immediately indicates in which band most of the energy is released.

Two general remarks can be made. The first is that all AGN emit almost constant power per decade of frequency between ~ 100 μm and ~ 100 keV, whereas at radio and gamma-ray energies they show quite different behaviors, with some sources being strong radio or gamma-ray emitters whereas others are not. The second important remark is that the spectral features, across the largest part of the electromagnetic spectrum, show close similarities for AGN spanning a range of luminosities over about seven orders of magnitude. It thus seems that a scaling relation with luminosity must exist in the central

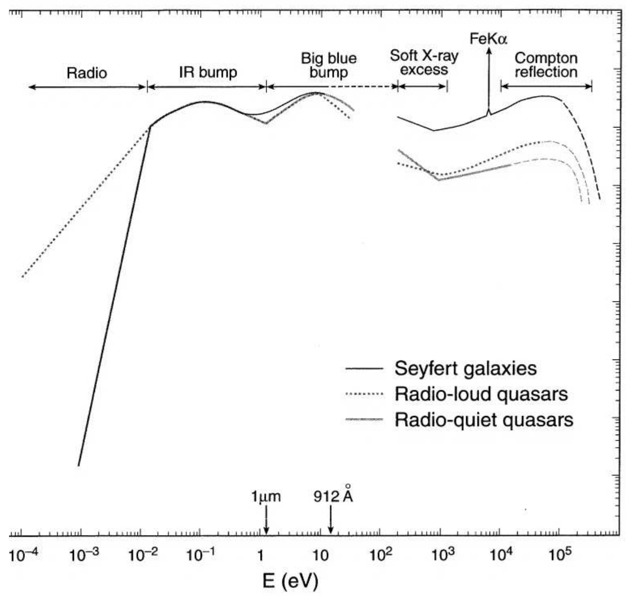

Figure 4.1: *Schematic Spectral Energy Distribution for different types of non-blazar AGN (from Koratkar & Blaes 1999).*

engines of AGN.

Apart from these overall similarities, the SEDs of AGN can be recognized to belong to two different classes: the *blazars*, which are dominated by non-thermal emission processes in the jets and the *"non-blazar"* AGN, in which the dominating process is the thermal emission from the accretion disk. In the following we will treat these two cases separately and describe them in more detail.

4.1.1 The non-blazar AGN

This class includes radio-quiet quasars, Seyfert galaxies, radio galaxies and steep-spectrum quasars. In Fig. 4.1 a schematic representation of the SED for Seyfert galaxies, radio-quiet and radio-loud quasars is shown.
The continuum can be quite well modeled with a flat underlying power law from the infra-red band up to the X-rays plus some evident spectral features deviating from it.

The first one is the drop in flux in the sub-millimeter band (*mm-break*) which distinguishes radio-loud from radio-quiet objects. In fact, in radio-loud quasars the drop is of the order of about two decades, whereas for the radio-quiet it is of the order of $\sim 5-6$ decades. It must be noted, however, that although the emitted radio power in radio-quiet objects is small compared to the total, it is not completely absent and it is still larger than in normal galaxies.
Fig. 4.1 shows that the flux between ~ 1 and ~ 100 μm for both classes (radio-loud and radio-quiet) rises, reaches a peak and decreases to a local minimum at ~ 1 μm, forming the so called *infra-red bump*. The infra-red bump typically contains one third of the total

bolometric luminosity of the thermally dominated objects.
A second prominent peak is situated between the near-infrared, around $\sim 1\ \mu$m, and the UV, past $\sim 1000\text{Å}$. This feature is called the *Big Blue Bump (BBB)*. In some objects the flux is still rising beyond $\sim 1000\text{Å}$ and probably peaks in the unobservable extreme UV region. The strength of the BBB is generally comparable to that of the infra-red bump.
On top of the BBB, placed around $\sim 3000\text{Å}$, there is another small bump.
Beyond the Lyman limit at 912Å up to the soft X-ray band (~ 0.1 keV) no radiation can reach us because of the absorption by the Galactic interstellar medium. This is unfortunate as the radiation in this frequency range is responsible for the ionization of the BLR and of the NLR. An analysis of the emission lines can, however, provide insight into the properties of the extreme UV radiation.
In the soft X-ray domain an excess of emission appears with respect to the extrapolation of the hard X-ray power law to lower energies. This *soft X-ray excess* is sometimes believed to be the high energy tail of the BBB peaking in the extreme UV.
In the hard X-rays a component with flat slope ($\alpha_{\rm x} \sim 0.9$) emerges and sometimes additional features like the Fe Kα emission line and a Compton reflection hump above ~ 10 keV.
Above few hundred keV the non-blazar AGN are not strong emitters, contrary to the blazars (see §4.1.2).

Objects observed at a large angle with the line of sight (type 2) appear to have less prominent BBBs and stronger soft X-ray absorption than more aligned objects (type 1) in agreement with the unification scenario.

4.1.2 The blazars

Blazars are the most radio-loud AGN and therefore are regarded as jet-dominated objects. An example of their typical SED is given in Fig. 4.2. The typical shape is that of a "camel's back" with two broad bumps.

BL Lacs are currently classified either as *Low-energy-peaked BL Lacs (LBL)* or as *High-energy-peaked BL Lacs (HBL)* according to the definition proposed by Padovani & Giommi (1995). The bump at lower energies peaks typically at infra-red/optical wavelengths in LBL and in the UV/soft X-rays band in HBL. LBL are more extreme objects than HBL in having higher polarization, higher variability, larger bolometric luminosity and larger core dominance[1]. Compared to LBL, FSRQ have both similar broad band spectra, with the first peak falling in the IR/optical, and extreme properties.

Contrary to non-blazar objects the radio emission joins smoothly the infra-red emission suggesting a common non-thermal origin. After the peak the continuum falls gradually towards a minimum and rises again reaching a second peak in the gamma-ray band. Blazars are in fact strong emitters at $E \gtrsim 100$ MeV as discovered by the EGRET experiment on board the *Compton Gamma-Ray Observatory* (von Montigny et al. 1995). In many cases the gamma-ray luminosity is even dominating that in the other wavebands.

[1] The *core dominance* of a source is defined as the ratio of its core to its extended radio emission, usually measured at 5 GHz.

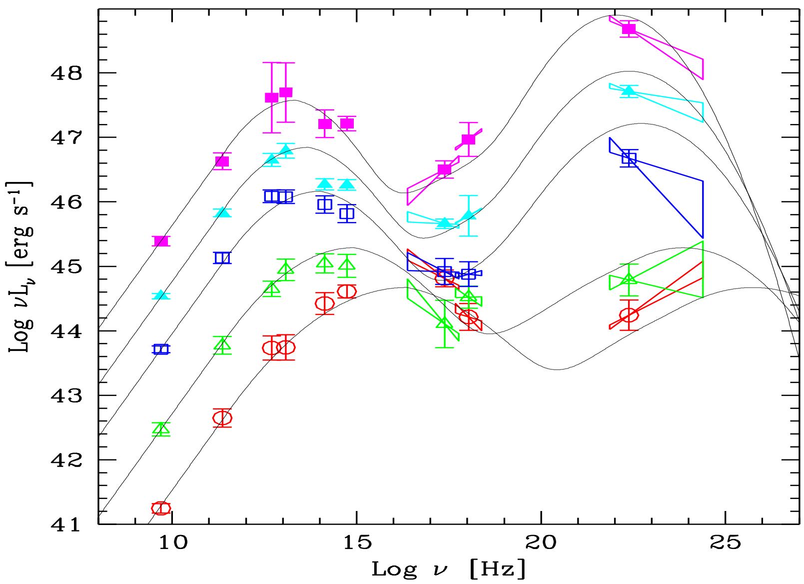

Figure 4.2: *Average spectral energy distributions of blazars from Donato et al. (2001).*

4.2 Continuum emission mechanisms

In the previous section we have given a general description of the AGN SED without discussing which emission mechanisms could produce it. In the following we treat the most plausible emission mechanisms proposed for each waveband.

Radio: Radio emission in radio-loud AGN is firmly believed to be synchrotron emission from a population of relativistic electrons residing in jets. The radio spectral index is usually flat ($\alpha_{\rm r} \lesssim 0.5$) in the core of a radio source and steep ($\alpha_{\rm r} \gtrsim 0.5$) in the outer lobes. The power law form of the spectrum results naturally if the energy distribution of the emitting particles is also a power law, that is, if the number of particles per energy interval is given by:

$$N(E) \sim E^{-p} \tag{4.1}$$

The *particle distribution index* p is related to the spectral index α through $\alpha = (p-1)/2$ (Rybicki & Lightman 1979).
The steeper slope of the lobes is believed to be the result of the aging of the plasma. At higher energies electrons cool faster and the energy distribution is thus depleted, directly reflecting in a steepening of the emitted spectrum.
In blazars, observed at small angles, the synchrotron radio emission from the jet is highly beamed.
As we have seen in Chapter 2, GPS and CSS differ from the classical radio sources because they are compact, with a convex radio spectrum around few GHz and an overall steep spectral index at energies above the peak. Synchrotron self-absorption seems to be the likely cause of this behavior.
Radio-quiet AGN rarely show a jet+lobes radio structure similar to classical radio sources

and at a considerable lower luminosity level. Frequently, the radio emission has a complex diffuse morphology. In these cases it is conjectured that the radio emission originates from a mixture of thermal and non-thermal processes associated with starbursts.

Infra-red: Since in radio-quiet AGN the extrapolation of the radio emission into the IR band lies far below the observed IR flux and since the IR emission shows no rapid variability, the IR bump is generally attributed to thermal emission by dust, heated by the optical/UV radiation from the central energy source. The range of temperatures required is wide, from ~ 50 to ~ 1000 K. In this scenario the drop in flux around $\sim 1\ \mu$m is easily explained by the maximum temperature of ~ 2000 K that dust can reach before sublimation takes place and both the dust opacity to UV/radiation and its radiative efficiency decline.
In blazars the non-thermal radio emission smoothly merges with the infra-red emission, which is therefore naturally interpreted as the high energy continuation of the synchrotron emission.
The IR emission in non-blazar radio-loud AGN is likely a combination of both the thermal and non-thermal components discussed above.

Optical/UV: The currently most favored interpretation for the BBB in radio-quiet and non-blazar radio-loud AGN is thermal radiation produced by the gas in the accretion disk. The small bump at $\sim 3000\mathring{A}$ is the sum of the contributions from the Balmer continuum, the blending of higher order Balmer lines and the blending of the Fe II lines.
The blazars lack the BBB and their optical/UV radiation is just the steepening side of the synchrotron bump.

X-rays and gamma-rays: Radio-quiet AGN usually exhibit a soft X-ray excess which is generally believed to be the high energy tail of the BBB, whose peak is situated in the unobservable extreme UV band. Lobe-dominated radio-loud AGN often show the same soft X-ray excess.
In the hard X-rays, the spectrum of radio-quiet AGN is usually a power law with $\alpha_{\rm x} \sim 0.9$ (Williams et al. 1992). This X-ray radiation is mainly regarded as the result of inverse Compton scattering of optical/UV photons from the disk off electrons in a hot corona above the disk. Above ~ 10 keV a hump is usually observed originating from reflection from cold material (the accretion disk or the torus). In association with this, a fluorescence Fe Kα emission line is often observed at 6.4 keV. The non-blazar radio-loud AGN have similar X-ray spectra, but with somewhat flatter slopes ($\alpha_{\rm x} \sim 0.7$), weaker Fe lines, and usually no reflection humps. No strong emission is known above ~ 100 keV for radio-quiet and lobe-dominated radio-loud AGN.
As we have seen, blazars have very peculiar overall spectra compared to other AGN. The first bump is thought to originate from synchrotron emission whereas the second from inverse Compton scattering of photons which could either be the synchrotron photons themselves (Synchrotron Self-Compton, SSC) or external photons either from the accretion disk or reprocessed in the emission lines region (External Compton, EC). In LBL and FSRQ this second peak is situated in the hard X-ray/gamma-ray band, at lower energies with respect to the HBL. As a consequence, for blazars, the X-ray band contains contributions from both the synchrotron emission and the inverse Compton emission, giving

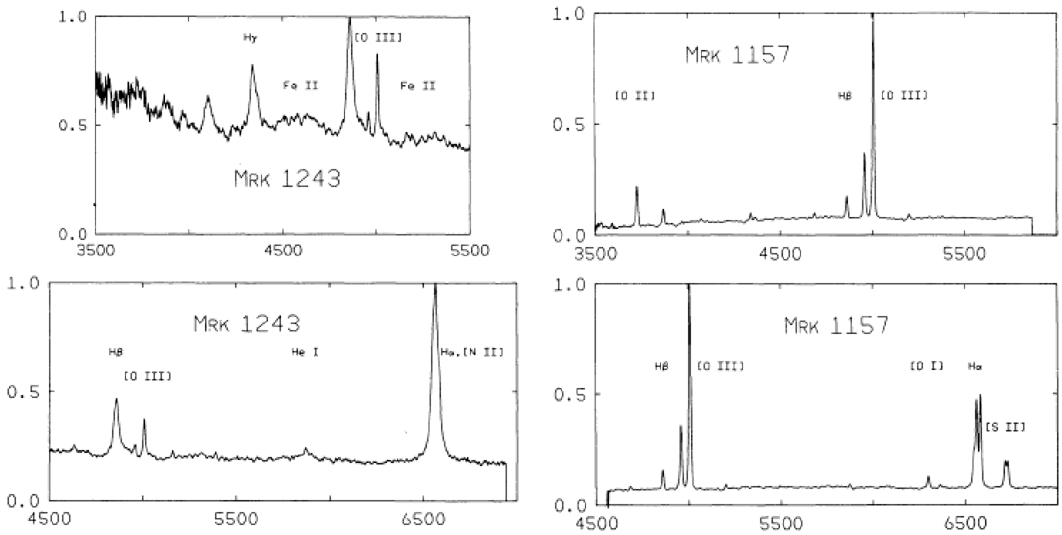

Figure 4.3: *Optical spectra of a Seyfert 1 galaxy (left panels) and of a Seyfert 2 galaxy (right panels) (Osterbrock 1989).*

rise to a wide range of slopes. In HBL the X-ray emission is the high energy tail of the synchrotron emission and the resulting slope is steep; for LBL and FSRQ it is the rising part of the inverse Compton bump and thus the slope is flat. The strong gamma-ray emission is produced in all blazars through inverse Compton scattering.

4.3 Emission lines

As we have seen in Chapter 2 a distinguishing property of all AGN (except the BL Lacs) is the presence of strong emission lines in their spectra, rarely seen in normal galaxies. The emission lines consist basically of two types and are used for the definition of type 1 and type 2 AGN: lines with broad profiles and lines with narrow profiles. In Fig. 4.3 two examples of type 1 and type 2 spectra are shown.

The broad lines have $FWHM \gtrsim 1000$ km s^{-1} and originate mainly from H, He, C, O, Mg, Si. No forbidden lines are detected among the broad emission lines, which means that the density in the BLR must be high in order to rapidly collisionally de-excite the energy levels which could give rise to the forbidden transitions on longer time scales. From this argument a lower limit to the electron density is $n_e > 10^8$ cm^{-3}. However, the detection of the CIII] semi-forbidden emission lines implies $n_e < 10^{10}$ cm^{-3}.
The narrow lines have $FWHM \lesssim 1000$ km s^{-1}, still broader though than those of normal galactic nuclei. Typical narrow lines are those produced by H, He, FeII, MgII, CIV. Several forbidden lines are also detected as narrow emission lines like the prominent [OIII], O[II] and [NII], [OI] and [SII]. From the intensity ratios of the forbidden lines it is found that in the NLR the electron density is $n_e = 10^3 - 10^4$ cm^{-3}.
It must be noted that both the broad and the narrow emission lines have profiles too broad to be interpreted as thermal motion. Instead, it is believed that the Doppler broadening

is caused by the high bulk velocity of the gas moving in the deep gravitational potential well of the supermassive black hole.

The lines are emitted from the gas in the NLR and BLR photo-ionized by the continuum emission from the center of the AGN. The main supporting evidence for this scenario is the simultaneous presence of a wide range of ionization stages which cannot be obtained by collisional ionization at the temperatures inferred from the line ratios. The broad band continuum from the central engine of the AGN can, on the other hand, supply the high energy photons necessary to overcome the high ionization potentials.

The broad emission lines are known to be variable and to respond to the variations of the continuum flux, accordingly to the photoionization scenario, with a certain delay. Measuring this delay and assuming that the BLR clouds follow Keplerian orbits around the black hole, it is possible to estimate the size of the BLR. This technique is known as *reverberation mapping* and the inferred BLR sizes are of the order of light-days up to light-months. No variability has been observed in the narrow lines so far. They are produced much farther from the center than the broad lines and do not respond to continuum variations. The NLRs usually have dimensions of the order of few kpc, in some cases they extend up to $10 - 100$ kpc.

4.4 Absorption lines

We will only briefly mention the absorption lines in AGN. Some are intrinsic to the AGN and some are believed to originate from matter along the path of the light from the AGN to us.
The latter are detected mostly in high-z quasars, whose light has the highest probability to interact with the intergalactic medium in between. Two kinds of absorption lines are observed in these cases, metal absorption line systems and the Lyα forest.
The metal line systems are groups of many absorption lines in the quasars' spectra with a common redshift (smaller than the quasar's redshift) produced by elements like CIV and MgII.
The Lyα forest is a closely-packed sequence of absorption lines bluewards of the quasars' Lyα emission line. They do not belong to a single redshift system as in the case of the metal lines. It is believed that they are produced through Lyα absorption of the redshifted quasar radiation at shorter wavelengths than the Lyα emission line by many intergalactic clouds situated along the line of sight at lower redshifts.
BAL QSO show broad absorption lines bluewards of the corresponding emission lines in a sort of P-Cygni profile. As we have seen in Chapter 2 these lines are regarded as intrinsic to the quasars, produced in a high velocity outflow in the direction towards the observer. The connection with the emission line is the main evidence for an intrinsic origin.

Chapter 5

The sample and the data

For the study of AGN two different approaches are generally followed. The first is to analyse a large number of objects, either by studying the collective properties of sources belonging to a certain class or to highlight common/different trends for separate classes which can be interpreted in terms of unified schemes.
The second approach is to concentrate on interesting individual objects by performing accurate spectroscopic, spatial and timing analyses, a work favored by the new generation of both space and ground based observatories (XMM-Newton, *Chandra*, VLT, HST, INTEGRAL, etc.), which combine a high degree of sensitivity with good spatial, spectral and temporal resolution. This approach provides direct insight into the physics and the structure of an AGN testing its various components (see Fig. 3.1). However, the objects under study are usually, for obvious reasons, the most luminous or the most peculiar ones, therefore their properties might not be typical for the majority of AGN.
In this work we want to explore the issue of AGN unification from an X-ray perspective. In fact, although the X-ray properties of AGN have been investigated by now for about three decades, the results have not been included in the description of the standard picture.

In the following we describe the construction of the sample to be studied and its properties. We explain what data were collected for each source and we discuss the advantages and the limitations of such a sample.

5.1 The sample

For the above purposes we require a very large sample of AGN for which X-ray data are available. The ROSAT satellite performed an *All-Sky Survey* (RASS) in the soft $0.1-2.4$ keV X-ray band in 1990/91 (Trümper 1983). The second RASS processing yielded 145,060 sources with detection likelihood ≥ 7 (Voges et al. 1999), of which a large fraction are AGN. Additional data from several years of ROSAT pointed observations are also available. No previous or subsequent X-ray satellite accomplished an equivalent survey in terms of combined sensitivity and sky coverage and the data are now entirely stored in an easily accessible public archive. The ROSAT archive was thus the main source of the objects for our sample.
We are primarily interested in radio-loud AGN, so the second requirement was the detec-

Name of survey/catalog	Frequency
3rd Cambridge Radio Catalog (3C)	178 MHz
4th Cambridge Radio Catalog (4C)	178 MHz
5th Cambridge Radio Catalog (5C)	408 MHz, 1.407 GHz
6th Cambridge Radio Catalog (6C)	151 MHz
7th Cambridge Radio Catalog (7C)	151 MHz
8th Cambridge Radio Catalog (8C)	38 MHz
Strong Radio Source Surveys (S1, S2, S3, S4, S5)	5 GHz
Parkes Radio Catalog (PKS)	Several frequencies
Molonglo Reference Catalogue of Radio Sources (MRC)	408 MHz
Bologna Catalogs of Radio Sources (B2, B3)	408 MHz
MIT-Green Bank 5 GHz Surveys (MG1, MG2, MG3, MG4)	5 GHz
Faint Images of the Radio Sky at Twenty Centimeters (FIRST)	1.4 GHz
1987 Green Bank Radio Survey (87GB)	4.85 GHz

Table 5.1: *The radio catalogs searched with NED.*

tion of radio emission from each source (which, however, does not necessarily imply that the object is radio-loud).
To select X-ray (in the ROSAT band) and radio emitting AGN we made use of the *NASA Extragalactic Database (NED)*. We selected all sources in NED either defined as galaxies or quasars[1] which were labeled both as X-ray sources and radio sources belonging to one of several well known radio catalogs. The searched radio catalogs together with the observing frequencies are listed in Table 5.1.

Among the objects returned by NED we chose only those fulfilling some further requirements. We selected only the ROSAT sources (and not, for example, *Einstein* or ASCA sources). We required from all sources to have a measured optical magnitude and excluded those for which no redshift is available because we wanted to calculate luminosities. For 15 objects we performed a series of optical spectroscopical observations at the Skinakas Observatory in Crete (see Appendix A for an extensive report). We were able to measure the redshift and give a classification for 13 of them.
In the radio-loud AGN unification scheme the FRI/FRII classification holds a fundamental role, but unfortunately only for a relatively small number of sources in our sample this information is available. We searched the literature for FRI/FRII sources that were not listed as X-ray sources in NED and we performed a cross-correlation with the RASS and other ROSAT catalogs (the first and the second ROSAT source catalogues of pointed PSPC observations, the ROSAT Wide Field Camera catalogue, the Supper-Voges cat-

[1]In NED the difference between quasars and galaxies is that *quasars* are pointlike AGN whose host galaxy is not visible, whereas *galaxies* appear extended.

Classification	Number
Quasars	943
BL Lacs	270
Radio galaxies	131
GPS/CSS	68
Seyfert galaxies	383
NLSy1s	31
LINERs	37
Starbursts	14
HII galaxies	10
AGN	36
No classification	337

Table 5.2: *The composition of the database in terms of the classification of the sources from the literature.*

alogues of pointed HRI observations, the first ROSAT HRI catalogue and the White, Giommi & Angelini ROSAT source catalogue of pointed PSPC observations) to look for possible X-ray detections that could be added to our sample. This attempt yielded a few dozen additional sources.

We have searched the literature and the ROSAT archive for the required data and additional information for every single source. We recorded the redshift, the optical magnitude, the radio flux, the radio spectral index when measured, the optical position, the X-ray count rate/flux and the X-ray position. The V magnitude was preferred, however, if this was not available, the B magnitude was used and extrapolated to the V band assuming a power law spectrum with energy index $\alpha_o = 0.5$. We collected radio fluxes at 5 GHz or, when these were not found, at other frequencies such as at 1.4 GHz and 408 MHz. We recorded separately the core and the extended radio fluxes whenever they were given. References were carefully kept for all data. The ROSAT X-ray count rate between $0.1 - 2.4$ keV and the X-ray position were mostly extracted from the ROSAT archive.
Some sources detected by ROSAT and for which results from their data analysis are reported in the literature do not turn up as X-ray sources in NED. Therefore we searched systematically papers reporting on ROSAT observations of large samples of AGN to look for such sources which could be added to our sample. In these cases the X-ray flux, luminosity or an upper limit given in the paper was used.
We also checked the literature for any possible information about the AGN classification, radio morphology, host galaxy type and cluster/group membership.

The resulting sample consists of 2260 sources of different types with known redshift, optical, radio and X-ray fluxes. The total sample is given in Table 1 at the end of the thesis, with the data and relevant information for each source. The composition of the sample according to the classification of the sources given in the literature is summarized in Table 5.2.

5.2 Properties of the sample

Our sample selection certainly has some limitations but we believe that this does not dramatically influence the results of our work. It is clear that the objects in our sample are heterogeneously selected, originally belonging to different radio catalogs with different observational frequencies, sensitivities, level of completeness, etc. This fact leads to unknown selection biases and we cannot easily define the degree of completeness. One selection bias clearly present in our sample is the exclusion of highly obscured AGN, due to the soft X-ray selection of our objects. As a consequence, the relative numbers of type 1 and type 2 AGN in our sample do not reflect the real relative numbers according to the unified scheme. However, we believe that our sample is representative of the AGN population, at least the radio-loud, because its heterogeneity tends to minimize any systematic selection bias.

The strongest quality of our sample is its large size compared to previous works which allows both a good statistical treatment with the determination of the bulk trends and the location of "outliers". These atypical objects, while not affecting the determination of the collective properties of the sources, have to be investigated in more detailed studies.

Furthermore, objects from all AGN classes are contained within our sample as a consequence of its heterogeneity. Basically all radio-loud AGN types and also radio-quiet objects (but not radio-silent!) are present with quite a significant number of objects each, allowing the study of subsamples and tests for the unified scheme.

A critical issue is related to the errors given for the fluxes. They are beyond our control, in many cases they are not available and they reflect the heterogeneity of the original measurements. Therefore, for our analysis we have used error estimates based on conservative assumptions which will be discussed later on.

As a final remark it must be noted that the collected information is not always complete and may change. New sources are constantly observed and better data are steadily supplied. However, "real-time" updates are not feasible and we think that, due to the large size of our sample, our results are quite robust with respect to the progressive improvement of the databases. Nonetheless, the sample should be updated whenever new data become available.

5.3 Calculation of luminosities

For the calculation of the X-ray, radio and optical luminosities we assume a Friedmann cosmology with $H_0 = 50$ km s^{-1} Mpc^{-1} and $q_0 = 0.5$. We do not use the cosmological parameters from recent WMAP data in order to facilitate comparisons with previous studies. The effects of different cosmologies are especially evident at high redshifts, but negligible at low redshifts. As all FRI galaxies in our sample have $z < 0.25$ and most of the BL Lacs ($\sim$86%) have $z < 0.5$ we are confident that the cosmology used does not significantly affect the main results for these sources. The FRII galaxies have a mean redshift of ~ 0.3 and a maximum value of ~ 0.7, whereas the mean redshift of the quasars is ~ 0.8 and the maximum value is ~ 1.9. Therefore, for these two classes of objects the choice of the cosmology might be critical. Using a WMAP cosmology would produce higher luminosities than those calculated with our adopted cosmology, especially for objects at redshift $\gtrsim 0.5$. The mean luminosities and, consequently, also the beaming factors for FRI galaxies

and radio-loud quasars (see Chapter 8) might thus be underestimated. However, the main results about both, the spectral energy distributions of these sources and the correlations between their luminosities in different bands should not be significantly affected, as the choice of a different cosmology would modify all luminosities by the same amount.
From the $0.1 - 2.4$ keV count rate we calculate the corresponding X-ray flux using the ROSAT PSPC *energy-to-counts conversion factor (ECF)* (ROSAT AO-2 technical appendix, 1991), assuming absorption by the galactic neutral hydrogen column density ($N_{\rm H}$) and a power law photon index of $\Gamma_{\rm X} = 2.1$ for all sources. The dependence of the ECF on $\Gamma_{\rm X}$ is described by curves in the $\Gamma_{\rm X}$-ECF plane corresponding to different values of constant $N_{\rm H}$. For a given photon index, the ECF for the galactic $N_{\rm H}$ towards a source is derived by interpolation between the given curves of constant $N_{\rm H}$. For sources observed with the ROSAT HRI the corresponding ECF was used. Allowing for a range of photon indices of $\Gamma_{\rm X} \sim 1.5 - 2.5$, including the typical values for different AGN classes (Brinkmann et al. 1994, Brinkmann et al. 1995), does not appreciably change the ECF; the variations in the X-ray flux are only of the order of $\sim 5\%$. A more critical parameter is the amount of galactic absorption towards the source. At a photon index $\Gamma_{\rm X} = 2.1$ changes in the galactic $N_{\rm H}$ of $\sim 10^{20}$ cm^{-2} produce flux differences of the order of 10%. We used FTOOLS to obtain the galactic $N_{\rm H}$ for each source. This is derived from the HI maps by Dickey & Lockman (1990) averaging the available $N_{\rm H}$ measurements within 1 degree from the position of the source, weighted by the inverse of the distance from it. For some prominent objects, accurate $N_{\rm H}$ measurements towards the sources from Elvis et al. (1989), Lockman & Savage (1995) and Murphy et al. (1996) are available.
Having calculated the ECF the $0.1 - 2.4$ keV X-ray flux is obtained by:

$$f_{\rm X} = \frac{CR}{ECF} \tag{5.1}$$

where CR is the X-ray count rate.
The monochromatic 2 keV flux is calculated from the X-ray flux in Eq. (5.1) or from the flux given in the literature (see §5.1) by adopting $\Gamma_{\rm X} = 2.1$.

The $0.1 - 2.4$ keV and the monochromatic luminosities are calculated according to:

$$L_{\rm X} = f_{\rm X} 4\pi D_{\rm L}^2 K(z) \tag{5.2}$$

where $f_{\rm X}$ is either the $0.1 - 2.4$ keV flux or the 2 keV flux, $D_{\rm L}$ is the luminosity distance and $K(z)$ is the K-correction term:

$$K(z) = (1+z)^{-(1-\alpha_{\rm x})} \tag{5.3}$$

for which we used the energy index $\alpha_{\rm x} = \Gamma_{\rm X} - 1 = 1.1$.

The optical luminosity is calculated in the V band, centered on a wavelength of $\lambda = 5500\mathring{A}$, by converting magnitudes to fluxes and then fluxes to luminosities using an equation analogous to Eq. (5.2), but with an optical energy index $\alpha_{\rm o} = 0.5$ (Worrall et al. 1987, Brotherton et al. 2001) for the K-correction.
When only the B ($\lambda = 4400\mathring{A}$) magnitude is available we convert B fluxes to V fluxes

assuming again a power law with $\alpha_o = 0.5$.

A similar procedure is followed for the 5 GHz radio luminosities. Both the radio core luminosity (when available) and the total radio luminosity are calculated. In cases where we only know the radio flux at 1.4 GHz or 408 MHz we extrapolate the flux to 5 GHz assuming a power law with slope $\alpha_r = 0.5$ (see §5.4 for a discussion on the error committed with such an assumption). The same value is taken for the K-correction.

5.4 Errors

Our sample is selected such that we cannot rely on accurate determinations of the errors on fluxes and luminosities. The errors on the measurements quoted in the literature are heterogeneous and, in many cases not available. Furthermore, to calculate fluxes and luminosities, we need to make general assumptions on the spectral and absorption properties of the sources. In fact, the possibility of performing a detailed X-ray, radio and optical spectral analysis of all 2260 sources is precluded by the large size of the sample, the often limited statistical quality of the data and the inaccessibility of the radio and optical data. Only for a minority of objects in our sample spectral and absorption data are provided in the literature. For a consistent approach we made the same assumptions about the spectral and absorption properties for all sources and we are confident that our results do not depend dramatically on them.
Variability, commonly found in AGN, might affect as well the calculated fluxes and luminosities, which are obtained from non-simultaneous data. In the X-rays a large fraction of radio-loud quasars show variability, however by less than a factor of two (Brinkmann et al. 1997) and only few objects by more than a factor of 4 or 5.
We therefore used the following conservative estimates for the total errors:

Errors on the optical measurements quoted in the literature can vary from very small (~ 0.01 mag) up to large values (~ 0.10 mag) in a few cases. With a conservative value of $\Delta V \sim 0.10$ mag, we get a $\sim 4\%$ error on the flux. The error on flux might be larger for sources for which we have to transform B band into V band fluxes due to the assumption made on the optical spectral shape. If we assume $\Delta B \sim 0.10$ mag, a power law spectrum with spectral index $\alpha_o = 0.5$ and possible variations of the optical slope of $\Delta\alpha_o = 0.5$ we obtain errors of the flux of $\sim 6\%$. When we calculate the luminosity a further contribution to the total error originating from the uncertainty of the spectral index comes from the K-correction term. This error will be larger for sources at higher redshifts. Assuming as before $\alpha_o = 0.5$ and $\Delta\alpha_o = 0.5$ leads eventually to a total error in the range $\sim 6 - 38\%$ corresponding to the minimum and maximum redshift in our sample ($z_{\rm min} = 0.0007$, $z_{\rm max} = 4.715$). Using the average redshift of our sample ($\bar{z} = 0.5$) the error is $\sim 11\%$. To account for other possible sources of uncertainty such as, for example, variability we will adopt a 20% total error on the optical luminosity as a conservative estimate.

The errors on the radio fluxes quoted in the literature are usually smaller than $\sim 5\%$ and only in few cases they are as large as $\sim 15\%$. However, the radio spectral index $\alpha_r = 0.5$ used for the extrapolation of fluxes to 5 GHz and for the K-correction can actually vary a lot among different kinds of AGN and among different radio source components (e.g. the core and the lobes). Assuming, like in the optical case, variations of $\Delta\alpha_{\rm r} = 0.5$ and a typical 5% error on the measured flux we obtain an uncertainty of $\sim 28\%$ on the extrapolated flux. However, the extrapolation to 5 GHz applies only for less than 1/4 of our sample. The contribution from the K-correction at $\bar{z} = 0.5$ yields 10% and 29% errors on the radio luminosity in the case where we use the direct flux measurement at 5 GHz with 5% error and in the case where we use the extrapolated flux with 28% error, respectively. As a conservative estimate we use a 30% total error on the radio luminosity for all sources.

The uncertainty on the X-ray flux, calculated through the energy-to-counts conversion factor, is dependent on variations of both the photon index $\Gamma_{\rm X}$ and the hydrogen column density $N_{\rm H}$. As discussed in §5.3 the corresponding errors on the estimated flux are of the order of 5 and 10%, respectively. Combining them leads to a $\sim 11\%$ error for the flux. Taking into account the K-correction term at $\bar{z} = 0.5$ with, as in §5.3, a possible range of photon indices of $\Gamma_{\rm X} \sim 1.5 - 2.3$ (Brinkmann et al. 1994, Brinkmann et al. 1995) the total error on the X-ray luminosity is $\sim 14\%$. Allowing for variability and further possible sources of uncertainty the total error will be taken as 20%.

5.5 Statistical tools

To address the problem of AGN unification we use a statistical approach. In this paragraph we describe the statistical methods applied in the analysis of our sample reported in the following chapters. These typically involve the estimate of mean luminosities and dispersions, two-sample tests for the hypothesis that two populations have the same distribution, correlation and regression analyses.

Statistical techniques can be divided in two large groups, parametric and non-parametric. Parametric methods assume that the data are drawn from a known distribution function (e.g. Gaussian or exponential). Non-parametric methods make no assumptions and derive the parent distribution function from the data themselves. They are frequently based on Maximum-Likelihood techniques and they can be used when the underlying distribution of a population of objects is *a priori* unknown.

A frequent problem in the analysis of astronomical data is the presence of upper limits or "left-censored data". Excluding these data points leads to significant loss of information and sometimes to misleading results. A branch of statistics, called *Survival Analysis*, has been developed at first by scientists working in biomedical and clinical research fields as well as in industrial reliability testing and econometrics and was later adapted for astronomical applications. Most of the survival analysis techniques for astronomical usage are implemented in the stand-alone package ASURV developed by Isobe T., LaValley M. & Feigelson E., available to the astronomical community without charge from StatCodes, the statistical website located at Penn State University (http://www.astro.psu.edu/statcodes/). Since the underlying distribution functions for the astronomical objects are usually unknown only the non-parametric methods are implemented in ASURV. In our statistical analysis we have made extensive use of ASURV rev. 1.2, which provides the methods presented in Feigelson & Nelson (1985) and Isobe, Feigelson & Nelson (1986) as discussed below.

In spite of the ability of ASURV to deal with upper limits, it does not take into account the errors in the analysis. However, the estimated errors on the luminosities for our sample are not negligible (see §5.4) and their inclusion might influence the results of the statistical methods used. Therefore, as a complementary approach, we have applied additional methods which cannot account for upper limits but include errors, a Maximum-Likelihood technique for the calculation of the means and the Fasano & Vio (1988) Orthogonal Distance Regression (ODR) analysis code (see §§ 5.5.1 and 5.5.4). In this case only the detections were considered. Conclusions are finally drawn from the comparison of the various methods.

5.5.1 Estimate of the mean and dispersion

The ASURV package provides routines to calculate the so called *Kaplan-Meier estimator*, a non-parametric Maximum-Likelihood estimate of the true distribution. Once known, an estimate of the mean and of its error can be calculated taking properly into account the upper limits (Feigelson & Nelson 1985), however, not the measurement errors. If no upper limits are present the results are consistent with the standard formula $\bar{x} = \sum x_i/n$ for the mean.
We also evaluate jointly the 90% confidence level contours of the best-fit values of the mean and intrinsic dispersion, i.e. deconvolved from the measurement errors, of the distributions through a Maximum-Likelihood technique (Avni 1976, Maccacaro et al. 1988, Worrall & Wilkes 1990), excluding objects with upper limits that cannot be treated with this method. In the following chapters both results from the Kaplan-Meier estimator and the Maximum-Likelihood technique will be shown for comparison.

5.5.2 Two-sample tests

The most often used standard procedure to test the hypothesis that two populations are drawn from the same distribution is Student's t-test. However, when the underlying distribution is not known it cannot be applied. When all data points are detections a Wilcoxon test (also called Mann-Whitney U-test) can instead be performed. This is the non-parametric equivalent of the t-test, however, it is not adequate to work in the presence of upper limits. The software in ASURV provides four different two-sample tests which are both non-parametric and can deal with censored data. These are the Gehan's test, either with permutation or hypergeometric variance, the *logrank* test, the Peto & Peto and the Peto & Prentice tests. Except for the logrank test, they are all generalizations of the Wilcoxon test. They differ in the way the censored data points are scored and in the formula for the variance. All of them consist of calculating a quantity called the *test statistic* L and a variance σ directly from the data. The ratio L/σ is, under the null hypothesis that the two samples belong to the same parent population, approximately normally distributed when the number of objects is large. The null hypothesis is rejected at the significance level α when $|L/\sigma| \geq z_{\alpha/2}$, where $z_{\alpha/2}$ is the value for which the area

under a standard Gaussian distribution in the interval $[-z_{\alpha/2}, z_{\alpha/2}]$ is $1-\alpha$.
These tests show different efficiencies in the determination of reliable significance levels depending on several factors, such as the censoring pattern and the relative size of the two samples, the shape of the true underlying distribution and the weights assigned to the censored data. However, all of them perform better than the parametric tests when the assumed model is incorrect. In general, in the absence of a well-defined criterium to choose a certain test, a frequently adopted procedure is to apply all tests and compare their results. If large discrepancies are observed there are reasons to believe that some of the requirements for the correct application of the test are not fulfilled and firm conclusions cannot be drawn from their results. In the following analysis we will adopt this procedure and, since good agreement is reached by all tests in all cases, we will show for simplicity only the results from the Peto & Prentice test, which has proven to be less vulnerable to small sizes and heavy and unequal censoring of the samples (Latta 1981). When no upper limits are present we will give results from the Gehan's test, to which the Peto & Prentice test reduces in the absence of censoring.

5.5.3 Correlation analysis

The purpose of correlation analysis is to determine the existence of a relationship between two variables. The standard non-parametric techniques involve the calculation of, for example, the Spearman's ρ or Kendall's τ correlation coefficients. Generalized versions of both for the case of censored data are implemented in ASURV (Feigelson & Nelson 1985). A frequent question in the analysis of correlations is whether they are induced by a common dependence on a third variable. This is typically the case for correlations between luminosities in different wavebands in flux-limited samples, which can originate from the common dependence on redshift. To deal with this problem partial correlation coefficients have been used and Akritas & Siebert (1996) developed a method to determine the partial Kendall's τ correlation coefficient in the presence of upper limits. In our study we will first calculate the generalized Kendall's τ correlation coefficient with ASURV and then the partial Kendall's τ correlation coefficient with the code of Akritas & Siebert (1996) to check if the correlation between the luminosities at two given frequencies is still significant after the exclusion of the effect of redshift.

5.5.4 Regression analysis

If a correlation is present, the regression analysis yields the parameters of the relation between the variables. ASURV provides three methods to perform a linear regression analysis. The EM (Expectation-Maximization) algorithm is a parametric method which calculates the regression coefficients assuming a normal distribution for the residuals. The Buckley & James (1979) method is similar to the previous one but makes use of the Kaplan-Meier distribution derived from the data and is, thus, non-parametric. The Schmitt (1985) regression method allows the use of upper limits for both the dependent and independent variables. An estimate of the significance level of the linear relationship can be found treating the quantity $z = b/[Var(b)]^{1/2}$ (where b is the slope of the regression line and $Var(b)$ its variance) as an approximately normal distributed variable, in the same way as for the two-sample tests (Isobe et al. 1986). In the following chapters we will present the results of the regression analysis with the non-parametric Buckley & James method when only one variable is affected by upper limits and the Schmitt regression when both variables are censored. The EM algorithm gave very similar results to the Buckley & James method in most cases, however, since we do not know *a priori* the true distribution of the residuals, the use of the second is conceptually more correct.

The drawback of all techniques above is that they do not take into account the errors on the variables. Since we estimated errors for the luminosities of the order of $20-30\%$ this might be a severe limitation. Another disadvantage is that the regression lines appear to change according to the choice of the independent and dependent variables, i.e. the slope of a regression line is not the inverse of the slope obtained exchanging the variables. In this case the bisector of the two fitted lines can be a better representation of the data (Feigelson & Babu 1992).

In order to include the errors we have also performed a linear regression using the code of Fasano & Vio (1988). It uses errors on both variables and carries out an Orthogonal Distance Regression (ODR), which minimizes the residuals perpendicular to the line. Furthermore, the regression line is not affected by the exchange of the variables. However, since it cannot distinguish between upper limits and detections, only the latter are used for the calculation of the regression parameters.

In what follows we will show the results from the Buckley-James or Schmitt regression, giving the parameters of the bisector of the two fitted lines obtained alternating the dependent and independent variable. We will also show the results from the Fasano & Vio technique and we will draw conclusions from the comparison of the two methods.

Chapter 6

The data: the FRI/FRII dichotomy

6.1 Introduction

In the unification scheme for radio-loud objects, the Fanaroff-Riley classification, based on radio morphology and 178 MHz flux density, plays a crucial role. In fact, the unification acts separately on two different populations of objects, those with FRI morphology (FRI galaxies and BL Lacs) at lower radio luminosities and those with FRII morphology (FRII galaxies and radio-loud quasars) at higher luminosities. The reason for this dichotomy is not understood and it is a key problem in the study of AGN unification. Nonetheless, several explanations have been proposed for it, falling into one of two categories, extrinsic or intrinsic.

Intrinsic explanations attribute the dichotomy to fundamental differences in the jets or in the engines of the two classes. Possible differences could be the jet composition, the black hole masses and spins, and details of the geometrical and physical properties of the accretion process (Celotti & Fabian 1993, Reynolds et al. 1996, Wilson & Colbert 1995, Meier 1999). The extrinsic explanations assume that the central engines of FRI and FRII sources are similar, possibly differing only in power, and that the type of radio source depends on the kind of interactions with the ambient medium. Therefore, weaker jets will be more easily disrupted and produce FRI morphologies, whereas more powerful jets will be able to dig through the surrounding matter for longer distances producing FRII morphologies (Bicknell 1995).

The strongest evidence for an extrinsic origin comes from observations of sources with mixed morphologies, i.e. of FRI and FRII type on opposite sides of the core (Gopal-Krishna & Wiita 2000). An extrinsic explanation, however, does not seem to be able to account for the basic difference between FRI/BL Lacs and FRII/radio-loud quasars, i.e. the absence of optical/UV lines in the first class of objects compared to the strong emission features observed in the second. Of course, both intrinsic and extrinsic effects might play a role in determining the appearance of a radio source.

Finally, Owen & Ledlow (1994) found that the break between FRI and FRII sources shifts to higher radio luminosities for higher optical magnitudes of the host galaxies, as if producing a powerful FRII radio source would become increasingly more difficult for larger galaxy masses.

Among our sample 177 sources are classified either as FRI or FRII (2 of them have an intermediate morphology, but will be included in the FRI group). The majority of them, 139 objects, have an absolute magnitude $M_{\rm V} > -23$ and we will refer to them as the FRI or FRII *galaxies*. The remaining 38 objects have $M_{\rm V} < -23$ and thus are formally defined as *quasars*. From the galaxies, 57 are FRI whereas 82 are FRII. Among the quasars, 26 have FRII morphology, whereas 12 belong to the FRI class. The latter are not really a new class of objects (so far no radio-loud quasars with FRI morphology are known). They are optically much brighter than typical FRI galaxies but they do not differ from them in other properties, like the radio and X-ray luminosities (see below for a discussion). The host galaxies of these objects are usually ellipticals with peculiar features, such as dust lanes or distorted morphologies due to interactions with a companion galaxy. Apart from their optical properties, they could be regarded as normal FRI galaxies. As an example, Centaurus A belongs to this group.
54 of the 139 galaxies are also known to reside in a cluster (36 FRI and 18 FRII).

In this chapter we present the analysis of the data for the FRI and FRII radio sources. We will discuss and compare their luminosity properties and the results from their regression and correlation analyses.

6.2 Luminosity distributions

It must be remarked that the shapes of the luminosity distributions for our sample might not be representative for the true distributions because they could be biased by various selection effects. For example, radio-quiet AGN are included in our database only if they are radio detected, so that, amongst the radio-quiet population, we are selecting the most nearby and prominent objects.
However, we can investigate the ranges of luminosities and calculate the mean and related scatter, and then compare the results for the different classes. The ranges of luminosities cover several orders of magnitude, therefore, to avoid that the statistical parameters are dominated by the largest values giving misleading results, we calculate the logarithmic means and dispersions.
Two methods are used to this purpose, described in §5.5. The first involves the calculation of the Kaplan-Meier estimator for the distribution of luminosities and it includes the upper limits. The second calculates the mean and intrinsic dispersion of the distribution together with the 90% confidence level contours through a Maximum Likelihood technique (Avni 1976, Maccacaro et al. 1988, Worrall & Wilkes 1990), with the underlying assumption that the points follow a Gaussian distribution around the mean. In this case, only the detections have been utilized and it is found that the two methods give results which are in very good agreement when no upper limits are present.

6.2.1 The X-ray luminosity distributions

In Table 6.1 we list the average values of the logarithm of the X-ray luminosity for different subclasses; in Fig. 6.1 we show the distribution of radio-loud/radio-quiet and FRI/FRII sources compared to the total sample. In Fig. 6.2 the 90% confidence level contour plots

of the mean luminosities and intrinsic dispersions for the FRI/FRII population are presented, distinguishing between quasars and galaxies and between cluster and non-cluster sources.
The X-ray luminosity distribution for the total sample is the sum of different contributions, stretching over ~ 8 orders of magnitude. There is significant overlap between the distributions of radio-quiet and radio-loud objects. However, radio-quiet objects extend to slightly lower luminosities than the radio-loud which, on the other hand, reach luminosities of the order of $L_{\rm X} \sim 10^{48}$ erg s^{-1}, about two orders of magnitude higher than the most X-ray luminous radio-quiet objects. A two-sample Peto-Prentice generalized Wilcoxon test (see Table 6.5 and the description of the test in §5.5) rejects the hypothesis that radio-quiet and radio-loud objects are drawn from the same X-ray luminosity distribution. Zamorani et al. (1981) found from a study of quasars observed by Einstein that the average luminosity of radio-loud AGN is about three times higher than that of radio-quiet objects, whereas in our sample the difference is only of ~ 1.5 times. This is not surprising since we are selecting only the most radio and X-ray luminous radio-quiet objects.
As can be seen in Fig. 6.1, FRI radio galaxies are on average less X-ray luminous than the FRII, but with some overlap. However, Fig. 6.2 shows that the 90% confidence contour plots of FRI and FRII galaxies, either in cluster or not, are well separated, implying a significant difference between the X-ray luminosities of these two classes. The FRI "quasars" do not differ significantly from the FRI galaxies in terms of their X-ray luminosities, whereas the hypothesis that FRII quasars belong to the same population as the FRII galaxies is rejected at 5% significance level by a two-sample test. It therefore seems that the atypical features of FRI "quasars" are limited to the optical band and do not extend to the soft X-rays. In the case of FRII quasars, on the other hand, the larger X-ray luminosities are in agreement with the scenario in which these sources are observed at smaller viewing angles with respect to the galaxies of same morphology and, therefore, their emission is beamed.
The intrinsic dispersion of FRI galaxies is rather large, with $\log \sigma \gtrsim 1$, whereas for the FRII galaxies it is lower ($\log \sigma \sim 0.9$), but still consistent inside the errors with that of the FRI sources.

A significant contribution to the X-ray luminosity of radio galaxies, especially of FRI class, could come from clusters. In order to investigate the effects of cluster emission on the X-ray luminosities we have cross-correlated our sample of radio galaxies with three cluster catalogs (Böhringer et al. 2000, Böhringer et al. 2004). For 26 sources we could find a measurement of the cluster X-ray luminosity in which they reside, ranging from $\sim 10^{42} - 10^{44}$ erg s^{-1}. With such values clusters might contribute significantly to the emission from the active nucleus in the radio galaxies. However, when we compare the luminosities of cluster and non-cluster FRI galaxies, a two-sample test does not reject the hypothesis that they are both drawn from the same parent distribution (see Table 6.5). For 4 sources we could use the fluxes found in the literature, from accurate spatial analyses (mostly from ROSAT-HRI data), which should exclude most of the cluster contribution. For most of the other sources the X-ray count rate has been obtained from pointed PSPC observations using a small extraction radius (~ 20 arcsec) and thus also likely avoiding a considerable contamination from cluster emission. Therefore, although the presence of a cluster certainly affects to a certain amount the X-ray luminosity of the FRI sources, we judge that the effect is not so strong as to significantly alter the results of the following

Average X-ray luminosities

Group (1)	$N_{\rm tot}$ (2)	$N_{\rm up}$ (3)	$\log L_{\rm X}^{\rm KM}$ (4)	$\log L_{\rm X}^{\rm ML\dagger}$ (5)
Total sample	2260	85	44.53 ± 0.03	44.57 ± 1.32
Radio-loud	1682	85	44.91 ± 0.03	44.97 ± 1.08
Radio-quiet	578	0	43.48 ± 0.05	43.47 ± 1.30
FRI galaxies (in cluster)	36	2	42.79 ± 0.21	42.88 ± 1.22
FRI galaxies (not in cluster)	21	2	42.43 ± 0.27	42.56 ± 1.14
FRI galaxies	57	4	42.66 ± 0.17	42.77 ± 1.20
FRII galaxies (in cluster)	18	6	43.73 ± 0.25	44.14 ± 0.85
FRII galaxies (not in cluster)	64	26	43.38 ± 0.19	44.02 ± 0.89
FRII galaxies	82	32	43.46 ± 0.16	44.05 ± 0.89
FRI quasars	12	0	42.29 ± 0.32	42.29 ± 1.06
FRII quasars	26	6	44.59 ± 0.26	45.01 ± 0.75

† Detections only.

Table 6.1: *Column 1: group of objects. Column 2: total number of objects. Column 3: number of upper limits. Column 4: mean of the* $0.1 - 2.4$ *keV luminosity in erg* s^{-1} *and related error from the generalized Kaplan-Meier estimator. Column 5: mean luminosity and intrinsic dispersion from the Maximum-Likelihood technique (see § 5.5.1).*

correlation analysis. Further proof for this comes from the strong correlation with the radio core emission, of certain non-thermal origin, found in § 6.3.3. The presence of such a correlation argues in favor of a mainly non-thermal origin also for the X-ray emission. The effect of cluster emission might be to increase the scatter of the X-ray luminosities, but the slopes of the correlations will be unaffected. Therefore, for the purposes of the subsequent analysis, we will not exclude cluster sources in order to be able to apply the regression techniques to a statistically more significant number of objects, which would be drastically reduced taking only non-cluster sources.
FRII galaxies are less affected by cluster emission even if a tendency, however not significant according to a two-sample test (see Table 6.5), for sources in cluster to be on average brighter can also be observed.

6.2.2 The optical luminosity distributions

In Table 6.2 we list the average optical luminosities for the various subclasses considered and in Fig. 6.3 and 6.4 we show the luminosity distributions and 90% confidence level contour plots of the mean luminosities and intrinsic dispersions, respectively.

The optical luminosity distribution of the whole sample extends over a wide range, from

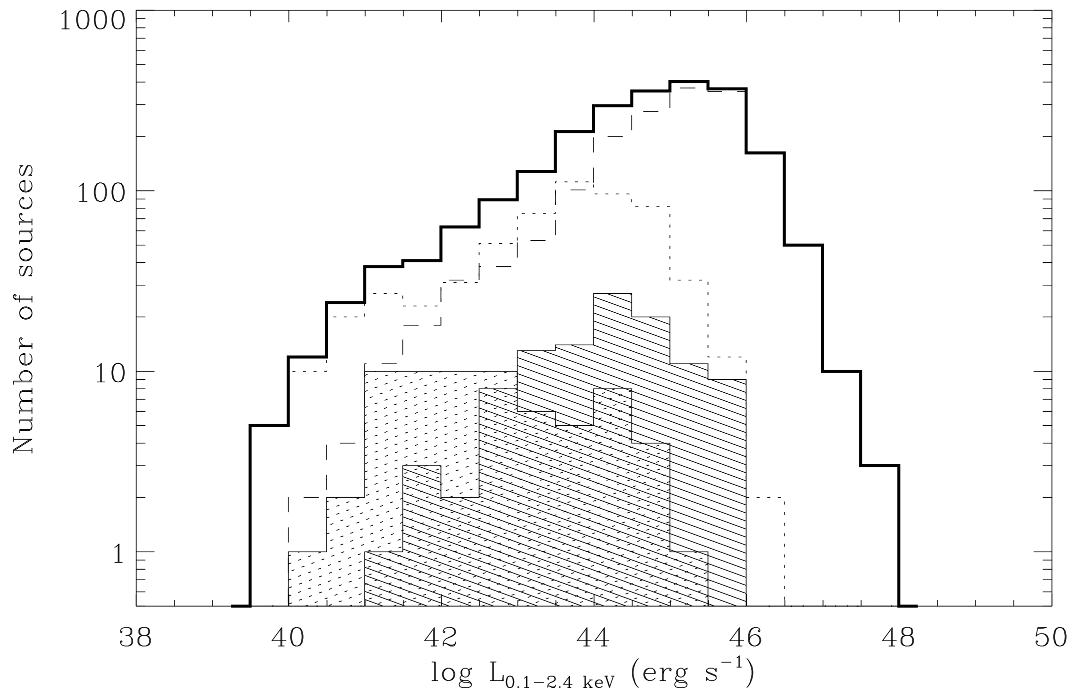

Figure 6.1: *X-ray luminosity distributions for the FRI (dotted area) and FRII (dashed area) radio sources, superposed on that for the total sample (thick line). The dotted and the dashed lines show the X-ray luminosity distributions of radio-quiet and radio-loud objects, respectively.*

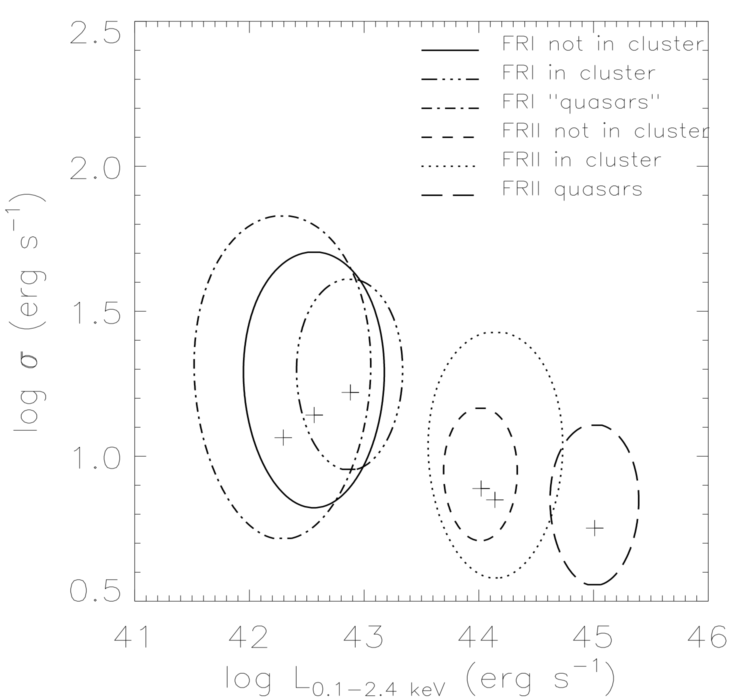

Figure 6.2: 90% *confidence level contour plots for the* $0.1 - 2.4$ *keV X-ray luminosity and intrinsic dispersion of FRI/FRII radio galaxies, in clusters and not in clusters, and for FRI/FRII quasars. The crosses indicate the average* $\log\ L_X$ *and* $\log\ \sigma$*.*

Average optical luminosities

Group (1)	$N_{\rm tot}$ (2)	$\log L_{\rm V}^{\rm KM}$ (3)	$\log L_{\rm V}^{\rm ML}$ (4)
Total sample	2260	30.09 ± 0.02	30.10 ± 0.85
Radio-loud	1682	30.26 ± 0.02	30.26 ± 0.85
Radio-quiet	578	29.61 ± 0.03	29.60 ± 0.69
FRI galaxies (in cluster)	36	29.47 ± 0.05	29.47 ± 0.30
FRI galaxies (not in cluster)	21	29.44 ± 0.05	29.44 ± 0.19
FRI galaxies	57	29.46 ± 0.04	29.48 ± 0.27
FRII galaxies (in cluster)	18	29.46 ± 0.08	29.46 ± 0.32
FRII galaxies (not in cluster)	64	29.41 ± 0.04	29.41 ± 0.32
FRII galaxies	82	29.42 ± 0.04	29.42 ± 0.29
FRI quasars	12	30.05 ± 0.05	30.05 ± 0.13
FRII quasars	26	30.54 ± 0.10	30.54 ± 0.48

Table 6.2: *Column 1: group of objects. Column 2: total number of objects. Column 3: mean of the V-band luminosity in erg s^{-1} Hz^{-1} and related error from the generalized Kaplan-Meier estimator. Column 4: mean luminosity and intrinsic dispersion from the Maximum-Likelihood technique (see § 5.5.1). All optical luminosities are detections.*

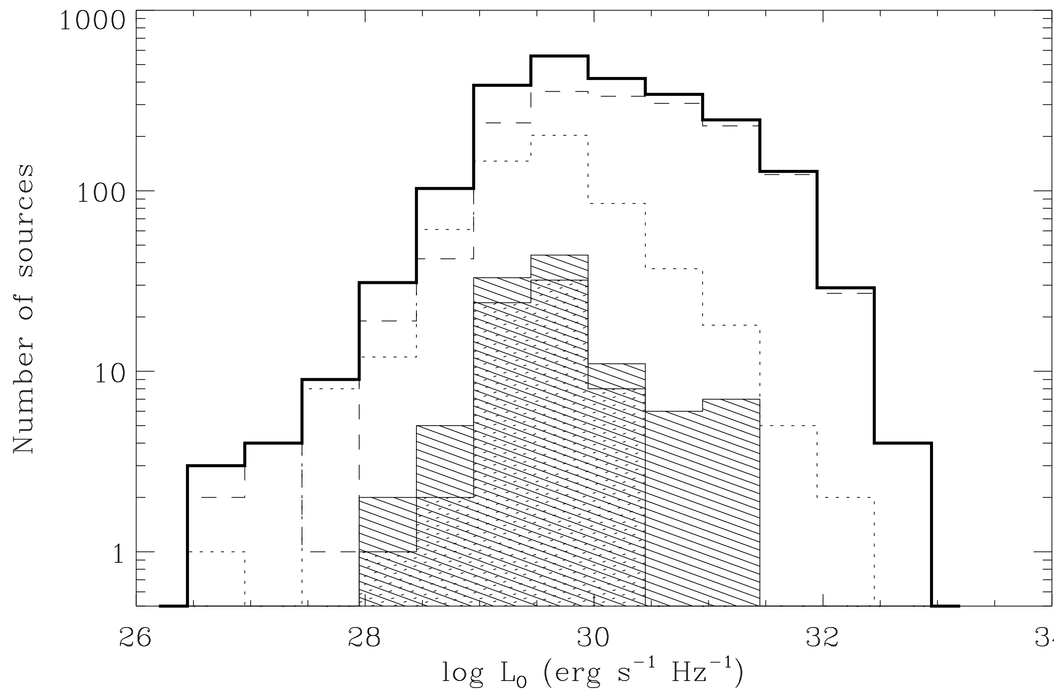

Figure 6.3: *Optical V-band luminosity distributions for the FRI (dotted area) and FRII (dashed area) radio galaxies, superposed on that for the total sample (thick line). The dotted and the dashed lines show the optical luminosity distributions of radio-quiet and radio-loud objects, respectively.*

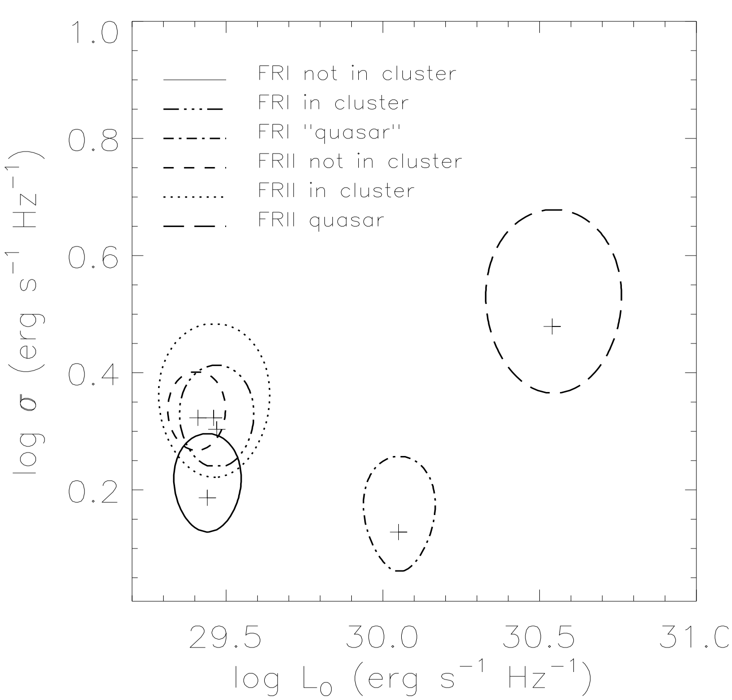

Figure 6.4: 90% *confidence level contour plots for the optical V-band luminosity and intrinsic dispersion for FRI/FRII radio galaxies, in clusters and not in clusters, and for FRI/FRII quasars. The crosses indicate the average* $\log\ L_O$ *and* $\log\ \sigma$.

$\sim 10^{27}$ to $\sim 10^{33}$ erg s^{-1} Hz^{-1}. Radio-quiet and radio-loud objects share a common range of values, except for the highest luminosity bin ($\sim 10^{33}$ erg s^{-1} Hz^{-1}), occupied only by radio-loud objects. Radio-quiet objects have a significantly lower mean optical luminosity than radio-loud objects, confirmed by a Peto-Prentice two-sample test.
Fig. 6.4 shows that, if we exclude the quasars, both the FRI and FRII galaxies cluster in the same relatively narrow range of luminosities and their intrinsic dispersions are small and very similar, with $\log\sigma = 0.27$ and $\log\sigma = 0.29$, respectively. A two-sample test excludes at 5% significance level that their average optical luminosities belong to different populations. No difference is found for cluster and non-cluster sources.
The quasars clearly exhibit larger optical luminosities, which is not surprising since they are defined to be brighter than $M_{\rm V} = -23$.
The optical luminosities of the FRI/FRII galaxies agree well with those of normal non-active ellipticals, whose optical magnitudes in the B band can range from about -15 to -23. In fact, the FRI/FRII galaxies in our sample cluster around $M_{\rm B} \sim -22$. The above results all suggest that in FRI and FRII galaxies we are probably observing the stellar emission from the host galaxies, whereas the optical emission from the active nucleus is either hidden (for example via obscuration), too weak to be resolved or the nucleus radiates anisotropically.
In the case of FRII quasars (as we have remarked above FRI quasars are all peculiar objects and do not constitute a separate class from the FRI galaxies) we are likely observing a beamed non-thermal optical component outshining the stellar emission.

6.2.3 The total radio luminosity distributions

Fig. 6.5 shows the total radio luminosity distributions for the various classes considered. The average luminosities and the 90% confidence level contour plots of the mean luminosities and intrinsic dispersions are presented in Table 6.3 and Fig. 6.6, respectively.

The radio luminosity distribution of the whole sample, extending over about ten orders of magnitude, appears to be the superposition of two distinct broad distributions, the radio-quiet and the radio-loud populations. The separation between the two is not clear-cut as there is a region of overlap around $\sim 10^{30} - 10^{31}$ erg s^{-1} Hz^{-1}. The hypothesis that the two classes belong to the same population can be rejected at the 5% significance level by a Peto-Prentice two-sample test.
The distributions for FRI and FRII galaxies are also well distinct, although they overlap between $\sim 10^{31} - 10^{33}$ erg s^{-1} Hz^{-1}. However, the original FRI/FRII classification is based on 178 GHz luminosities, whereas we use here a frequency of 5 GHz. Furthermore, subsequent studies (Owen & Ledlow 1994) revealed that the FRI/FRII separation actually also depends on the optical luminosity of the galaxy. This and the existence of intermediate or anomalous objects (like Hercules A, an FRI radio galaxies with radio power typical of an FRII) contributes to the blurriness of the FRI/FRII boundary.
The FRI/FRII dichotomy is more evident considering the mean luminosities of the objects. In Fig. 6.6 the sources nicely separate into two groups regardless of the quasar or galaxy classification.
The intrinsic dispersions of the total luminosities for both FRI and FRII sources are very similar and cluster around $\log\sigma \sim 1$.

Average total radio luminosities

Group (1)	$N_{\rm tot}$ (2)	$\log L^{\rm KM}_{\rm 5GHz,tot}$ (3)	$\log L^{\rm ML}_{\rm 5GHz,tot}$ (4)
Total sample	2260	32.23 ± 0.04	32.15 ± 1.94
Radio-loud	1682	33.08 ± 0.03	33.02 ± 1.38
Radio-quiet	578	29.73 ± 0.04	29.72 ± 0.92
FRI galaxies (in cluster)	36	31.59 ± 0.18	31.58 ± 0.84
FRI galaxies (not in cluster)	21	31.59 ± 0.19	31.58 ± 0.84
FRI galaxies	57	31.59 ± 0.13	31.58 ± 1.00
FRII galaxies (in cluster)	18	33.62 ± 0.24	33.64 ± 1.02
FRII galaxies (not in cluster)	64	33.50 ± 0.10	33.50 ± 0.80
FRII galaxies	82	33.53 ± 0.10	33.52 ± 0.85
FRI quasars	12	31.51 ± 0.28	31.50 ± 0.92
FRII quasars	26	33.86 ± 0.18	33.86 ± 0.90

Table 6.3: *Column 1: group of objects. Column 2: total number of objects. Column 3: mean of the 5 GHz total luminosity in erg s^{-1} Hz^{-1} and related error from the generalized Kaplan-Meier estimator. Column 4: mean luminosity and intrinsic dispersion from the Maximum-Likelihood technique (see § 5.5.1). No upper limits are present.*

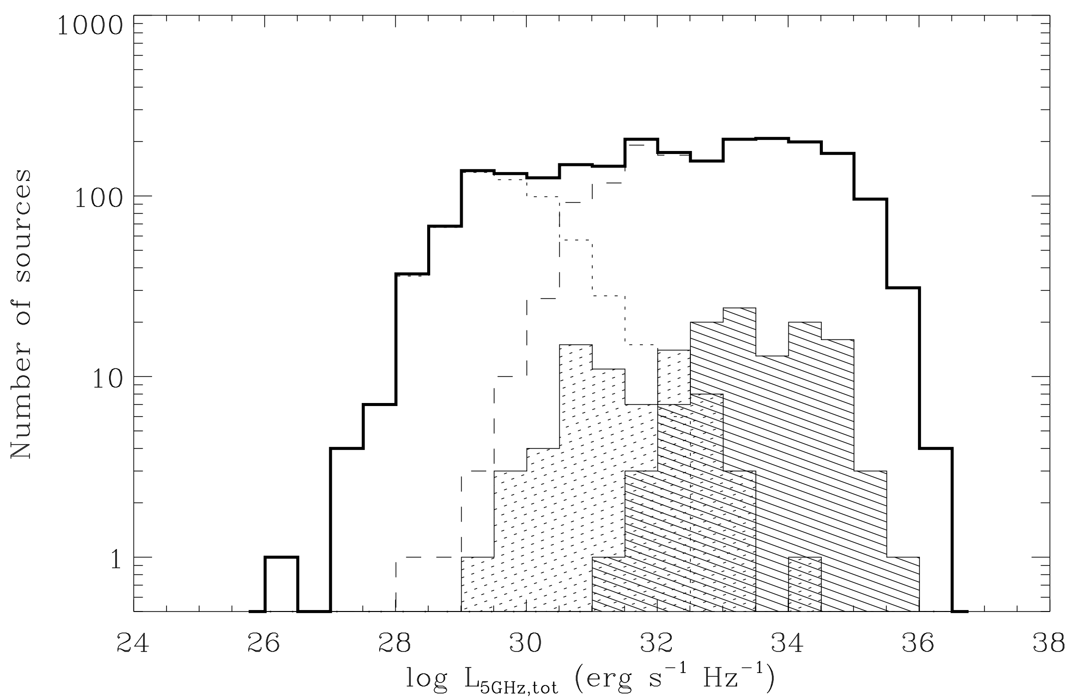

Figure 6.5: *Total* 5 *GHz radio luminosity distributions for the FRI (dotted area) and FRII (dashed area) radio galaxies, superposed on that for the total sample (thick line). The dotted and dashed lines show the total radio luminosity distributions of radio-quiet and radio-loud objects, respectively.*

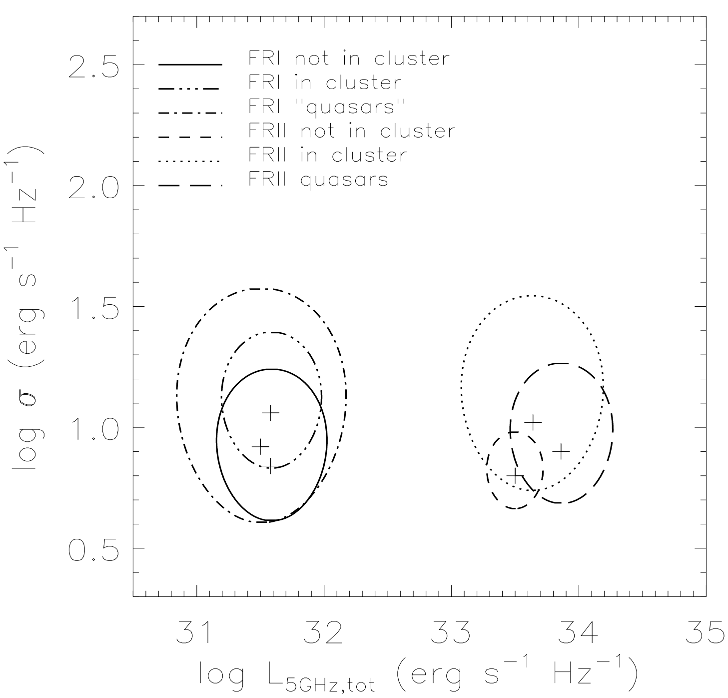

Figure 6.6: 90% *confidence level contour plots for the total* 5 *GHz luminosity and intrinsic dispersion for FRI/FRII radio galaxies, in clusters and not in clusters, and for FRI/FRII quasars. The crosses indicate the average* log $L_{\mathrm{R,tot}}$ *and* log σ*.*

Average core radio luminosities

Group (1)	$N_{\rm tot}$ (2)	$\log L^{\rm KM}_{\rm 5GHz,core}$ (3)	$\log L^{\rm ML}_{\rm 5GHz,core}$ (4)
Total sample	2260	32.30 ± 0.06	32.30 ± 1.62
Radio-loud	1682	32.47 ± 0.05	32.47 ± 1.47
Radio-quiet	578	29.39 ± 0.21	29.40 ± 1.42
FRI galaxies (in cluster)	36	30.46 ± 0.19	30.46 ± 1.02
FRI galaxies (not in cluster)	21	30.85 ± 0.26	30.84 ± 1.06
FRI galaxies	57	30.60 ± 0.16	30.60 ± 1.05
FRII galaxies (in cluster)	18	31.56 ± 0.26	31.56 ± 0.92
FRII galaxies (not in cluster)	64	31.36 ± 0.15	31.36 ± 0.88
FRII galaxies	82	31.42 ± 0.13	31.42 ± 0.90
FRI quasars	12	30.74 ± 0.31	30.74 ± 0.86
FRII quasars	26	32.39 ± 0.28	32.38 ± 1.22

Table 6.4: *Column 1: group of objects. Column 2: total number of objects. Column 3: mean of the 5 GHz core luminosity in erg* s^{-1} Hz^{-1} *and related error from the generalized Kaplan-Meier estimator. Column 4: mean luminosity and intrinsic dispersion from the Maximum-Likelihood technique (see § 5.5.1). No upper limits are present.*

6.2.4 The core radio luminosity distributions

The average core radio luminosities for different groups of objects are presented in Table 6.4, whereas Figs. 6.7 and 6.8 show their distributions and 90% confidence level contour plots, respectively.
Core fluxes are available for 789 sources ($\sim 35\%$) of our sample, of which 744 radio-loud and only 45 radio-quiet. Among the 177 sources with known Fanaroff-Riley morphology, 45 FRI and 49 FRII galaxies as well as 9 FRI and 10 FRII quasars have measured core fluxes.

The core radio luminosity distribution of the whole sample extends over the same range as the total radio luminosity distribution, with the radio-loud sources having significantly brighter cores by ~ 3 orders of magnitude.
Fig. 6.8 shows that FRI and FRII sources separate less sharply according to their radio morphology than in the case of the total radio luminosity (Fig 6.6). However, from a two-sample test, there seems to be a significant difference in the core luminosity distributions of FRI and FRII galaxies, with the FRII having brighter cores. This might suggest that the radio total luminosity which, for these sources, is basically produced by the extended lobes, is correlated with the core luminosity. This is indeed what is found in § 6.3.4.
The FRII quasars clearly display larger core luminosities than galaxies of the same radio morphology. Like in the optical and X-ray bands this can be interpreted in terms of smaller viewing angles and larger beaming factors for the quasars than for the FRII galaxies.

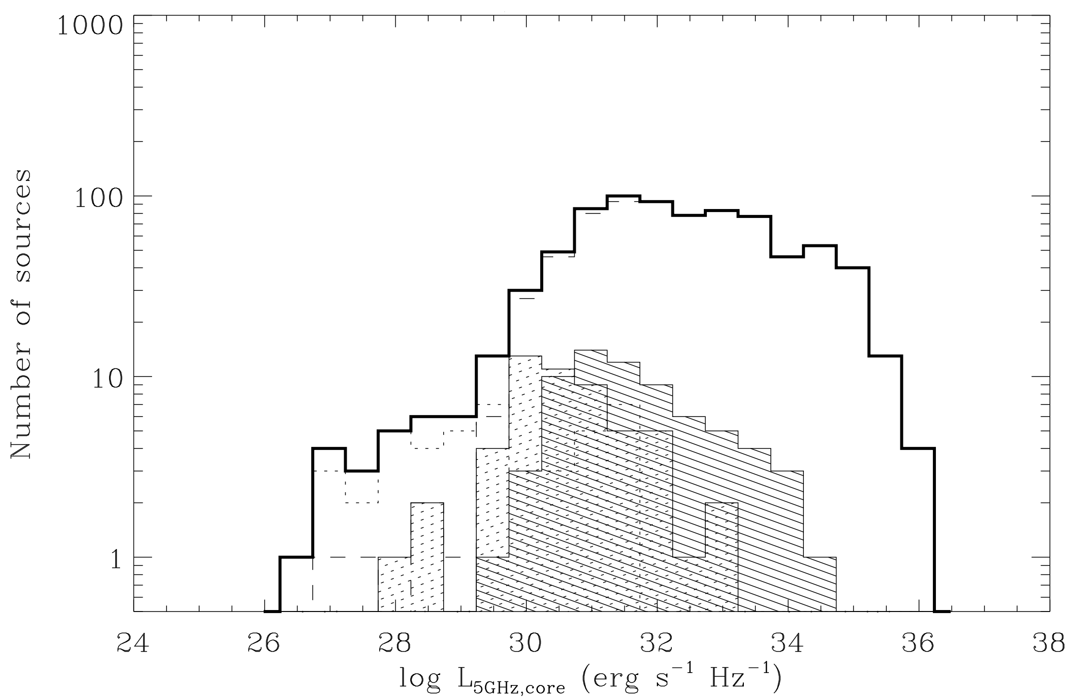

Figure 6.7: 5 *GHz core radio luminosity distributions for the FRI (dotted area) and FRII (dashed area) radio galaxies, superposed on that for the total sample (thick line). The dotted and dashed lines show the core radio luminosity distributions of radio-quiet and radio-loud objects, respectively.*

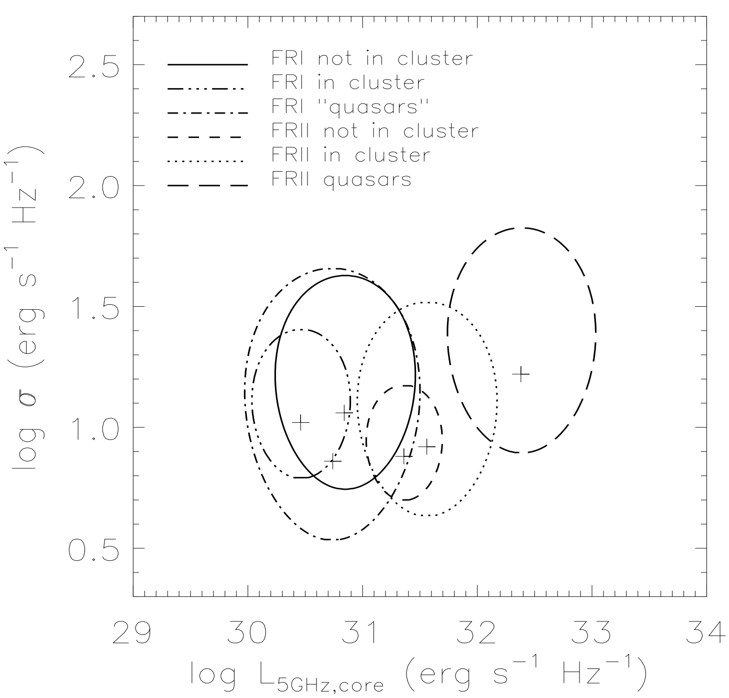

Figure 6.8: 90% *confidence level contour plots for the* 5 *GHz core luminosity and intrinsic dispersion for FRI/FRII radio galaxies, in clusters and not in clusters, and for FRI/FRII quasars. The crosses indicate the average* $\log L_{\mathrm{R,core}}$ *and* $\log \sigma$.

Two-sample tests

	$\log L_{0.1-2.4\ \mathrm{keV}}$		$\log L_{\mathrm{V}}$		$\log L_{5\mathrm{GHz,tot}}$		$\log L_{5\mathrm{GHz,core}}$	
Groups (1)	Stat. (2)	Prob. (3)	Stat. (4)	Prob. (5)	Stat. (6)	Prob. (7)	Stat.	Prob.
Radio-loud vs. radio-quiet	23.83	0.0	16.15	0.0	34.30	0.0	9.79	0.0
Cluster vs. non-cluster FRI	0.90	0.37	1.01	0.31	0.05	0.96	0.57	0.57
Cluster vs. non-cluster FRII	0.82	0.41	0.72	0.47	1.11	0.27	0.54	0.59
FRI galaxies vs. FRI quasars	0.99	0.32	5.21	0.0	0.45	0.65	0.19	0.85
FRII galaxies vs. FRII quasars	4.71	0.0	7.66	0.0	1.87	0.06	2.84	0.0
FRI vs. FRII (all sources)	3.40	0.0	0.53	0.60	8.55	0.0	3.72	0.0

Table 6.5: *Results of the Peto-Prentice generalized Wilcoxon tests. Column 1: the two samples tested. Columns 2 and 3, 4 and 5, 6 and 7, 8 and 9: the test statistics and the probability that the two samples belong to a common distribution (null hypothesis). For the optical and radio case we give results from a Gehan's Wilcoxon test (see §5.5.2).*

The FRI "quasars" do not show different core properties from those of the FRI galaxies, a further evidence that the active nucleus in these sources has not dissimilar properties than those in FRI galaxies and that their anomalous optical luminosities have to be attributed to peculiarities of the host galaxies.
As already noted for the optical, X-ray and total radio luminosities, cluster and non-cluster sources have average core luminosities consistent with each other.
As in the case of the total luminosities the intrinsic dispersions of both FRI and FRII sources are significantly large and close to $\log \sigma \sim 1$.

6.3 Correlation and regression analysis

Unified schemes of AGN predict the existence of correlations between the emission in different wavebands. The study of these correlations can provide information about the emission mechanisms, the connection between them and, eventually, on what are the beamed and parent populations of the AGN unified scheme. The existence of a good correlation between the X-ray and radio core luminosity is well established by previous works. From the analysis of Einstein data of a sample of 3CR radio galaxies Fabbiano et al. (1984) found tight correlations for both FRI and FRII galaxies, with slopes $b = 0.77 \pm 0.18$ and $b = 1.05 \pm 0.15$, respectively. The X-ray luminosity was also discovered to be correlated with the total radio emission, but through the dependence on the core luminosity. Fabbiano et al. (1984) also obtained weaker correlations between the optical and both the X-ray and radio core luminosities. Later on, Brinkmann et al. (1994) confirmed a tight

X-ray -to - radio core luminosity relationship for FRI and FRII radio galaxies together, with slope $b = 0.89 \pm 0.11$, whereas the X-ray - to - optical correlation ($b = 0.70 \pm 0.43$) was attributed to the presence of some outliers. Separating FRI and FRII galaxies, Siebert et al. (1996) found statistically significant correlations between the X-ray and radio core luminosities of slopes $b = 1.00 \pm 0.18$ and $b = 0.58 \pm 0.26$, respectively. However, no correlation could be determined with the optical luminosity. The weak relationship between the optical and radio core luminosities found by Fabbiano et al. (1984) could not be confirmed by subsequent works.

Figs. 6.9-6.15 show the correlations between luminosities at different frequencies for the objects in our sample. In the top panel of each figure the data for the FRI and FRII sources are superposed onto those for the total sample, to highlight the regions where they lie. In the bottom panels, only the FRI and FRII radio galaxies are plotted for clarity.
In the following we present the results from the correlation and regression analyses for the subsamples of FRI and FRII sources. In order to check if a correlation between two variables exists we calculate the Kendall's τ correlation coefficient. To determine if the correlations could be induced by the effect of a third variable (redshift) we calculate also the partial Kendall's τ correlation coefficient. We use generalized versions applicable to censored data for both methods (see §5.5).
For the regression analysis we present results from two techniques, described in § 5.5: the non-parametric Buckley-James and the Fasano & Vio regressions. When using the first method we will include the upper limits and we will show the parameters of the bisector of the two regression lines obtained by taking each variable as the independent or dependent one. For the second method we use only detections and errors on both variables.
The results from the correlation and regression analyses are given in Table 6.6 and 6.7, respectively.

6.3.1 The radio - to - optical luminosity correlations

The top panel of Fig. 6.9 shows the total radio versus the optical luminosity for the FRI and FRII sources superposed onto the total sample, whereas the bottom panel shows the FRI and FRII objects only. No clear trend is visible when taking together all sources. At a given optical luminosity, the radio galaxies (the objects to the left of the vertical line in the bottom panel of Fig. 6.9) can have a wide range of total radio power, with the FRII basically found above $L_{5\mathrm{GHz,tot}} \sim 10^{32}$ erg s^{-1} Hz^{-1} and the FRI below it. The boundary between FRI and FRII galaxies is not neat, as already remarked in § 6.2.3, resembling more a transitional region where both types of sources coexist.
A small subgroup is separated from the bulk of the FRII galaxies into the quasar region and, in this case, the radio emission appears to be correlated to the optical one with a rather steep slope of $b = 2.18 \pm 0.38$ (from the Fasano & Vio regression). This is confirmed by a Kendall's τ test at the 5% level and the effect of redshift does not alter the significance of the correlation (see Table 6.6).
The FRI "quasars" move from the FRI galaxies region towards quasar-like optical luminosities, however, with comparable radio luminosities as discussed previously.

Considering the core radio luminosity, there is some indication for a trend with op-

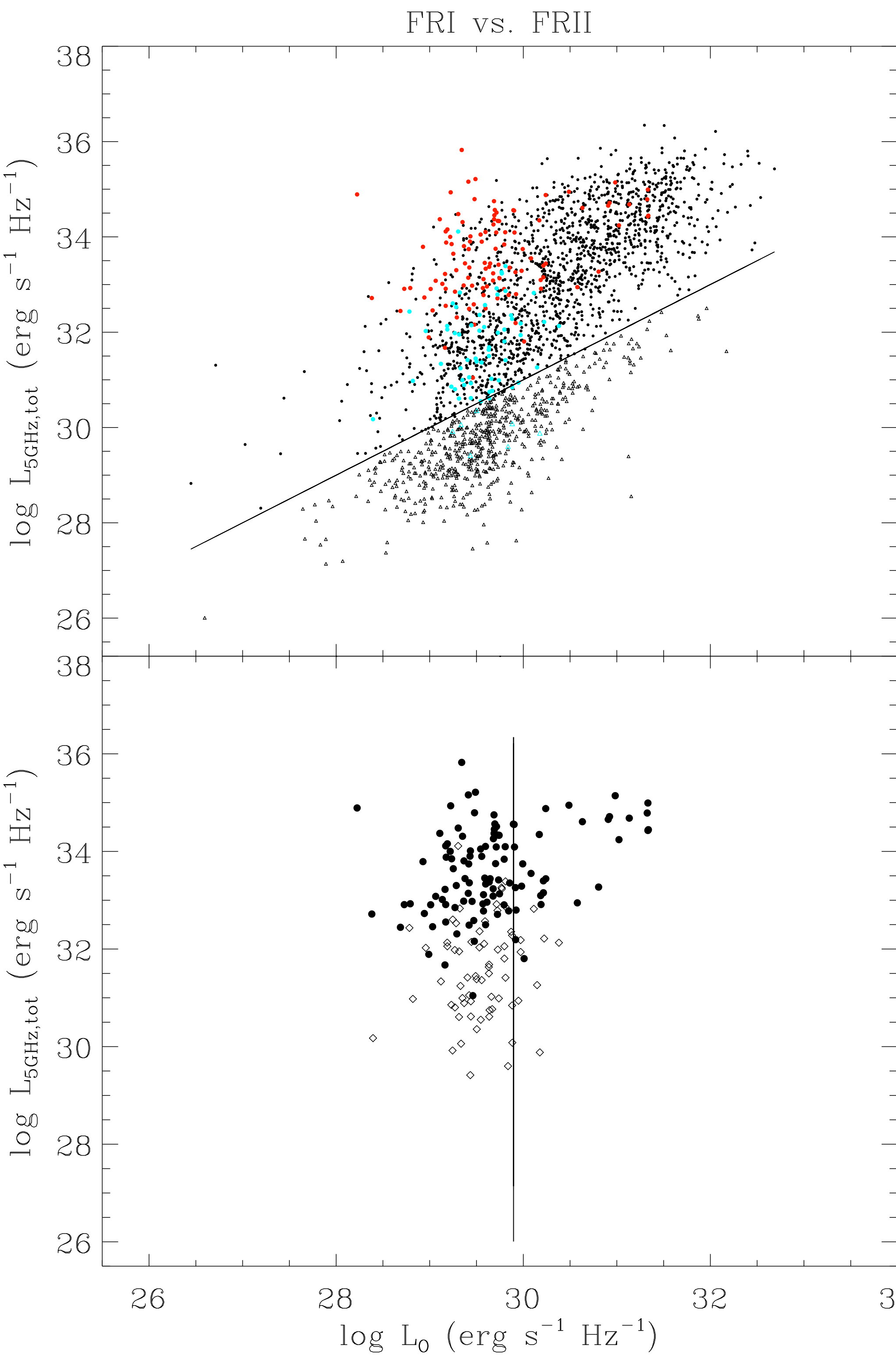

Figure 6.9: *Top panel: the* $L_{\rm R,tot}$*-*$L_{\rm O}$ *plane for the FRI (blue) and the FRII (red) galaxies superposed on the rest of the sample (black). The straight line is the formal division between radio-loud (circles) and radio-quiet (triangles) objects (see § 2.3). Bottom panel: the* $L_{\rm R,tot}$*-*$L_{\rm O}$ *plane for FRI (diamonds) and FRII (circles) galaxies only. Also shown is the line for which* $M_{\rm V} = -23$*, which conventionally separates galaxies from quasars.*

tical luminosity when all sources are taken together (see Fig 6.10). The presence of a correlation is confirmed by both a Kendall's τ and a partial Kendall's τ test for the FRII sources, quasars and galaxies, but not for the FRII galaxies alone. For the FRII quasars this correlation might be induced by the redshift dependence of both luminosities. No correlation is found for the FRI sources.
The absence of a correlation between the optical and radio luminosities in FRI and FRII galaxies is not surprising considering that the optical emission originates from the stars (see § 6.2.2), whereas the radio emission is connected with the AGN and therefore they are not intimately related. As we will see in Chapters 7 and 8, a tight correlation is observed between the optical and radio emission when core fluxes are taken in both wavebands.
We will see in Chapter 8 that a significant correlation is actually found for quasars, even allowing for redshift effects, when a much larger number of objects is analyzed.

6.3.2 The X-ray - to - optical luminosity correlations

Fig. 6.11 shows the X-ray versus optical luminosity for the FRI and FRII sources compared to the rest of the sample (top panel) and for FRI and FRII sources only (bottom panel). It appears that no common trend is present when all FRI/FRII sources are taken together, but a correlation might be present for the FRII quasars with a Fasano & Vio slope of $b = 1.86 \pm 0.33$. However, this is not significant at the 5% level if the redshift is included, probably due to the reduced number of objects used (see Chapter 8 for the analysis of a larger sample of quasars).
The narrow range in optical luminosities for the FRI and FRII galaxies is again evident. The FRII galaxies are mostly found at higher and the FRI at lower X-ray luminosities, however, the boundary between the two classes is even more ill-defined than in the case of the radio luminosities (§ 6.3.1), with several FRI galaxies lying within the FRII X-ray luminosity range. It is interesting to note, that these sources are the same that are found at the boundary between the FRI and FRII regions in the $L_{\rm R,tot}$-$L_{\rm O}$ plane (Fig. 6.9) and they might well represent transitional objects.

6.3.3 The X-ray - to - radio luminosity correlations

The X-ray versus total radio luminosity plane is shown in Fig. 6.12. This figure indicates that, unlike in the previous cases, a common trend exists for all sources. Separating the objects according to their radio morphology results in a significant correlation for the FRI sources, quasars plus galaxies, with a slope $b = 1.48 \pm 0.16$, whereas for the FRII sources it is likely induced by a common redshift dependence of $L_{\rm X}$ and $L_{\rm R,tot}$.
The correlation is confirmed for the FRI galaxies alone with a slope similar to that including also FRI "quasars", whereas no correlation is found for the FRII galaxies, perhaps due to the numerous X-ray upper limits. The FRII quasars appear to be correlated only through the effect of redshift. This is not what is usually obtained for radio-loud quasars (Zamorani et al. 1981, Worrall et al. 1987, Brinkmann et al. 1997), however, the best correlation is observed between the X-ray and the radio core luminosities and the number of objects considered here is small.

The bottom panel of Fig 6.13 shows a much clearer trend, similar for FRI and FRII sources, between the X-ray and core radio luminosities than when the total radio luminosity is used. For FRI and FRII galaxies alone the slopes of the observed correlations are

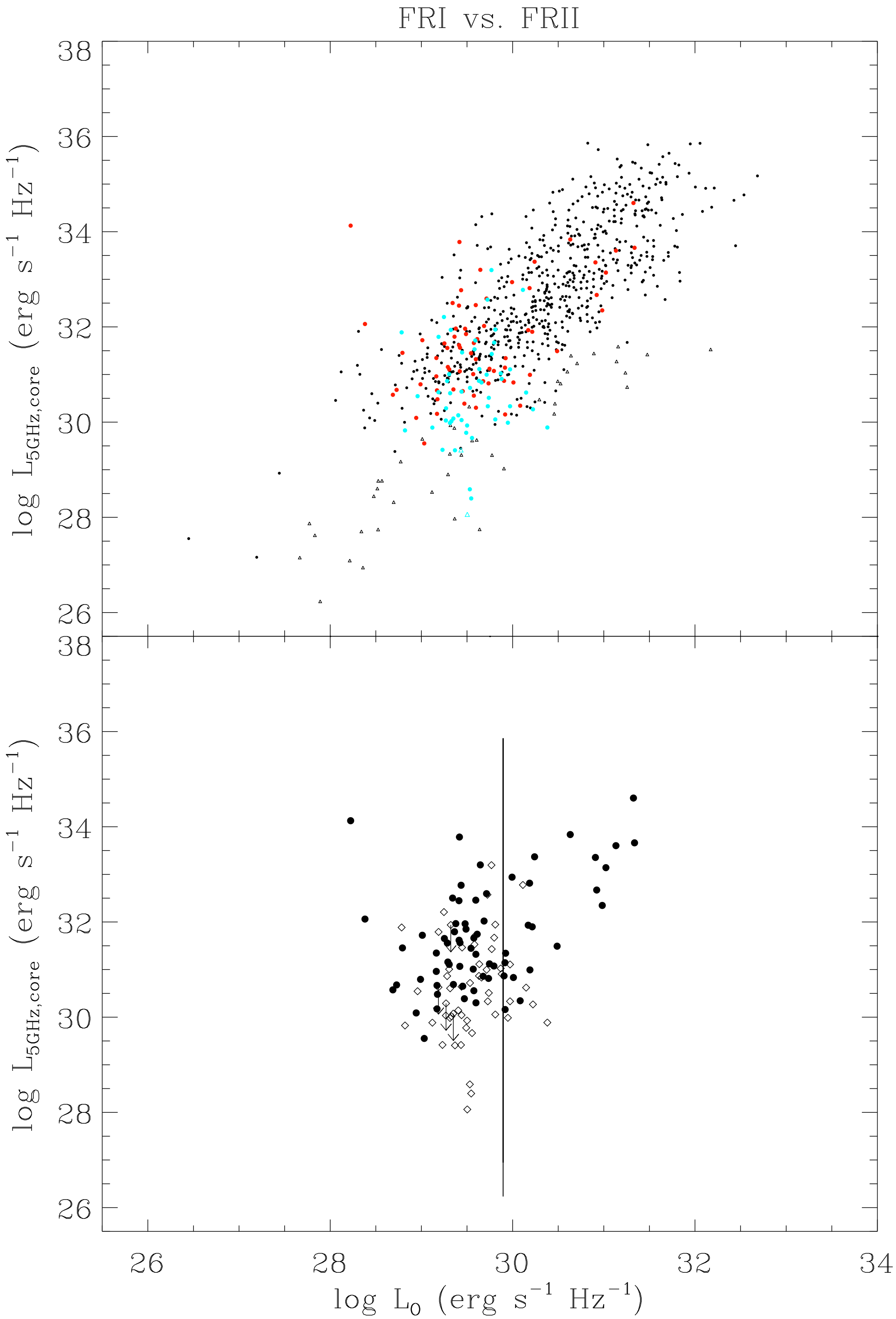

Figure 6.10: *Top panel: the $L_{\rm R,core}$-$L_{\rm O}$ plane for the FRI (blue) and the FRII (red) galaxies superposed on the rest of the sample (black). Bottom panel: the $L_{\rm R,core}$-$L_{\rm O}$ plane for FRI (diamonds) and FRII (circles) galaxies only. Also shown is the line for which $M_{\rm V} = -23$, which conventionally separates galaxies from quasars.*

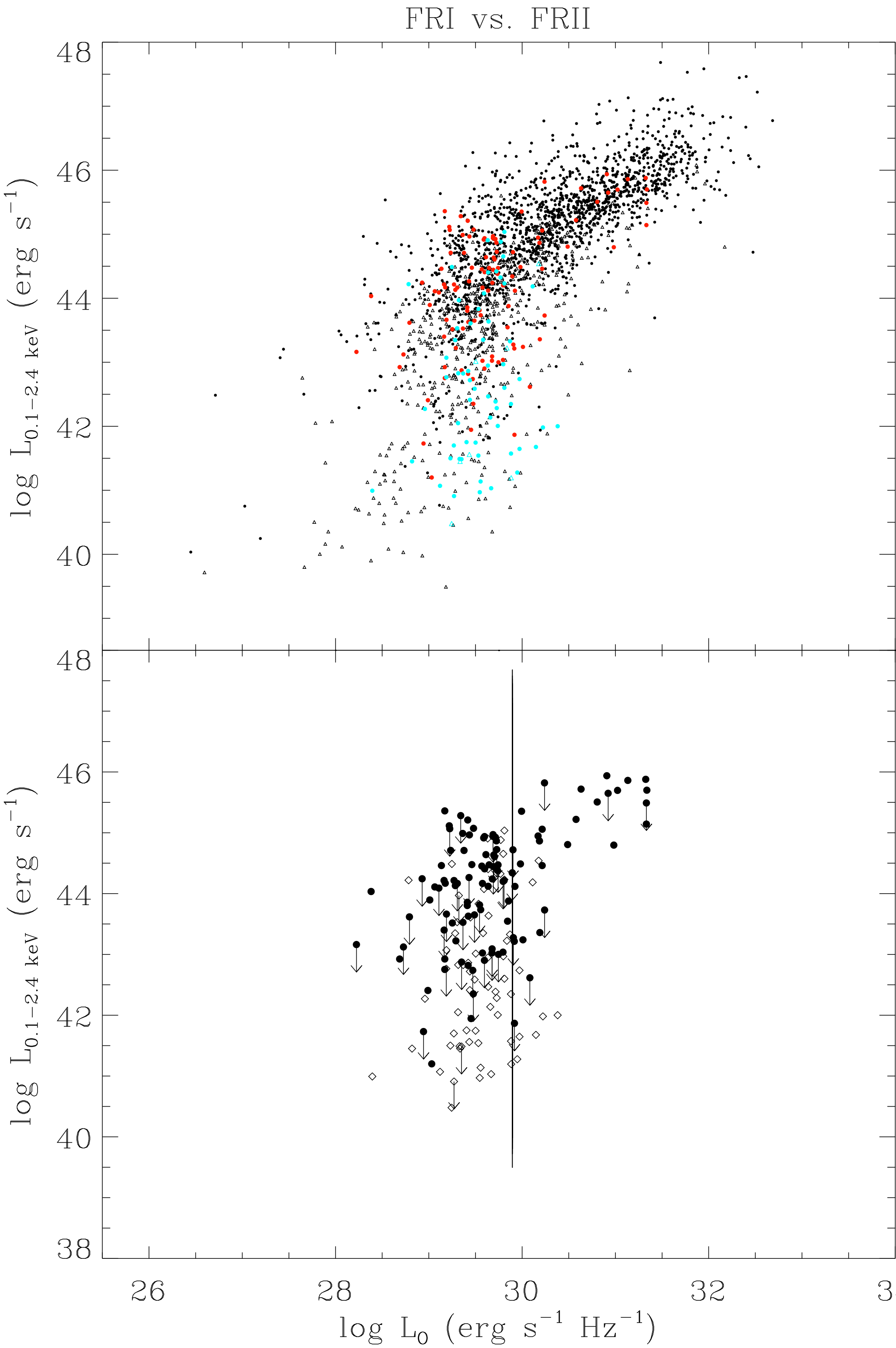

Figure 6.11: *Top panel: the L_X-L_O plane for the FRI (blue) and the FRII (red) galaxies superposed on the total sample (black). Radio-loud objects are shown as circles and radio-quiet as triangles. Bottom panel: the L_X-L_O plane for the FRI (diamonds) and FRII (circles) galaxies only. Also shown here is the line for which $M_V = -23$, which conventionally separates galaxies from quasars, and the upper limits on the X-ray luminosities*

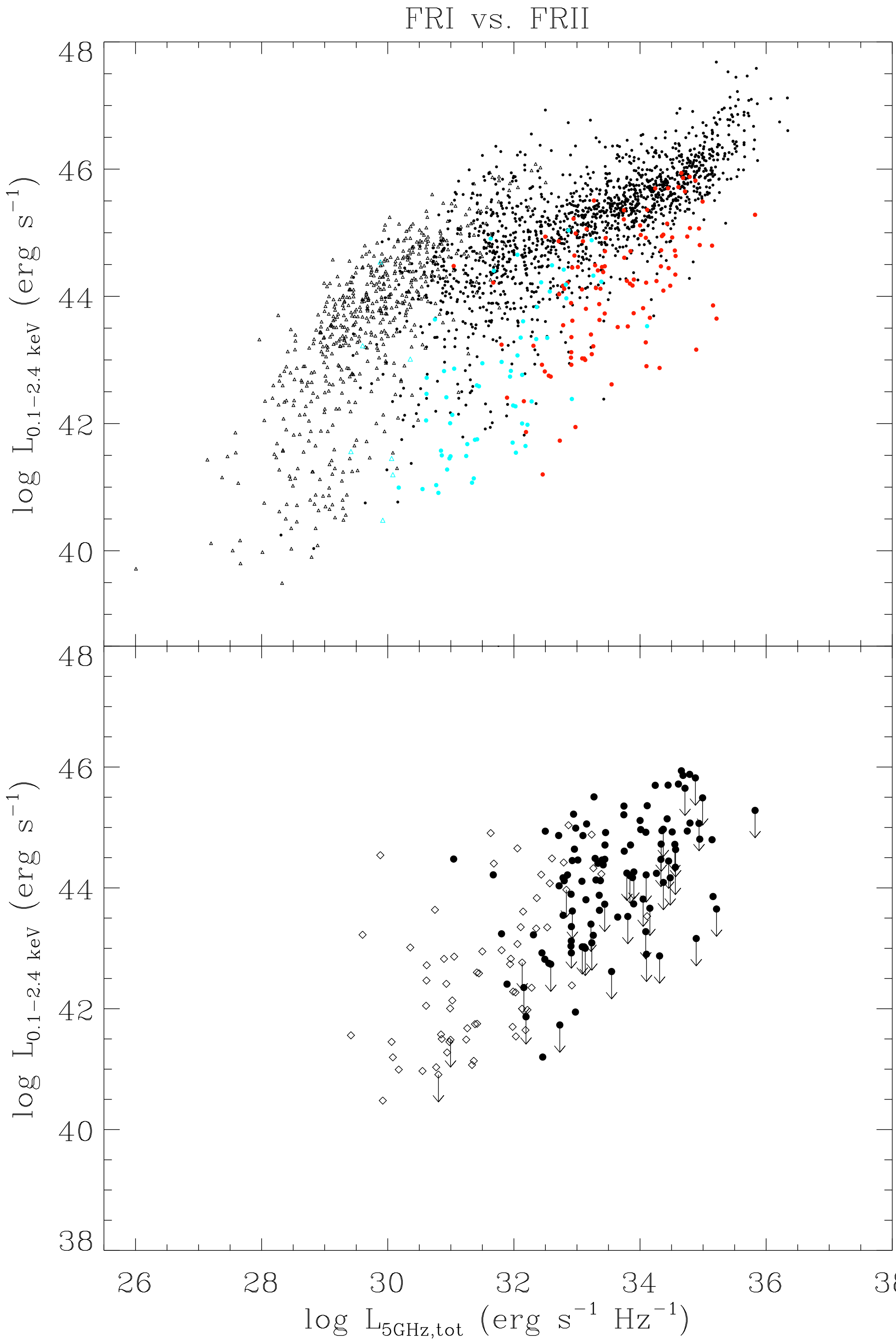

Figure 6.12: *Top panel: the* L_X-$L_{R,tot}$ *plane for the FRI (blue) and the FRII (red) galaxies superposed on the total sample (black). Radio-loud objects are shown as circles and radio-quiet as triangles. Bottom panel: the* L_X-$L_{R,tot}$ *plane for the FRI (diamonds) and FRII (circles) galaxies only. Also shown here are the upper limits on the X-ray luminosities (arrows).*

consistent with each other ($b = 1.16 \pm 0.13$ and $b = 1.23 \pm 0.15$, respectively), whereas for the FRII quasars the slope of the regression line is flatter ($b = 0.78 \pm 0.09$). All correlations are significant according to the Kendall's τ test, also after taking into account possible redshift effects. A better determination of this correlation for the FRII quasars is given in Chapter 8.

6.3.4 The radio - to - radio luminosity correlations

The total versus core radio luminosities are plotted in Fig. 6.14. The top panel shows the FRI/FRII sources and the rest of the objects in the sample with an available core flux measurement. Many sources are distributed along a straight line of approximately a slope of unity. These are mostly flat-spectrum quasars and BL Lacs, i.e. core-dominated sources, for which the total flux almost coincides with the strongly beamed core flux. The FRI/FRII sources are lobe-dominated objects and, in fact, are found at larger total luminosities with respect to this line. In the bottom panel of Fig. 6.14 only the FRI/FRII sources are plotted.

We have subtracted the core radio luminosity from the total one and used this as a measure of the extended luminosity. Fig. 6.15 shows the dependence of $L_{\mathrm{R,ext}}$ on $L_{\mathrm{R,core}}$. The difference in extended luminosity between FRI and FRII sources is evident. The galaxies of both classes are found to follow linear correlations with similar slopes inside the errors ($b = 0.86 \pm 0.11$ and $b = 0.98 \pm 0.13$, respectively). However, the correlation for FRII sources is only marginally significant when the redshift is included in the analysis. No correlation is found for the FRII quasars, probably smeared by relativistic beaming which is likely relevant in these sources.

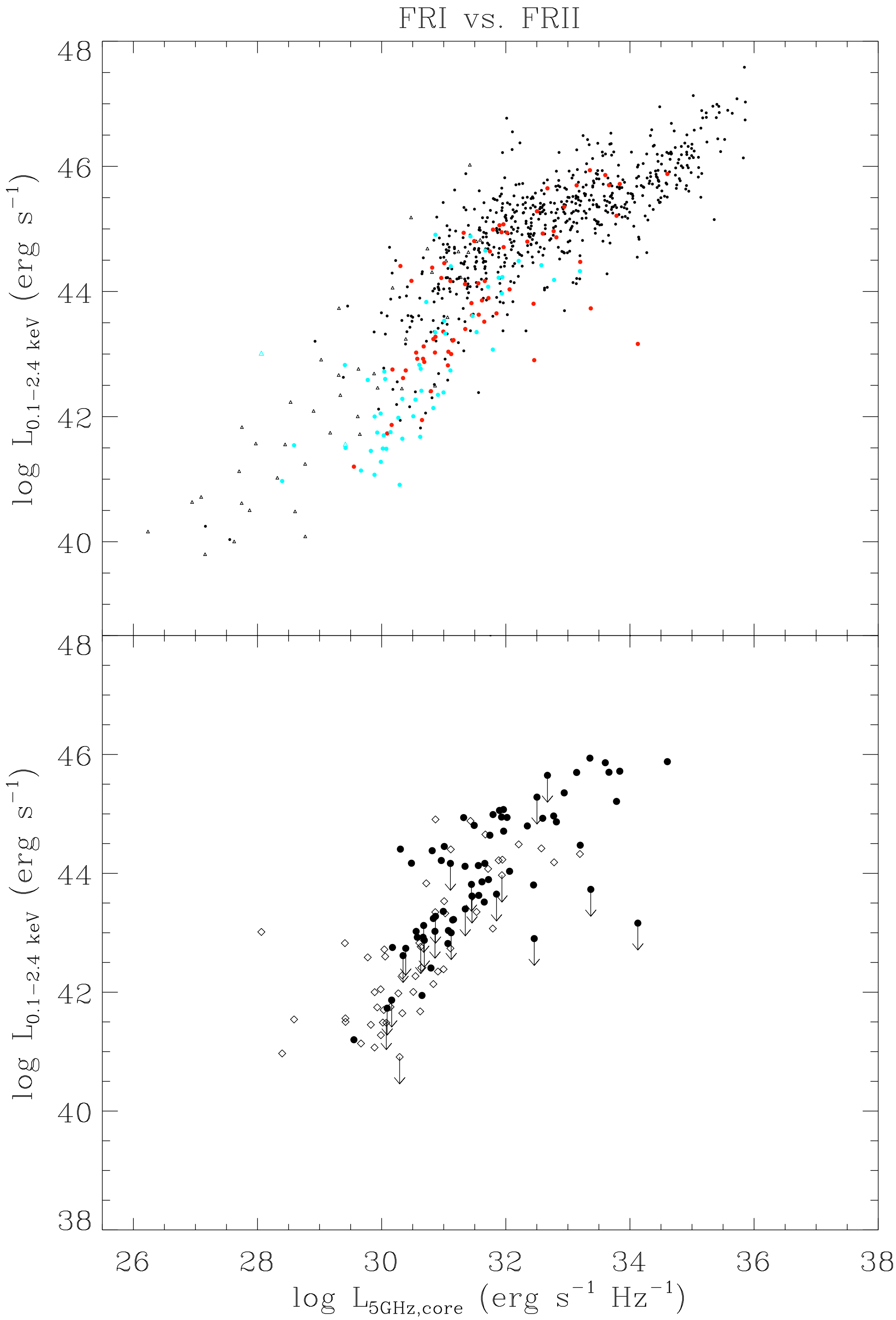

Figure 6.13: *Top panel: the L_X-$L_{R,core}$ plane for the FRI (blue) and the FRII (red) galaxies superposed on the total sample (black). Radio-loud objects are shown as circles and radio-quiet as triangles. Bottom panel: the L_X-$L_{R,core}$ plane for the FRI (diamonds) and FRII (circles) galaxies only. Also shown here are the upper limits on the X-ray luminosities (arrows).*

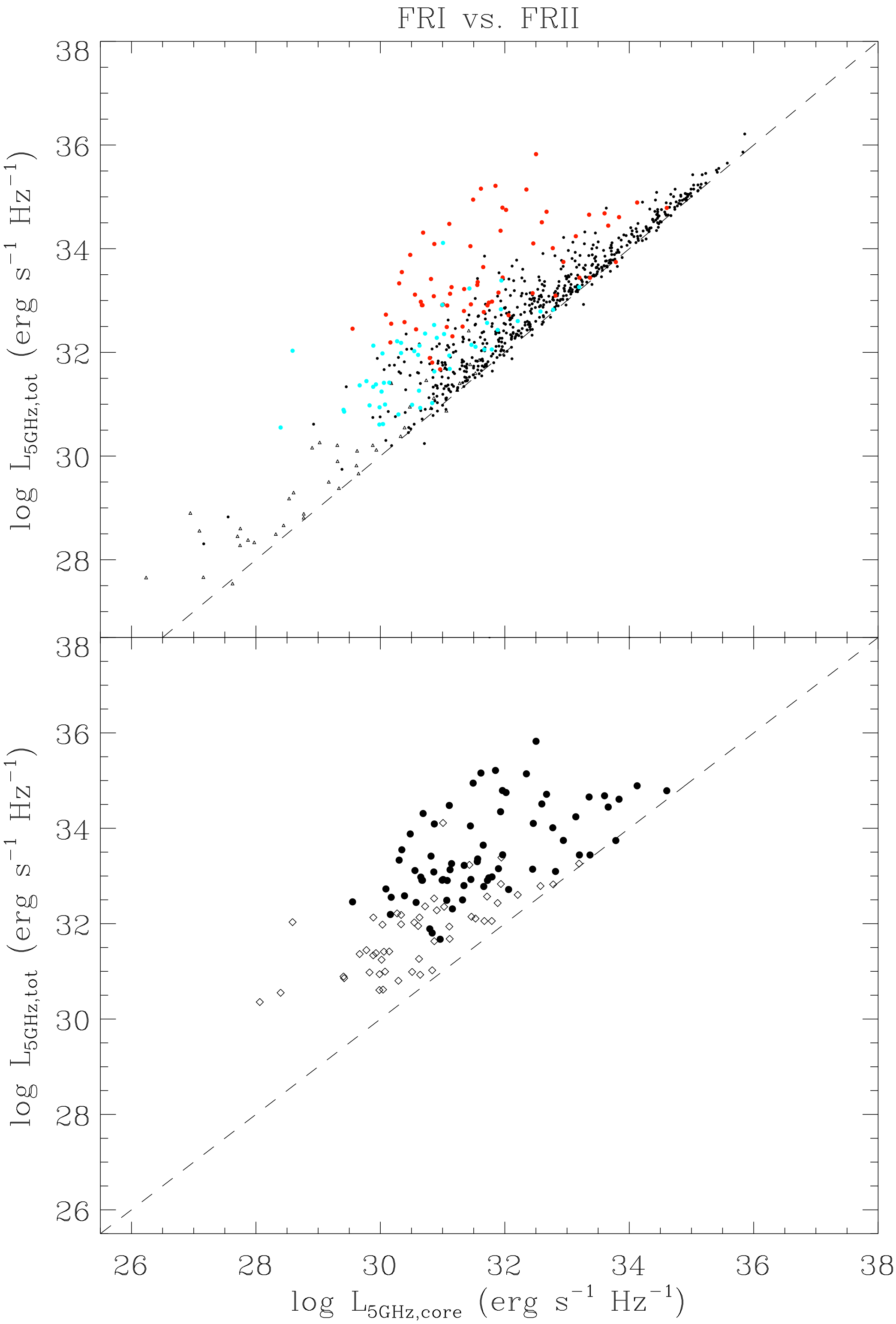

Figure 6.14: *Top panel: the* $L_{R,tot}$-$L_{R,core}$ *plane for the FRI (blue) and the FRII (red) galaxies superposed on the total sample (black). Radio-loud objects are shown as circles and radio-quiet as triangles. Bottom panel: the* $L_{R,tot}$-$L_{R,core}$ *plane for the FRI (diamonds) and FRII (circles) galaxies only. In both panels the line for which* $L_{R,tot} = L_{R,core}$ *is drawn.*

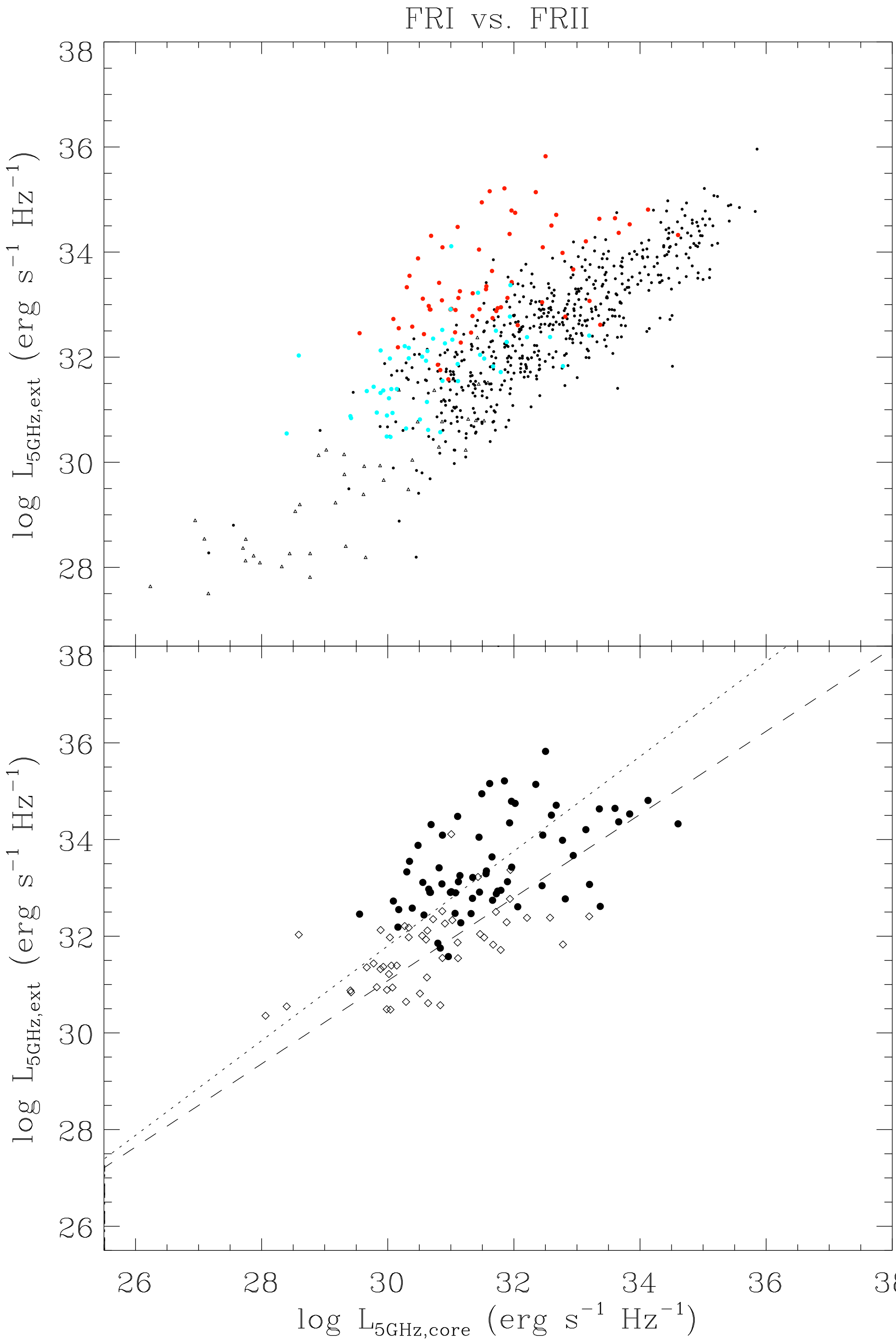

Figure 6.15: *Top panel: the $L_{R,ext}$-$L_{R,core}$ plane for the FRI (blue) and the FRII (red) galaxies superposed on the total sample (black). Radio-loud objects are shown as circles and radio-quiet as triangles. Bottom panel: the $L_{R,ext}$-$L_{R,core}$ plane for the FRI (diamonds) and FRII (circles) galaxies only. The regression lines for FRI (dashed) and FRII (dotted) galaxies are also plotted.*

Correlation analysis

Correlation	Groups	Kendall's τ		Partial Kendall's τ	
		Stat.	Prob.	Stat.	Prob.
(1)	(2)	(3)	(4)	(5)	(6)
Radio (total)/optical	FRI galaxies	1.75	0.08	1.80	0.06
	FRII galaxies	2.37	0.02	1.06	0.28
	FRII QSO	3.51	0.0	2.53	0.01
Radio (core)/optical	FRI galaxies	1.51	0.13	1.70	0.08
	FRII galaxies	0.90	0.37	0.34	0.74
	FRII QSO	3.32	0.0	2.02	0.04
X-ray/optical	FRI galaxies	3.57	0.0	4.43	0.0
	FRII galaxies	0.93	0.35	0.69	0.48
	FRII QSO	3.22	0.0	1.83	0.07
X-ray/radio (total)	FRI galaxies	5.10	0.0	3.98	0.0
	FRI galaxies+QSO	4.80	0.0	2.98	0.0
	FRII galaxies	1.20	0.23	1.14	0.26
	FRII QSO	2.41	0.02	0.01	0.98
X-ray/radio (core)	FRI galaxies	5.32	0.0	4.54	0.0
	FRI galaxies+QSO	5.84	0.0	4.80	0.0
	FRII galaxies	3.99	0.0	3.83	0.0
	FRII QSO	4.08	0.0	3.18	0.0
Radio (total)/radio (core)	FRI galaxies	5.85	0.0	5.40	0.0
	FRI galaxies+QSO	6.10	0.0	4.94	0.0
	FRII galaxies	3.64	0.0	2.59	0.01
	FRII QSO	2.48	0.01	1.08	0.28
Radio (extended)/radio (core)	FRI galaxies	4.93	0.0	4.31	0.0
	FRI galaxies+QSO	4.97	0.0	3.83	0.0
	FRII galaxies	3.27	0.0	1.76	0.08
	FRII QSO	1.64	0.10	0.37	0.70

Table 6.6: *Column 1: type of correlation. Column 2: groups of objects. Columns 3 and 4, 5 and 6: test statistics and relative probability that a correlation is not present for the generalized Kendall's τ and generalized partial Kendall's τ test, respectively. The hypothesis of zero correlation coefficient is rejected at 5% significance level if the probability does not exceed 0.05.*

Table 6.7: **Regression analysis**

Correlation (1)	Group (2)	Buckley-James (3)	Fasano & Vio (4)
$\log L_{\rm R,tot} - \log L_{\rm O}$	FRII galaxies	$a = -10.36$ $b = 1.50 \pm 0.37$ $\sigma = 0.921$	$a = -129.2 \pm 22.88$ $b = 5.52 \pm 0.78$ $\sigma_{\rm int} = 2.44 \pm 0.62$ Weighted rms= 1.610
	FRII QSO	$a = -21.11$ $b = 1.80 \pm 0.26$ $\sigma = 0.774$	$a = -32.95 \pm 11.60$ $b = 2.18 \pm 0.38$ $\sigma_{\rm int} = 0.62 \pm 0.15$ Weighted rms= 0.782
$\log L_{\rm R,core} - \log L_{\rm O}$	FRII QSO	$a = -42.72$ $b = 2.46 \pm 0.38$ $\sigma = 0.956$	$a = -62.09 \pm 15.72$ $b = 3.10 \pm 0.51$ $\sigma_{\rm int} = 1.09 \pm 0.32$ Weighted rms= 1.027
$\log L_{\rm X} - \log L_{\rm O}$	FRI galaxies	$a = -57.24$ $b = 3.26 \pm 0.70$ $\sigma = 1.152$	$a = -202.1 \pm 32.11$ $b = 8.31 \pm 1.09$ $\sigma_{\rm int} = 4.73 \pm 1.48$ Weighted rms= 2.253
	FRII QSO	$a = -10.43$ $b = 1.81 \pm 0.28$ $\sigma = 0.713$	$a = -119.4 \pm 10.03$ $b = 1.86 \pm 0.33$ $\sigma_{\rm int} = 0.47 \pm 0.14$ Weighted rms= 0.677
$\log L_{\rm X} - \log L_{\rm R,tot}$	FRI galaxies	$a = 5.95$ $b = 1.16 \pm 0.12$ $\sigma = 1.228$	$a = -1.48 \pm 5.04$ $b = 1.40 \pm 0.16$ $\sigma_{\rm int} = 1.29 \pm 0.30$ Weighted rms= 1.133
	FRI galaxies+QSO	$a = 6.158$ $b = 1.15 \pm 0.13$ $\sigma = 1.314$	$a = -4.05 \pm 5.24$ $b = 1.48 \pm 0.16$ $\sigma_{\rm int} = 1.65 \pm 0.40$ Weighted rms= 1.284
	FRII QSO	$a = 13.21$ $b = 0.93 \pm 0.15$ $\sigma = 0.900$	$a = 13.69 \pm 5.65$ $b = 0.92 \pm 0.17$ $\sigma_{\rm int} = 0.41 \pm 0.14$ Weighted rms= 0.627
$\log L_{\rm X} - \log L_{\rm R,core}$	FRI galaxies	$a = 10.25$ $b = 1.06 \pm 0.10$ $\sigma = 1.082$	$a = 7.27 \pm 3.90$ $b = 1.16 \pm 0.13$ $\sigma_{\rm int} = 0.75 \pm 0.26$ Weighted rms= 0.864
	FRI galaxies+QSO	$a = 9.66$ $b = 1.08 \pm 0.09$ $\sigma = 1.054$	$a = 5.16 \pm 3.62$ $b = 1.23 \pm 0.12$ $\sigma_{\rm int} = 0.75 \pm 0.24$ Weighted rms= 0.873

Table 6.7: *Continued on next page.*

Table 6.7: *(continued)*

Correlation (1)	Group (2)	Buckley-James (3)	Fasano & Vio (4)
	FRII galaxies	$a = 13.58$ $b = 0.96 \pm 0.11$ $\sigma = 0.984$	$a = 5.24 \pm 4.68$ $b = 1.23 \pm 0.15$ $\sigma_{\rm int} = 0.61 \pm 0.15$ Weighted rms= 0.781
	FRII QSO	$a = 15.74$ $b = 0.89 \pm 0.08$ $\sigma = 0.700$	$a = 19.70 \pm 3.12$ $b = 0.78 \pm 0.09$ $\sigma_{\rm int} = 0.15 \pm 0.05$ Weighted rms= 0.380
$\log L_{\rm R,tot} - \log L_{\rm R,core}$	FRI galaxies	$a = 6.70$ $b = 0.82 \pm 0.08$ $\sigma = 0.953$	$a = 5.80 \pm 2.83$ $b = 0.85 \pm 0.09$ $\sigma_{\rm int} = 0.41 \pm 0.12$ Weighted rms= 0.648
	FRI galaxies+QSO	$a = 7.11$ $b = 0.81 \pm 0.07$ $\sigma = 0.932$	$a = 6.33 \pm 2.58$ $b = 0.83 \pm 0.08$ $\sigma_{\rm int} = 0.38 \pm 0.10$ Weighted rms= 0.629
	FRII galaxies	$a = 2.63$ $b = 0.98 \pm 0.14$ $\sigma = 1.117$	$a = -2.64 \pm 4.90$ $b = 1.15 \pm 0.16$ $\sigma_{\rm int} = 0.95 \pm 0.17$ Weighted rms= 0.975
	FRII QSO	$a = 8.18$ $b = 0.79 \pm 0.15$ $\sigma = 1.261$	$a = 7.27 \pm 2.58$ $b = 0.82 \pm 0.16$ $\sigma_{\rm int} = 0.75 \pm 0.23$ Weighted rms= 0.834
$\log L_{\rm R,ext} - \log L_{\rm R,core}$	FRI galaxies	$a = 6.47$ $b = 0.83 \pm 0.09$ $\sigma = 1.081$	$a = 5.28 \pm 3.33$ $b = 0.86 \pm 0.11$ $\sigma_{\rm int} = 0.58 \pm 0.14$ Weighted rms= 0.763
	FRI galaxies+QSO	$a = 6.96$ $b = 0.81 \pm 0.09$ $\sigma = 1.076$	$a = 5.97 \pm 3.12$ $b = 0.84 \pm 0.10$ $\sigma_{\rm int} = 0.57 \pm 0.13$ Weighted rms= 0.759
	FRII galaxies	$a = 0.60$ $b = 1.04 \pm 0.15$ $\sigma = 1.111$	$a = 2.40 \pm 4.16$ $b = 0.98 \pm 0.13$ $\sigma_{\rm int} = 1.01 \pm 0.17$ Weighted rms= 1.003

Table 6.7: *Results of the regression analysis for the subsamples of Table 6.6. Column 1: type of correlation. Column 2: groups of objects. Column 3: Buckley-James regression parameters of the bisector of the two fitted lines (see § 5.5.4). Column 4: Fasano & Vio regression parameters. Only detections have been used for the Fasano & Vio regression.*

6.4 Summary of results

From the above discussion, the following results can be summarized:

- No dependence of the optical luminosity on the radio morphology is observed. The optical emission of radio galaxies is likely dominated by the stellar emission of the host galaxies with luminosities typical of the most massive non-active ellipticals.
- At a given optical luminosity, a wide range of both, total radio and X-ray luminosities, are observed for the radio galaxies. FRI and FRII galaxies clearly form two distinct groups, with the latter having significantly larger X-ray and total radio luminosities.
- The difference between the core radio luminosities of FRI and FRII galaxies is less pronounced than that observed for the total radio luminosities, with some indications that the radio cores of FRII galaxies are brighter.
- The luminosity properties of the radio galaxies in and outside clusters do not differ significantly. Only for FRI galaxies there is some indication of a cluster contribution to their X-ray luminosity, which might be unresolved.
- A subgroup of FRI and FRII sources formally classify as quasars with properties which distinguish them from the galaxies. All FRI "quasars" are objects with peculiar host galaxies and they differ from the galaxies only in having enhanced optical luminosity, whereas they are basically undistinguishable considering their radio and X-ray properties.
  The FRII quasars have a total radio power typical of FRII galaxies, but their X-ray, optical and radio core luminosities are significantly larger, indicative of the presence of relativistic beaming.
- The X-ray luminosity is correlated with the core radio luminosity of FRI and FRII galaxies. No good correlation is observed with the total radio luminosity for the galaxies. This supports the scenario in which the X-ray emission is also mainly non-thermal connected to the active nucleus and not to a hot gaseous corona.
- For the FRII quasars the data suggest a linear relation of the X-rays with both the total and core radio luminosities, with slopes of $b \sim 0.9$ and $b \sim 0.8$, respectively, however, the hypothesis that the observed relationship with the total radio luminosity is induced by redshift cannot be rejected. The X-ray luminosity as well seems to be correlated to the optical through a common redshift dependence. However, the number of FRII quasars considered is not sufficiently large to draw firm conclusions.
- There are indications that the extended/lobe radio power is positively correlated with the core luminosity only in FRI sources, whereas for the FRII galaxies this is probably caused by redshift effects.
- In general, the correlations for sources with FRII morphology are more affected by redshift. This might be due to their larger redshift range ($z \sim 0.03 - 1.9$) compared to that of FRI sources which have $z \lesssim 0.25$.

6.5 Discussion

We have seen that FRI and FRII galaxies show comparable optical luminosities which can be attributed to the stellar emission of the host galaxies. The majority of them have absolute magnitudes around $M_{\rm V} = -22.0$, falling in the range of massive ellipticals. On one hand, this result suggests that strong radio sources can only be sustained when a certain galaxy mass is reached. On the other hand, the masses of the supermassive black holes are correlated to the bulge magnitudes (Kormendy & Richstone 1995, Ferrarese & Merritt 2000), therefore our findings support a substantial similarity of black hole mass ranges in FRI and FRII galaxies. This is in agreement with recent results by Marchesini, Celotti & Ferrarese (2004) who estimate black hole masses for a sample of FRI and FRII galaxies and radio-loud quasars through the use of the black hole mass - host bulge magnitude correlation. Therefore an intrinsic explanation for the FRI/FRII dichotomy relying on the black hole mass only seems unlikely.

The dependence of the FRI/FRII classification on the optical luminosity of the host galaxy found by Owen & Ledlow (1994) has been interpreted by Bicknell (1995) and Gopal-Krishna et al. (1996) in terms of extrinsic models in which the environment plays the decisive role. From our data we cannot confirm a clear optical luminosity dependence of the dichotomy. However, we use 5 GHz and V-band frequencies instead of the 1.4 GHz and R magnitudes originally adopted by Owen & Ledlow (1994), where the dichotomy might be more apparent. Recent results by Lara et al. (2004) actually favor a sharp break between FRI and FRII sources in total radio power at 1.4 GHz in contrast with Owen & Ledlow (1994), so that this issue is still being debated.

The X-ray luminosity appears to be well correlated to the core radio luminosity in all sources. This is commonly taken as an indication for a non-thermal origin, likely from inverse Compton or Synchrotron-Self Compton scattering of the radio synchrotron photons. Therefore, contrary to what is observed for the optical band, both the X-ray and radio emission are closely related to the central AGN. Furthermore, FRI galaxies are found to have lower luminosities than the FRII at both frequencies, implying lower power engines.

FRII quasars have higher optical, X-ray and radio core luminosities compared to FRII galaxies. The optical luminosity appears to be correlated with both the total and core radio power and possibly with the X-ray luminosity, implying that in these sources a nuclear component boosted by relativistic beaming is dominating in the optical band, contrary to the case of the galaxies. The stronger X-ray and core radio emission compared to the FRII galaxies also suggest that in FRII quasars relativistic beaming plays a non-negligible role. The presence of beaming is also in agreement with the lack of a correlation between the extended and core radio luminosities in these sources.

The results discussed above suggest that FRI and FRII sources have similar black hole masses but different powers. The extrinsic scenario assumes that both FRI and FRII galaxies have similar engines, possibly differing only in power, and that the interactions of the jets with the environment determine the resulting radio morphology. The similarity in black hole masses inferred from our data apparently supports an extrinsic explanation.

However, at a closer look, this is not capable to account for the rather sharp division into high-power (FRII) and low-power (FRI) objects. In fact, in this scenario, a significant overlap, tracing that observed for the black hole masses, of their luminosity distributions would be expected but not the observed bimodal behavior with FRI and FRII sources found separately at low and high luminosities. The only way to reproduce this bimodal distribution given a common range of black hole masses would be to vary some other fundamental parameter (e.g. the accretion rate or the black hole spin), leading eventually to an intrinsic scenario. We therefore believe that some intrinsic explanation is required and is more consistent with the observations.

A possible parameter which could explain the dichotomy might be the accretion rate. Objects with higher accretion rates would have disks with higher bolometric luminosities and, likely, more powerful outflows/jets. With black hole masses of the order of $10^8 - 10^9 M_{\odot}$ the emission of the disk would be mostly in the optical/UV range, providing the photons necessary to ionize the emission line regions. The higher the accretion rate, the higher the ionizing flux and the stronger the emission lines. At the same time, a higher accretion rate would imply more powerful jets with higher radio and X-ray luminosity, capable of producing a FRII morphology.

The case with lower accretion rate would, on the other hand, result in lower bolometric luminosities, lower ionizing flux, weaker emission lines and weaker jet power and X-ray/radio luminosities. The radio morphology associated to this case would then be of FRI type.

Chapter 7

The data: FRI galaxies vs. BL Lac objects

7.1 Introduction

In the context of the unification scheme for AGN BL Lac objects are the beamed counterparts of FRI galaxies. Two kinds of BL Lacs are found, X-ray selected (XBL) and radio-selected (RBL), depending on the waveband of their discovery. RBL show extreme properties (i.e. polarization, variability, etc.) whereas XBL are more "quiet". A quantitative classification of BL Lacs separates these objects into *High-energy-peaked (HBL)* and *Low-energy-peaked (LBL)*(Padovani & Giommi 1995) depending on whether the synchrotron peak frequency falls into the IR/optical or into the UV/X-ray band, respectively. Most of the RBL are LBL and most of the XBL are HBL.
Recently it has been proposed (Fossati et al. 1998, Donato et al. 2001) that HBL, LBL and flat-spectrum radio-loud quasars (FSRQ) belong to a single family of objects whose emission is governed by similar physical processes. They form the so called *blazar sequence* in which, going from HBL to LBL to FSRQ, the synchrotron peak frequency moves from $10^{16}-10^{17}$ Hz to $10^{13}-10^{14}$ Hz, the inverse Compton peak frequency shifts from $10^{24}-10^{25}$ Hz to $10^{21}-10^{22}$ Hz and the ratio of the inverse Compton and synchrotron peak luminosities (the *γ-ray dominance*) increases. The fundamental parameter governing the blazar sequence is believed to be the source luminosity, independent of its classification. Sources with higher luminosities have lower peak frequencies, stronger γ-ray emission and more extreme properties.
As the parent population of BL Lac objects, FRI galaxies are expected to show similar SEDs as Low-energy and High-energy-peaked objects. The SEDs of FRI galaxies are, however, only poorly sampled and thus this issue can currently not be investigated directly. Trussoni et al. (2003) analyzed the SEDs of a few FRI galaxies and found indications that they are not monotonic with peaks and minima of emission, like the BL Lacs. However, only few data points are available so that large uncertainties remain.
The unification scheme for FRI galaxies and BL Lac objects has been tested in several ways, such as by comparing the isotropic properties of the two classes or by analyzing their luminosity functions taking into account relativistic beaming (Urry & Padovani 1995). Another way has been to compare the nuclear properties of BL Lacs with those of FRI

galaxies, after correcting for relativistic beaming effects (Chiaberge et al. 2000, Capetti et al. 2000). In order to match the luminosity properties of FRI galaxies with those of "de-beamed" BL Lacs the authors postulate the presence of a velocity structure in the jet, with a fast spine dominating the emission of BL Lacs and a slow layer, dominant in FRI galaxies. This jet structure might be able to explain the discrepant values of the beaming factors obtained for the BL Lacs and FRI galaxies with different methods. In fact, higher beaming factors ($\delta = 15-20$) result from the observation of superluminal motions or from accurate fits of the SEDs, whereas lower values $\delta = 4-6$ are required from the simple comparison of the luminosities of BL Lac objects and FRI galaxies in a given waveband (see Eq. (3.5)). The existence of such a velocity structure is currently an open question.

In this chapter we want to address the subject of BL Lac/FRI galaxy unification with a multiwavelength approach, using radio, optical and X-ray data. There are 270 BL Lac objects in our sample and 68 sources with FRI morphology. The objects that we defined in Chapter 6 as FRI "quasars" are here included in the group of FRI galaxies due to their similar properties (see Chapter 6). One FRI source resulted to be also optically classified as a BL Lac and is included in the first group. 3 BL Lacs turned out to have wrong redshift measurements and are excluded from the analysis. Among the BL Lacs, 24 are classified either as RBL or LBL and 49 either as XBL or HBL. To further increase the number statistics of each of these two classes we have defined the BL Lacs in our sample lacking a classification as LBL or HBL according to the criterium of Fossati et al. (1998): objects having $\alpha_{\rm rx} \gtrsim 0.75$ are labeled as LBL and those with $\alpha_{\rm rx} \lesssim 0.75$ as HBL. We obtain in total 179 HBL and 88 LBL. The HBL are more numerous as a consequence of the X-ray selection of our sample.
Core radio fluxes are available for 105 BL Lac objects (38 LBL and 67 HBL) and 54 FRI galaxies. The core optical fluxes from HST observations of 25 FRI galaxies are given in Chiaberge et al. (1999) and Capetti et al. (2002). These fluxes will be used to compare the nuclear properties of BL Lacs and FRI galaxies.

7.2 Luminosity distributions

We study the properties of the luminosity distributions of BL Lac objects compared to those of FRI galaxies as described in § 6.2. The average luminosities from the Kaplan-Meier estimator and the Maximum Likelihood technique for the two classes are given in Table 7.1. Upper limits are present in the X-rays for 4 FRI galaxies only.
The optical luminosities of the FRI galaxies are calculated from the core fluxes given in Chiaberge et al. (1999) and Capetti et al. (2002) extrapolated to the V band. The luminosities of the BL Lac objects are calculated from their total magnitudes, since in these objects the contribution of the host galaxy is negligible.

7.2.1 The total radio luminosity distributions

Fig. 7.1 displays the total radio luminosity distributions for the various classes and Fig. 7.2 the 90% confidence level contour plots of their mean luminosities and intrinsic dispersions. An inspection of Fig. 7.2 shows that BL Lacs have larger total radio luminosities than FRI galaxies and the difference is found to be significant at the 5% level. However, the total

Average luminosities

Luminosity (1)	Group (2)	$\log L^{\rm KM}$ (3)	$\log L^{\rm ML}$ (4)
$L_{0.1-2.4\ \rm keV}$ (erg s^{-1})	FRI galaxies	42.59 ± 0.15	$42.68 \pm 1.18^{\dagger}$
	BL Lacs	44.90 ± 0.05	44.90 ± 0.85
	LBL/RBL	44.54 ± 0.10	44.53 ± 0.97
	HBL/XBL	45.07 ± 0.05	45.07 ± 0.71
$L_{\rm O,core}$ (erg s^{-1} Hz^{-1})	FRI galaxies	26.95 ± 0.19	26.94 ± 0.93
	BL Lacs	29.81 ± 0.04	29.81 ± 0.67
	LBL/RBL	30.07 ± 0.09	30.07 ± 0.85
	HBL/XBL	29.69 ± 0.04	29.69 ± 0.52
$L_{\rm 5GHz,tot}$ (erg s^{-1} Hz^{-1})	FRI galaxies	31.57 ± 0.12	31.57 ± 0.96
	BL Lacs	32.00 ± 0.07	32.01 ± 1.06
	LBL/RBL	32.89 ± 0.13	32.88 ± 1.18
	HBL/XBL	31.56 ± 0.05	31.57 ± 0.66
$L_{\rm 5GHz,core}$ (erg s^{-1} Hz^{-1})	FRI galaxies	30.62 ± 0.14	30.62 ± 1.02
	BL Lacs	31.96 ± 0.09	31.96 ± 0.90
	LBL/RBL	32.42 ± 0.18	32.42 ± 1.10
	HBL/XBL	31.70 ± 0.08	31.70 ± 0.64

† Detections only.

Table 7.1: *Column 1: luminosity. Column 2: group of objects. Column 3: mean of luminosity and related error from the generalized Kaplan-Meier estimator. Column 4: mean of luminosity and intrinsic dispersion from the Maximum-Likelihood technique (see § 5.5.1).*

radio emission in FRI galaxies is dominated by the extended lobes and in BL Lacs by the core, so that the comparison might be misleading. A separate comparison of the extended and core emission in the two classes is more meaningful and will be discussed in §§ 7.2.2 and 7.3.1. Among BL Lacs, LBL have larger total radio luminosities than HBL at 5% significance level, consistently with the different shapes of their SEDs. Since their emission in the radio band is dominated by the core this also implies that LBL have stronger cores than HBL (see also § 7.2.2).
The intrinsic dispersion for FRI galaxies is large ($\log \sigma_{\rm intr} \sim 1$) and comparable to that for all BL Lacs taken together. However, when LBL and HBL are separated the intrinsic dispersion is much lower for the HBL ($\log \sigma_{\rm intr} = 0.66$) than for the LBL ($\log \sigma_{\rm intr} = 1.18$)

7.2.2 The radio core luminosity distributions

Considering the radio core luminosity distributions (Fig. 7.3) and the 90% confidence level contour plots of the mean luminosities and intrinsic dispersions (Fig. 7.4) the discrepancy between FRI galaxies and BL Lacs is larger than in the case of the total luminosities. The core luminosities of LBL are significantly higher than those of HBL, but the difference appears to be less pronounced than in the case of total radio luminosities. However, the average radio core luminosity of HBL is unexpectedly larger than their average total luminosity, in contradiction with the fact that the core emission constitutes only part of the total emission. The reason for this is probably that, due to their low radio brightness, core luminosities are available only for a fraction of HBL and therefore the average core luminosity quoted in Table 7.1 is probably only an upper limit.
The intrinsic dispersions of FRI galaxies and all BL Lacs are close to unity and LBL have a much larger value ($\log \sigma_{\rm intr} = 1.10$) than HBL ($\log \sigma_{\rm intr} = 0.64$), similar to the case of the total radio luminosities.

7.2.3 The optical luminosity distributions

The optical luminosity distributions for the various classes are shown in Fig. 7.5, whereas the 90% confidence level contour plots for the mean luminosities and intrinsic dispersions are presented in Fig. 7.6.
The (total) luminosities of BL Lacs are significantly larger than those of the FRI galaxies when only their optical cores are considered. If the optical emission of BL Lacs, as usually found, is dominated by the active nucleus, then the above result means that the cores of BL Lacs are optically more luminous than those of FRI galaxies, in agreement with the relativistic beaming scenario. LBL have significantly larger optical luminosities than HBL at 5% level, as expected from their different SEDs.
The FRI galaxies have quite large intrinsic dispersion ($\log \sigma_{\rm intr} = 0.93$), more similar to that of LBL ($\log \sigma_{\rm intr} = 0.85$) than to that of HBL ($\log \sigma_{\rm intr} = 0.52$).

7.2.4 The X-ray luminosity distributions

Fig. 7.7 shows the X-ray luminosity distributions for the various classes, whereas Fig. 7.8 displays the 90% confidence level contour plots of their mean luminosities and intrinsic dispersions.
The X-ray emission of BL Lacs is thought to be non-thermal, a fact supported by the

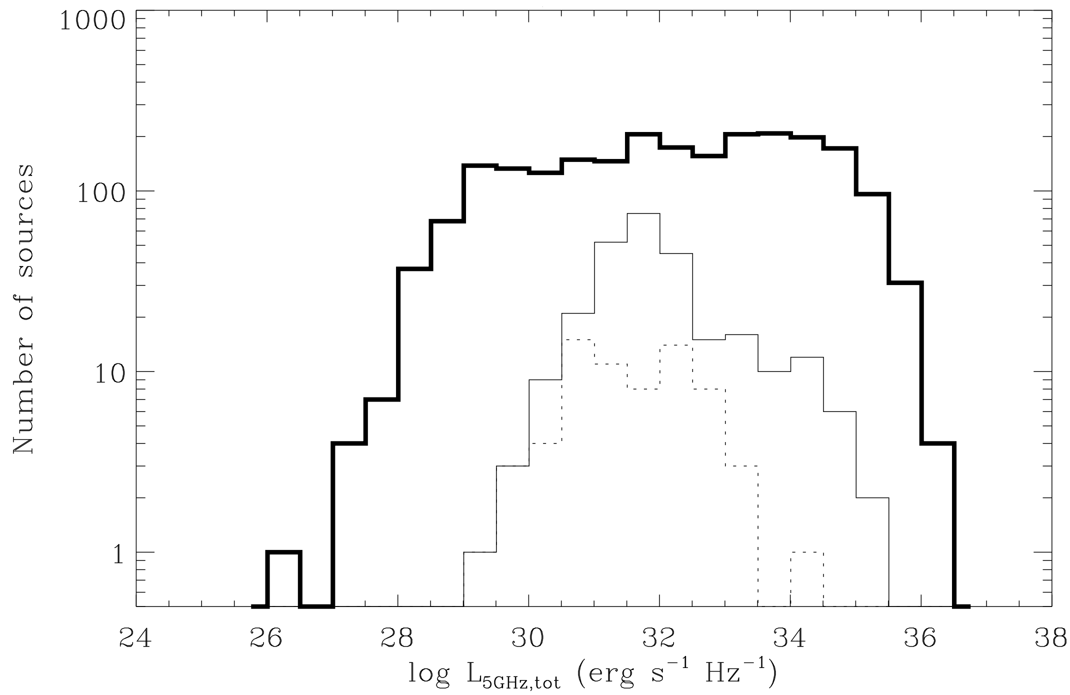

Figure 7.1: *Total* 5 *GHz radio luminosity distributions for the FRI galaxies (dotted line), the BL Lacs (thin solid line) and the total sample (thick solid line).*

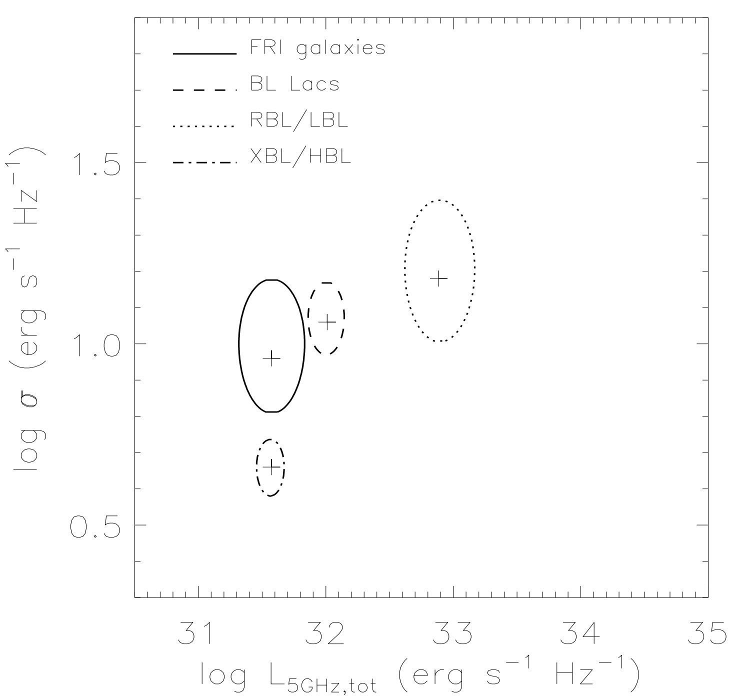

Figure 7.2: 90% *confidence level contour plots for the total* 5 *GHz luminosity and intrinsic dispersion of FRI galaxies and BL Lacs. Also shown are the contours for LBL/RBL and HBL/XBL, separately. The crosses indicate the average* $\log\ L_{\rm R,tot}$ *and* $\log\ \sigma$*.*

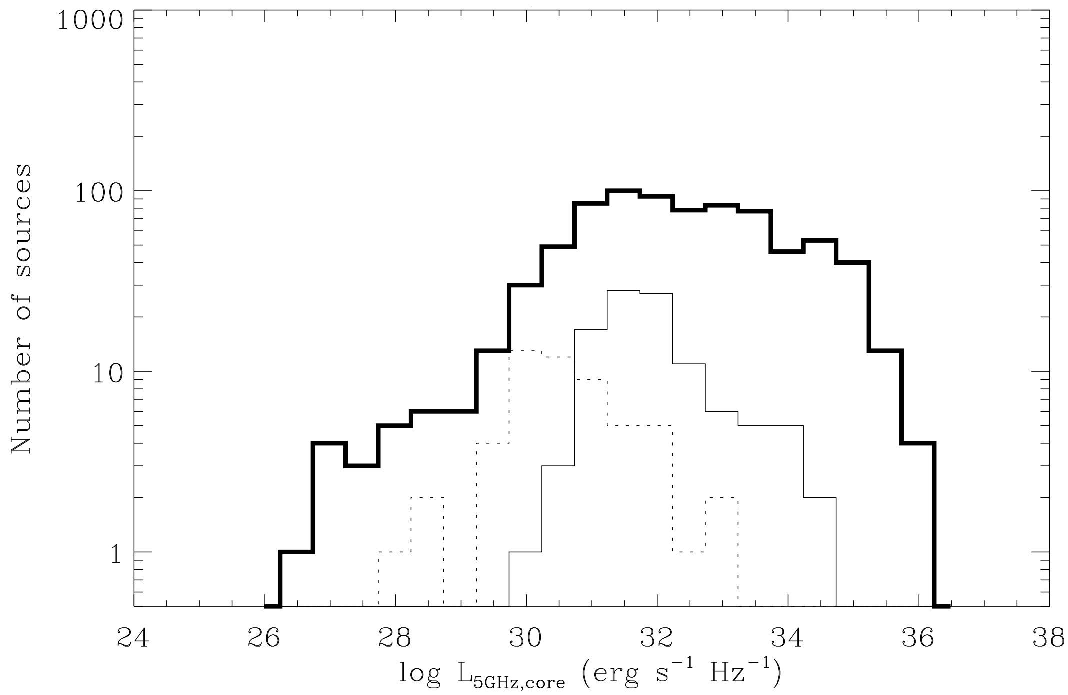

Figure 7.3: 5 *GHz core radio luminosity distributions for the FRI galaxies (dotted line), the BL Lac objects (thin solid line) and the total sample (thick solid line).*

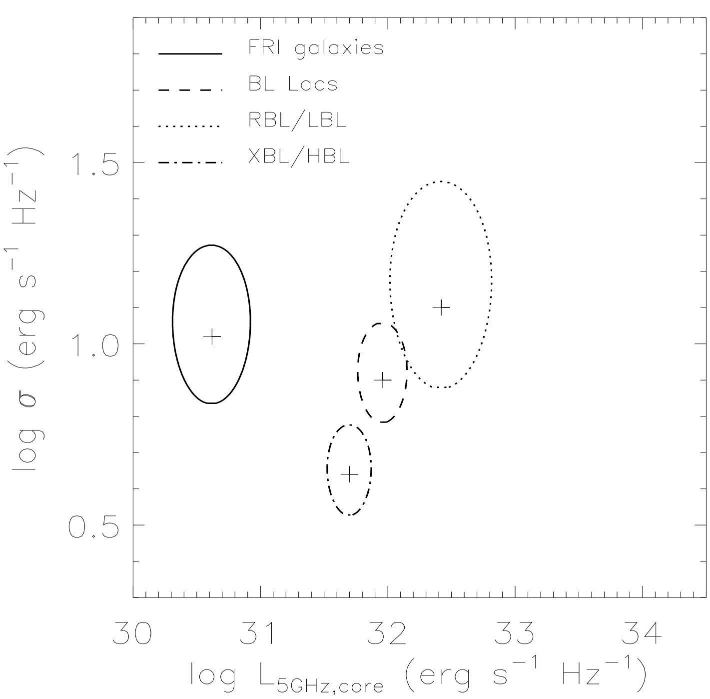

Figure 7.4: 90% *confidence level contour plots for the* 5 *GHz core luminosity and intrinsic dispersion of FRI galaxies and BL Lacs. Also shown are the contours for LBL/RBL and HBL/XBL, separately. The crosses indicate the average* $\log\ L_{\mathrm{R,core}}$ *and* $\log\ \sigma$*.*

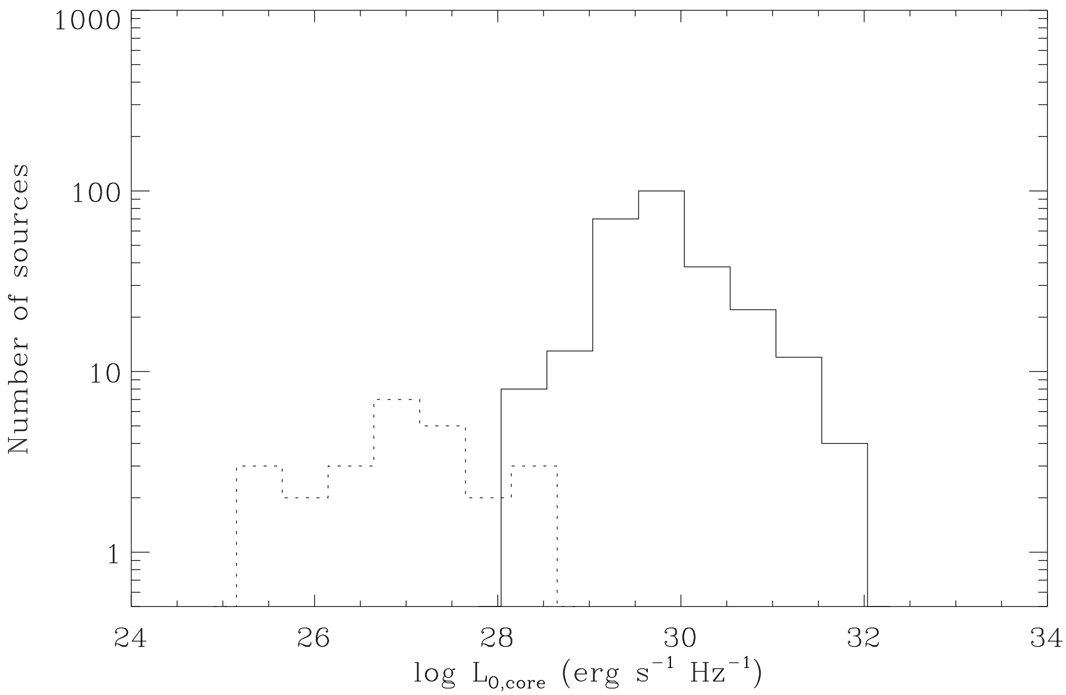

Figure 7.5: *Optical V-band luminosity distributions for the FRI galaxies (dotted line) and the BL Lac objects (solid line).*

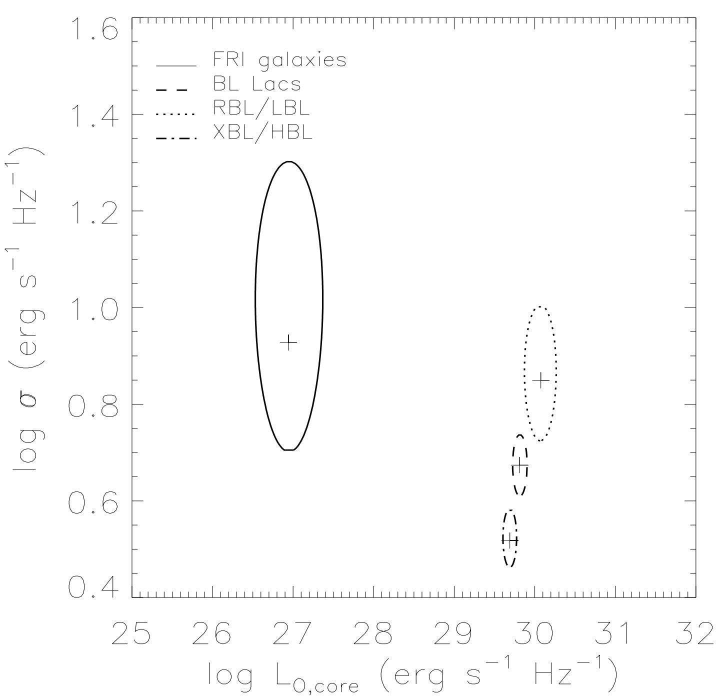

Figure 7.6: 90% *confidence level contour plots for the optical V-band luminosity and intrinsic dispersion of FRI galaxies and BL Lacs. Also shown are the contours for LBL/RBL and HBL/XBL, separately. The crosses indicate the average* log L_O *and* log σ*.*

shape of their SEDs (see Chapter 4) and by the correlation with the core radio emission (see § 7.3.4). We have seen in Chapter 6 that also in the FRI sources the X-ray luminosity appears to correlate with the radio luminosity, likely implying a non-thermal origin from the nucleus rather than a thermal origin from the hot corona of the host galaxy (Hardcastle & Worrall 1999). We can therefore conclude that the X-ray luminosities of both FRI galaxies and BL Lacs originate mostly from their active nuclei and that also in X-rays the cores of BL Lac objects are brighter than those of FRI galaxies. HBL are significantly more X-ray luminous than LBL, consistently with their SEDs and observational classifications. FRI galaxies show a large intrinsic dispersion of $\log \sigma_{\rm intr} = 1.18$, whereas LBL and HBL display lower values of $\log \sigma_{\rm intr} = 0.97$ and $\log \sigma_{\rm intr} = 0.71$, respectively.

7.3 Correlation and regression analysis

Previously, the X-ray and total radio luminosities of the BL Lac objects were found to be tightly correlated by Brinkmann et al. (1996) with slopes $b = 0.53{\pm}0.14$ and $b = 1.09{\pm}0.11$ for XBL and RBL, respectively. These authors also obtained weaker correlations of the optical with both the X-ray and radio luminosities, however, without a clear separation between XBL and RBL.
The correlation between the X-ray and radio core luminosities of FRI galaxies is known to exist since Einstein and ROSAT observations (Fabbiano et al. 1984, Brinkmann et al. 1994, Siebert et al. 1996) as discussed briefly in § 6.3. The almost linear correlation of the radio with the optical core luminosities of FRI galaxies has been evidenced by Chiaberge et al. (1999) and has been used to support the non-thermal origin of the optical core emission in these objects.

In this section we present the results of the correlation and regression analyses for FRI galaxies and BL Lacs using the statistical methods described in Chapter 5. To determine the statistical significance of the correlations we calculate generalized versions for censored data of both the Kendall's τ and partial Kendall's τ coefficients. We perform both the Buckley-James regression, allowing for the presence of upper limits, and the Fasano & Vio regression, considering only detections and including the errors on the variables. The Fasano & Vio regression also provides an estimate of the intrinsic dispersion of the correlation. The results are given in Table 7.2 and will be discussed in § 7.5.

7.3.1 The radio - to - radio luminosity correlations

Figs. 7.9 and 7.10 show the total versus core and the extended versus core radio luminosities for the whole sample (Fig. 7.9, top panel) and for FRI galaxies and BL Lacs only (bottom panel of Fig. 7.9 and Fig. 7.10), where the extended luminosity is obtained by subtracting the core from the total luminosity. The luminosities of the BL Lac objects appear to be dominated by the core, whereas the FRI galaxies are lobe-dominated. In fact, at a given core luminosity the FRI galaxies have on average an extended luminosity about an order of magnitude larger than that of BL Lacs. LBL appear to be the objects with the largest core luminosities, reaching $L_{\rm R,core} \gtrsim 10^{34}$ erg s^{-1} Hz^{-1}, about an order of magnitude higher than the maximum value reached by HBL. A few FRI galaxies appear to be more

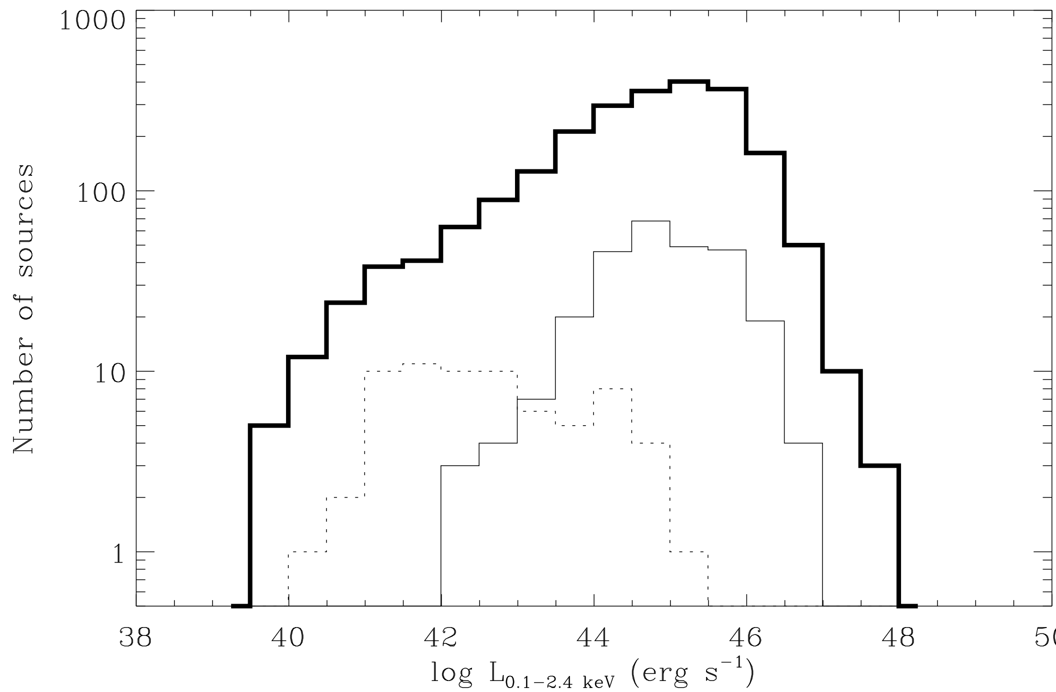

Figure 7.7: *X-ray luminosity distributions for the FRI galaxies (dotted line), the BL Lacs (thin solid line) and the total sample (thick solid line).*

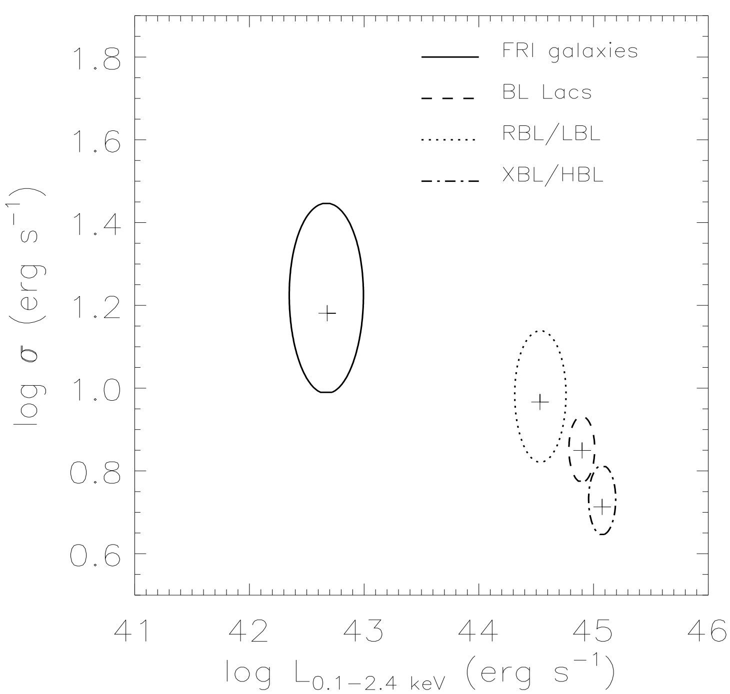

Figure 7.8: 90% *confidence level contour plots for the* $0.1 - 2.4$ *keV X-ray luminosity and intrinsic dispersion of FRI galaxies and BL Lacs. Also shown are the contours for LBL/RBL and HBL/XBL, separately. The crosses indicate the average* $\log\ L_{\mathrm{X}}$ *and* $\log\ \sigma$.

core-dominated, suggesting that they could be beamed, perhaps because they are observed at smaller viewing angles.

FRI galaxies and BL Lacs have comparable ranges of extended luminosities, following almost parallel trends of $L_{\rm R,ext}$ versus $L_{\rm R,core}$ (see Fig. 7.10). These results are expected in the framework of the unified scheme where the isotropic radiation from the extended lobes is of comparable intensity for all viewing angles, whereas the strongly beamed core emission from the relativistic jets is dominant in objects observed at small angles, i.e. BL Lacs. Therefore, with decreasing viewing angle a source will move progressively to the right of Fig. 7.10 at constant extended luminosity.

Both LBL and HBL lie approximately on the same correlation between $\log L_{\rm R,ext}$ and $\log L_{\rm R,core}$ (Fig. 7.10) of slope $b \sim 1$. This implies that $L_{\rm R,core} \propto L_{\rm R,ext}$ and that the *core-dominance*, defined as $R_{\rm C} = L_{\rm R,core}/L_{\rm R,ext}$, is approximately constant and equal in both classes. As $R_{\rm C}$ is usually taken as an indicator of the amount of beaming (Urry & Padovani 1995), this cannot account for the different properties of LBL and HBL. The correlation seems to be less tight for HBL, for which a significant dispersion is observed.

7.3.2 The radio - to - optical luminosity correlations

In Fig. 7.11 the relation between the total radio and optical luminosities for BL Lac objects and FRI galaxies is shown with respect to the rest of the sample; Fig. 7.12 shows the relation between the radio core and optical luminosities for the BL Lacs and the FRI galaxies only.

FRI galaxies and BL Lacs occupy approximately the same region in the $L_{\rm R,tot}$-$L_{\rm O,tot}$ plane. Some BL Lacs, however, reach higher luminosities than the galaxies at both frequencies. It has already been remarked that the similar ranges of $L_{\rm R,tot}$ observed in FRI galaxies and BL Lacs is a coincidence, since their radio emission arises mostly from spatially well separated regions, the lobes in the first class and the core in the second one.
When considering only the core luminosities a clear separation between FRI galaxies and BL Lacs becomes apparent. LBL/RBL separate neatly from HBL/XBL with the first ones lying above, and the second ones below, an approximate luminosity between $\sim 10^{32} - 10^{33}$ erg s^{-1} Hz^{-1}. The radio core luminosity seems to be well correlated with the optical in both, FRI galaxies and BL Lacs (see Table 7.2). The slope of the Fasano & Vio regression line is $b \sim 1$ for the galaxies and steeper for the BL Lacs. However, amongst the BL Lacs, sources classified either as LBL or HBL appear to follow separate correlations (see Fig. 7.12). HBL follow a correlation with very similar slope ($b = 1.09 \pm 0.08$) to that of the FRI galaxies ($b = 1.13 \pm 0.18$) inside the errors, whereas LBL have a much steeper slope ($b = 1.51 \pm 0.15$). FRI galaxies and LBL show a large dispersion ($\log \sigma_{\rm intr} = 0.70 \pm 0.42$ and $\log \sigma_{\rm intr} = 0.56 \pm 0.19$, respectively) about the regression line, whereas for the HBL it is much smaller ($\log \sigma_{\rm intr} = 0.16 \pm 0.04$). All correlations are highly significant at the 5% level.
The slope of the correlation for the FRI galaxies is comparable to that found by Chiaberge et al. (1999), whereas we cannot confirm the close similarity found by Brinkmann et al. (1996) between the correlations for LBL and HBL, which appear instead to be clearly different.

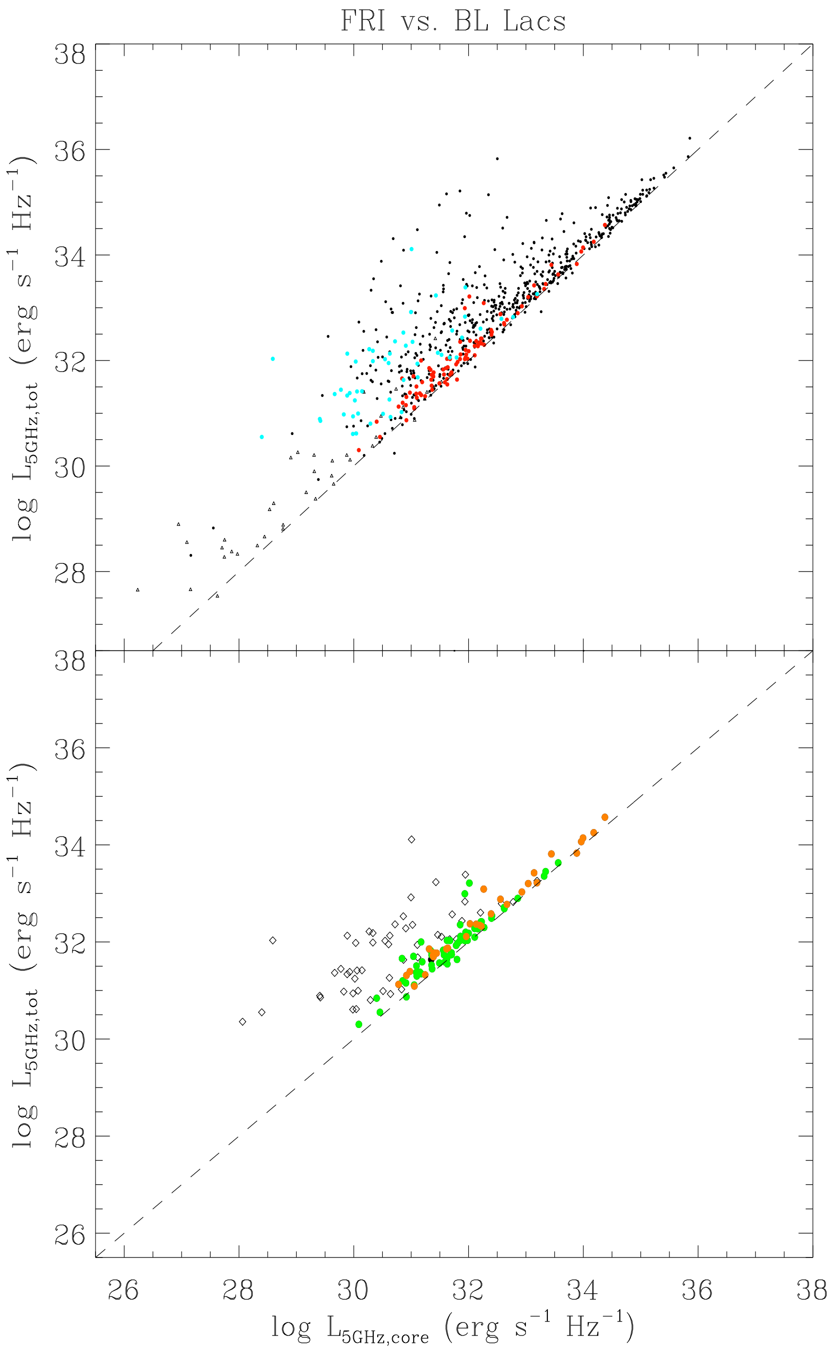

Figure 7.9: *Top panel: the* $L_{\rm R,tot}$*-*$L_{\rm R,core}$ *plane for the FRI galaxies (blue) and the BL Lacs (red) superposed on the total sample (black). Radio-loud objects are shown as circles and radio-quiet as triangles. Bottom panel: the* $L_{\rm R,tot}$*-*$L_{\rm R,core}$ *plane for the FRI galaxies (diamonds) and BL Lacs (circles) only. LBL/RBL are plotted in yellow and HBL/XBL in green. In both panels the line for which* $L_{\rm R,tot} = L_{\rm R,core}$ *is drawn.*

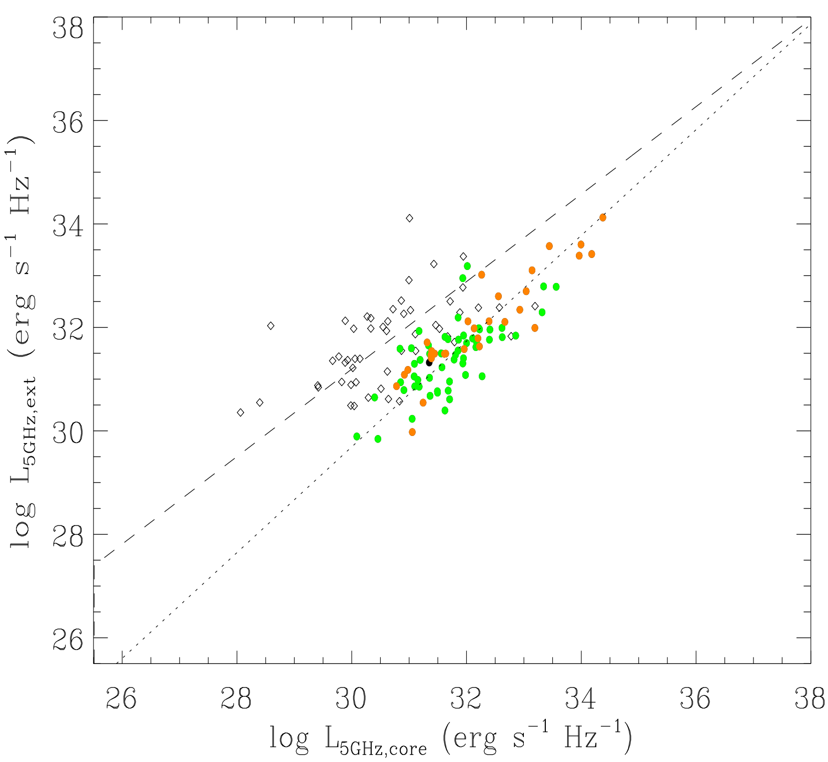

Figure 7.10: *The $L_{\mathrm{R,ext}}$-$L_{\mathrm{R,core}}$ plane for the FRI galaxies (diamonds) and the BL Lacs (circles). LBL/RBL are plotted in yellow and HBL/XBL in green. The regression lines for FRI galaxies (dashed) and BL Lacs (dotted) are also plotted, with slopes of* $b = 0.84 \pm 0.11$ *and* $b = 1.02 \pm 0.06$*, respectively.*

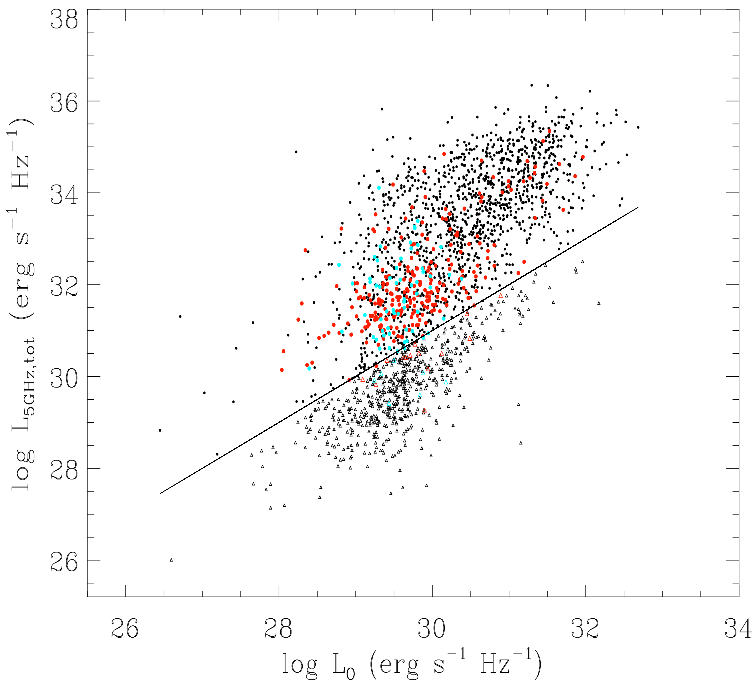

Figure 7.11: *The $L_{\mathrm{R,tot}}$-L_{O} plane for the FRI galaxies (blue) and the BL Lacs (red) superposed on the rest of the sample (black). The straight line represents the formal division between radio-loud (circles) and radio-quiet (triangles) objects (see §2.3).*

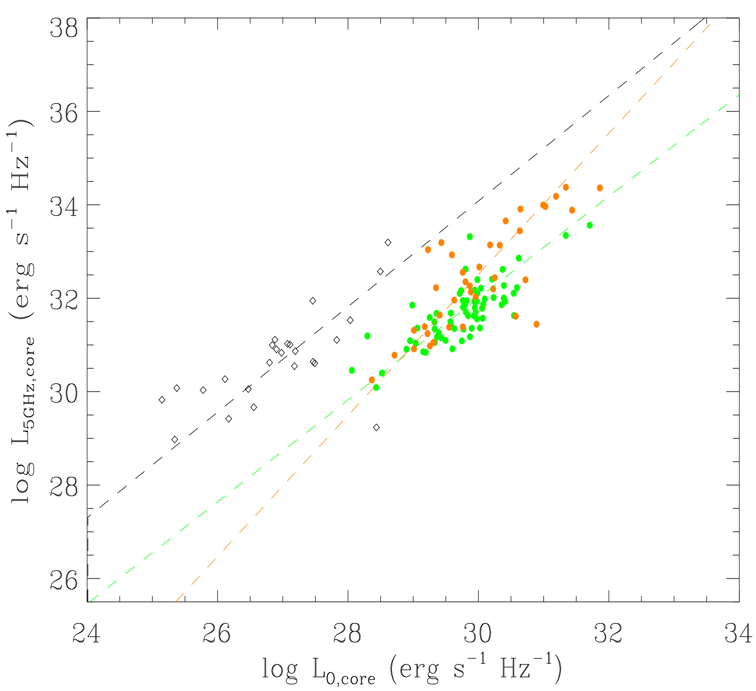

Figure 7.12: *The $L_{\mathrm{R,core}}$-$L_{\mathrm{O,core}}$ plane for the FRI galaxies (diamonds) and the BL Lacs (circles). HBL/XBL are plotted in green and LBL/RBL in yellow. The total optical luminosity is used for the BL Lacs. Also plotted are the Fasano & Vio regression lines for FRI galaxies (black), HBL (green) and LBL (yellow).*

7.3.3 The X-ray - to - optical luminosity correlations

Fig. 7.13 shows the X-ray versus optical luminosities for FRI galaxies and BL Lac objects superposed on the rest of the sample, where the total optical luminosity has been used for both classes. Fig. 7.14 shows the X-ray - to - optical plane for FRI galaxies and BL Lacs only, where the optical core emission has been considered in the case of the galaxies. Figs. 7.13 and 7.14 clearly show that FRI galaxies have on average lower X-ray luminosities than all BL Lacs taken together and of both HBL and LBL taken separately, as already found in § 7.2.4. Considering only the optical core luminosities (see Fig. 7.14), the FRI galaxies follow a trend with intermediate slope ($b = 1.33 \pm 0.20$) with respect to LBL ($b = 1.25 \pm 0.09$) and HBL ($b = 1.72 \pm 0.11$) (see also Table 7.2). The intrinsic dispersion is larger for the galaxies ($\log \sigma_{\rm intr} = 0.88 \pm 0.22$), whereas LBL and HBL have $\log \sigma_{\rm intr} = 0.46 \pm 0.09$ and $\log \sigma_{\rm intr} = 0.61 \pm 0.07$. In all cases we find that the correlations are highly significant.

7.3.4 The X-ray - to - radio luminosity correlations

The top and bottom panels of Fig. 7.15 show, respectively, the X-ray versus total radio luminosities for FRI galaxies and BL Lacs superposed on the rest of the sample and for FRI galaxies and BL Lacs only. The X-ray versus core radio luminosity plane is shown in Fig. 7.16. In these two figures the different trends for LBL and HBL appear more clearly. A linear relationship with slope $b = 1.23 \pm 0.12$ is found between the X-ray and radio core luminosities of FRI galaxies. The correlation is significant at 5% level. The luminosities of BL Lacs are also correlated, but they separate into two branches corresponding to LBL and HBL, with much flatter ($b = 0.79 \pm 0.06$) and steeper ($b = 1.32 \pm 0.12$) slope than that for the galaxies, respectively.
As in the previous cases, the FRI galaxies are the objects showing the largest intrinsic dispersion, with $\log \sigma_{\rm intr} = 0.75 \pm 0.24$, compared to LBL and HBL with $\log \sigma_{\rm intr} = 0.16 \pm 0.03$ and $\log \sigma_{\rm intr} = 0.35 \pm 0.09$, respectively.

7.4 Unification of FRI galaxies and BL Lac objects

To test the unified scheme for BL Lacs and FRI galaxies we will compare the nuclear properties of the two classes. We include in the analysis all BL Lacs with given radio core fluxes and we use their total X-ray and optical luminosities. In fact, the nuclear origin of the emission in the X-ray and optical bands is quite reliably established for these sources. For the FRI galaxies, where the contribution from the host galaxy is usually not negligible, the situation is somewhat more complicated. We select only those sources for which optical and radio core fluxes are available. For the X-ray luminosities we rely on the results of Chapter 6 and of previous works (e.g. Hardcastle & Worrall 1999) which showed that the X-ray emission is mainly non-thermal, originating from the nucleus rather than from a hot gaseous corona.
The final subsample of sources with available nuclear luminosities thus consists of 25 FRI galaxies and 105 BL Lac objects.

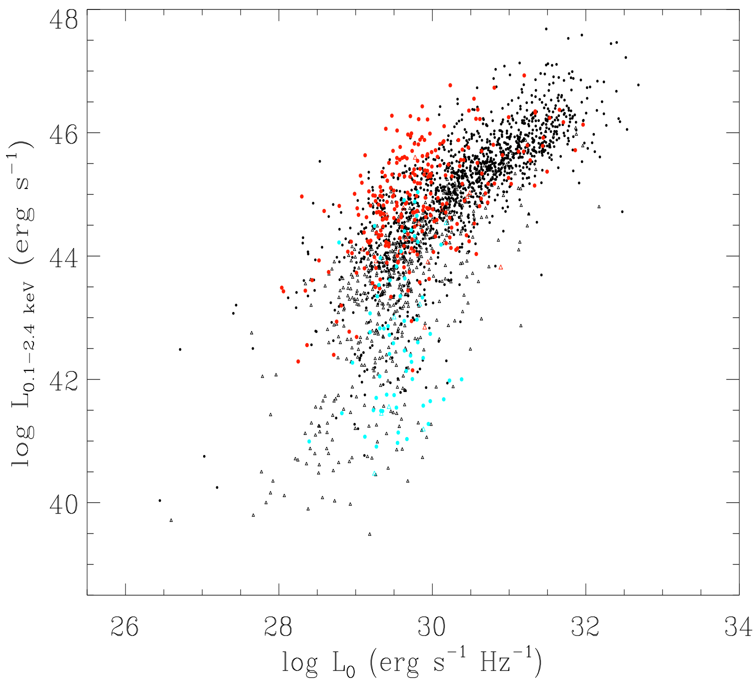

Figure 7.13: *The L_X-$L_{O,tot}$ plane for the FRI galaxies (blue) and the BL Lac objects (red) superposed on the total sample (black). Radio-loud objects are shown as circles and radio-quiet as triangles.*

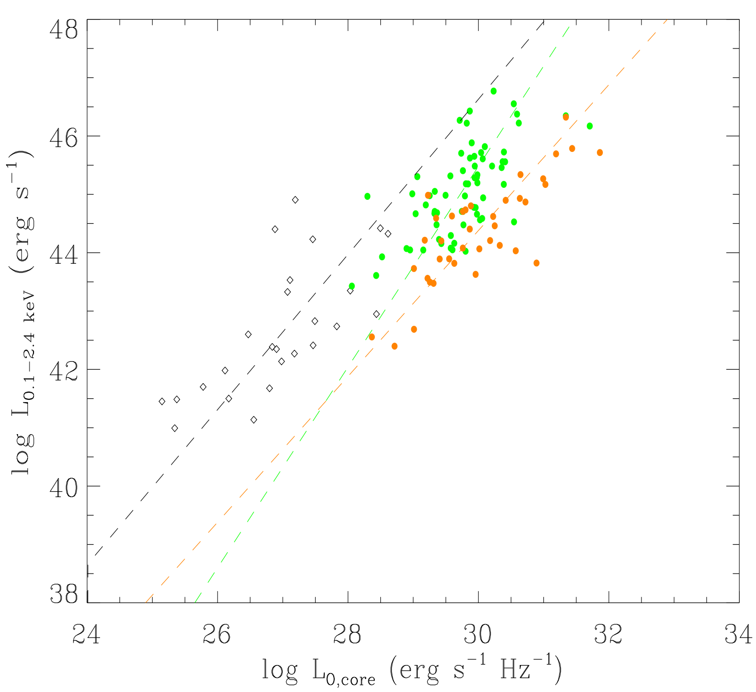

Figure 7.14: *The L_X-$L_{O,core}$ plane for the FRI galaxies (diamonds) and the BL Lac objects (circles). HBL/XBL are plotted in green and LBL/RBL in yellow. The total optical luminosity is used for the BL Lacs. Also plotted are the Fasano & Vio regression lines for FRI galaxies (black), HBL (green) and LBL (yellow).*

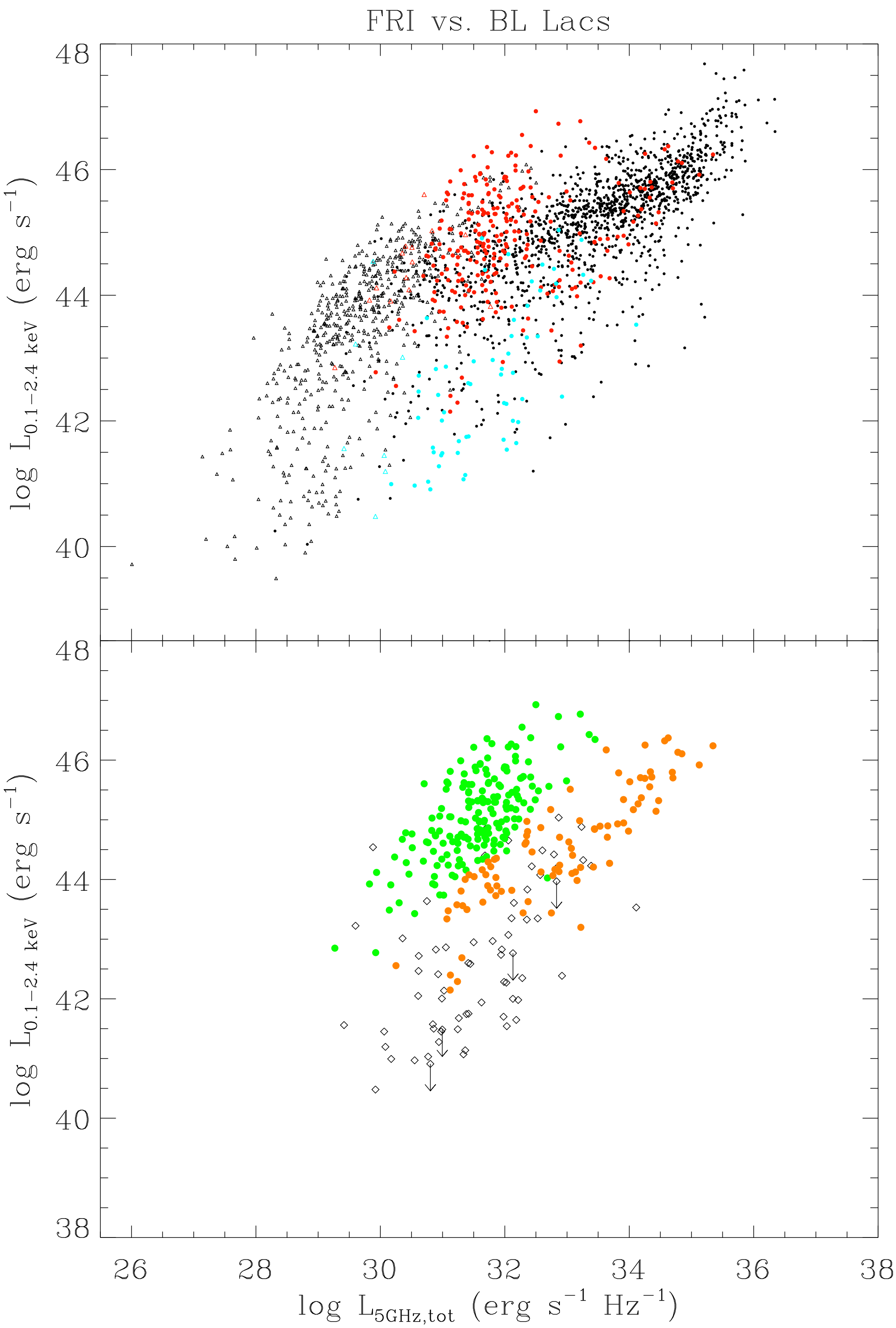

Figure 7.15: *Top panel: the L_X-$L_{R,tot}$ plane for the FRI galaxies (blue) and the BL Lacs (red) superposed on the total sample (black). Radio-loud objects are shown as circles and radio-quiet as triangles. Bottom panel: the L_X-$L_{R,tot}$ plane for the FRI galaxies (diamonds) and BL Lacs (circles) only. HBL/XBL are plotted in green and LBL/RBL in yellow. Arrows indicate upper limits on the X-ray luminosities.*

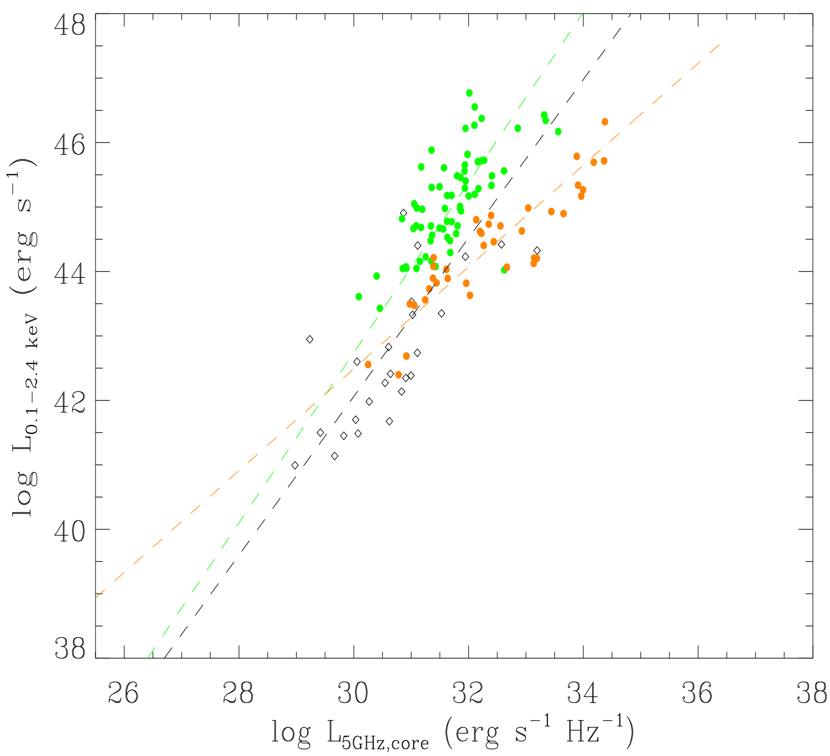

Figure 7.16: *The L_X-$L_{R,core}$ plane for the FRI galaxies (diamonds) and the BL Lacs (circles). HBL/XBL are plotted in green and LBL/RBL in yellow. Also shown here are the upper limits on the X-ray luminosities (arrows). Also plotted are the Fasano & Vio regression lines for FRI galaxies (black), HBL (green) and LBL (yellow).*

Regression analysis

Correlation (1)	Group (2)	Buckley-James (3)	Fasano & Vio (4)
$\log L_{\rm R,core} - \log L_{\rm O,core}$	FRI galaxies	$a = 3.13$ $b = 1.03 \pm 0.16$ $\sigma = 1.032$	$a = 0.18 \pm 4.95$ $b = 1.13 \pm 0.18$ $\sigma_{\rm int} = 0.70 \pm 0.42$ Weighted rms= 0.820
	LBL	$a = -8.67$ $b = 1.37 \pm 0.12$ $\sigma = 0.852$	$a = -12.79 \pm 4.65$ $b = 1.51 \pm 0.15$ $\sigma_{\rm int} = 0.56 \pm 0.19$ Weighted rms= 0.750
	HBL	$a = 0.75$ $b = 1.04 \pm 0.07$ $\sigma = 0.552$	$a = -0.70 \pm 2.53$ $b = 1.09 \pm 0.08$ $\sigma_{\rm int} = 0.16 \pm 0.04$ Weighted rms= 0.427
$\log L_{\rm X} - \log L_{\rm O,core}$	FRI galaxies	$a = 10.41$ $b = 1.20 \pm 0.17$ $\sigma = 1.073$	$a = 6.73 \pm 5.48$ $b = 1.33 \pm 0.20$ $\sigma_{\rm int} = 0.88 \pm 0.22$ Weighted rms= 0.909
	LBL	$a = 9.88$ $b = 1.15 \pm 0.07$ $\sigma = 0.822$	$a = 6.88 \pm 2.75$ $b = 1.25 \pm 0.09$ $\sigma_{\rm int} = 0.46 \pm 0.09$ Weighted rms= 0.684
	HBL	$a = 6.10$ $b = 1.31 \pm 0.08$ $\sigma = 0.758$	$a = -6.12 \pm 3.21$ $b = 1.72 \pm 0.11$ $\sigma_{\rm int} = 0.61 \pm 0.07$ Weighted rms= 0.795
$\log L_{\rm X} - \log L_{\rm R,core}$	FRI galaxies	$a = 9.66$ $b = 1.08 \pm 0.09$ $\sigma = 1.054$	$a = 5.16 \pm 3.62$ $b = 1.23 \pm 0.12$ $\sigma_{\rm int} = 0.75 \pm 0.24$ Weighted rms= 0.873
	LBL	$a = 19.17$ $b = 0.78 \pm 0.05$ $\sigma = 0.656$	$a = 18.79 \pm 1.98$ $b = 0.79 \pm 0.06$ $\sigma_{\rm int} = 0.16 \pm 0.03$ Weighted rms= 0.408
	HBL	$a = 8.27$ $b = 1.16 \pm 0.09$ $\sigma = 0.709$	$a = 3.14 \pm 3.76$ $b = 1.32 \pm 0.12$ $\sigma_{\rm int} = 0.35 \pm 0.09$ Weighted rms= 0.619

Table 7.2: *Results of the regression analysis for FRI galaxies and BL Lacs. Column 1: type of correlation. Column 2: groups of objects. Column 3: Buckley-James regression parameters of the bisector of the two fitted lines (see § 5.5.4). Column 4: Fasano & Vio regression parameters. For the Fasano & Vio regression only detections have been used.*

7.4.1 Modeling the Spectral Energy Distributions

Following a common approach (Landau et al. 1986, Comastri et al. 1995, Sambruna et al. 1996, Fossati et al. 1998, Wolter et al. 1998) we have parameterized the synchrotron peak of the Spectral Energy Distribution (SED) of all BL Lacs and FRI galaxies in our subsample with a parabola of the form:

$$\log(\nu L_\nu) = a(\log\nu)^2 + b\log\nu + c \tag{7.1}$$

The coefficients of the parabola are calculated solving the system of three equations in three unknowns for each source. This approach ignores the measurement errors and can thus lead to incorrect results. However, due to the paucity of data points, a fitting procedure including these errors yields coefficients of the parabolae basically undistinguishable from those obtained from a simple parameterization. The resulting parabolae are shown in Fig. 7.17 and 7.18 for the FRI galaxies and the BL Lac objects, respectively.

All of the SEDs of BL Lacs and most of those of FRI galaxies can be modeled by convex (downward) parabolae. However, 6 FRI galaxies require concave (upward) parabolae. A concave shape might be obtained if the frequency of the minimum between the synchrotron and the inverse Compton peaks falls close to the V-band and we observe the rising side of the inverse Compton bump in the X-rays (see Fig. 4.2). This might happen for FRI galaxies considering that, in the relativistic beaming scenario, the double-peaked shape of the SED is expected to be preserved but shifted to lower frequencies with respect to the BL Lacs. However, the required beaming factor would be quite large, at least of the order of ten or more.

Another possibility is that, since the data points are from non-simultaneous observations, variability might have affected the true shape of the SED. In this case our parabolic model would not be reliable. On the other hand, this is usually not a problem for the FRI galaxies which do not show strong variability.

The most likely possibility is that the SEDs of these objects are atypical. In fact, almost all of them show peculiar features, such as dust lanes (M 84, 3C 270, 4C +26.42), highly distorted radio structures (3C 288) or intermediate FRI/FRII radio properties (Her A). Therefore, these objects are probably not representative of the FRI class and we will consider the parameterization of their SEDs as not reliable.

From the parabolic model it is in principle possible to calculate the peak frequency $\nu_{\rm peak}$ and the corresponding power $\nu_{\rm peak}L_{\nu_{\rm peak}}$. By applying the parabolic parameterization to the curves in Fig. 4.2 from Donato et al. (2001) it can be found that, in general, the thus calculated $\nu_{\rm peak}$ agrees with the true peak position within an error of $\sim 10\%$ and the $\nu_{\rm peak}L_{\nu_{\rm peak}}$ within $\lesssim 10\%$. Therefore, $\nu_{\rm peak}$ can be used in the majority of cases as a good criterium to distinguish between LBL and HBL. In fact, it can be seen from Fig. 7.19 that most of the objects with $\alpha_{\rm rx} \lesssim 0.75$ corresponding to the definition of HBL (Fossati et al. 1998) have $\nu_{\rm peak} \gtrsim 10^{14-15}$ Hz, whereas those with $\alpha_{\rm rx} \gtrsim 0.75$ corresponding to LBL have $\nu_{\rm peak} \lesssim 10^{14-15}$ Hz. Only the FRI galaxies have too high or too low $\nu_{\rm peak}$ with respect to their $\alpha_{\rm rx}$. Those with very low $\nu_{\rm peak}$ are the peculiar objects discussed above, for which the parabolic parameterization of their SED very likely cannot be applied. However, the $\alpha_{\rm rx}$ criterium has been defined for BL Lacs and not for the FRI galaxies. The fact that at a given peak frequency the FRI galaxies have larger $\alpha_{\rm rx}$ than BL Lacs might be an indication that the X-ray emission is more beamed than the radio emission when the viewing angle

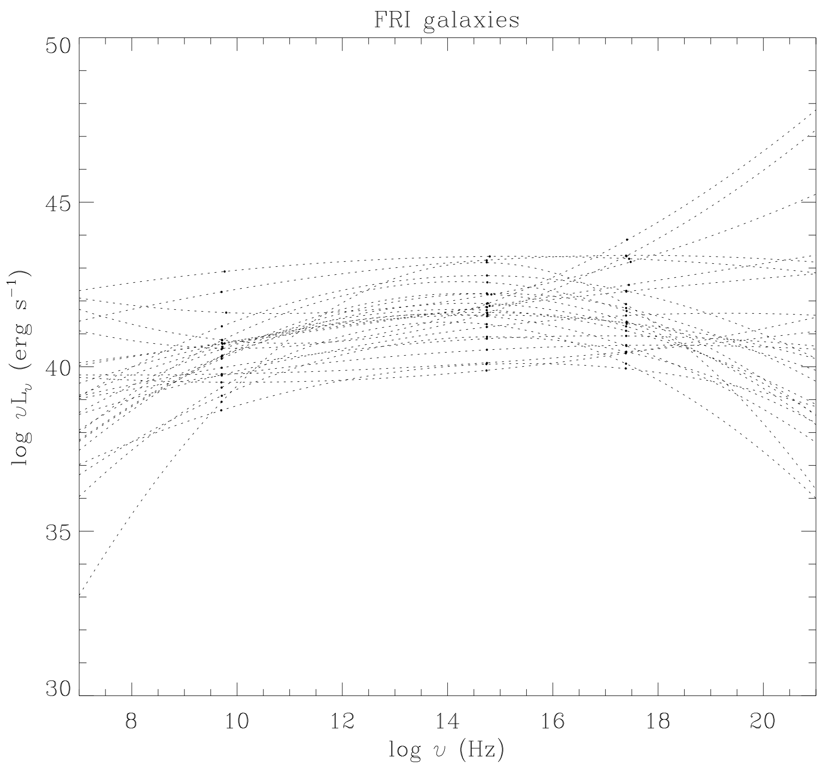

Figure 7.17: *The parabolic parameterizations of the SEDs of FRI galaxies.*

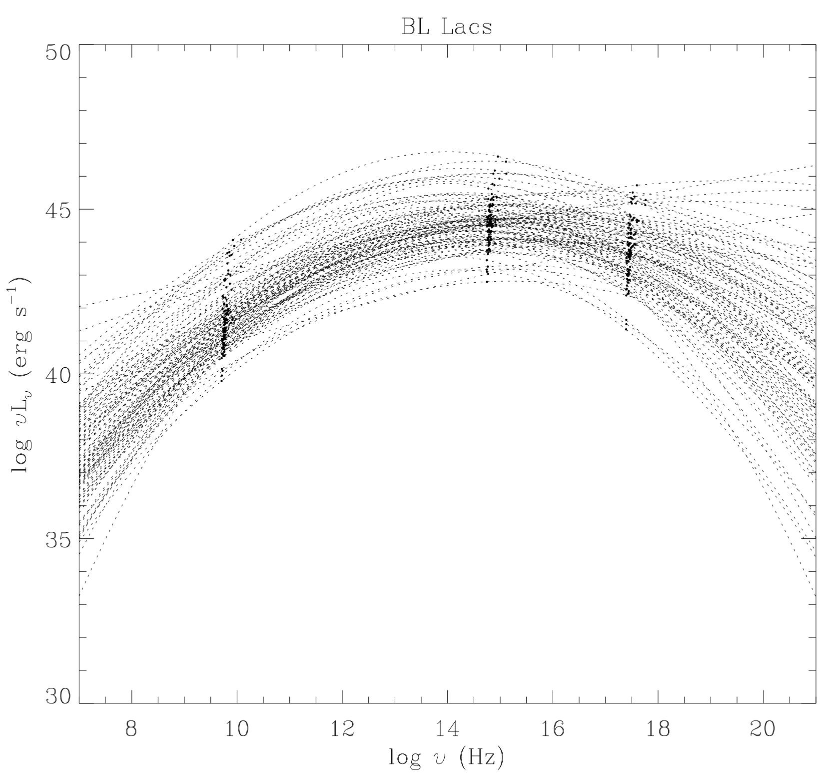

Figure 7.18: *The parabolic parameterizations of the SEDs of BL Lacs.*

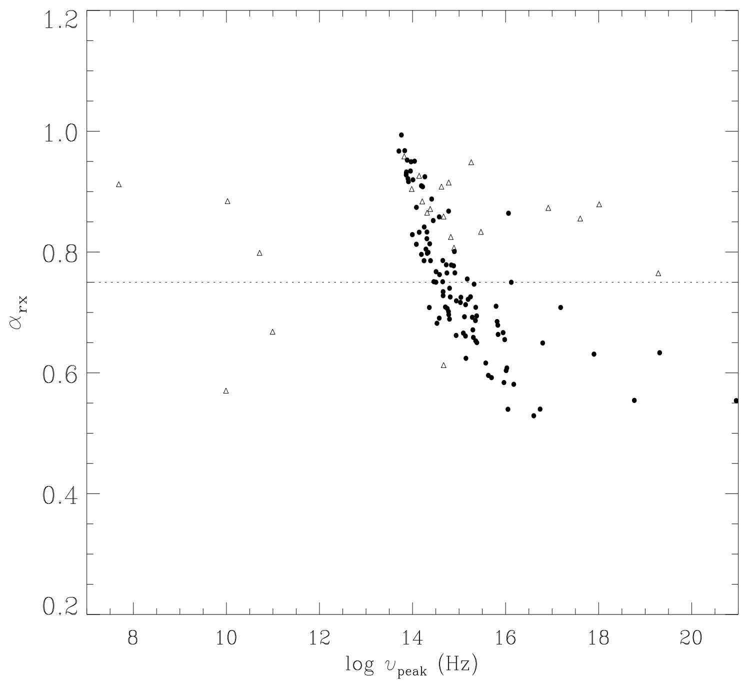

Figure 7.19: *The broad band spectral index α_{rx}, calculated at 5 GHz and 1 keV, plotted versus* $\log \nu_{peak}$ *as obtained from the parabolic parameterization of the SEDs of the FRI galaxies (triangles) and BL Lac objects (circles).*

becomes smaller.

Excluding the peculiar sources with a concave parabola, the ν_{peak} of both BL Lacs and FRI galaxies fall in the range from $\sim 10^{13}$ to 10^{20} Hz with no statistically significant difference ($z = 0.27$, *prob.* $= 0.79$ from a two-sample test) at the 5% level between the two classes. On the other hand, BL Lacs have significantly higher $\nu_{peak}L_{\nu_{peak}}$ than FRI galaxies ($z = 7.04$, *prob.* $= 0$, see Fig. 7.20). This is in agreement with the beaming model where the luminosities are shifted to higher values by an amount δ^4 (in the case of an isotropic source) and the frequencies only by δ (see Eq. 3.6 and 3.3). The largest discrepancies between the two classes are therefore expected in the luminosities and not in the peak frequencies where a significant overlap should be observed.

7.4.2 Beaming the SEDs of FRI galaxies

If, as currently believed, the FRI galaxies are the parent population of BL Lac objects their nuclear properties should be consistent with those of BL Lacs after relativistic beaming has been taken into account. Therefore, to test if the results are consistent with the claim that BL Lacs are the beamed counterparts of FRI galaxies, we apply relativistic beaming to the parabolic SEDs of FRI galaxies from § 7.4.1 and we calculate the "beaming tracks" in the various luminosity-luminosity planes. The frequencies and the monochromatic luminosities are beamed according to Eq. (3.3) and (3.5). As a first step the same amount of beaming, i.e. the same δ, has been used in all three wavebands. For the spectral indices α we use the slopes calculated locally from the parabolic parameterization of the SED of each source.

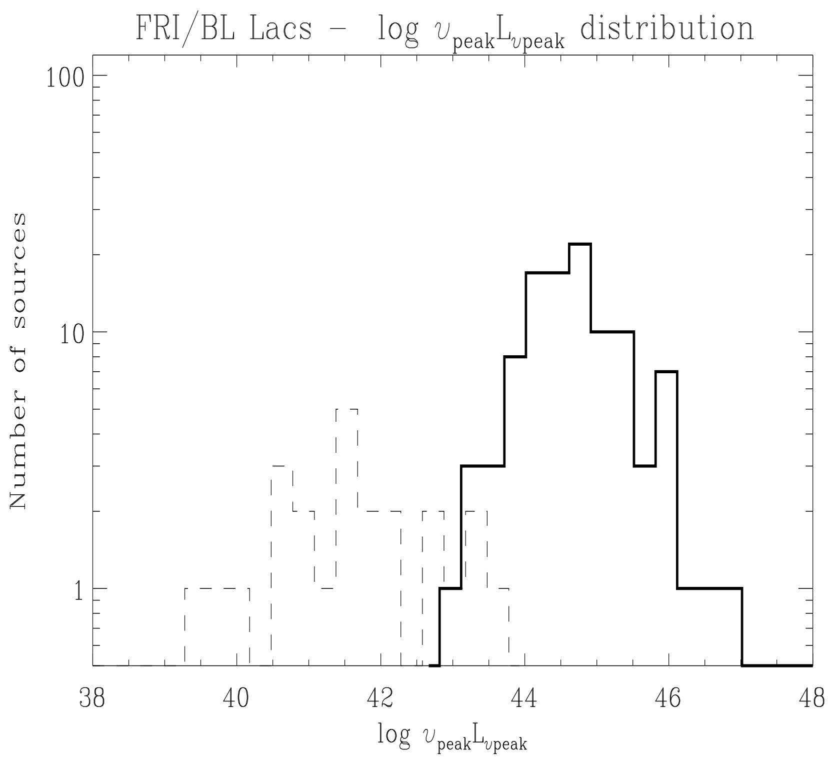

Figure 7.20: *The $\nu_{\mathrm{peak}}L_{\nu_{\mathrm{peak}}}$ distributions of FRI galaxies (dashed line) and BL Lacs (solid line).*

We checked if the use of these slopes is appropriate by comparing those inferred from the SEDs in Fig. 4.2 with those obtained from their parabolic parameterization. In general the parabolic slopes can differ considerably from the true ones, however, the discrepancies in the beaming tracks obtained in the two cases do not significantly affect the results.
The resulting beaming tracks for five selected objects with $\nu_{\rm peak}$ which are representative of the whole range of values obtained for the FRI galaxies are shown in Figs. 7.21-7.23.

In every luminosity-luminosity plane the beamed FRI galaxies appear to fall into the BL Lac region for $\delta = 4 - 10$. However, most of the objects with beaming tracks crossing the HBL region of the $L_{\rm X} - L_{\rm O}$ plane tend to fall in the LBL region of the $L_{\rm X} - L_{\rm R}$ and $L_{\rm R} - L_{\rm O}$ planes, as if the radio emission were too much enhanced with respect to that in the other two bands. We therefore apply different beaming factors in the three wavebands to see if better results could be obtained. As shown in Fig. 7.24-7.26, we find good agreement between the luminosities of "beamed" galaxies and BL Lacs for $\delta_{\rm x} = 4$, $\delta_{\rm o} = 5$ and $\delta_{\rm r} = 2$ (assuming p=2, see Eq. (3.5)). The majority of the beamed objects fall now consistently in the HBL regions in all of the luminosity-luminosity planes. The objects with a concave SED also fall mostly in the HBL regions, however, the results are in this case not reliable since we are not sure that their SEDs can be well represented by a parabola.
In § 7.5 the choice of these beaming factors will be further justified.

7.5 Interpretation of results

In this section we discuss the main results of the regression analyses and of the modeling of the SEDs of the objects, reported in §§ 7.3 and 7.4.1, in the context of the unification scheme for FRI galaxies and BL Lacs.

7.5.1 Low-energy and High-energy-peaked FRI galaxies

Since two kinds of BL Lac objects exist, LBL and HBL, if the unification scheme is valid it is expected to find these subclasses also among their parent objects, i.e. the FRI galaxies. As remarked in the introduction of this chapter, there is some evidence, although still not constraining, that this is the case (Trussoni et al. 2003). From the parabolic parameterization of the SED of the FRI galaxies in our sample, described in § 7.4.1, we find that 19 have $\nu_{\rm peak} \gtrsim 10^{14-15}$ Hz, and would thus be associated to HBL since beaming would shift it to even higher values. The only objects with unusual $\nu_{\rm peak} << 10^{14}$ Hz are those with a concave parabolic SED that, as we have already remarked in § 7.4.1, are all atypical FRI galaxies. Leaving them aside, it seems that only HBL-like galaxies are present in our sample. This is also supported by the results of § 7.4.2 where we have found that almost all objects would fall in the HBL region if their luminosities were beamed.
The absence of Low-energy-peaked FRI galaxies might, however, be the consequence of selection effects. From the average luminosities listed in Table 7.1 it is possible to estimate the "amount of beaming" using Eq. (3.5) which, taking the logarithms, transforms into:

$$\log L_\nu^{\rm beamed} - \log L_\nu^{\rm unbeamed} = (p + \alpha_\nu) \log \delta_\nu = \Delta_\nu \tag{7.2}$$

The quantity Δ_ν depends both on the beaming factor δ_ν and on the spectral slope α_ν. Since we have found that our FRI galaxies are essentially all High-energy-peaked objects,

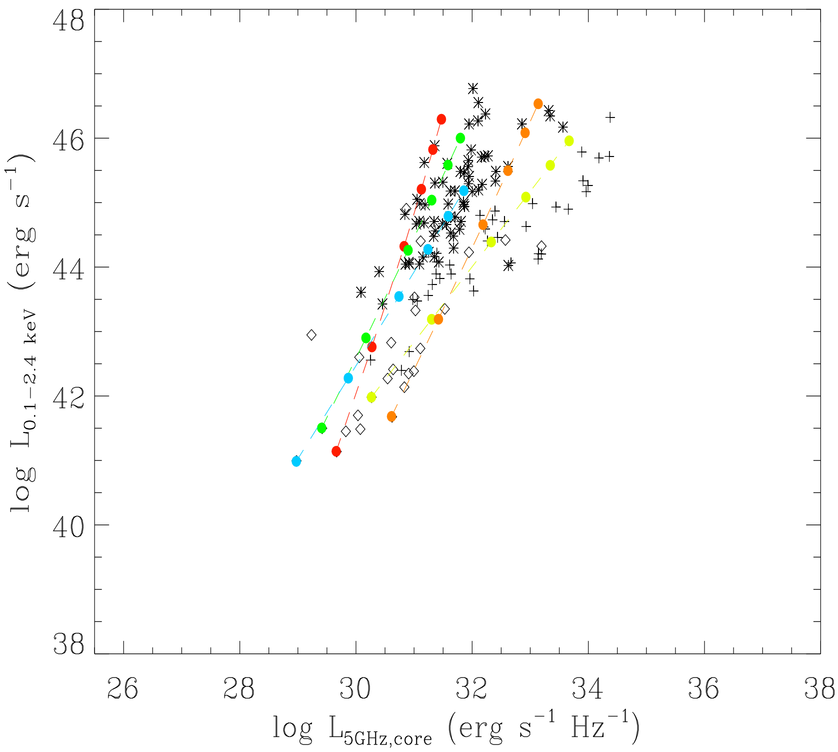

Figure 7.21: *Beaming tracks in the L_{X}-$L_{\mathrm{5GHz,core}}$ plane for 5 FRI galaxies. FRI galaxies are represented by diamonds, LBL by crosses and HBL by stars. The colored circles lying on the beaming tracks correspond to increasing values of* $\delta = 0, 2, 4, 6, 8, 10$.

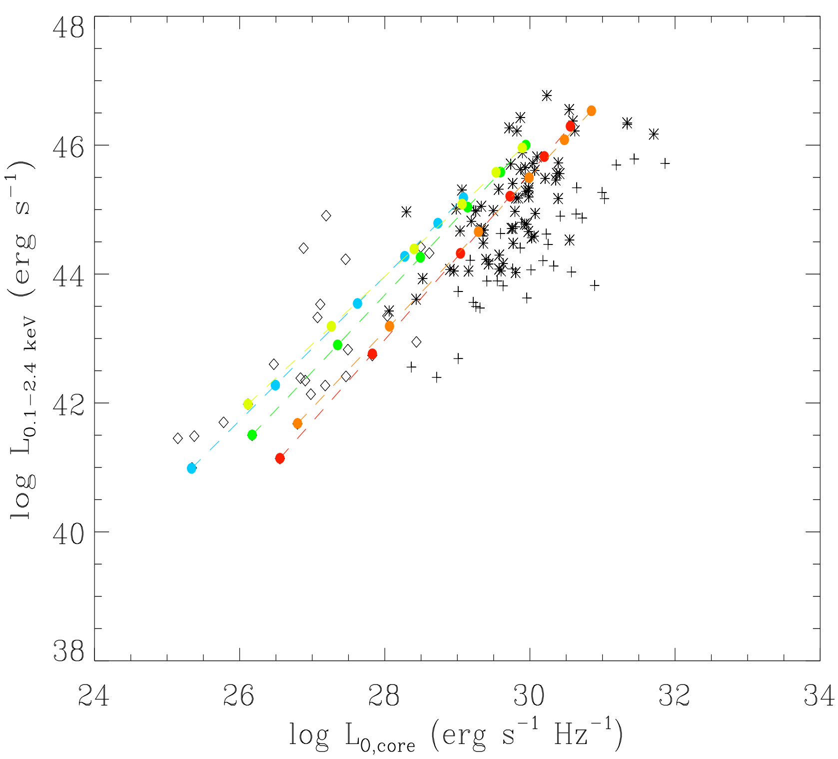

Figure 7.22: *Beaming tracks in the L_{X}-$L_{\mathrm{O,core}}$ plane for 5 FRI galaxies. FRI galaxies are*

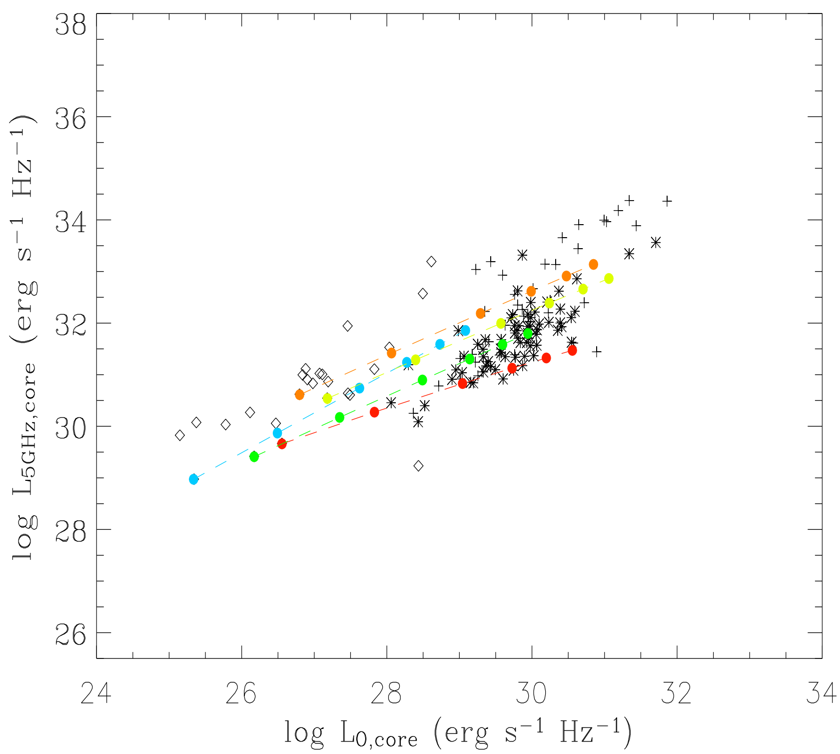

Figure 7.23: *Beaming tracks in the $L_{R,core}$-$L_{O,core}$ plane for 5 FRI galaxies. FRI galaxies are represented by diamonds, LBL by crosses and HBL by stars. The colored circles lying on the beaming tracks correspond to increasing values of $\delta = 0, 2, 4, 6, 8, 10$.*

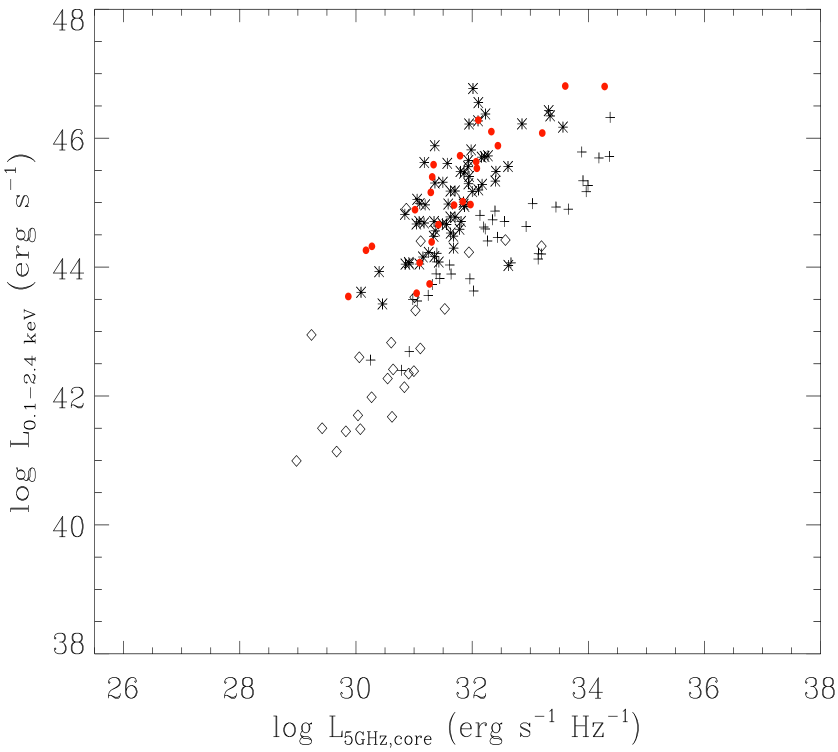

Figure 7.24: *Results from the application of relativistic beaming to the FRI galaxies with $\delta_{\mathrm{r}} = 2$ and $\delta_{\mathrm{x}} = 4$ (red circles) compared to the BL Lacs. FRI galaxies are represented by diamonds, LBL by crosses and HBL by stars.*

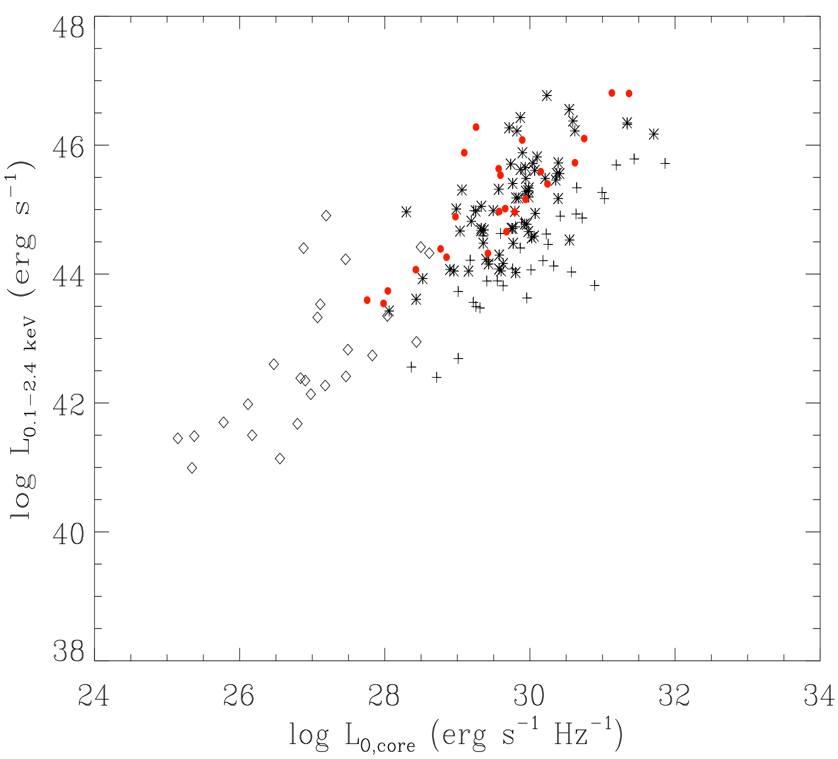

Figure 7.25: *Results from the application of relativistic beaming to the FRI galaxies with $\delta_{\mathrm{r}} = 4$ and $\delta_{\mathrm{x}} = 5$ (red circles) compared to the BL Lacs. FRI galaxies are represented by*

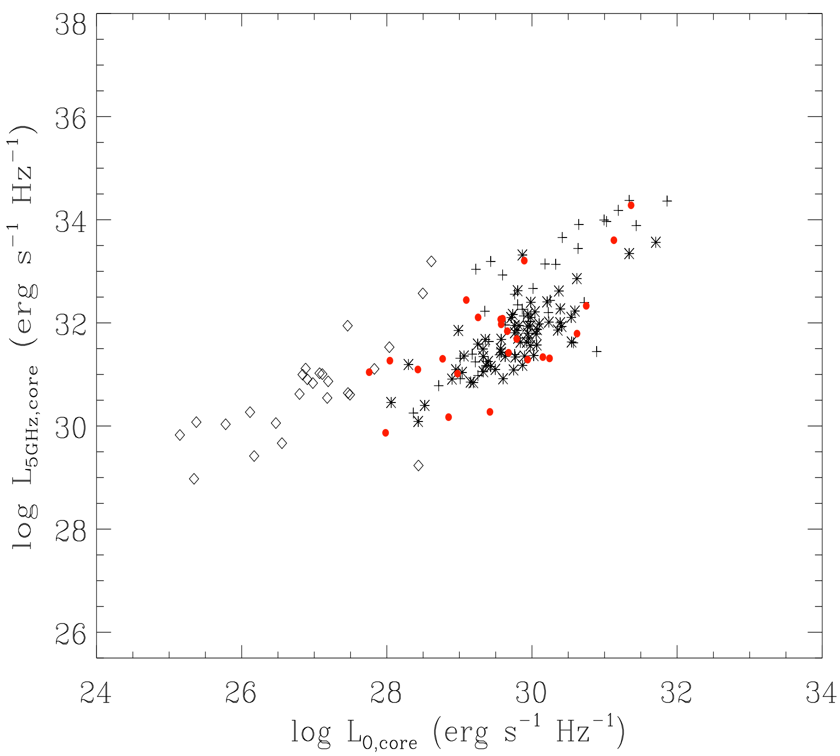

Figure 7.26: *Results from the application of relativistic beaming to the FRI galaxies with* $\delta_r = 2$ *and* $\delta_o = 5$ *(red circles) compared to the BL Lacs. FRI galaxies are represented by diamonds, LBL by crosses and HBL by stars.*

in order to get δ_ν we compare their luminosities with those of HBL only. As spectral slopes we use the average values of those obtained from the parameterized SEDs of the single objects, namely $\alpha_{\rm x} = 1.0$, $\alpha_{\rm r} = 0.6$ and $\alpha_{\rm o} = 0.9$. For p=3(2) we get $\delta_{\rm x} \sim 4(8)$, $\delta_{\rm r} \sim 2(3)$ and $\delta_{\rm o} \sim 5(10)$. Assuming, in agreement with the currently accepted scenario, that the same amount of beaming applies to both HBL and LBL we can use these values to calculate the expected luminosities of *LBL-like* FRI galaxies from those of LBL. We obtain luminosities $L_{\rm X} \sim 10^{42}$ erg s^{-1}, $L_{\rm R,core} \sim 10^{31}$ erg s^{-1} Hz^{-1} and $L_{\rm O,core} \sim 10^{28}$ erg s^{-1} Hz^{-1}. These are of the same order as those of FRI galaxies in our sample. In particular, LBL-like objects do not seem to be excluded because of too low X-ray or optical core luminosities and, even using a higher radio beaming factor comparable to those in the other two bands would still lead to detectable cores. On the other hand, the assumption that the same beaming factors apply to both LBL and HBL could be incorrect.
A possibility with important consequences for the unified scheme might be that LBL-like FRI galaxies do not exist. The best way to further investigate this point would be to perform a detailed sampling of the SEDs of radio galaxies at as many frequencies as possible, with both high spatial resolution and sensitivity. It is hopeful that this will become feasible in the future with the help of improved instrumentation, both in space and on the ground.

7.5.2 The amount of beaming in BL Lacs

Comparing the nuclear luminosities of HBL with those of FRI galaxies we find that $\delta_{\rm x} = 4(8)$, $\delta_{\rm r} = 2(3)$ and $\delta_{\rm o} = 5(10)$ for p=3(2) (see § 7.5.1). Beaming the FRI luminosities using these Doppler factors reproduces quite well the behavior of HBL in the various luminosity-luminosity planes. Therefore it appears that our data indicate a similar amount of beaming in the X-ray and optical bands, but lower at radio frequencies. To estimate the beaming in the radio band we have used an average spectral index $\alpha_{\rm r} = 0.6$, but the value obtained from measurements is $\alpha_{\rm r} = 0.14$. Using this, however, does not change much the inferred $\delta_{\rm r}$ which remains of the order 2(3).
This low beaming factor might also be explained by the presence of a decelerating jet, as proposed for example by Georganopoulos & Kazanas (2003) and supported also by VLBA (Marscher 1999) and VLBI (Edwards & Piner 2002) observations. We know from variability studies that the X-rays are produced much closer to the central black hole than the radio emission. Therefore, if the jet is decelerating between these two emission regions, a lower beaming factor is expected in the radio band. However, this model cannot be proved by our data.

7.5.3 Luminosity correlations and unification scheme

We will now analyze wether the correlations found for FRI galaxies and BL Lacs are in agreement with the predictions of the unified scheme.
In the extremely simple model in which only one component is responsible for the emission at all observed wavelengths, the slopes of the correlations should not change when relativistic beaming is applied to the luminosities of the objects. FRI galaxies and BL Lacs should therefore exhibit correlations with similar slopes inside the statistical errors. In fact, assuming that a certain class of objects follows the correlation:

$$\log \mathcal{L}_1 = a + b \log \mathcal{L}_2 \tag{7.3}$$

applying Eq. (3.5) to $\mathcal{L}_1$ and $\mathcal{L}_2$ would lead to a relationship between the beamed luminosities:

$$\log L_1 = \alpha + \beta \log L_2 \tag{7.4}$$

where:

$$\alpha = a + (p + \alpha_1) \log \delta_1 - b(p + \alpha_2) \log \delta_2 \tag{7.5}$$

and $\beta = b$. The slope b does not change, independently of the values adopted for the spectral slopes α_1 and α_2 and the beaming factors δ_1 and δ_2. The effect of beaming is simply to shift the intercept of the regression line, either to higher or to lower luminosities.

To better show the effect of relativistic beaming on the luminosity correlations we have performed a few simulations. We consider, as an example, the case of the X-ray - to - radio core correlation of FRI galaxies but the results can be generalized to any pair of luminosities. Fig. 7.27 shows the case in which the luminosities of the parent population are beamed assuming that the Doppler factors and spectral indices are the same for all sources, but different in the two wavebands. Values corresponding to $\delta_{\rm r} = 2$ and $\delta_{\rm x} = 12$ have been chosen to make the effect of beaming more evident and $\alpha_{\rm r} = 0.0$ and $\alpha_{\rm x} = 1.0$ have been used to approximately mimic the case of High-energy-peaked objects. As it can be seen, the effect of beaming has, in this case, the only effect of moving the regression line to higher luminosity in the vertical direction, but the slope is unchanged.

We can therefore compare the regression parameters (given in Table 7.2) of the FRI galaxies with those of BL Lacs and check if they are consistent with this model. We will use the results for the HBL only since, as discussed above, the FRI galaxies in our sample are exclusively associated with this class.
Only in the case of the $L_{\rm R,core}$-$L_{\rm O,core}$ correlation the slopes for FRI galaxies and HBL are similar within the errors, consistently with the hypothesis that the same component is responsible for the emission at both wavelengths. In the other two cases the slope of the HBL is significantly steeper than that of the FRI galaxies.

To investigate how, in the context of a simple beaming model involving only one emission component, the slope of a correlation can vary we have performed further simulations changing the assumptions on the beaming factors and the spectral indices of the sources. Figs. 7.28 and 7.29 show the results obtained assuming that, in the first case, the beaming factors differ among the sources and are gaussianly distributed, and, in the second case, that the beaming factor is a linear function of the luminosity of the objects. In both simulations there are some indications that the slope changes, however, the scatter of the beamed objects is too large with respect to what is actually found and the overall behavior does not reproduce well that observed for the HBL in our sample. Therefore, although a range of Doppler factors might contribute to modify the slope of a correlation, the results above do not provide strong evidence that this is decisive. We also remark that using different distributions for the beaming factors (i.e. uniform, bimodal, etc.) or beaming

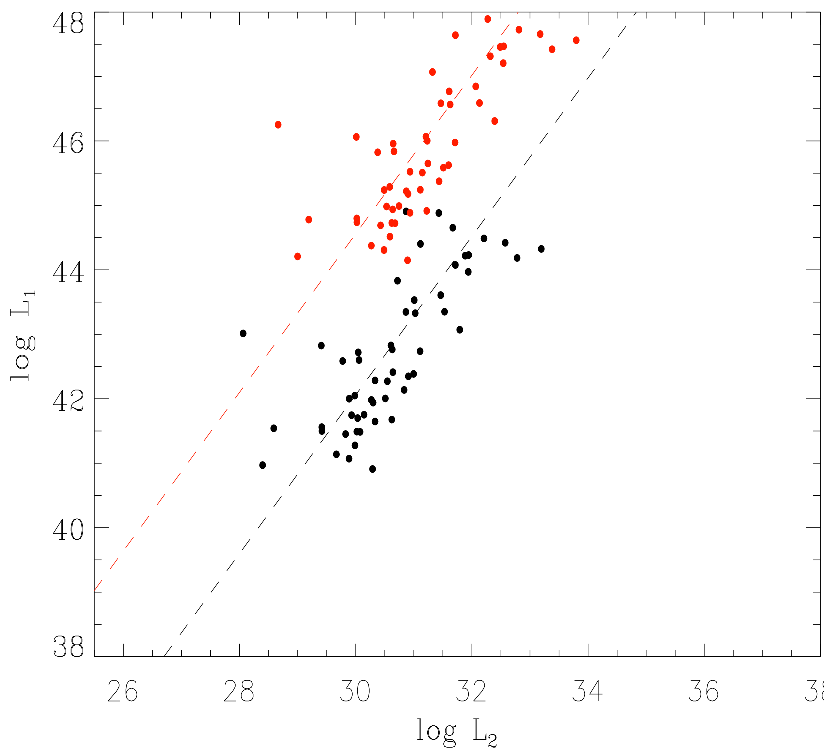

Figure 7.27: *Simulation of the effect of relativistic beaming onto a population of objects characterized by a linear correlation between two given luminosities. Unbeamed and beamed objects, together with their best fit regression lines, are plotted in black and red, respectively. The black dots are the real X-ray and radio core luminosities of the FRI galaxies. The same beaming factors ($\delta_1 = 12$ and $\delta_2 = 2$) and spectral indices ($\alpha_1 = 1.0$ and $\alpha_2 = 0.0$) have been used for all sources.*

only 10% of one of the luminosities or using a range of spectral indices for the sources, all lead to very little changes in the slope of the correlations.

None of the attempts to interpret the different slopes of the correlations of the unbeamed and beamed populations in terms of simple relativistic beaming models with only one emission component have been successful. It seems, therefore, that more emission components are required. Since different slopes are found for both correlations involving the X-ray luminosity it is reasonable to postulate the existence of (at least) an additional X-ray component. The simplest model capable to explain the observed change in slope would thus be that in FRI galaxies the first component is dominant, whereas the second one is too weak or hidden, and in BL Lacs the second component becomes prominent with respect to the first one due, for example, to relativistic beaming. Both components should be correlated to the radio and optical emission but with different slopes, as observed. A similar two-component model has been suggested before for the radio-loud quasars (Zamorani et al. 1981, Browne & Murphy 1987, Kembhavi 1993, Baker et al. 1995) a fact which would establish a close relationship between the emission mechanisms in the two classes of objects (but see also the discussion of § 8.4.1).
A possible candidate for this additional component is unresolved thermal emission from the hot corona of the host galaxy. However, it is difficult to explain how this could be so tightly correlated with the radio and optical emission. A tentative and qualitative justification for such correlations might be that with larger gas masses of the hot corona, and thus larger X-ray luminosities, more fuel is available for the AGN, consequently resulting in an overall increased power and therefore also in larger radio and optical luminosities. However, the nature of such a component cannot be established by these data and it would be desirable to determine it through a detailed X-ray spectral analysis, either from XMM or Chandra observations, of a large sample of FRI galaxies, with both higher sensitivities and spatial resolution than ROSAT.

7.6 Summary of results

- BL Lac objects, both LBL and HBL, differ from FRI galaxies in having brighter cores at all wavelengths, in agreement with the relativistic beaming scenario. LBL are brighter than HBL in the optical and in the radio bands, whereas HBL are significantly brighter in X-rays, consistently with the different shapes of their SEDs.

- BL Lac objects and FRI galaxies have a comparable range of extended radio luminosities, however, the objects in the second class are less core-dominated, as predicted by the unified scheme. LBL and HBL appear similarly core-dominated.

- The nuclear luminosities at all wavelengths are highly correlated in both, BL Lacs and FRI galaxies. HBL and FRI galaxies follow a similar $L_{\rm R,core}$-$L_{\rm O,core}$ correlation with a slope $b \sim 1$, whereas the slopes of the $L_{\rm X}$-$L_{\rm O,core}$ and $L_{\rm X}$-$L_{\rm R,core}$ are different for FRI galaxies ($b = 1.33 \pm 0.20$ and $b = 1.23 \pm 0.12$, respectively) and HBL ($b = 1.72 \pm 0.11$ and $b = 1.32 \pm 0.12$, respectively). All slopes found for the LBL differ from those of the other two classes ($b = 1.51 \pm 0.15$, $b = 1.25 \pm 0.09$ and $b = 0.79 \pm 0.06$ for the $L_{\rm R,core}$-$L_{\rm O,core}$, $L_{\rm X}$-$L_{\rm O,core}$ and $L_{\rm X}$-$L_{\rm R,core}$ correlations, respectively).

- From the modeling of the SEDs of the FRI galaxies the estimated synchrotron peak

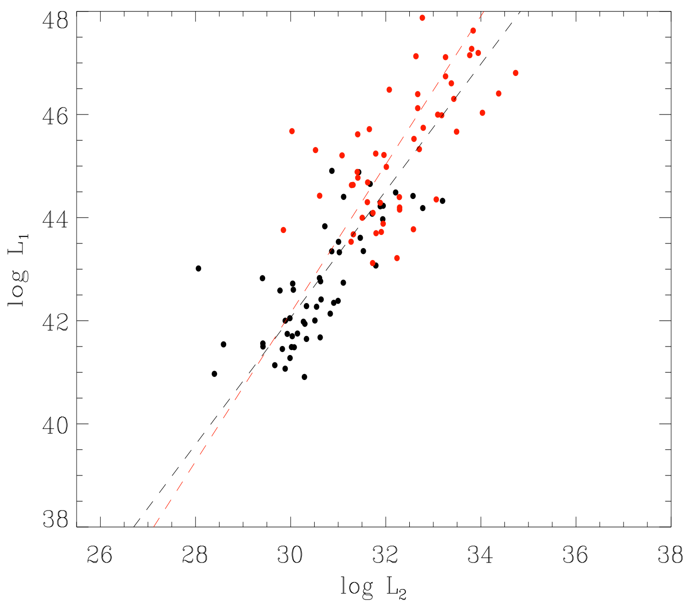

Figure 7.28: *Simulation of the effect of relativistic beaming onto a population of objects characterized by a linear correlation between two given luminosities. Unbeamed and beamed objects, together with their best fit regression lines, are plotted in black and red, respectively. The black dots are the real X-ray and radio core luminosities of the FRI galaxies. A Gaussian distribution of beaming factors is assumed and the same spectral indices (*$\alpha_1 = 1.0$ *and* $\alpha_2 = 0.0$*) for all sources have been used.*

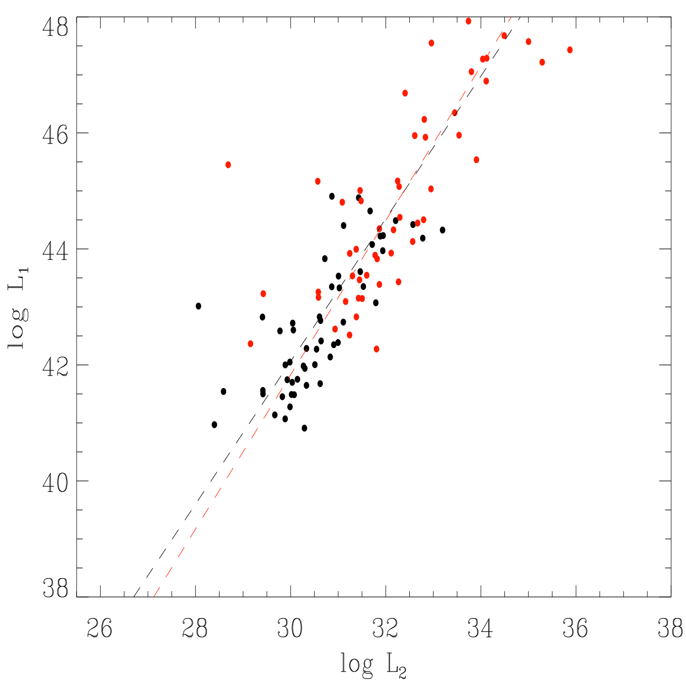

Figure 7.29: *Simulation of the effect of relativistic beaming onto a population of objects characterized by a linear correlation between two given luminosities. Unbeamed and beamed objects, together with their best fit regression lines, are plotted in black and red, respectively. The black dots are the real X-ray and radio core luminosities of the FRI galaxies. A beaming factor depending linearly on the luminosity is assumed and the same spectral*

frequencies are consistent with those of HBL-like objects except for a few peculiar sources. Selection effects seem not to have played any role in excluding LBL-like objects from our sample. A better sampling of the SEDs of FRI galaxies is needed to further investigate the existence of Low-energy-peaked objects in this class.

- Similar beaming factors ($\delta \sim 4-5$) are required in the X-ray and optical bands in order to interpret the BL Lacs (HBL) as the beamed counterparts of the FRI galaxies. A lower value appears to be required in the radio band ($\delta \sim 2-3$). A possible way to explain such a lower value is by means of a jet decelerating between the regions of X-ray and radio emission.
- The analysis of the correlations in the three wavebands leads to the requirement of (at least) two emission components in the X-ray band. Both components have to be correlated with the radio and optical emission. The nature of this second component cannot be determined from our data.

Chapter 8

The data: FRII galaxies vs. radio-loud quasars

8.1 Introduction

In the context of the unified scheme for radio-loud AGN FRII radio galaxies are considered to be the unbeamed counterparts of radio-loud quasars. With decreasing viewing angle the same object would be classified progressively as a Narrow Line Radio Galaxy (NLRG), then as a Broad Line Radio Galaxy (BLRG) or, at higher luminosities, as a Steep Spectrum Radio Quasar (SSRQ), and finally as a Flat Spectrum Radio Quasar (FSRQ). BLRG and SSRQ show both broad and narrow emission lines in their optical spectra contrary to the NLRG which have only narrow lines. However, the radio emission of all these three classes is dominated by the extended lobes and not by the core as in FSRQ.

The unification of SSRQ with FSRQ dates back to the relativistic beaming model proposed by Orr & Browne (1982). They determined the distribution of the core-dominance, defined as $R_{\rm C} = L_{\rm R,core}/L_{\rm R,extended}$ for a sample of randomly oriented sources and fitted it to the observed one for a complete sample of quasars. Using 5 GHz luminosities they found $R_{\rm C}(90^\circ) = 0.024$ at transverse orientation and a bulk Lorentz factor of $\Gamma \sim 5$.

Later on, Browne & Murphy (1987) developed this model further including also the X-ray emission, which is postulated to have two components, one directly proportional to the radio core emission and beamed at small viewing angles, and the other isotropic. Only for angles $\lesssim 15^\circ$ the beamed X-ray emission appears to be dominant with respect to the isotropic component. Different correlations are found between the X-ray and radio core luminosities of SSRQ and FSRQ, with slopes $b = 0.40 \pm 0.06$ and $b = 0.70 \pm 0.07$, respectively.

Kembhavi (1993) refined the Browne & Murphy (1987) model in order to estimate the separate contributions of the two X-ray components using the radio data.

Baker et al. (1995) confirmed the existence of tight correlations between the X-ray and the radio core luminosities of radio-loud quasars, with a slope ($b = 0.36 \pm 0.10$) in the case of SSRQ, flatter than that for FSRQ ($b = 0.79 \pm 0.05$). The presence of both an isotropic and a beamed anisotropic component for the X-ray emission is capable to explain such behavior supporting the Kembhavi (1993) model.

It must also be remarked that, from the analysis of Einstein data, two X-ray components

were already proposed for the quasars by Zamorani et al. (1981) in order to explain the larger X-ray luminosities of radio-loud with respect to the radio-quiet objects and their different spectral properties.
FSRQ are also included in the *blazar sequence* (Fossati et al. 1998, Donato et al. 2001, see § 7.1) with Low-energy-peaked and High-energy-peaked BL Lacs. They are the objects with the lowest synchrotron peak frequencies ($\nu_{\rm peak} < 10^{14}$ Hz) and the highest bolometric luminosities. Recently, however, Padovani et al. (2003) discovered some FSRQ with broad band spectral indices $\alpha_{\rm ro}$ and $\alpha_{\rm ox}$ typical of HBL, a fact which might question the blazar sequence scenario if supported by more data.

Our sample contains 94 FRII radio galaxies and 862 radio-loud quasars (RLQ) (of which 14 are also classified as FRII). We could collect radio core fluxes from the literature for 380 quasars and 56 FRII galaxies. Among these galaxies, 23 also have optical core fluxes (of which 8 are upper limits) from HST observations, reported in Chiaberge et al. (2002).
In X-rays many FRII galaxies have only upper limits, with 37 non-detections out of 94 objects, representing $\sim$ 39% of the total. A radio spectral index is available for 608 quasars: 387 are FSRQ ($\alpha_{\rm r} < 0.5$) and 221 are SSRQ ($\alpha_{\rm r} \geq 0.5$). For 286 quasars (187 FSRQ and 99 SSRQ) we have information on both the core flux and radio spectral index. 33 radio galaxies are also classified as NLRG and 17 as BLRG. Radio core fluxes are available for 23 NLRG and 13 BLRG and optical core fluxes for 8 NLRG and 9 BLRG only.

8.2 Luminosity distributions

In this section we analyse the properties of the luminosity distributions of FRII galaxies and radio-loud quasars. In Figs. 8.1-8.8 the histograms of the radio core, optical and X-ray luminosities and the 90% confidence contour plots of their means and intrinsic dispersions are presented; numerical values of the means and dispersions from both the Kaplan-Meier estimator and the Maximum Likelihood technique are given in Table 8.1. Results are shown separately for SSRQ, FSRQ, NLRG and BLRG. The optical luminosities of FRII galaxies are calculated from the core fluxes given in Chiaberge et al. (2000) extrapolated to the V band; those of radio-loud quasars are calculated from their total magnitudes.

8.2.1 The total radio luminosity distributions

Fig. 8.1 shows the distributions of the total radio luminosities of FRII galaxies and radio-loud quasars compared to the total sample and Fig. 8.2 displays the 90% confidence level contour plots of the mean luminosities and intrinsic dispersions. It seems that both, FRII galaxies and radio-loud quasars, share a common range of total radio luminosities, from $\sim 10^{30}$ to $\sim 10^{36}$ erg s^{-1} Hz^{-1}. However, a two-sample test finds a difference between the average luminosities for the two classes, which is significant at the 5% level ($z = 3.17$, *prob.* = 0.001). NLRG and SSRQ have comparable total radio luminosities, whereas BLRG appear to have slightly lower values. However, the difference with NLRG is only marginally significant ($z = 1.93$, *prob.* = 0.05) at the 5% level. FSRQ have significantly higher values than all other classes.

Average luminosities

Luminosity (1)	Group (2)	$\log L^{\mathrm{KM}}$ (3)	$\log L^{\mathrm{ML}}$ (4)
$L_{0.1-2.4\ \mathrm{keV}}$ (erg s^{-1})	FRII galaxies	43.46 ± 0.15	$44.09 \pm 0.87^{\dagger}$
	NLRG	42.89 ± 0.28	$43.75 \pm 1.00^{\dagger}$
	BLRG	44.24 ± 0.17	$44.32 \pm 0.65^{\dagger}$
	SSRQ	45.43 ± 0.04	45.43 ± 0.56
	FSRQ	45.69 ± 0.03	45.72 ± 0.60
$L_{\mathrm{O,core}}$ (erg s^{-1} Hz^{-1})	FRII galaxies	27.25 ± 0.30	$28.06 \pm 0.97^{\dagger}$
	NLRG	26.06 ± 0.23	$26.47 \pm 0.05^{\dagger}$
	BLRG	28.68 ± 0.16	$28.68 \pm 0.46^{\dagger}$
	SSRQ	30.72 ± 0.04	30.72 ± 0.57
	FSRQ	30.89 ± 0.03	30.90 ± 0.61
$L_{\mathrm{5GHz,tot}}$ (erg s^{-1} Hz^{-1})	FRII galaxies	33.53 ± 0.09	33.53 ± 0.86
	NLRG	33.70 ± 0.18	33.71 ± 1.06
	BLRG	33.17 ± 0.10	33.17 ± 0.40
	SSRQ	33.71 ± 0.05	33.71 ± 0.68
	FSRQ	34.37 ± 0.04	34.37 ± 0.80
$L_{\mathrm{5GHz,core}}$ (erg s^{-1} Hz^{-1})	FRII galaxies	31.43 ± 0.13	31.44 ± 0.94
	NLRG	31.12 ± 0.17	31.20 ± 0.80
	BLRG	31.82 ± 0.23	31.82 ± 0.82
	SSRQ	32.79 ± 0.08	32.78 ± 0.76
	FSRQ	33.99 ± 0.07	34.00 ± 0.90

† Detections only.

Table 8.1: *Column 1: luminosity. Column 2: group of objects. Column 3: mean of luminosity and related error from the generalized Kaplan-Meier estimator. Column 4: mean and intrinsic dispersion of luminosity from the Maximum-Likelihood technique.*

The intrinsic dispersions are significantly different from zero for all objects, with NLRG reaching a value of $\log \sigma_{\rm intr} \sim 1.1$ and the BLRG a much lower value of $\log \sigma_{\rm intr} \sim 0.4$. However, the total luminosities in the radio band are dominated by the core in FSRQ and by the lobes in the other classes, therefore it is necessary to compare separately the emission of these two components. This will be done in §§ 8.2.2 and 8.3.1.

8.2.2 The radio core luminosity distributions

The radio core luminosity distributions of FRII galaxies and radio-loud quasars are presented in Fig. 8.3 and the 90% confidence contour plots of the mean luminosities and intrinsic dispersions in Fig. 8.4.
It appears that, unlike what was observed for the total luminosities, the distributions of core luminosities for the two classes are more distinct, with that of the FRII galaxies moving to lower values in the range from $\sim 10^{29}$ to $\sim 10^{34}$ erg s^{-1} Hz^{-1}.
The hypothesis that the radio core luminosities of NLRG and BLRG belong to the same distribution can formally not be rejected ($z = 2.19$, $prob. = 0.03$). The core luminosities of SSRQ are significantly larger than those of both NLRG and BLRG and those of FSRQ are larger than for the SSRQ. These findings support the scenario in which NLRG, BLRG, SSRQ and FSRQ constitute a sequence of objects observed at progressively smaller viewing angles and therefore with increasingly beamed and more luminous cores.
As further support to this unified scheme, the hypothesis that the extended luminosities of FRII galaxies and radio-loud quasars, calculated by subtracting the core from the total luminosity, belong to the same distribution cannot be rejected at the 5% significance level ($z = 0.69$, $prob. = 0.49$).
The differences between intrinsic dispersions for the various classes are small, falling in a narrow range between $\log \sigma_{\rm intr} \sim 0.75 - 0.95$. Since NLRG and BLRG have very different intrinsic dispersions of the total but not of the core luminosities (see § 8.2.1) the former discrepancy has to be attributed to the extended emission. However, this is not easily explained in the context of the unified scheme.

8.2.3 The optical luminosity distributions

The optical luminosity of the host galaxy of a radio-loud quasar is usually dominated by the active nucleus. We can therefore compare the total optical luminosity of RLQ with the core optical luminosity of FRII radio galaxies.
The optical luminosity distributions of both FRII galaxies and radio-loud quasars are depicted in Fig. 8.5, whereas Fig. 8.6 shows the 90% confidence level contour plots of the mean luminosities and intrinsic dispersions for the various classes.
The distribution of the radio-loud quasars is situated at much larger optical luminosities than that of the galaxies, reaching $\sim 10^{33}$ erg s^{-1} Hz^{-1}, even if a few objects are found at values of $\sim 10^{27}$ erg s^{-1} Hz^{-1}, more typical of FRII galaxies.
FSRQ appear to have only a slightly higher average optical luminosity than SSRQ, however, a two-sample test finds this difference significant at the 5% level ($z = 3.10$, $prob. = 0.0$). Much larger, about three orders of magnitude, is the discrepancy between the optical core luminosities of FRII galaxies and those of both, SSRQ and FSRQ. Considering separately BLRG and NLRG it can be seen in Fig. 8.6 that the first class of objects has

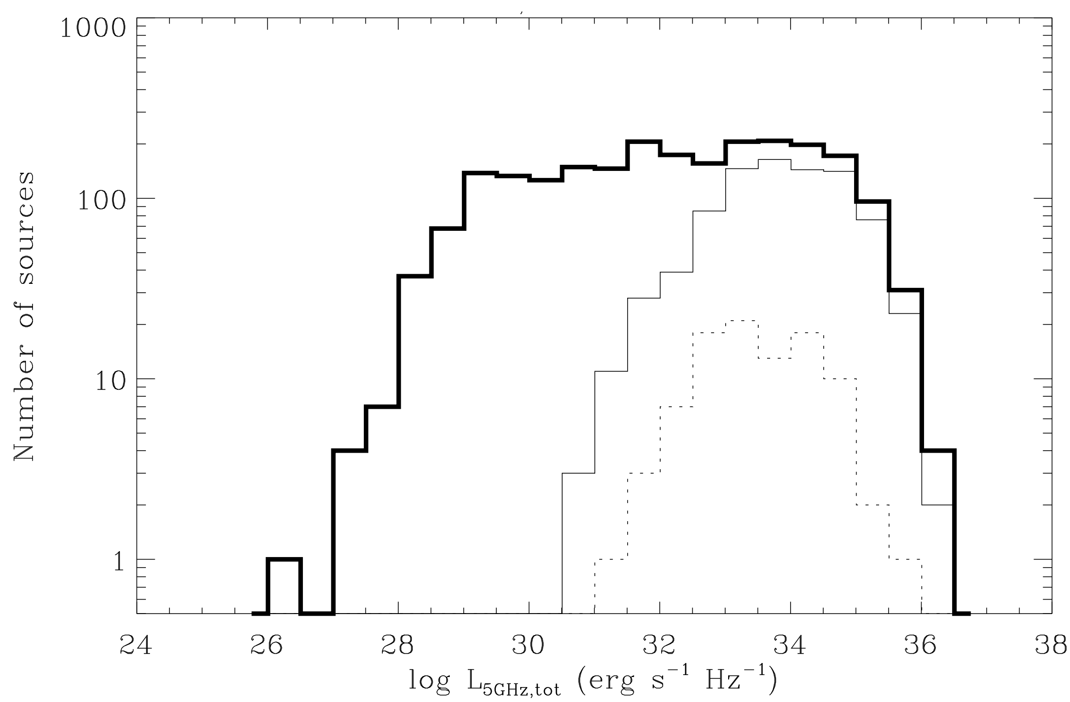

Figure 8.1: *Total* 5 *GHz radio luminosity distributions for the FRII galaxies (dotted line), the radio-loud quasars (thin solid line) and the total sample (thick solid line).*

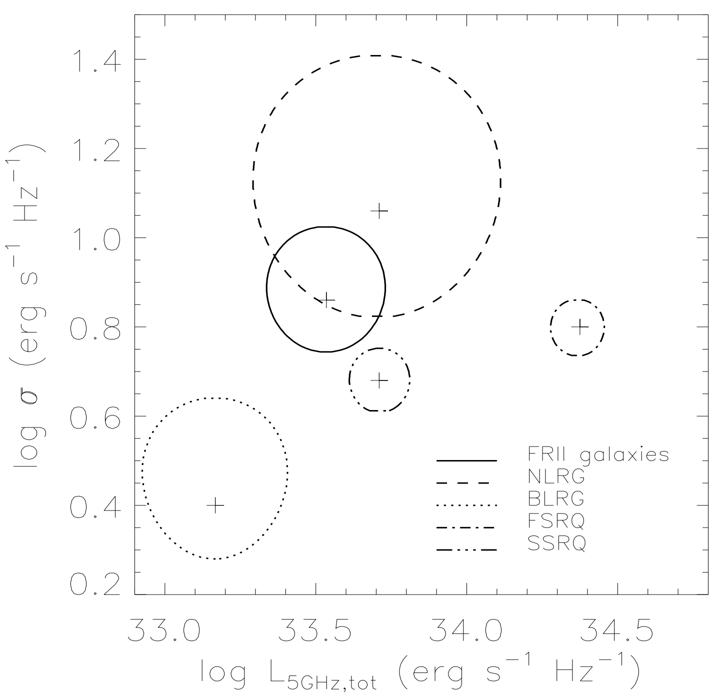

Figure 8.2: 90% *confidence level contour plots for the total* 5 *GHz luminosity and intrinsic dispersion of all FRII galaxies, NLRG, BLRG, SSRQ and FSRQ. The crosses indicate the average* log $L_{\mathrm{R,tot}}$ *and* log σ.

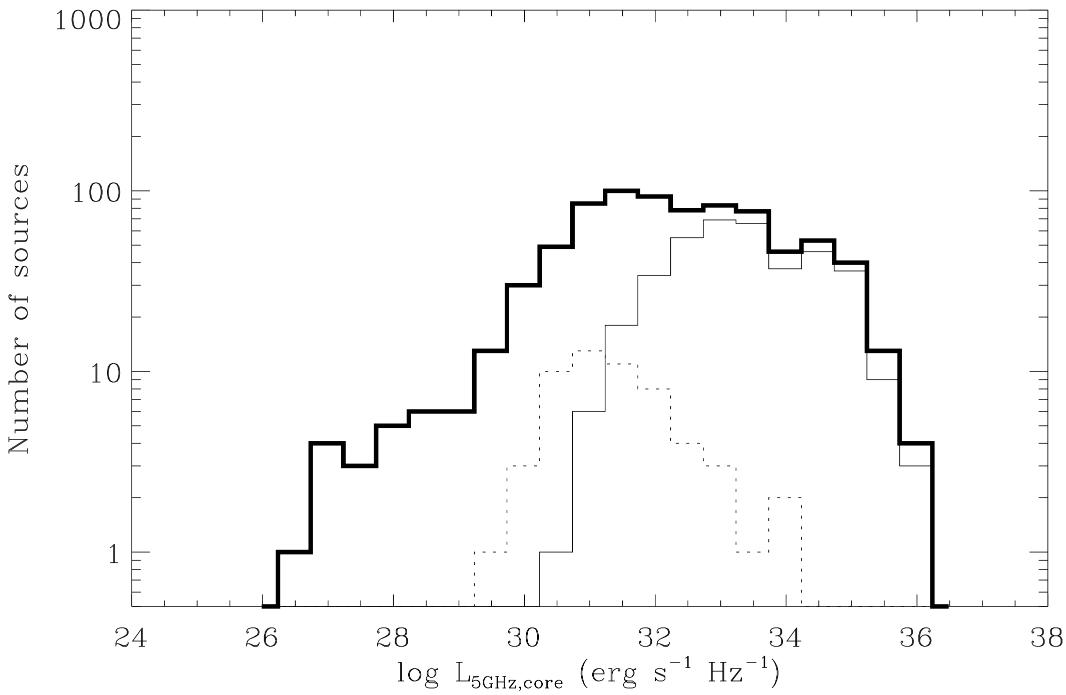

Figure 8.3: 5 *GHz core radio luminosity distributions for the FRII galaxies (dotted line), the radio-loud quasars (thin solid line) and the total sample (thick solid line).*

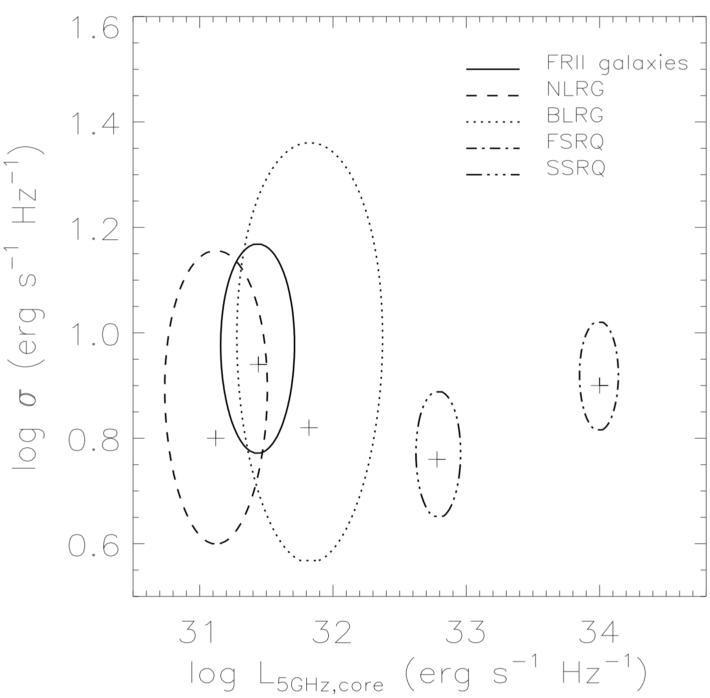

Figure 8.4: 90% *confidence level contour plots for the* 5 *GHz core luminosity and intrinsic dispersion of all FRII galaxies, NLRG, BLRG, SSRQ and FSRQ. The crosses indicate the average* $\log\ L_{\rm R,core}$ *and* $\log\ \sigma$.

luminosities more than two orders of magnitude larger than the second. However, it must be remarked that the number statistics is rather poor in this case, with only 9 and 8 objects in each class, respectively. The intrinsic dispersion is consistent with zero in the case of the NLRG alone, whereas it is larger for the BLRG. SSRQ and FSRQ have similar values around $\log \sigma_{\rm intr} \sim 0.6$.

8.2.4 The X-ray luminosity distributions

Similar to what was discussed in Chapter 7 for FRI galaxies and BL Lac objects, we can reasonably suppose that the X-ray emission in both, FRII galaxies and RLQ, is mainly non-thermal and of nuclear origin because it is known to be tightly correlated with that in the radio band (e.g. Hardcastle & Worrall 1999), also confirmed by the regression analysis discussed in § 8.3.4. We can therefore directly compare the X-ray properties of FRII galaxies with those of radio-loud quasars. Figs. 8.7 and 8.8 show their X-ray luminosity distributions and the 90% confidence level contour plots of their means and intrinsic dispersions, respectively.

The luminosities of FRII galaxies cover an interval of $\sim 10^{40} - 10^{46}$ erg s^{-1}, whereas those of radio-loud quasars range from $\sim 10^{42}$ to $\sim 10^{48}$ erg s^{-1}, with a wide overlap with the first class of objects.

The X-ray emission of both SSRQ and FSRQ is significantly stronger than that of FRII galaxies with luminosities higher by about two orders of magnitude, when upper limits are properly taken into account. SSRQ are less luminous than FSRQ and, according to a two-sample test, the difference is significant at the 5% level ($z = 4.75$, *prob.* $= 0.0$). Among the galaxies, BLRG have larger X-ray luminosities than NLRG and the hypothesis that they are drawn from the same distribution is also rejected at 5% significance level ($z = 3.18$, *prob.* $= 0.0$).

The above results are all in qualitative agreement with the unified scheme. The intrinsic dispersions of BLRG, SSRQ and FSRQ are approximately similar, around a value of $\log \sigma_{\rm intr} \sim 0.6$, whereas the NLRG show larger scatter with $\log \sigma_{\rm intr} \sim 1.0$.

8.3 Correlation and regression analysis

As we have seen in the introduction of this chapter good correlations of the X-ray with the radio core luminosity have been found for both SSRQ and FSRQ, however, with different slopes. This has suggested the existence of two X-ray components in radio-loud quasars. Significant correlations of the optical emission with both the X-ray and radio core emission have also been found (Browne & Murphy 1987, Baker 1997, Siebert et al. 1996, Brinkmann et al. 1997, Hardcastle & Worrall 1999) and are discussed in the various subsections below.

A good X-ray - to - radio core correlation is also known to exist for the FRII galaxies (Siebert et al. 1996, Hardcastle & Worrall 1999) and the close relationship between the optical and radio core luminosities was discussed in Chiaberge et al. (2000), although different trends were identified for BLRG and NLRG, with the first objects showing an optical excess with respect to the regression line obtained for the latter, coincident also with that found for FRI galaxies.

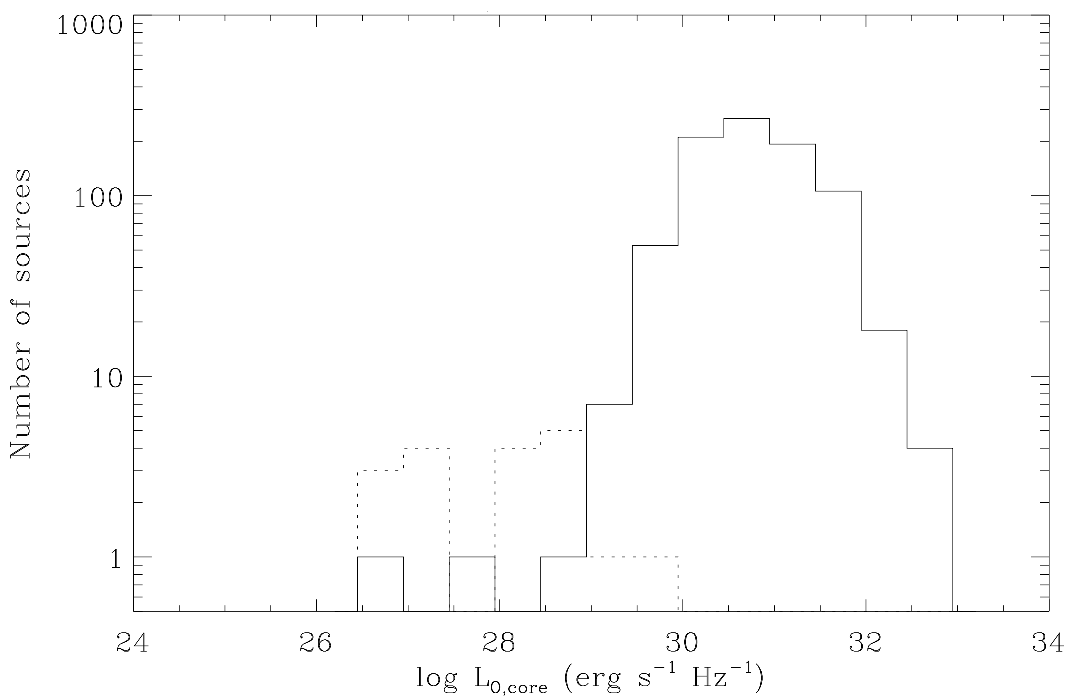

Figure 8.5: *Optical V-band luminosity distributions for the FRII galaxies (dotted line) and the radio-loud quasars (solid line). The total and core luminosities are used for the radio-loud quasars and the FRII radio galaxies, respectively.*

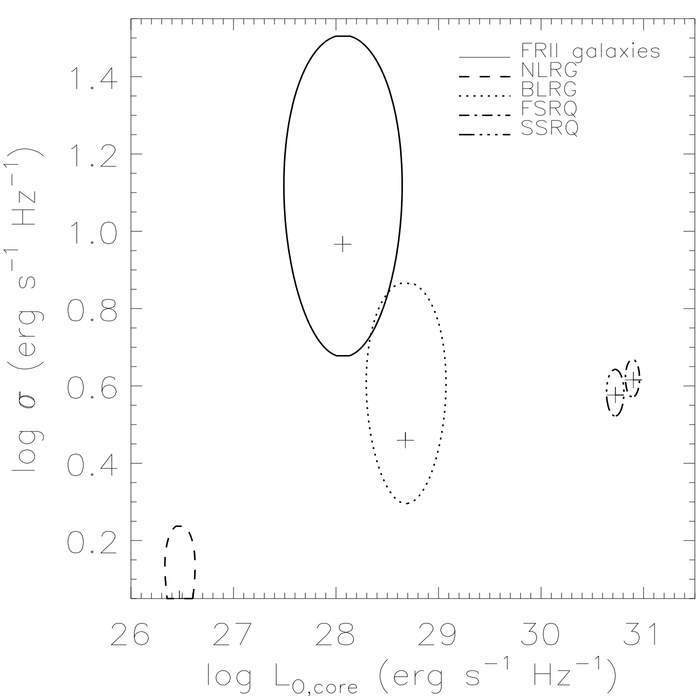

Figure 8.6: 90% *confidence level contour plots for the optical V-band luminosity of FRII galaxies, NLRG, BLRG, SSRQ and FSRQ. The total and core luminosities are used for the radio-loud quasars and the FRII radio galaxies, respectively.*

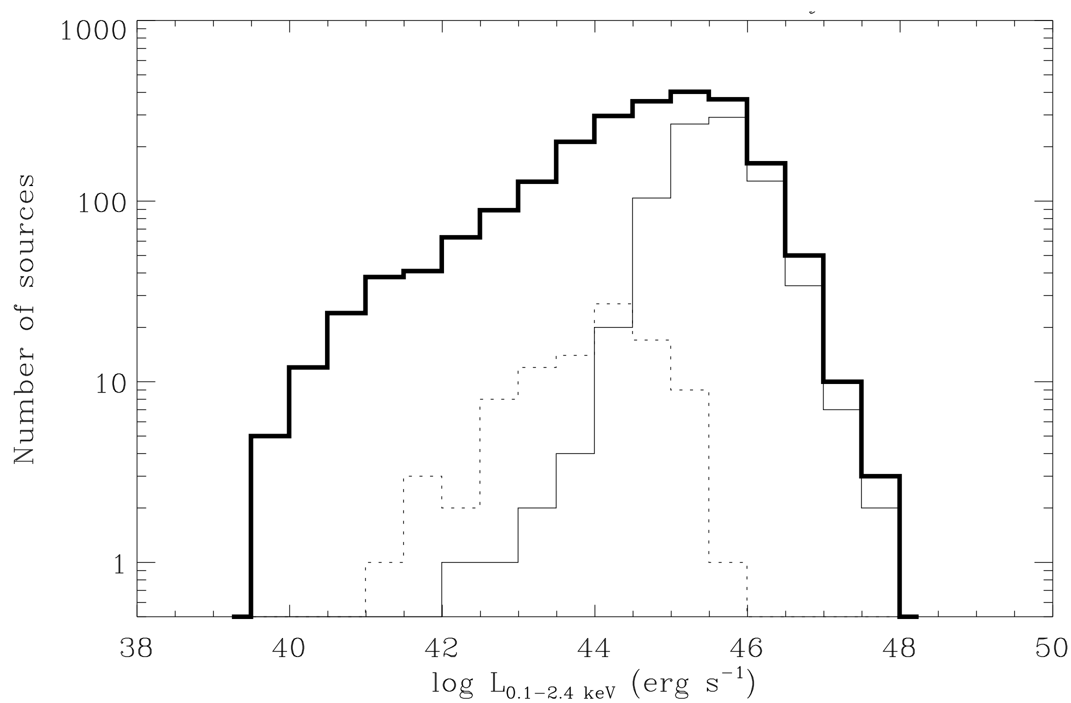

Figure 8.7: *X-ray luminosity distributions for the FRII galaxies (dotted line), the radio-loud quasars (thin solid line) and the total sample (thick solid line).*

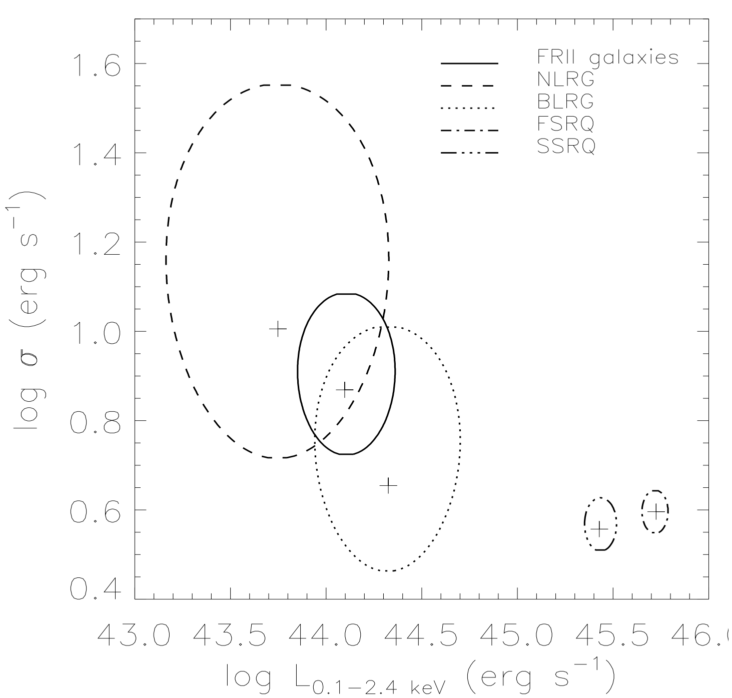

Figure 8.8: 90% *confidence level contour plots for the* $0.1 - 2.4$ *keV X-ray luminosity and intrinsic dispersion of FRII galaxies, NLRG, BLRG, SSRQ and FSRQ. The crosses indicate the average* $\log\ L_{\rm X}$ *and* $\log\ \sigma$.

In this section we present the results from the correlation and regression analyses for FRII galaxies and radio-loud quasars, using the statistical methods described in Chapter 5 and already utilized in Chapters 6 and 7. To determine the statistical significance of the correlations we calculate generalized versions of both the Kendall's τ and partial Kendall's τ coefficients for censored data. We perform both the Buckley-James regression, allowing for the presence of upper limits, and the Fasano & Vio regression, including errors on the variables and a calculation of the intrinsic dispersion of the correlation. The results are given in Table 8.2 and will be discussed in § 8.4.1.
We do not show the parameters of the regression lines for BLRG and NLRG separately because, in all cases, no significant correlations could be found due to the small number of objects with available radio and optical core fluxes. In all the other cases the correlations are significant at the 5% level.

8.3.1 The radio - to - radio luminosity correlations

Fig. 8.9 shows the radio total versus core luminosity for the whole sample (top panel) and for FRII galaxies and radio-loud quasars only (bottom panel). FRII radio galaxies appear as objects essentially dominated by their extended emission, FSRQ are core-dominated, whereas SSRQ display lower core luminosities with respect to their total emission, but still higher than those of the FRII galaxies. These are likely objects observed at intermediate viewing angles with respect to the galaxies and the core-dominated quasars.

Fig. 8.10 gives the radio extended versus core luminosities of the various objects and illustrates well the similarity of the extended emission of radio-loud quasars, both FSRQ and SSRQ, and FRII galaxies compared to the large range of their core emission. The slopes of the regression lines are similar within the errors for all the three classes and close to unity ($b = 1.24 \pm 0.16$ for the FRII galaxies, $b = 1.12 \pm 0.11$ for SSRQ, $b = 1.01 \pm 0.05$ for FSRQ). Going from the FRII galaxies to the SSRQ to the FSRQ the regression lines are just shifted towards higher core luminosities in agreement with the hypothesis that the core emission is enhanced by relativistic beaming, whereas the extended emission remains constant.

8.3.2 The radio - to - optical luminosity correlations

Figs. 8.11 and 8.12 show, respectively, the radio - to - optical planes for FRII galaxies and radio-loud quasars superposed on the rest of the sample and of FRII galaxies and radio-loud quasars only. In Fig. 8.11 the total luminosities are used for all objects in both wavebands, whereas in Fig. 8.12 the optical core luminosities are taken for the FRII galaxies and the radio core luminosities for both classes.
The radio and optical core luminosities appear to be correlated in both, FRII galaxies and radio-loud quasars. However, the results for FRII galaxies are based on only 23 objects of which 8 are upper limits (in the optical band). A clear trend is observed for radio-loud quasars, with FSRQ and SSRQ following almost parallel lines with similar slopes (within the statistical errors) of $b = 1.90 \pm 0.12$ and 2.18 ± 0.20, respectively. FSRQ are found at the higher end of the radio core luminosity distribution of radio-loud quasars. The FRII galaxies clearly do not follow the same correlation as the quasars, but have a much flatter trend with $b = 0.84 \pm 0.27$ (when the optical upper limits are considered). This

Regression analysis

Correlation (1)	Group (2)	Buckley-James (3)	Fasano & Vio (4)
$\log L_{\rm R,core} - \log L_{\rm O,core}$	FRII galaxies	$a = 8.23$ $b = 0.84 \pm 0.27$ $\sigma = 1.058$	$a = 16.48 \pm 4.28$ $b = 0.52 \pm 0.15$ $\sigma_{\rm int} = 0.30 \pm 0.06$ Weighted rms= 0.529
	SSRQ	$a = -11.91$ $b = 1.46 \pm 0.15$ $\sigma = 0.791$	$a = -34.03 \pm 6.13$ $b = 2.18 \pm 0.20$ $\sigma_{\rm int} = 0.85 \pm 0.12$ Weighted rms= 0.943
	FSRQ	$a = -9.80$ $b = 1.42 \pm 0.09$ $\sigma = 0.915$	$a = -24.66 \pm 3.68$ $b = 1.90 \pm 0.12$ $\sigma_{\rm int} = 0.95 \pm 0.11$ Weighted rms= 0.993
$\log L_{\rm X} - \log L_{\rm O,core}$	FRII galaxies	$a = 21.71$ $b = 0.79 \pm 0.09$	$a = 16.36 \pm 6.96$ $b = 0.97 \pm 0.25$ $\sigma_{\rm int} = 0.65 \pm 0.36$ Weighted rms= 0.749
	SSRQ	$a = 15.47$ $b = 0.98 \pm 0.04$ $\sigma = 0.573$	$a = 13.01 \pm 1.61$ $b = 1.05 \pm 0.05$ $\sigma_{\rm int} = 0.19 \pm 0.02$ Weighted rms= 0.452
	FSRQ	$a = 16.27$ $b = 0.95 \pm 0.04$ $\sigma = 0.679$	$a = 13.43 \pm 1.36$ $b = 1.05 \pm 0.04$ $\sigma_{\rm int} = 0.27 \pm 0.03$ Weighted rms= 0.538
$\log L_{\rm X} - \log L_{\rm R,core}$	FRII galaxies	$a = 13.58$ $b = 0.96 \pm 0.11$ $\sigma = 0.948$	$a = 5.24 \pm 4.68$ $b = 1.23 \pm 0.15$ $\sigma_{\rm int} = 0.61 \pm 0.15$ Weighted rms= 0.781
	SSRQ	$a = 23.50$ $b = 0.67 \pm 0.04$ $\sigma = 0.621$	$a = 23.58 \pm 1.59$ $b = 0.66 \pm 0.05$ $\sigma_{\rm int} = 0.12 \pm 0.02$ Weighted rms= 0.367
	FSRQ	$a = 22.94$ $b = 0.67 \pm 0.03$ $\sigma = 0.693$	$a = 22.87 \pm 1.11$ $b = 0.67 \pm 0.03$ $\sigma_{\rm int} = 0.15 \pm 0.02$ Weighted rms= 0.408

Table 8.2: *Results of the regression analysis for FRII galaxies and radio-loud quasars. Column 1: type of correlation. Column 2: groups of objects. Column 3: Buckley-James regression parameters of the bisector of the two fitted lines (see § 5.5.4). Column 4: Fasano & Vio regression parameters. For the Fasano & Vio regression only detections have been used.*

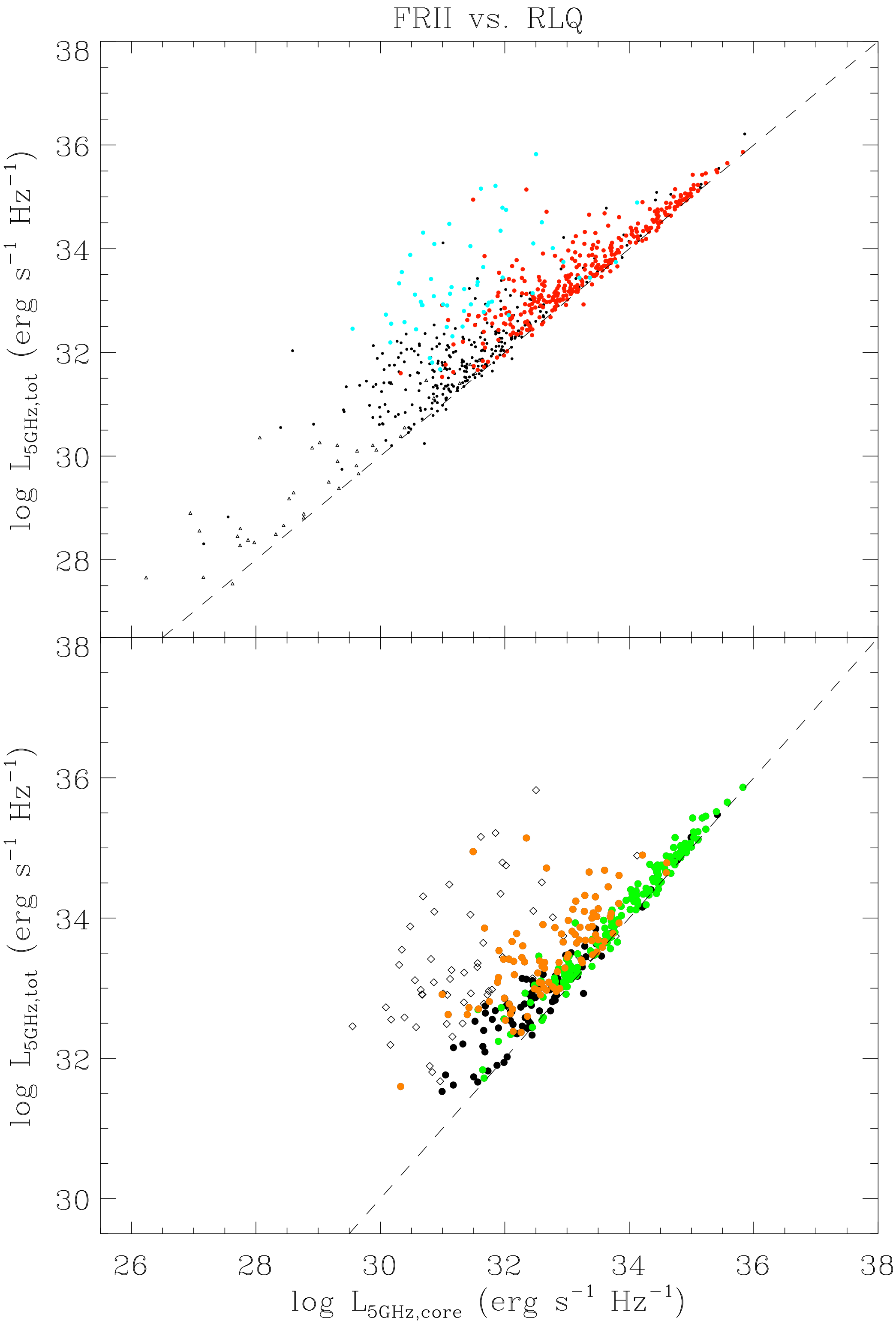

Figure 8.9: *Top panel: the* $L_{\rm R,tot}$-$L_{\rm R,core}$ *plane for the FRII galaxies (blue) and the radio-loud quasars (red) superposed on the total sample (black). Radio-loud objects are shown as circles and radio-quiet as triangles. Bottom panel: the* $L_{\rm R,tot}$-$L_{\rm R,core}$ *plane for FRII galaxies (diamonds) and radio-loud quasars (circles) only. FSRQ are plotted in green and SSRQ in yellow. In both panels the line for which* $L_{\rm R,tot} = L_{\rm R,core}$ *is drawn.*

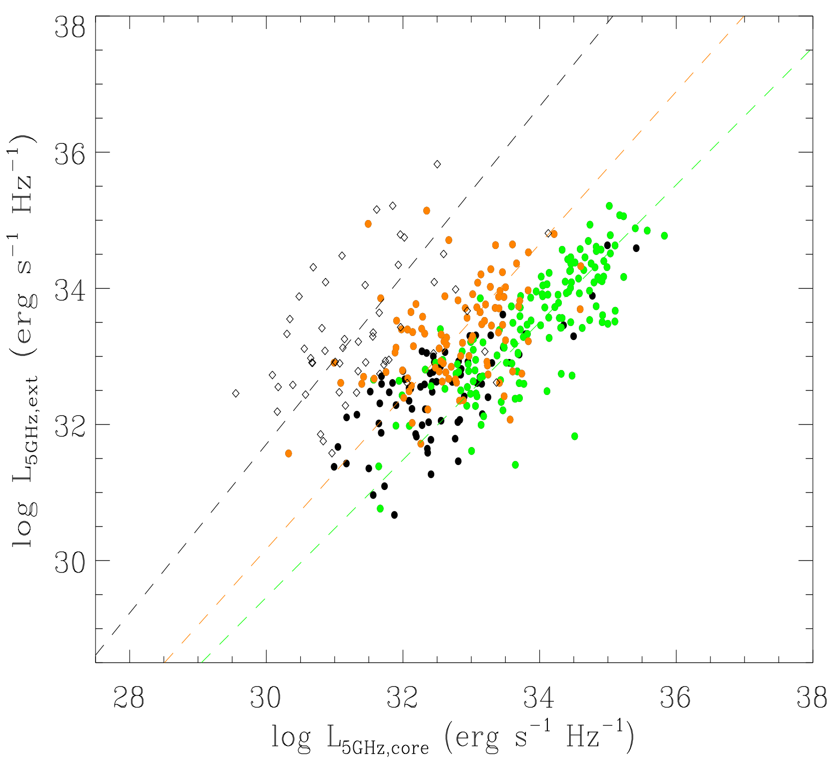

Figure 8.10: *The $L_{\mathrm{R,ext}}$-$L_{\mathrm{R,core}}$ plane for the FRII galaxies (diamonds) and the radio-loud quasars (circles). FSRQ are plotted in green and SSRQ in yellow. The regression lines for the three classes are also drawn.*

relationship is consistent inside the errors, with what has been found for the FRI galaxies ($b = 1.03 \pm 0.16$, see Chapter 7). The regression analyses for NLRG and BLRG do not yield well constrained parameters due to their low number, however, the NLRG appear to follow a correlation with slope $b \sim 0.8$, which is not very dissimilar from that of the FRI galaxies as a whole, considering the large errors. On the other hand, the BLRG show an optical excess with respect to this correlation. These results are in agreement with those of Chiaberge et al. (2000), however, it must be stressed that the samples considered are still too small to draw firm conclusions.
Browne & Murphy (1987) found correlations with slopes $b = 1.67 \pm 0.22$ for core-dominated quasars and $b = 3.45 \pm 0.87$ for lobe-dominated quasars[1]. These slopes are not much different from ours if we take into account the errors. However, we have a much larger sample of objects. Baker (1997) finds, using the EM algorithm and the Buckley-James method, that core-dominated quasars follow a correlation with slope $b = 1.43 \pm 0.20$, well in agreement with our result for FSRQ from the same regression technique.

8.3.3 The X-ray - to - optical luminosity correlations

In Figs. 8.13 and 8.14 the X-ray versus optical luminosities are plotted. In the first case, total luminosities are used for all objects in the V band and, in the second case, core luminosities are taken for the FRII galaxies.
The X-ray luminosity correlates with the optical one with a slope of about $b \sim 1$ for both SSRQ and FSRQ and small dispersions. The slope for the FRII galaxies ($b = 0.97 \pm 0.25$) is similar to that for the quasars, although with larger dispersion ($\log \sigma_{\rm intr} = 0.65 \pm 0.36$), when the Fasano & Vio regression is performed. However the number of objects is very small. When the upper limits in the optical and X-ray band are taken into account through a Schmitt's regression (Isobe et al. 1986) the slope becomes flatter ($b = 0.79 \pm 0.09$) than that found for the FRI galaxies ($b = 1.20 \pm 0.17$, see Chapter 7), probably due to the much more numerous X-ray upper limits.
The result that the slopes for FSRQ and SSRQ are essentially similar appears to be in disagreement with previous works by Brinkmann et al. (1997) who report values of $b = 0.86 \pm 0.11$ and $b = 0.79 \pm 0.16$, respectively. However, they are still consistent inside the errors and our determination of the regression parameters relies on larger samples of objects of both classes.

8.3.4 The X-ray - to - radio luminosity correlations

The X-ray versus the radio total and core luminosities are shown, respectively, in Figs. 8.15 and 8.16.
The bottom panel of Fig. 8.15 shows that the range of total radio luminosities is similar for FRII galaxies, SSRQ and FSRQ, ranging from $\sim 10^{32}$ to 10^{37} erg s^{-1} Hz^{-1}. However, the radio emission in the different classes originates from spatially well separated regions, mostly from the lobes in FRII galaxies and SSRQ, and mostly from the cores in FSRQ. The total luminosities of these objects are, therefore, as already discussed in § 8.2, not well suited to investigate their different properties.

[1] We have transformed to our notation the regression coefficients given in Browne & Murphy (1987) where the optical and radio luminosities were used as the dependent and independent variables, respectively.

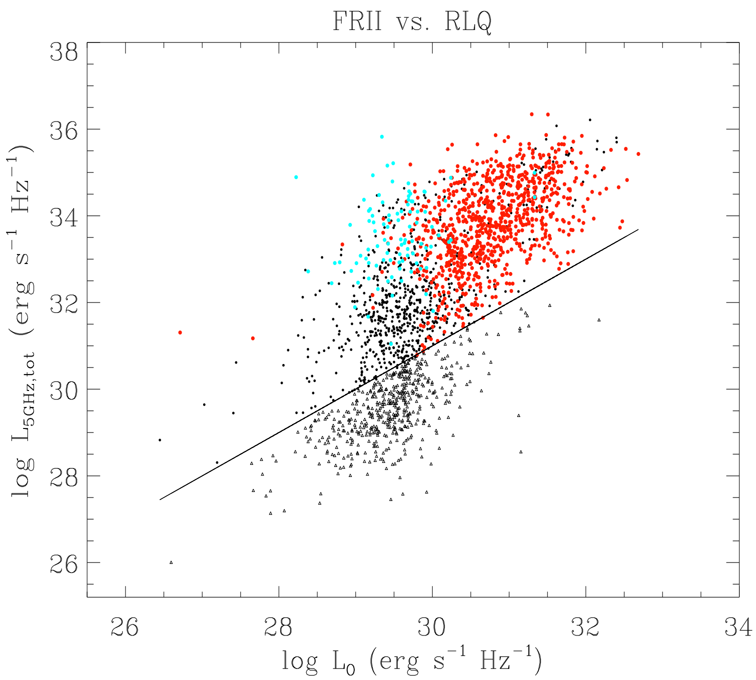

Figure 8.11: *The $L_{\rm R,tot}$-$L_{\rm O,tot}$ plane for the FRII galaxies (blue) and the radio-loud quasars (red) superposed on the rest of the sample (black). The straight line is the formal division between radio-loud (circles) and radio-quiet (triangles) objects (see § 2.3).*

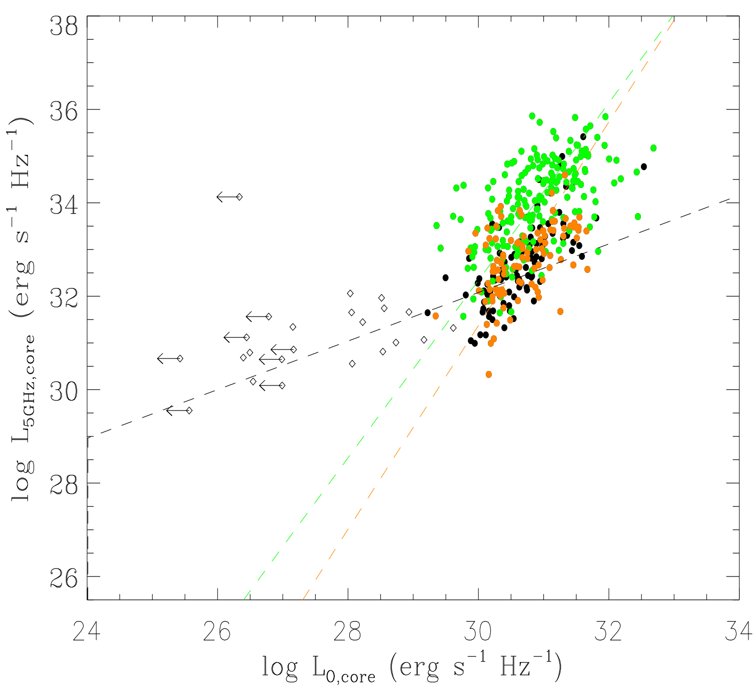

Figure 8.12: *The $L_{\rm R,core}$-$L_{\rm O,core}$ plane for the FRII galaxies (diamonds) and the radio-loud quasars (circles). Flat-spectrum quasars ($\alpha_{\rm r} < 0.5$) are plotted in green and steep-spectrum quasars ($\alpha_{\rm r} \geq 0.5$) in yellow. The total optical luminosity is used for the radio-loud quasars. The regression lines for the three classes are also drawn.*

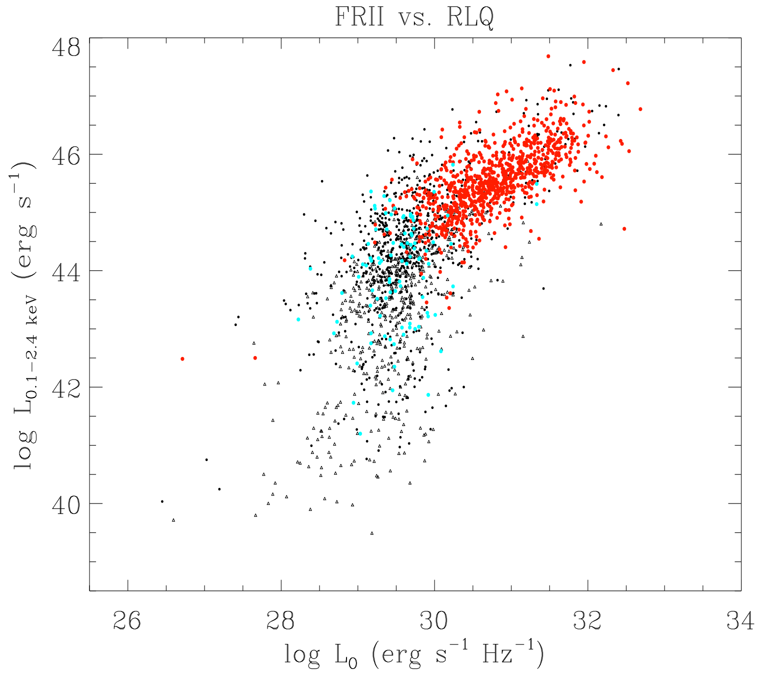

Figure 8.13: *The L_X-L_O plane for the FRII galaxies (blue) and the radio-loud quasars (red) superposed on the total sample (black). Radio-loud objects are shown as circles and radio-quiet as triangles.*

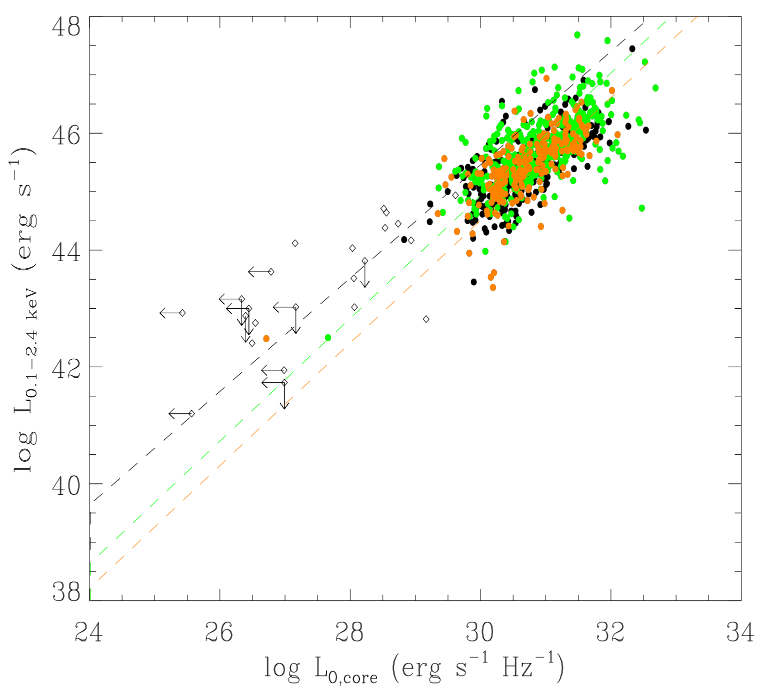

Figure 8.14: *The L_X-$L_{O,core}$ plane for the FRII galaxies (diamonds) and the radio-loud quasars (circles). Flat-spectrum quasars ($\alpha_r < 0.5$) are plotted in green and steep-spectrum quasars ($\alpha_r \geq 0.5$) in yellow. The total optical luminosity is used for the radio-loud quasars. The regression lines for the three classes are also drawn.*

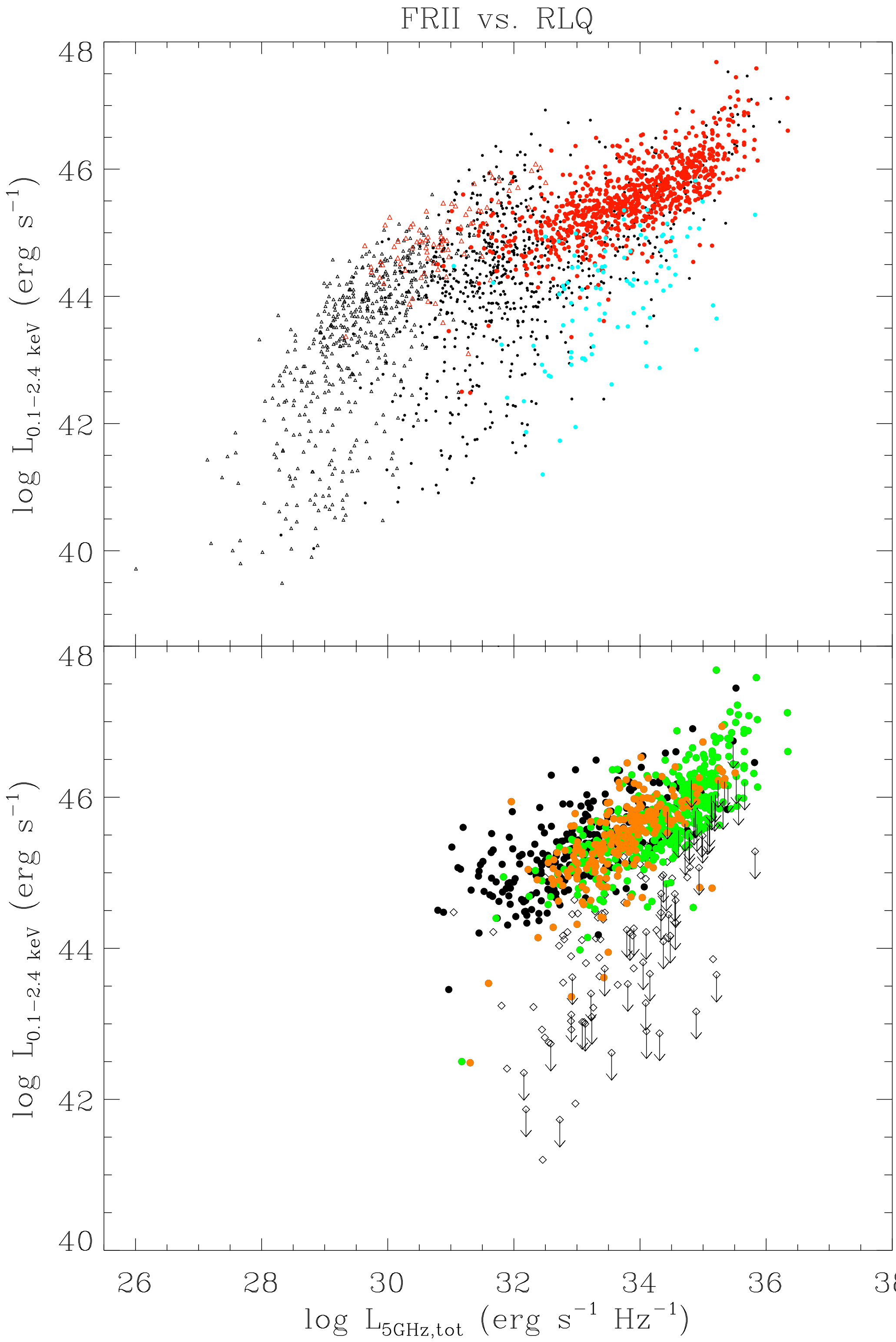

Figure 8.15: *Top panel: the L_X-$L_{R,tot}$ plane for FRII galaxies (blue) and radio-loud quasars (red) superposed on the total sample (black). Radio-loud objects are shown as circles and radio-quiet as triangles. Bottom panel: the L_X-$L_{R,tot}$ plane for FRII galaxies (diamonds) and radio-loud quasars (circles) only. Flat-spectrum quasars ($\alpha_r < 0.5$) are plotted in green and steep-spectrum quasars ($\alpha_r \geq 0.5$) in yellow. Also shown here are the upper*

A correlation seems to be present between the X-ray and core radio luminosities of the FRII galaxies, with a slope of $b = 0.96 \pm 0.11$. Also in this case SSRQ and FSRQ turn out to follow basically the same correlation of slopes $b = 0.66 \pm 0.05$ and $b = 0.67 \pm 0.05$, respectively with small dispersions ($\log \sigma_{\rm intr} = 0.12 \pm 0.02$ for SSRQ and $\log \sigma_{\rm intr} = 0.15 \pm 0.02$ for FSRQ). The FRII galaxies, therefore, do not show the same trend as the quasars.
Siebert et al. (1996) found for a sample of 30 FRII galaxies a slope of $b = 0.58 \pm 0.26$, whereas from a similar survival analysis we obtain a slightly steeper value, however for 56 objects. Hardcastle & Worrall (1999) find, for 41 FRII galaxies, an even steeper slope of $b = 1.52$ from a Schmitt regression but with a rather large error.
In the case of radio-loud quasars several authors report different slopes for SSRQ and FSRQ, in contrast with our results. Browne & Murphy (1987) quote slopes of $b = 0.70 \pm 0.07$ for core-dominated quasars and $b = 0.40 \pm 0.06$ for lobe-dominated quasars. The first value is well in agreement with that found here for the FSRQ, but the second is significantly flatter than for the SSRQ in our sample. Baker et al. (1995) confirm the discrepancy between FSRQ and SSRQ, with $b = 0.79 \pm 0.05$ and $b = 0.36 \pm 0.10$, respectively. Siebert et al. (1996) and Hardcastle & Worrall (1999) find slopes for the quasars, without distinguishing between FSRQ and SSRQ, of $b = 0.58 \pm 0.26$ and $b = 0.69$, respectively, consistent with our results. Brinkmann et al. (1997) obtain $b = 0.68 \pm 0.13$ for FSRQ and $b = 0.47 \pm 0.14$ for SSRQ, but consistent with a single slope within the mutual 1σ errors and with some indication for a steepening towards higher luminosities. However, a clear separation of SSRQ and FSRQ could not be confirmed.

As we have seen, our data argue in favor of similar X-ray - to - radio core correlations for both SSRQ and FSRQ in contrast with previous results. However, the discrepancy resulted to be weaker in Brinkmann et al. (1997) who analyzed much larger samples than those of Browne & Murphy (1987) and Baker et al. (1995), and, from the analysis of our even bigger sample, it seems to disappear. Therefore, the apparent discrepancy between the two classes might be the result of the small sizes of the samples combined with selection effects. In fact, Baker et al. (1995) select objects from two flux limited catalogs, the Molonglo Quasar Sample and the Parkes Flat-spectrum Sample, probably causing the inclusion of only the brightest SSRQ, truncating the low luminosity tail of their distributions. On the other hand, the luminosities of FSRQ usually lie above the flux limits of the samples, therefore their distribution is probably well reproduced. If SSRQ and FSRQ actually follow parallel correlations in the X-ray - to - radio core luminosity plane, as it is found in this work, with FSRQ just displaced towards higher values in both wavebands, the elimination of the low luminosity steep-spectrum objects would generate an artificial curved trend. Our sample, however, contains many more sources than those of Browne & Murphy (1987) and Baker et al. (1995), selected from several different radio catalogs and is therefore less affected by such selection effects, reproducing more realistically the trends for SSRQ and FSRQ.

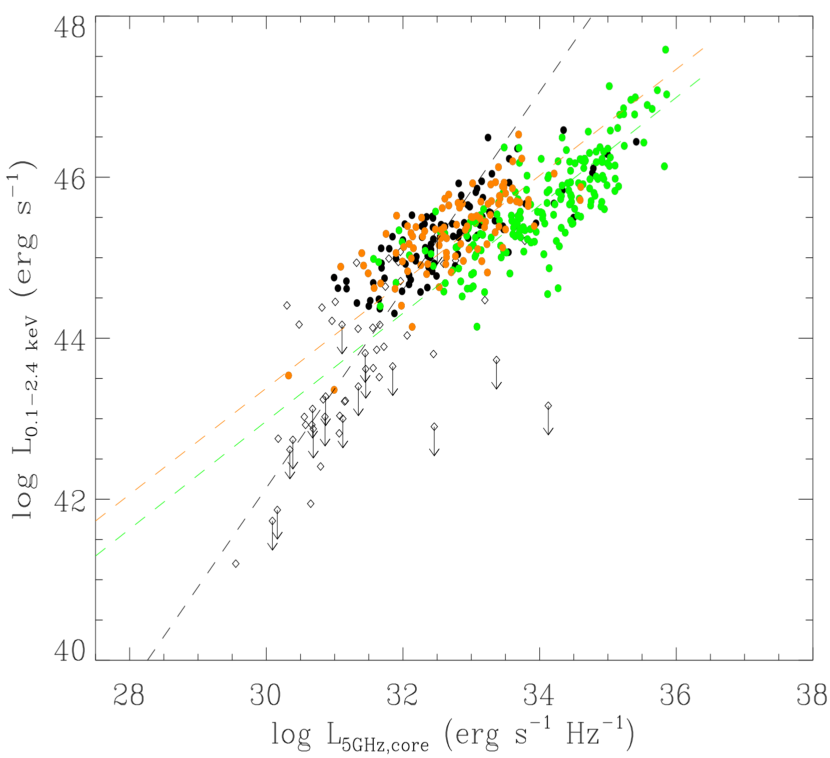

Figure 8.16: *The L_X-$L_{R,core}$ plane for the FRII galaxies (diamonds) and the radio-loud quasars (circles). Flat-spectrum quasars ($\alpha_r < 0.5$) are plotted in green and steep-spectrum quasars ($\alpha_r \geq 0.5$) in yellow. Also shown here are the upper limits on X-ray luminosities (arrows). The regression lines for the three classes are also drawn.*

8.4 Unification of FRII galaxies and radio-loud quasars

8.4.1 Interpretation of correlations

In § 7.5.3 we have seen that, in a simple beaming model in which only one component is responsible for the emission at all wavelengths, the slopes of the correlations between luminosities at two different frequencies for the unbeamed and beamed populations should be the same. This behavior is observed for FRII galaxies and radio-loud quasars in the case of the correlation between the radio extended and core luminosities (see Fig. 8.10), supporting, as discussed in § 8.3.1, the view that FSRQ, SSRQ, BLRG and NLRG are simply increasingly beamed versions of the same kind of objects.
The same behavior is also observed in the case of the X-ray - to - optical correlations, but not in the case of the radio - to - optical and X-ray - to - radio correlations, where the FRII galaxies show different slopes than the quasars.
In Chapter 7 we have interpreted the different slopes of the correlations for FRI galaxies and BL Lacs as a possible indication for the presence of more than one emission component. However, in the case of FRII galaxies and radio-loud quasars we propose a different scenario in which multiple emission components are not required. This is attained by taking into account absorption by gas or dust which, contrary to the case of FRI/BL Lacs, is believed to be substantial in FRII galaxies. Absorption is mostly effective at optical and soft X-ray wavelengths. The steeper slope of the X-ray - to - radio correlation for the FRII galaxies with respect to SSRQ and FSRQ might be explained in the context of this model by considering that two kinds of objects, BLRG and NLRG, actually constitute the group of FRII galaxies. BLRG are thought to be unbeamed quasars which, however, are observed at smaller viewing angles than the NLRG so that the obscuring region is, at least partially, out of sight, whereas NLRG are highly absorbed. Therefore the BLRG are expected to follow the same correlation as both FSRQ and SSRQ, only extrapolated at lower luminosities. On the other hand, since they are highly absorbed, NLRG should display smaller X-ray luminosities than expected from the extrapolation of this correlation. If we perform a regression analysis for BLRG and NLRG taken together we would obtain a steeper slope than the one found for the quasars. To test this we have attempted to calculate the regression parameters for the BLRG and the NLRG separately, although the number statistics of the two classes is rather small, especially for the BLRG (13 objects). The correlation for the BLRG is not statistically significant at the 5% level, however, the slope obtained from a Buckley-James regression, $b = 0.76 \pm 0.25$, is within the errors in good agreement with those for SSRQ and FSRQ, supporting the model above. The slope for the NLRG (23 objects) is much steeper ($b = 1.16 \pm 0.21$) and the correlation is, in this case, statistically significant at 5% level.
The slope of the radio - to - optical correlations for the various classes can be explained by the above model in a similar way. Absorption affects the optical emission from NLRG, but not from BLRG, resulting in a flatter slope for the FRII galaxies with respect to those found for SSRQ and FSRQ. In this case, however, the regression analyses performed for NLRG and BLRG separately do not reliably determine the parameters due to the very small number of objects in both classes (8 and 9 objects, respectively) and the presence of many upper limits.
The fact that the slopes of the X-ray - to - optical correlations are comparable for FRII

galaxies, SSRQ and FSRQ when the Fasano & Vio regression is used, suggests that both the optical and X-ray emission is absorbed by similar amounts. However, if the upper limits are taken into account with a Buckley-James regression, the slope for the FRII galaxies appears to be flatter than for the quasars, as if the optical emission were more absorbed.
The radio emission is unaffected by absorption, therefore, we would expect to observe similar extended - to - core luminosity correlations for FRII galaxies, SSRQ and FSRQ. This is indeed what we found in § 8.3.1.

We can estimate the amount of absorption in the optical and soft X-ray band in the following way. We assume that the X-ray - to - radio correlation for FSRQ also applies to FRII galaxies, if they are unobscured. The expected unabsorbed average X-ray luminosity can be calculated from the observed average radio core luminosity, which is unaffected by absorption. From the comparison with the observed X-ray luminosity we obtain the average neutral hydrogen column density for the FRII galaxies in our sample from $N_{\rm H} = -\ln(L_{\rm X}^{\rm abs}/L_{\rm X}^{\rm unabs})/\sigma_{\rm T})$ where $\sigma_{\rm T}$ is the Thomson cross-section. Using the Fasano & Vio regression parameters for FSRQ given in Table 8.2 we get $\log L_{\rm X}^{\rm unabs} = 43.71$ and taking the average X-ray luminosity of NLRG listed in Table 8.1 as $L_{\rm X}^{\rm abs}$ we finally obtain $N_{\rm H} \sim 3 \times 10^{22}$ cm^{-2}.
To estimate the absorption in the optical band we use the radio - to - optical correlation of FSRQ and we determine the expected unabsorbed average optical luminosity of NLRG, which turns out to be $\log L_{\rm O}^{\rm unabs} = 29.35$. Comparing this value with the observed, $\log L_{\rm O}^{\rm abs} = 26.06$, we obtain the extinction of $A_{\rm V} \sim 2.81$. Next we calculate the reddening due to dust from the equation $R_{\rm V} = A_{\rm V}/E(B-V)$, taking the standard Galactic value of $R_{\rm V} = 3.1$ (Schultz & Wiemer 1975). The result is $E(B-V) = 0.91$ which can be converted into a neutral hydrogen column density through the gas - to - dust ratio given by $N_{\rm H}/E(B-V) = 5.8 \times 10^{21}$ cm^{-2} (Bohlin et al. 1978), in the case of the Milky Way. We finally obtain $N_{\rm H} \sim 5.27 \times 10^{21}$ cm^{-2}, a lower value than that found from the X-rays. However, the standard Galactic gas - to - dust ratio might not apply to AGN and there is indeed some evidence that it might be higher (Maiolino et al. 2001, Willott et al. 2004), more similar to that found for the Small Magellanic Cloud. Using this ratio ($N_{\rm H}/E(B-V) = 5.2 \times 10^{22}$ cm^{-2}, Bouchet et al. 1985) instead of the Galactic one, the neutral hydrogen column density would be $N_{\rm H} \sim 4.72 \times 10^{22}$ cm^{-2}, well in agreement with the value found in the X-rays.

8.4.2 The amount of beaming in radio-loud quasars

To investigate the amount of beaming in radio-loud quasars we can apply Eq. 7.2 using the average radio core luminosities of radio-loud quasars, either SSRQ or FSRQ, and of NLRG as the beamed and unbeamed luminosities, respectively. We estimate the beaming factor in this band, under the assumption that $\alpha_{\rm r} = 0.5$. For FSRQ we find $\delta_{\rm r} = 7(14)$ and for SSRQ $\delta_{\rm r} = 3(4)$ for $p = 3(2)$.
In the X-ray and optical band we can repeat the calculus above, however, to correct for the effect of obscuration, we have to use the unabsorbed luminosities of NLRG estimated in § 8.4.1. For FSRQ we get $\delta_{\rm x} = 3(5)$ and $\delta_{\rm o} = 3(4)$ and for SSRQ $\delta_{\rm x} = 3(4)$ and $\delta_{\rm o} = 2(3)$

for $p = 3(2)$, where we have assumed $\alpha_{\rm x} = 1.0$ and $\alpha_{\rm o} = 0.5$. The values found in the three bands for SSRQ are well consistent with each other, whereas in the case of FSRQ the radio beaming factor is higher than those at X-ray and optical frequencies. Furthermore, the X-ray and optical beaming factors of both SSRQ and FSRQ are similar, contrary to the hypothesis that the latter are more beamed than the former. It appears that, going from SSRQ to FSRQ, only the radio emission is further boosted.

The simple relativistic beaming scenario is not capable to explain these findings. Interestingly, the result above could be explained by a model in which the radio emission of quasars is dominated by the jet and that in the optical and X-ray bands by the accretion disk. In this scenario the X-ray and optical luminosities of SSRQ and FSRQ are expected to be comparable because the disk emission is not beamed. The lower X-ray luminosities of the FRII galaxies are interpreted both in terms of intervening absorption and of an anisotropy of the disk emission due to purely geometrical reasons. Maraschi & Tavecchio (2003) actually proposed a model in which FSRQ are disk-dominated objects, contrary to BL Lacs which are jet-dominated. In their model both FSRQ and BL Lacs have similar masses of $10^8 - 10^9 M_{\odot}$, but the latter have accretion rates much lower than the Eddington limit. A further attractive aspect of this scenario is that it would also agree with the results of Chapter 6 for the parent populations of radio-loud quasars and BL Lacs, namely FRII and FRI galaxies for which a similar case has been envisaged.

It must be remarked that the validity of this model is not in contrast with the observed properties of the correlations discussed in § 8.4.1. Even if we assumed a "pure" beaming scenario the correlations can be equally well interpreted in the context of the disk model. In fact, recalling Eq. 7.4, we see that the effect of beaming on a correlation, independent of the choice of the Doppler factors and of the spectral indices in the two bands, is just to shift the regression line either to higher or to lower values. However, the effect would be the same if the enhancement of the luminosities in radio-loud quasars were due to a disk viewed pole-on instead of edge-on through obscuring matter. Therefore, neither the conclusions of § 8.4.1 about the amount of absorption in the galaxies and about the increasingly smaller viewing angles of NLRG, BLRG, SSRQ and FSRQ are affected by the chosen model. The only difference is that relativistic beaming is required in the radio band, but it is not the main cause of the larger luminosities of SSRQ and FSRQ in the optical and X-ray bands, even if it might contribute to the emission.

8.4.3 Modeling the Spectral Energy Distributions

In this section we discuss the Spectral Energy Distributions of FRII galaxies and radio-loud quasars. Although a disk or a jet origin of the emission from FSRQ in the optical and X-ray band is still discussed and investigated they usually show double-peaked SEDs similar to those of BL Lacs. In a pure beaming model, i.e. in the jet scenario, the same shape should be observed for SSRQ, BLRG and NLRG. However, in the disk scenario a dependence of the luminosities on the viewing angle, similar to the case of relativistic beaming, is also present and we could expect that the general shape of the SEDs of the galaxies is also preserved. We can thus apply the same parabolic parameterization of the synchrotron peak that we have used for BL Lacs and FRI galaxies in § 7.4.1. However, we have seen that NLRG are likely strongly absorbed in the X-ray and optical bands. BLRG are probably partially obscured, since the expected unabsorbed luminosities of

FRII galaxies are still larger than those observed for these objects (see § 8.4.1). As a consequence, the shape of the SEDs might be altered, strongly in NLRG and less heavily in BLRG, but still sufficient to produce misleading results.
Nonetheless, we attempt to parameterize the SEDs of the 9 BLRG in our sample to further investigate this point, but not those of NLRG because 6 out of 8 objects have upper limits either in the optical or the X-ray band or in both. The results for BLRG, SSRQ and FSRQ separately are shown in Figs. 8.17-8.19.

The SEDs of both FSRQ and SSRQ appear to be well represented by a parabolic form in all cases except two FSRQ for which we obtain an upward parabola. For one of these objects, PKS 0528+134, we could retrieve a well sampled SED from NED which shows that the minimum between the synchrotron and inverse Compton peaks might occur around the V band. In this case, we could be actually parameterizing this minimum explaining why we find a concave parabola. The same might be true for the second object, S5 0212+73, however, its SED is less well determined than in the previous case. Variability can also have affected the shape of these SEDs, which is obtained from non-simultaneous data.
For BLRG we find convex parabolae for all of them, however 6 out of 9 objects have a rather flat curvature. This might have been produced as a consequence of the suppression of some of the optical flux due to obscuration as discussed above. On the other hand, the three BLRG with larger curvature are the most luminous in our sample, more similar to SSRQ, and probably obscuration in these objects is negligible, if not absent.
Therefore, these results suggest that we can rely on the parabolic parameterization of the SEDs only in the case of radio-loud quasars, but not in the case of BLRG for which absorption effects are important.

Fig. 8.20 shows the distributions of $\log \nu L_\nu$ calculated at the peak frequency for FSRQ and SSRQ. Both classes share a wide range of values, from $\sim 10^{44} - 10^{46.5}$ erg s^{-1}, however, FSRQ reach luminosities of $\sim 10^{48}$ erg s^{-1}, about two orders of magnitude higher than SSRQ.
Fig. 8.21 shows the broad band spectral index $\alpha_{\rm rx}$ calculated at 5 GHz and 1 keV plotted versus $\log \nu_{\rm peak}$. A part from PKS 0528+134 and S5 0212+73 which are discussed above and which have a peak (actually a minimum) frequency of $\sim 10^{12.7}$ and $\sim 10^{10.5}$ Hz, respectively, most $\nu_{\rm peak}$ of both FSRQ and SSRQ fall in the range between $\sim 10^{13} - 10^{15}$ Hz, with only a few objects having $\nu_{\rm peak} > 10^{15}$ Hz.
The large majority of FSRQ have $\alpha_{\rm rx} > 0.75$ and $\nu_{\rm peak} < 10^{15}$ Hz as typically found for these objects. 14 of them have $\alpha_{\rm rx} < 0.75$ among which, however, only three have also $\nu_{\rm peak} > 10^{15}$ Hz. The others have $\nu_{\rm peak} \gtrsim 10^{14}$ Hz, close to the boundary usually taken to distinguish between Low-energy-peaked and High-energy-peaked objects. Therefore, our data do not provide strong evidence in favor of the existence of High-energy-peaked FSRQ as proposed by Padovani et al. (2003).

The significant absorption found in FRII galaxies implies that we cannot model their SEDs reliably and, consequently, we are unable to construct their beaming tracks similarly to what was done for the FRI sources. We do not know their intrinsic luminosities and we cannot evaluate from their SEDs the spectral indices in the various wavebands needed to apply Eq. 3.5.

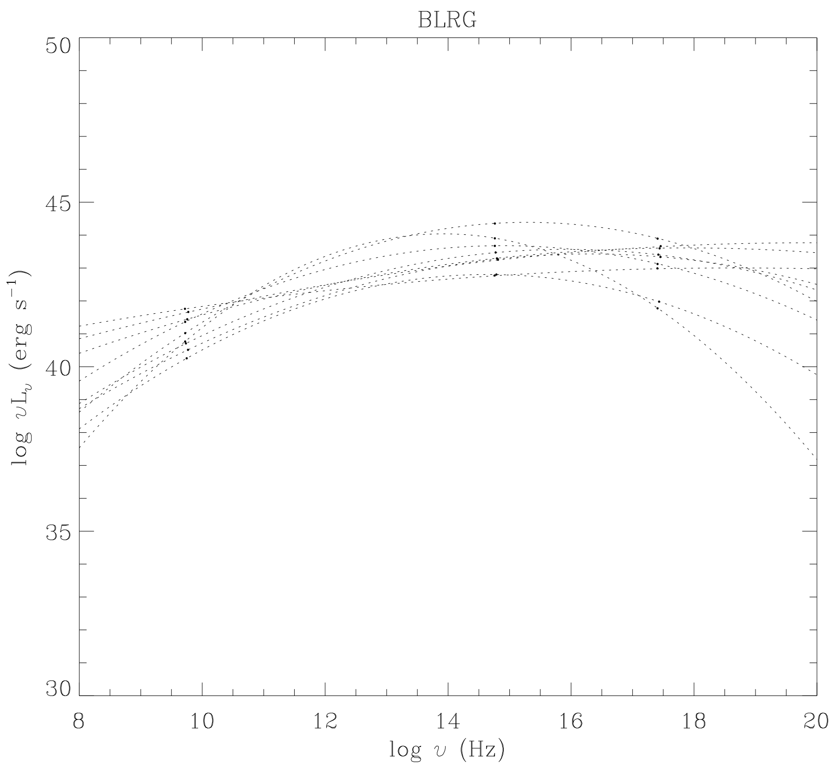

Figure 8.17: *The parabolic parameterizations of the SEDs of BLRG.*

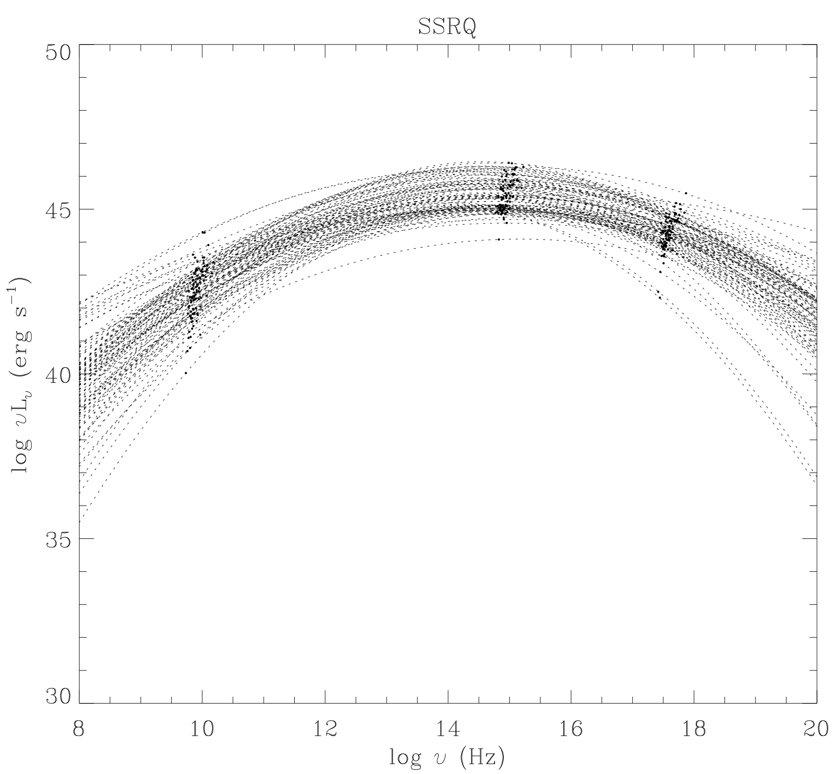

Figure 8.18: *The parabolic parameterizations of the SEDs of SSRQ.*

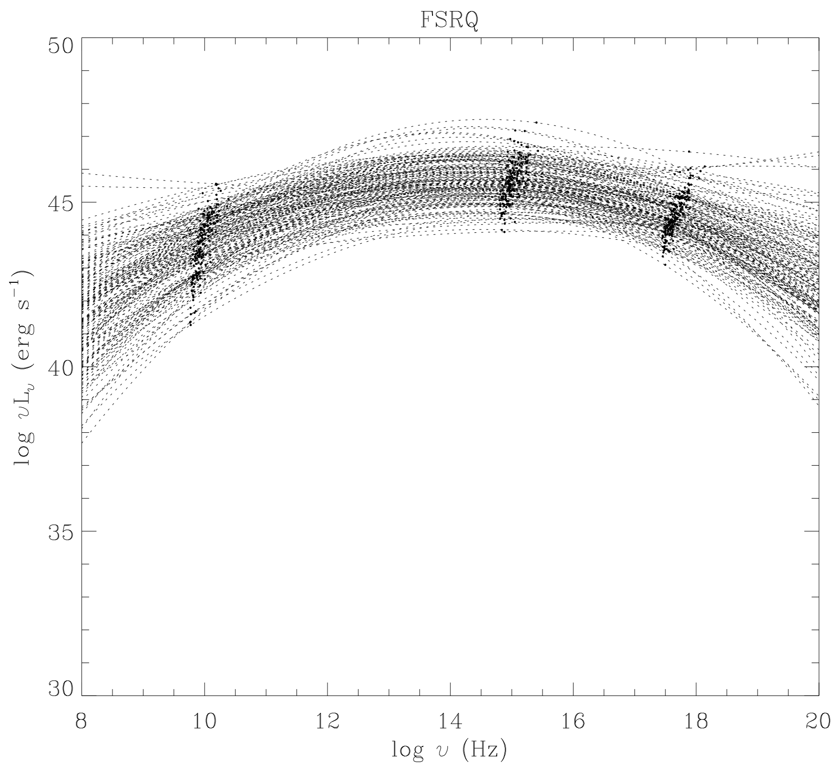

Figure 8.19: *The parabolic parameterizations of the SEDs of FSRQ.*

8.5 Summary of results

- At all wavelengths considered NLRG, BLRG, SSRQ and FSRQ form a sequence of increasing core luminosities, supporting the unified scheme scenario that these are intrinsically similar objects observed at decreasing viewing angles.
- We find significant correlations at the 5% level for all classes and between luminosities at all wavelengths.
- From the correlation analyses between luminosities it is inferred that absorption is significant in NLRG with estimated hydrogen column densities of the order of $N_{\rm H} \gtrsim 10^{22}$ cm^{-2}. Obscuration is also found to affect the BLRG, at least partially.
- Similar beaming factors are required in the X-ray and optical bands for SSRQ and FSRQ, whereas further beaming appears to be present in the radio band to go from SSRQ to FSRQ. This is best interpreted by a model in which the radio emission comes from the jet and is more boosted in FSRQ than in SSRQ, whereas the emission in the other two bands is mainly produced by the disk viewed pole-on in the radio-loud quasars and observed edge-on through obscuring matter in the galaxies.
- Taking into account the absorption in FRII galaxies the parameters of the regression lines for the various classes are in agreement with both, a pure simple beaming model involving only one emission component in all wavebands, and with a model in which the disk and the jet are responsible for the emission at different frequencies.

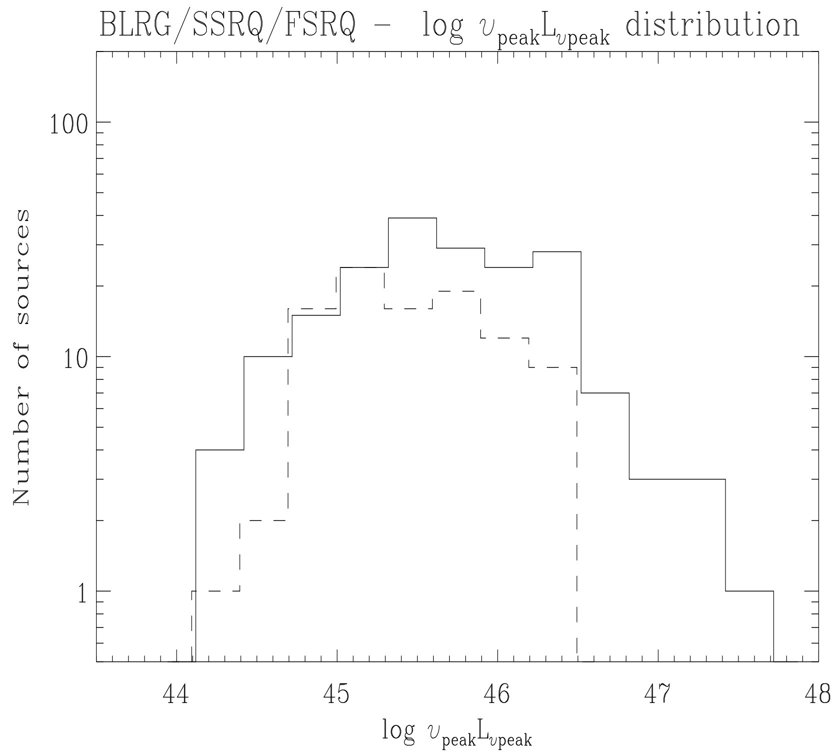

Figure 8.20: *The* $\nu_{\rm peak}L_{\nu_{\rm peak}}$ *distributions of SSRQ (dashed line) and FSRQ (solid line).*

- A parabolic model appears to be applicable to the SEDs of both SSRQ and FSRQ in analogy to the BL Lacs. The model is not appropriate, however, for most BLRG, probably due to the effect of absorption which significantly decreases the optical flux.

- The synchrotron peak frequencies obtained from the parabolic models of the SEDs of FSRQ are almost all typical of Low-energy-peaked objects ($\nu_{\rm peak} \lesssim 10^{15}$ Hz). Only for three objects we find higher values characteristic of High-energy-peaked objects, in contrast with the existence of a blazar sequence. However, the small number of such objects does not provide strong evidence in support of the existence of High-energy-peaked FSRQ.

- We are unable to calculate the beaming tracks of FRII galaxies because the presence of significant absorption in these objects hampers the correct determination of their optical and X-ray luminosities.

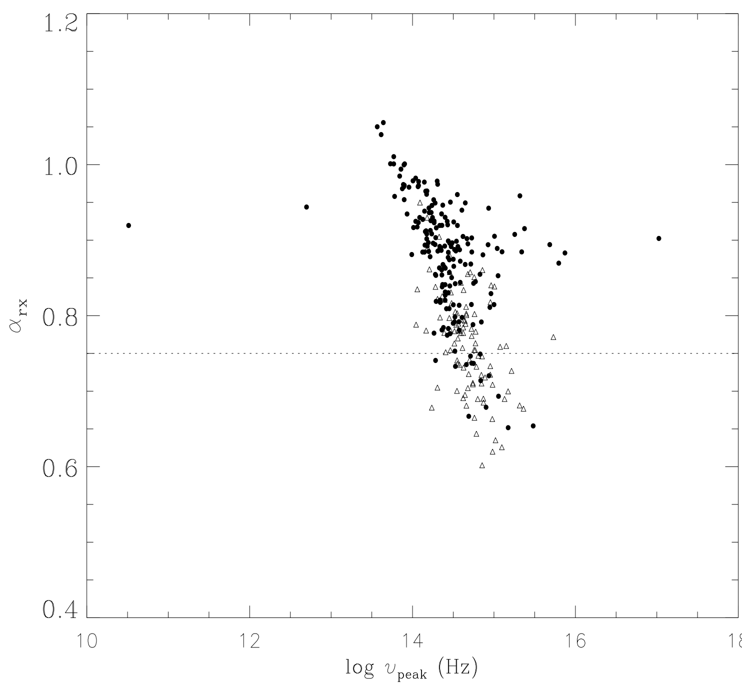

Figure 8.21: *The broad band spectral index α_{rx}, calculated at 5 GHz and 1 keV, plotted versus $\log \nu_{peak}$ as obtained from the parabolic parameterization of the SEDs of the SSRQ (triangles) and FSRQ (circles) in our sample.*

Chapter 9

Conclusions and prospects

The multiwavelength study of large samples of AGN, as carried out in this work, has proved to be a powerful method to analyse the properties of these objects and to test unification schemes, which aim at explaining the AGN classification in terms of orientation effects. At the same time it can provide a broad view on the general features of AGN, a framework for detailed studies of single sources and a sound starting point for more refined investigations. In spite of the limited information available for each single source this approach is capable of leading to important conclusions without the need to know the properties of the objects in detail. Although it cannot convey precise information as deeper studies of single AGN, these acquire more significance if interpreted in the light of the broader picture supplied by such a method.
In § 9.0.1 we summarize the main results from this thesis concerning the unification of radio-loud AGN and in § 9.0.2 we outline possible future developments.

9.0.1 Résumé

The results of this thesis, reported in the previous chapters, are in general agreement with the standard unified scheme in which FRI and FRII galaxies are the misaligned counterparts of BL Lac objects and radio-loud quasars, respectively. However, the details of such unification have been found to diverge in some cases from previous knowledge and potential complications have been highlighted, requiring further deep investigations. Due to the increased number of objects in all classes with respect to previous works we were able to better constrain their properties in the different wavebands considered and the correlations between them. Tight relationships are confirmed to exist for the emission at different wavelengths from the nucleus of all sources. However, the parameters can vary a lot, depending on the frequencies and on the classes considered.

The luminosity properties of FRI galaxies and BL Lacs generally appear to support their unification based on the relativistic beaming scenario alone. However, BL Lacs are usually divided into Low-energy-peaked and High-energy-peaked objects and an analogous separation might be supposed among the FRI galaxies. Contrary to the expectations all of them seem to be High-energy-peaked. Even if selection effects are not completely excluded to have produced such a result, due to the important consequences on the FRI/BL Lac unified scheme, this point certainly needs a thorough investigation.
Although relativistic beaming is sufficient to account for the different observational prop-

erties of BL Lacs and FRI galaxies, simple one-component models for the emission at all frequencies fail to explain the correlations found. Only the introduction of more emission components could provide a better interpretation of the calculated parameters of the regression lines. In particular, at least two components are required in the X-ray band, whereas, in the radio and optical bands, the data are still consistent with the presence of only one emission component.

Contrary to the case of FRI galaxies and BL Lacs, absorption by dust or gas appears to play a major role in the unification of FRII galaxies and radio-loud quasars. Accounting for this, only one emission component, relativistically boosted in the quasars and obscured in the galaxies, is needed to explain the observed correlations. Apparently, this is in disagreement with previous results claiming that two X-ray components should be present, one dominant in SSRQ and the other in FSRQ. However, we have seen that the results from previous works might originate from the much smaller sizes of the samples studied combined with selection effects due to the flux limitations of the catalogs from which the sources were drawn. From the estimate of the relative amount of beaming in SSRQ and FSRQ we found that the data are inconsistent with the hypothesis that the latter are more beamed than the first, except in the radio band. We have suggested that these results might be in better agreement with a model in which the radio-loud quasars are disk-dominated objects (at least in the X-ray and optical band) and not jet-dominated like the BL Lacs.

The comparison of our data for FRI and FRII galaxies argue in favor of fundamental differences in the central engines of these sources. The discrepancy, however, can probably not be ascribed to different black hole masses, which, on the contrary, can be inferred to be similar. The determining parameter might be the accretion rate, high, close to the Eddington limit in FRII sources and low, sub-Eddington, in FRI galaxies. This would also be in nice agreement with the results described above indicating that the emission from FSRQ is disk-dominated and that from BL Lacs is jet-dominated. Could it also be that the large amount of absorbing matter in FRII galaxies/FSRQ is related to the high accretion rate postulated in these objects?

9.0.2 Prospects

An immediate possible future development of this work is the extension and updating of the database to other wavelengths, such as the infra-red, hard X-rays and gamma-rays, covering as much of the electromagnetic spectrum as possible. Data on emission lines should also be added when available. Spectral information in every waveband might also be included, especially exploiting new, high quality data from the current observatories and telescopes. In particular, new X-ray data from Chandra and XMM could be used.

A general impression originating from this work is that the unified scheme is essentially based on the study of relatively few, well observed "parent" objects, i.e. FRI and FRII galaxies, whereas the majority of them are not considered for various reasons. For example, only a minority of both FRI and FRII galaxies are detected in X-rays, and are thus included in this work, and only for an even smaller number of objects the photon counts are high enough to allow a spectral analysis. For many radio galaxies a clear Fanaroff-Riley

classification is not possible, either because of peculiar morphologies or because they are unresolved in the radio band. Therefore, detailed studies of more of these objects should be promoted at all wavelengths. This would allow to construct their SEDs, thus determining directly if both Low-energy-peaked and High-energy-peaked FRI galaxies exist, and to better identify their emission mechanisms. XMM and Chandra observations would be crucial because they would allow to resolve the various X-ray components and to determine the amount of absorption, two topics that this work has revealed to be fundamental to correctly interpret the observed luminosity correlations. However, a part from a few nearby objects these topics are still poorly analyzed.
Equally deep studies of BL Lacs and FSRQ, more easily available than for the galaxies due to their much higher luminosities, are helping and will help in the near future to better understand the relative importance of the jet and disk emission in these objects.

Furthermore, several minor AGN classes are not considered by the unification scheme but are emerging to be a non negligible fraction of the total population and are promising carriers of information on the AGN phenomenon. Some examples are Low Luminosity AGN, LINERs, the long known Low Excitation Radio Galaxies, the Gigahertz-Peaked and Compact Steep-Spectrum sources. Since all classes are present in our database with a significant number of objects each, the next step would be to concentrate on them, performing a statistical study that can be compared to that described in this work. At the same time it would be very useful to propose sufficiently large samples of these sources for detailed systematic observations.

In the present study we have not investigated the role played by cosmic evolution in determining the properties of the different classes of radio-loud AGN. However, its effects might be considerable, especially for the quasar class, which shows the largest redshifts. A further development of this work thus might be the analysis of the properties of the objects in our sample, divided into several redshift bins. This is certainly possible for the quasar and BL Lacs subsamples formed by hundreds of objects, whereas it might be problematic for the much less numerous FRI and FRII galaxies.
From the detailed analyses of the XMM observations of four high-redshift objects ($z > 2$) we already found indications that quasars' properties might evolve with cosmic epoch (Ferrero & Brinkmann 2003). The two radio-loud quasars analyzed in this work present X-ray spectral slopes of $\Gamma \lesssim 1.5$ in the $0.2 - 10$ keV band, flatter than what is usually observed at low redhifts. They are also X-ray brighter, with luminosities of the order of $L_{2-10\ \mathrm{keV}} \sim 10^{45}$ erg s^{-1}. The absorption properties of high-redshift quasars are also different from those of their low-redshift counterparts, frequently showing neutral hydrogen column densities exceeding the Galactic value. However, Ferrero & Brinkmann (2003) find extra absorption only in one object, classified as a GPS source, suggesting an interesting connection between the early stages of radio-loud AGN and the presence of large amounts of absorbing matter. As stated above, GPS sources certainly deserve a thorough investigations.

Appendix A

Skinakas observations of 15 ROSAT sources

For the calculation of the X-ray, radio and optical luminosities of the sources in our sample their redshifts are needed, however, for some of them, no redshift was given in NED or in the literature. Since our aim was to have as many sources as possible in our database to allow an accurate statistical study, we checked which, among the objects in our sample without redshift, could be observed from the Skinakas observatory in Crete. The basic requirements for their observability were: an apparent optical magnitude $m_{\mathrm{V}} \leq 17$, declination $\delta \geq 10°$ and visibility at night in the summer period during which the observatory is operative. 15 sources resulted to be observable and we thus organized an observation campaign at the Skinakas observatory to directly observe them and take their spectra. For 13 sources for which at least one emission or absorption line was clearly detected we could determine the redshift.
In the following we will give a description of the Skinakas observatory, of the telescope and the CCD camera used. A summary of the observations and the data reduction will be also presented together with the results.

A.1 The Skinakas observatory

The Skinakas observatory has been built as a result of a scientific collaboration between the University of Crete, the Foundation for Research and Technology-Hellas and the Max-Planck-Institut für extraterrestrische Physik in Germany. It is located about 60 km from Heraklion, in Crete, on the Ida mountain (1750 m.) at a longitude of 24^h 53' 57" East and at a latitude of 35° 12' 43" North.
The main instrument is a modified Ritchey-Cretien 1.3 m telescope with a focal length of 985.7 cm and an equatorial mount. A second instrument is also available, a Schmidt-Cassegrain flat field 30 cm telescope with focal length of 940 cm and equatorial mount as well.
For our observations we made use of the 1.3 m telescope, equipped with a ISA CCD camera, with 2000×800 15 μm pixels, back illuminated and cooled by means of liquid nitrogen. On the light path a reflection grating is introduced. When used in the 0th order mode it simply works like a mirror reflecting the light on the CCD to produce an image.

Table A.1: The sample of sources observed at the Skinakas observatory

Name	m_V	Date of obs.
MCG +05-33-047	15.50	22nd June 2002
CGCG 195-013	15.60	
NPM1G +29.0397	16.27	
CGCG 170-018	15.60	
CGCG 435-002	15.70	25th July 2002
LEDA 214269	15.48	
2MASXiJ1611392+381241	16.35	
UGC 10782	15.60	
4C +26.11	16.50	26th July 2002
CGCG 1556.3+2019	15.70	
RGB J1652+403	16.40	
MCG +06-37-023	15.00	
CGCG 0250.9+3613	15.20	4th August 2002
PKSJ 2130+0308	17.00	
CG 1329	17.00	

When used in the 1st order mode it works as a spectrometer, dispersing the light into its wavelength components. In this case, in order to get only the light coming from the interesting object, a slit (with several possible widths) is positioned before the grating. The spectrum of the source will be seen on the CCD as a horizontal strip, where the pixels in the x-direction will correspond to different wavelengths.
A filter wheel with 6 positions, a flat spectrum lamp and a calibration lamp are also provided.

A.2 The observations

We have observed in total 15 sources during four nights. The names of the sources and the dates of the observations are given in Table A.1. These are all of the sources from our sample without redshift, with $m_V \leq 17.0$ and declination $\delta \geq -10°$, the requirements for the feasibility of their observations at Skinakas.
Each night of observations we followed the steps described below:

- refilling of liquid nitrogen to cool down the CCD camera.
- 1 sec exposure taken with the closed mirror in the 0th order mode to check the *bias*, due to the read-out noise of the CCD; five 1 sec exposures were actually taken in order to make an average.
- short exposure of a flat spectrum lamp in the 1st order mode to measure the response of the system formed by the CCD plus the grating; the response is not flat and because the CCD is much more sensitive to the red wavelengths, five exposures were

taken to increase the signal-to-noise in the blue band; a light diffusor was simulating the incidence of light from infinity.

- five short exposures in the 1st order mode of a calibration lamp with known emission lines; this enables to assign the correct wavelength to each pixel of the CCD for the data reduction.
- centering of the telescope on a bright star both to calibrate the coordinate system and to focus the telescope; to focus the telescope an exposure of 1 sec is taken in order to check the FWHM of the PSF of the star, then the focus is changed to reduce it as much as possible.
- approximate centering of telescope on the first interesting object and short exposures (in the imaging mode) of the slit alone and the field, to check for the position on the CCD of the slit and the object; the object is then moved in the center of the slit; we used a slit 320 μm wide.
- finding of a guiding star in the neighboring field of the object and start of *guiding* (the telescope and the dome follow the object in its movement through the sky).
- two exposures of $\sim$ 30 min of the object in 1st order mode. Two exposures are necessary to identify and eliminate cosmic rays, because it is very unlikely that two cosmic rays hit the same pixel in both exposures.
- two 1 sec exposures for the bias and one short exposure for the calibration lamp as at the beginning of the observation.
- start with a new object

In addition to the studied sources the spectrum of one standard star is also taken during each night. This is a star for which its flux at certain wavelengths is known and this allows the flux calibration during the data analysis. All the data related to the observations were subsequently transferred to CD-roms.

A.3 The data reduction

To analyse the data we used FIGARO, a data reduction software created at Caltech and further developed at the Anglo-Australian Observatory. It is mainly conceived for processing optical and infrared data.
After transforming each data file into a format readable by FIGARO, we followed the same procedure of analysis for each source. We first calculated the mean value of the intensity of all the bias images and we subtracted them to all the corresponding images/spectra (i.e. flats, lamps, fields, slits and data). We then cleaned all the flats from cosmic rays and we took their median. We added all the counts of the pixels of this average spectrum on the x-axis and we divided it by the number of pixels in the y-direction. The result is used to divide every row of the average flat spectrum by it in order to correct for the different sensitivity of different pixels. This yielded a calibrated flat spectrum which we used to divide the data and the lamp files. These files were then cleaned from cosmic rays.

After checking again for the respective positions of the slit and the source (in the field file), we added the counts of all pixels of the data images on the y-axis. This allowed us to identify the position of the source in the y-direction and consequently select the regions from which to extract the source spectrum and the background (or the sky). Two background regions, one on the left and one on the right of the source position, were generally chosen and then averaged. Both the skies' and the sources' spectra were divided by the number of pixels in each selected area, then the background was subtracted and the net spectra originating from the two 30 min exposures were averaged.
Having finally obtained the spectrum of the source, we proceeded with the wavelength and flux calibration. The wavelength calibration was performed averaging the five initial lamp exposures and taking the spectrum from the central rows of the CCD where the source was usually positioned. We then identified some known emission lines and got the others by fitting. The whole procedure can be performed by the FIGARO command *arc*. This first wavelength calibrated spectrum was used afterwards to calibrate all the other lamp spectra taken during the observation and these in turn were used to calibrate the sources' spectra.
To calibrate the flux the standard star was used. Its spectrum was retrieved from the Internet in form of a table and compared to the observed one. With a series of FIGARO commands the flux calibration was generated and then applied to the sources' spectra.
As a final step we checked if we observed the right object by retrieving finding charts from the NED or SkyView and comparing with our field images.

A.4 Results

The redshifts determined with the spectral analysis are listed in Table A.2. The classification for each object is also given.

The redshifts have been obtained on the base of the detection of at least two features, either emission or absorption lines, except for 2MASXiJ1611392+381241, for which only one feature has been clearly detected.
A classification as a *normal galaxy* means that only absorption features were observed in the spectra. The presence of narrow emission lines led to the classification of type 2 AGN or starburst; a further distinction between the two classes would imply the determination of line ratios, not done so far. Type 1 AGN are the sources for which broad emission lines were detected.
For two objects we could not determine the redshifts: 4C +26.11, the faintest object in the sample, and RGB J1652+403 now classified as a BL Lac in the literature, so that its spectrum could be intrinsically featureless.

Table A.2: Redshifts and classifications for the sample of sources observed at the Skinakas observatory

Name	z	Class
CGCG 435-002	0.0375	AGN type 2/Starburst
CGCG 0250.9+3613	0.0471	Normal galaxy
4C +26.11		
MCG +05-33-047	0.0639	Normal galaxy
CGCG 1556.3+2019	0.0461	AGN type 2/Starburst
PKSJ 2130+0308	0.0877	Normal galaxy
LEDA 214269	0.0295	AGN type 1
CG 1329	0.0475	AGN type 1
CGCG 195-013	0.0296	AGN type 1
2MASXiJ1611392+381241	0.0647	Normal galaxy
RGB J1652+403		BL Lac?
NPM1G +29.0397	0.0680	AGN type 2/Starburst
MCG +06-37-023	0.0628	Normal galaxy
UGC 10782	0.0379	AGN type 1
CGCG 170-018	0.0452	Normal galaxy

References

Adams T.F., 1974, ApJ 188, 463
Akritas M.G. & Siebert J., 1996, MNRAS 278, 919
Antonucci R., 1984, ApJ 278, 499
Antonucci R. & Miller J.S., 1985, ApJ 297, 621
Antonucci R. & Barvainis R., 1990, ApJ 363, L17
Antonucci R., 1993, ARA&A 31, 473
Avni Y., 1976, ApJ 210, 642
Baade W. & Minkowski R., 1954, ApJ 119, 206
Baker J., Hunstead R.W. & Brinkmann W., 1995, MNRAS 277, 553
Baker J., 1997, MNRAS 286, 23
Barthel P.D., 1989, ApJ 336, 606
Bicknell G.V., 1995, ApJS 101, 29
Bohlin R.C., Savage B.D. & Drake J.F., 1978, ApJ 224, 132
Boller T., 2000, NewAR 44, 387
Bouchet P., Lequeux J., Maurice E., et al., 1985, A&A 149, 330
Böhringer, H., Voges, W., Huchra, J.P., et al. 2000, ApJS, 129, 435
Böhringer, H., Schücker, P., Guzzo, L., et al. 2004, A&A, 425, 367
Brinkmann W., Siebert J. & Boller T., 1994, A&A 281, 355
Brinkmann W., Siebert J., Reich W., et al., 1995, A&AS 109, 147
Brinkmann W., Siebert J., Kollgaard R.I. & Thomas H.C., 1996, A&A 313, 356
Brinkmann W., Yuan W. & Siebert J., 1997, A&A 319, 413
Brinkmann W., Laurent-Muehleisen S.A., Voges W., et al., 2000, A&A 356, 445
Brotherton M.S., Green R.F., Kriss G.A., et al., 2001, AAS 33, 1514
Browne I.W.A. & Murphy D.W., 1987, MNRAS 226, 601
Buckley J. & James I., 1979, Biometrika 66, 429
Capetti A., Trussoni E., Celotti A., et al., 2000, MNRAS 318, 493
Capetti A., Celotti A., Chiaberge M., et al., 2002, A&A 383, 104
Celotti A., Maraschi L., Ghisellini G., et al., 1993, ApJ 416, 118
Celotti A. & Fabian A.C., 1993, MNRAS 264, 228
Chiaberge M., Capetti A. & Celotti A., 1999, A&A 349, 77
Chiaberge M., Celotti A., Capetti A. & Ghisellini G., 2000, A&A 358, 104
Chiaberge M., Capetti A. & Celotti A., 2002, A&A 394, 791
Comastri A., Molendi S. & Ghisellini G., 1995, MNRAS 277, 297
Dickey J.M. & Lockman F.J., 1990, ARA&A 28, 215
Donato D., Ghisellini G., Tagliaferri G. & Fossati G., 2001, A&A 375, 739
Dunlop J.S., McLure R.J., Kukula M.J., et al., 2003, MNRAS 340, 1095
Edwards P.G. & Piner B.G., 2002, ApJ 579, L67
Elvis M., Lockman F.J. & Wilkes B.J., 1989, AJ 97, 777
Elvis M., 2000, ApJ 545, 63
Fabbiano G., Miller L., Trinchieri G., et al., 1984, ApJ 277, 115
Fanaroff B.L. & Riley J.M., 1974, MNRAS 167, 31
Fasano G. & Vio R., 1988, BICDS 35, 191
Feigelson E.D. & Nelson P.I., 1985, ApJ 293, 192
Feigelson E.D. & Babu G.J., 1992, ApJ 397, 55
Ferrarese L. & Merritt D., 2000, ApJ 539, L9
Ferrero E. & Brinkmann W., 2003, A&A 402, 465
Fossati G., Maraschi L., Celotti A., et al. 1998, MNRAS 299, 433
Georganopoulos M. & Kazanas D., 2003, ApJ 594, 27
Ghisellini G. & Maraschi L., 1989, ApJ 340, 181
Gopal-Krishna, Wiita P.J. & Hooda J.S., 1996, A&A 316, L13

Gopal-Krishna & Wiita P.J., 2000, A&A 363, 507
Hamann F., Korista K.T. & Morris S.L., 1993, ApJ 415, 541
Hardcastle M.J. & Worrall D.M., 1999, MNRAS 309, 969
Hill G.J., Goodrich R.W. & DePoy D.L., 1996, ApJ 462, 163
Hoyle F. & Fowler W.A., 1962, MNRAS 125, 169
Hoyle F. & Fowler W.A., 1963, *Nature* 197, 533
Isobe T., Feigelson E.D. & Nelson P.I., 1986, ApJ 306, 490
Kellermann K.I., Sramek R., Schmidt M., et al., 1989, AJ 98, 1195
Kembhavi A., 1993, MNRAS 264, 683
Koratkar A. & Blaes O., 1999, PASP 111, 1
Kormendy J. & Gebhardt K., 2001, *20th Texas Symposium on Relativistic Astrophysics*, AIP Conf. Proc. 586, eds. J.C. Wheeler & H. Martel (Melville, NY:AIP), 363
Kormendy J. & Richstone D.O., 1995, ARA&A 33, 581
Laing R.A., Jenkins C.R., Wall J.V. & Unger S.W., 1994, *The First Stromlo Symposium: The Physics of Active Galaxies*, ASP Conference Series, Vol. 54, 1994, G.V. Bicknell, M.A. Dopita, and P.J. Quinn, Eds., p.201
Landau R., Golisch B., Jones T.J., et al., 1986, ApJ 308, 78
Laor A., 2003, astro-ph 0312417
Lara L., Giovannini G., Cotton W.D., et al., 2004, A&A 421, 899
Latta R.B., 1981, J. Am. Statistical Association 26, 713
Lockman F.J. & Savage B.D., 1995, ApJS 97, 1
Maccacaro T., Gioia I.M, Wolter A., et al., 1988, ApJ 326, 680
MacLeod J.M. & Andrew B.H., 1968, ApL 1, 243
Maiolino R., Marconi A., Salvati M., et al., 2001, A&A 365, 28
Maraschi L. & Rovetti F., 1994, ApJ 436, 79
Maraschi L. & Tavecchio F., 2003, ApJ 593, 667
Marchesini D., Celotti A. & Ferrarese L., 2004, MNRAS 351, 733
Marscher A.P., 1999, APh 11, 19
Meier D.L., 1999, ApJ 522, 753
Miller J.S., Goodrich R.W. & Mathews W.G., 1991, ApJ 378, 47
Mulchaey J.S., Mushotzky R.F. & Weaver K.A., 1992, ApJ 390, L69
Murphy E.M., Lockman F.J., Laor A. & Elvis M., 1996, ApJS 105, 369
Mushotzky R.F., 1982, ApJ 256, 92
O'Dea C.P., 1998, PASP 110, 493
Orr M.J.L. & Browne I.W.A., 1982, MNRAS 200, 1067
Osterbrock D.E., 1989, *Astrophysics of Gaseous Nebulae and Active Galactic Nuclei*, University Science Books
Owen F.N. & Ledlow M.J.,1994, *The First Stromlo Symposium: The Physics of Active Galaxies*, ASP Conference Series, Vol. 54, 1994, G.V. Bicknell, M.A. Dopita, and P.J. Quinn, Eds., p.319
Padovani P. & Giommi P., 1995, ApJ 444, 567
Padovani P., Perlman E.S., Landt H., et al., 2003, ApJ 588, 128
Perley R.A., Fomalont E.B & Johnston K.J, 1979, AJ 85, 649
Rees M.J., 1984, ARA&A 22, 471
Reynolds C.S., Di Matteo T., Fabian A.C., et al., 1996, MNRAS 283, 111
Richstone D.O., 2002, *Reviews in Modern Astronomy* 15, ed. R.E. Schielicke (Wiley), 57
Rybicki G. & Lightman A.P., 1979, *Radiative Processes in Astrophysics*, New York, John Wiley and Sons
Sambruna R.M., Maraschi L. & Urry C.M., 1996, ApJ 463, 444
Scheuer P.A.G & Readhead A.C.S, 1979, *Nature* 277, 182
Schmidt M., 1963, *Nature* 197, 1040
Schmidt M., 1968, ApJ 151, 393
Schmitt J.H.M.M., 1985, ApJ 293, 178

Schödel R., Ott T, Genzel R., et al., 2002, *Nature* 419, 694
Schultz G.V. & Wiemer W., 1975, A&A 43, 133
Seyfert C.K., 1943, ApJ 97, 28
Siebert J., Brinkmann W., Morganti R., et al., 1996, MNRAS 279, 1331
Tran H.D., 2001, ApJ 554, L19
Trümper J., 1983, Adv. Space Res. 27, 1404
Trussoni E., Capetti A., Celotti A., et al., 2003, A&A 403, 889
Urry C.M. & Padovani P., 1995, PASP 107, 803
Vèron-Cetty M.P. & Vèron P., 1993, *A Catalogue of Quasars and Active Galactic Nuclei*, 6th edition, ESO Scientific Report No. 13, ESO Publications
Visvanathan N., 1969, ApJ 155, L133
Voges W., Aschenbach B., Boller T., et al., 1999, A&A 349, 389
von Montigny C., Bertsch D.L., Chiang J., et al., 1995, ApJ 440, 525
Weymann R.J., Morris S.L., Poltz C.B., et al., 1991, ApJ 373, 23
White R.L., Becker R.H., Gregg M.D., et al., 2000, ApJS 126, 133
Williams O.R., Turner M.J.L., Stewart G.C., et al., 1992, ApJ 389, 157
Willott C.J., Simpson C., Almaini O., et al., 2004, ApJ 610, 140
Wilson A.S., Braatz J., Heckman T.M., et al., 1993, ApJ 419, L61
Wilson A.S. & Colbert E.J.M., 1995, ApJ 438, 62
Wolter A., Comastri A., Ghisellini G., et al., 1998, A&A 335, 899
Worrall D.M., Giommi P., Tananbaum H. & Zamorani G., 1987, ApJ 313, 596
Worrall D.M. & Wilkes B.J., 1990, ApJ 360, 396
Zamorani G., Henry J.P., Maccacaro T., et al., 1981, ApJ 245, 357

List of publications

Brinkmann W., Ferrero E., Gliozzi M., *XMM-Newton observation of the BAL Quasar PHL 5200: The big surprise*, 2002, A&A 385, 31

Brinkmann W., Grupe D., Branduardi-Raymont G., Ferrero E., *XMM-Newton observation of PG 0844+349*, 2003, A&A 398, 81

Ferrero E., Brinkmann W., *XMM-Newton observations of four high-z quasars*, 2003, A&A 402, 465

Brinkmann W., Papadakis I. E., Ferrero E., *XMM-Newton observations of the two X-ray weak quasars PG 1411+442 and Mrk 304*, 2004, A&A 414, 107

Brinkmann W., Arévalo P., Gliozzi M., Ferrero E., *X-ray variability of the Narrow Line Seyfert 1 Galaxy PKS 0558-504*, 2004, A&A 415, 959

Curriculum Vitae

I. Personal data

Name: Elisa Ferrero

Date of birth: December 9th, 1973

Place of birth: Pinerolo (Torino), Italy

Nationality: Italian

Home address: Marktplatz 1, 69117 - Heidelberg, Germany

Work address: Landessternwarte - Königstuhl, 69117 - Heidelberg, Germany

Telephone numbers: +49 (0)6221 4322257 (home), +49 (0)6221 509223 (office)

E-mail: eferrero@lsw.uni-heidelberg.de

Fax: +49 (0)6221 509202

II. Education

- November 1st, 2004 - present date: post-doctoral position at the Landessternwarte in Heidelberg.

- September 1st, 2001 - October 31st, 2004: PhD student at the International Max-Planck Research School on Astrophysics (IMPRS) and at the Max-Planck-Institut fuer extraterrestrische Physik, Garching (Germany) with a thesis on the subject: "AGN unification - the X-ray perspective". Supervisors: Dr. Wolfgang Brinkmann, Prof. Gregor Morfill

- January 25th, 2001: Italian Physics Diploma (Diploma di Laurea) at the University of Turin (Universita' degli Studi di Torino), with a final mark of 110/110 e lode. Subject of the thesis: "X-ray emission properties of extragalactic radio sources in the context of unified schemes for the Active Galactic Nuclei". Supervisors: Prof. Silvano Massaglia, Prof. Edoardo Trussoni.

- July 1992: Italian High School Diploma (scientific area) at Liceo Scientifico Marie Curie in Pinerolo (Torino), with a final mark of 60/60.

The sample of AGN

Description of Table 1:

Col.	Units	Label	Explanations
1		RXJ Name	ROSAT name
2		Name	Alternative name
3		RA(J2000)	Right ascension at epoch J2000
4		DEC(J2000)	Declination at epoch J2000
5		z	redshift
6	mag	$m_{\rm V}$	Apparent V magnitude
7	Jy	$F_{\rm 5GHz}^{\rm core}$	5 GHz core flux
8	Jy	$F_{\rm 5GHz}$	5 GHz total flux
9		$\alpha_{\rm r}$	radio spectral index
10	erg s^{-1} cm^{-2}	$F_{0.1-2.4\ {\rm keV}}$	unabsorbed $0.1-2.4$ keV flux
11		Type	NED classification
12		Host	Type of host galaxy
13		Class.	Spectral classification
14		FR	Fanaroff-Riley classification

Note on $\mathbf{m_V}$: a * denotes a B apparent magnitude.

Note on $\mathbf{F_{5GHz}^{core}}$ and $\mathbf{F_{5GHz}}$: a # indicates a flux at 1.4 GHz; a *&* indicates a flux at 408 MHz.

Note on $\mathbf{F_{0.1-2.4\ keV}}$: for some sources the $0.1-2.4$ keV luminosity is given instead of the flux and this is indicated by a *.

Note on Type: *G*=galaxy, *Q*=quasar, *C*=in cluster.

Note on Host: *E*=elliptical, *S*=spiral, *0*=S0 galaxy, *c*=cD galaxy, *N*=N galaxy, *p*=peculiar or irregular, *d*=dwarf galaxy.

Note on Class.: *q*=quasar, *z*=BL Lac, *a*=AGN, *n*=NLRG, *w*=WLRG, *g*=GPS/CSS, *b*=BLRG, *1*=Seyfert 1, *2*=Seyfert 2, *s*= Seyfert galaxy, *9*=Seyfert 1.9, *8*=Seyfert 1.8, *5*=Seyfert 1.5, *l*=LINER, *r*=radio galaxy, *=starburst, *h*=HII galaxy, *!*=NLSy1.

Note on FR: *I*=Fanaroff-Riley 1 radio galaxy, *II*=Fanaroff-Riley 2 radio galaxy.

Table A.3: *The sample*

RXJ name (1)	Name (2)	RA(J2000) (3)	DEC(J2000) (4)	z (5)	m_V (6)	F_{5GHz}^{core} (7)	F_{5GHz} (8)	α_r (9)	$F_{0.1-2.4\ keV}$ (10)	Type (11)	Host (12)	Class. (13)	FR (14)
0000.0+0816	MCG +01-01-006	00 00 07.0	08 16 45.1	0.0387	16.00*	0.048	0.052	0.00	0.5084E-11	G	E	!	
0001.5+2113	TXS 2358+209	00 01 32.3	21 13 36.0	1.1060	19.10	0.108	0.119	0.60	0.2145E-11	Q		q	
	ESO 409- G 003	00 01 55.8	-27 37 38.0	0.0284	13.72	0.000	0.030#	0.00	0.9179E-12	GC	S		
0002.4+0321	NGC 7811	00 02 26.5	03 21 06.9	0.0255	15.06*	0.000	0.006#	0.00	0.4821E-11	G	0	5	
0003.1+2157	UGC 6	00 03 09.6	21 57 36.6	0.0219	14.62	0.000	0.028#	0.00	0.2313E-11	G	S	8	
	ESO 349- G 022	00 03 12.9	-35 56 13.5	0.0498	14.62*	0.000	0.517#	1.30	0.6044E-11	GC	0		
0003.8+0203	RBS 7	00 03 49.7	02 03 59.9	0.0978	16.39*	0.000	0.011#	0.00	0.4150E-11	GC	c		
	NVSSJ000409+..	00 04 09.5	45 26 25.6	0.1204	16.90	0.000	0.004#	0.00	0.4769E-11	G		1	
0004.2+4526		00 04 09.5	45 26 25.6	0.1209	16.90*	0.000	0.004#	0.00	0.5300E-11	G		1	
0004.9+1142	UGC 00032	00 04 58.5	11 42 03.3	0.0760	17.00	0.027	0.033	0.00	0.3922E-11	G	E	9	
0005.1-0133	LBQS 0002-0149	00 05 07.1	-01 32 46.4	1.7100	19.10	0.000	0.061	0.00	0.5727E-12	Q		q	
	UM 18	00 05 20.2	05 24 10.8	1.8870	16.21	0.000	0.296	0.00	0.4883E-12	Q		q	
	PKS 0003-282	00 05 58.7	-27 59 00.6	0.6250	17.20	0.000	0.309#	0.70	0.9294E-12	Q		q	
0005.9+1609	PG 0003+158	00 05 59.2	16 09 48.0	0.4509	16.40	0.121	0.350	0.50	0.7766E-11	Q		q	
0006.2-0623	PKS 0003-066	00 06 13.9	-06 23 35.3	0.3470	18.50	0.000	1.580	-0.13	0.1439E-11	G		z	
0006.3+2012	MRK 335	00 06 19.5	20 12 10.5	0.0258	13.85	0.000	0.008#	0.00	0.5545E-10	G	S	1	
0006.3+1052	NVSS J000620+..	00 06 20.3	10 51 51.3	0.1676	17.30*	0.000	0.012#	0.00	0.4200E-11	GC		z	
0006.3+1236	RGB J0006+125	00 06 23.0	12 35 53.1	0.9800	17.40	0.156	0.209	0.00	0.7755E-12	G		q	
0007.4+0240	LBQS 0004+0224	00 07 27.0	02 41 12.0	0.3000	18.00	0.000	0.007#	0.00	0.2479E-11	Q		q	
	RGB J0007+472	00 07 59.9	47 12 07.8	0.2800	18.30	0.067	0.000#	0.63	0.1393E-11	Q		z	
0008.2-0057	FIRSTJ000813.1-.	00 08 13.2	-00 57 53.3	0.1390	18.50	0.000	0.005#	0.00	0.1068E-11	G		1	
	RBS 16	00 08 35.4	-23 39 28.2	0.1470	17.90	0.000	0.036#	0.00	0.4004E-11	G		z	
0009.5+1803	RGB J0009+180	00 09 34.9	18 03 43.0	0.3100	17.00	0.070	0.270	0.00	0.1755E-11	G		q	
0009.5-3216	IC 1531	00 09 35.5	-32 16 36.7	0.0256	13.32*	0.000	0.350	-0.50	0.5163E-12	G	p		
	MRK 937	00 10 09.9	-04 42 37.6	0.0295	13.80	0.000	0.007#	0.00	0.4682E-11	G	S	1	
0010.4+2047	RGB J0010+207	00 10 28.7	20 47 49.7	0.6000	17.80	0.089	0.121	0.19	0.9794E-12	G		q	
0010.5+1058	MRK 1501	00 10 31.0	10 58 29.5	0.0893	15.40	0.151	0.435	-0.29	0.1341E-10	G	E	1	
0010.5+1724	4C +17.04	00 10 33.9	17 24 18.8	1.6010	17.33	0.960	0.989	-0.10	0.1226E-11	Q		q	
	PKS 0008-307	00 10 35.7	-30 27 45.9	1.1900	19.10	0.000	0.270	0.00	0.2816E-12	Q		q	
	PMN J0011-3620	00 11 14.7	-36 20 39.4	2.3240	21.30	0.000	0.066#	0.00	0.2842E-13	Q		q	
	ESO 409- G 025	00 11 21.7	-28 51 15.8	0.0609	12.90	0.000	0.011#	0.00	0.5854E-12	GC	E		
0011.5+0058	PMN J0011+0058	00 11 30.4	00 57 51.9	1.4941	17.88	0.000	0.135#	0.00	0.5245E-12	Q			
0011.9+2903	RGB J0012+290	00 12 01.9	29 03 22.6	0.2760	16.60*	0.000	0.027	0.00	0.1659E-11	Q		q	
	PMN J0012-1628	00 12 33.8	-16 28 06.5	0.1510	17.52*	0.000	0.095#	1.60	0.1616E-11	G			

Table A.3: *(continued)*

RXJ name (1)	Name (2)	RA(J2000) (3)	DEC(J2000) (4)	z (5)	m_V (6)	F_{5GHz}^{core} (7)	F_{5GHz} (8)	α_r (9)	$F_{0.1-2.4\ keV}$ (10)	Type (11)	Host (12)	Class. (13)	FR (14)
0013.5+4051	4C +40.01	00 13 31.1	40 51 37.1	0.2550	17.90	0.388	1.034	0.44	0.2025E-11	G	E	q	
	PKS 0011-304	00 13 41.2	-30 09 26.5	1.1110	20.21	0.000	0.223#	0.00	0.7712E-13	Q		q	
	NPM1G -19.0008	00 13 56.0	-18 54 06.8	0.0944	17.00*	0.000	0.029#	0.00	0.1026E-10	G		z	
	PKS 0012-312	00 14 37.9	-30 59 18.8	2.7850	19.70	0.000	0.193#	0.00	0.2131E-12	Q		q	
	TXS 0012+305	00 15 36.1	30 52 24.1	1.6190	16.30	0.000	0.081#	0.70	0.4977E-12	Q		q	
0016.3-1430	PKS 0013-14	00 16 19.8	-14 30 11.8	0.7664	17.00	0.000	0.250	1.14	0.2160E-11	Q		q	
0018.4+2947	RBS 42	00 18 27.7	29 47 30.4	0.1000	19.10	0.000	0.034#	0.00	0.1185E-10	Q		z	
0019.5+2956	NGC 0076	00 19 37.8	29 56 01.7	0.0244	14.00*	0.083	0.095	0.00	0.1088E-11	G	S		
0019.6+2602	4C +25.01	00 19 39.8	26 02 52.3	0.2840	15.90	0.310	0.435	0.23	0.3591E-11	Q		q	
	[HB89] 0016+731	00 19 45.8	73 27 30.0	1.7810	19.00	0.000	1.889	0.00	0.2926E-12	Q		q	
	IC 1543	00 20 55.4	21 51 57.7	0.0187	14.30*	0.000	0.008#	0.00	0.1160E-12	G	S		
0021.1-1909	PGC 001348	00 21 07.5	-19 10 05.6	0.0952	17.00*	0.000	1.082#	0.00	0.1700E-11	G	E		
0023.6-1753		00 23 39.4	-17 53 53.9	0.0535	15.40*	0.000	0.042#	0.00	0.1880E-11	G		5	
0024.4-2928	PKS 0021-29	00 24 30.1	-29 28 54.3	0.4060	20.00	0.000	1.000	0.66	0.4254E-11	Q		q	
0024.7+0032	LBQS 0022+0015	00 24 44.1	00 32 21.3	0.4040	17.20	0.000	0.027#	0.00	0.8843E-12	Q		q	
	MRC 0023-333	00 25 31.2	-33 02 47.9	0.0498	14.23*	0.000	0.410	1.23	0.3585E-11	GC	E	r	
	PKS 0023-26	00 25 49.1	-26 02 12.3	0.3220	19.50	0.000	3.410	0.70	<0.1700E-12	G		g	
0027.6+4514	RGB J0027+452	00 27 42.3	45 14 57.1	0.9710	17.80	0.091	0.073	0.00	0.1448E-11	G		q	
0028.1+3103	RGB J0028+310	00 28 10.7	31 03 47.0	0.5000	15.42	0.044	0.088	0.92	0.4490E-11	Q		q	
	PSGS 0026+0453	00 29 03.6	05 09 34.9	1.6330	19.80	0.000	0.352	0.20	0.1329E-12	Q		q	
	PG 0026+129	00 29 13.6	13 16 03.0	0.1420	15.41	0.000	0.007#	0.00	0.1187E-10	Q		q	
	S4 0026+34	00 29 14.2	34 56 32.2	0.6000	20.20*	0.000	1.219	0.26	0.1118E-12	G		g	
0029.7+0554	PKS 0027+056	00 29 45.9	05 54 40.7	1.3170	15.92	0.374	0.500	0.20	0.5831E-12	Q		q	
0030.2+3804	B3 0027+377	00 30 18.8	38 03 55.4	1.4500	18.40	0.047	0.054	0.80	0.1073E-11	Q		q	
	NVSSJ003035-..	00 30 35.9	-24 11 13.3	0.1381	17.43*	0.000	0.008#	0.00	0.1616E-11	GC			
0031.3+3015	RGB J0031+302	00 31 21.9	30 16 01.8	0.2000	18.20	0.076	0.044	0.10	0.1329E-11	G		1	
	PMN J0032-2649	00 32 33.0	-26 49 17.6	1.4700	18.30	0.000	0.135#	0.00	0.2053E-12	Q		q	
	PMN J0032-2849	00 32 33.1	-28 49 20.2	0.3239	18.80	0.000	0.161#	0.00	0.2522E-12	Q		z	
	NPM1G -20.0015	00 33 22.5	-20 39 08.2	0.0727	17.10*	0.000	0.009#	0.00	0.4567E-11	GC		2	
	ESO 540- G 001	00 34 13.8	-21 26 20.6	0.0268	13.70	0.000	0.043#	0.00	0.4578E-11	GC	S	8	
0034.2+0118	FBQS J0034+0118	00 34 19.2	01 18 35.8	0.8700	18.56	0.038	0.204	1.00	0.7137E-12	Q		q	
	PMN J0034-2134	00 34 30.8	-21 33 49.3	0.7640	22.90	0.000	0.168#	0.00	0.4379E-13	Q		q	
0034.7-0054	FBQS J0034-0054	00 34 43.9	-00 54 13.0	0.6560	20.00	0.067#	0.070#	0.00	0.7322E-12	G		q	
0035.8+5950	RGB J0035+598	00 35 52.6	59 50 04.6	0.0860	19.50	0.049	0.123	0.45	0.2776E-10	Q		z	

Table A.3: *(continued)*

RXJ name (1)	Name (2)	RA(J2000) (3)	DEC(J2000) (4)	z (5)	m_V (6)	F_{5GHz}^{core} (7)	F_{5GHz} (8)	α_r (9)	$F_{0.1-2.4\ keV}$ (10)	Type (11)	Host (12)	Class. (13)	FR (14)
0035.9-0912	FBQS J0035-0911	00 35 52.9	-09 11 50.4	1.0040	20.00	0.000	0.094#	0.00	0.5007E-12	Q		q	
0035.9+1553	[HB89] 0033+156	00 35 55.5	15 53 17.0	1.1600	18.00	0.123	0.153	0.88	0.5233E-12	Q		q	
0036.0+1838	3C 14	00 36 06.5	18 37 58.6	1.4690	20.00	0.000	0.610	1.08	0.6090E-12	Q		q	
	ARP 282	00 36 51.9	23 59 16.1	0.0161	13.70*	0.000	0.020#	0.00	0.8723E-13	G	S		
0037.7+3659	4C +36.01	00 37 46.1	36 59 10.9	0.3660	18.00	0.172	0.457	0.44	0.6033E-12	Q		q	
	[HB89] 0035-252	00 38 14.7	-24 59 02.2	1.1960	20.70	0.000	0.300	-0.80	0.2073E-11	Q		q	
0038.8-2458	[HB89] 0035-252	00 38 14.7	-24 59 02.2	1.1960	17.50*	0.000	0.413#	-0.80	0.2040E-11	Q		q	
	3C 17	00 38 20.5	-02 07 40.7	0.2197	18.02	2.814	2.720	0.72	0.1737E-11	G	E	b	II
0038.4+4136	B3 0035+413	00 38 24.8	41 37 06.0	1.3530	19.90	0.950	1.143	0.05	0.7600E-12	Q		q	
0038.4-3859	PKS 0035-39	00 38 26.9	-38 59 46.2	0.5960	16.29	0.000	0.440	0.55	0.9405E-12	Q		q	
0038.5+4128	PGC 2304	00 38 33.1	41 28 50.3	0.0725	17.00	0.000	0.005#	0.00	0.1986E-11	G		5	
	PMN J0039-2220	00 39 08.2	-22 20 01.3	0.0644	14.50*	0.000	0.117#	0.00	0.2333E-11	G	0		
	NGC 193	00 39 18.6	03 19 52.0	0.0145	12.21	0.000	0.650	0.70	0.1182E-12	G			I
	NVSSJ003942-...	00 39 42.9	-35 28 03.2	0.8360	17.86	0.000	0.092#	0.00	0.8900E-12	Q		q	
	RBS 91	00 40 16.4	-27 19 12.2	0.1720	19.20	0.000	0.160#	0.00	0.4275E-11	G		z	
0040.3+2933	UGC 00428	00 40 28.3	+29 33 21.2	0.0713	16.00*	0.000	0.015#	0.00	0.8900E-11	GC		a	
0040.8+1003	3C 018	00 40 50.5	10 03 22.7	0.1880	18.50	0.061	1.835	0.72	0.3048E-11	G		b	II
0040.9+3310	3C 19	00 40 55.0	33 10 08.0	0.4820	20.00*	0.000	1.250	0.99	0.6651E-12	G		w	II
0041.8-0918	MCG -02-02-086	00 41 50.5	-09 18 11.4	0.0557	13.50	0.036#	0.058#	0.00	0.8758E-10	GC	p		
0041.8+4021	MRK 957	00 41 53.4	40 21 17.9	0.0711	15.70	0.000#	0.017#	0.00	0.2453E-11	G		2	
	PKS 0039-44	00 42 09.4	-44 14 15.4	0.3460	19.50	0.000#	1.169	1.00	<0.3100E-12	G			
0042.6-1335		00 42 27.0	-13 35 33.9	0.2903	17.10*	0.000#	0.004#	0.00	0.1920E-11	G		q	
0042.6+3017	2MASXiJ0042399..	00 42 39.9	30 17 51.6	0.1408	17.40	0.000#	0.005#	0.00	0.3604E-11	G		5	
	LBQS 0040-2655	00 43 22.6	-26 39 05.0	1.0020	17.34	0.000#	0.078#	0.00	0.7223E-12	Q		q	
0043.7+3725	2MASXiJ0043425..	00 43 42.5	37 25 20.0	0.0799	17.40	0.000#	0.021#	0.00	0.3153E-11	G		1	
0043.8+2424	RGB J0043+244	00 43 52.1	24 24 21.1	0.0830	17.20	0.032#	0.050#	0.00	0.1135E-10	GC	c		
0043.9+3137	RGB J0043+316	00 43 59.8	31 37 20.0	0.6310	17.50	0.016	0.041	0.00	0.1441E-11	G		q	
0044.0+0102	PKS 0041+007	00 44 04.7	01 01 52.8	0.1117	17.30*	0.025	0.152	1.24	0.2970E-12	G			
	FBQS J0044+0052	00 44 13.7	00 51 41.0	0.9300	18.59	0.000	0.040#	0.00	0.2371E-12	G		q	
0043.9+1036	CGCG 435-002	00 44 16.5	10 34 56.6	0.0375	15.70*	0.000	0.055	0.00	0.5737E-12	G			
0044.5+1211	[HB89] 0041+119	00 44 34.9	12 11 11.9	0.2280	19.00	0.017	0.228	0.80	0.1673E-11	Q		q	
0044.9+1026	[HB89] 0042+101	00 44 58.7	10 26 53.7	0.5830	18.40	0.027	0.082	0.80	0.9881E-12	Q		q	
0044.9+1921	RGB J0044+193	00 44 59.1	19 21 40.8	0.1810	17.00	0.007	0.024	0.00	0.3653E-11	Q		q	
	HE 0043-2300	00 45 39.6	-22 43 55.0	1.5380	17.20	0.000	0.157#	0.00	0.8045E-12	Q		q	

Table A.3: *(continued)*

RXJ name (1)	Name (2)	RA(J2000) (3)	DEC(J2000) (4)	z (5)	m_V (6)	F_{5GHz}^{core} (7)	F_{5GHz} (8)	α_r (9)	$F_{0.1-2.4\ keV}$ (10)	Type (11)	Host (12)	Class. (13)	FR (14)
	PKS 0043-42	00 46 17.7	-42 07 51.5	0.1160	17.00*	0.000	2.980	0.87	<0.2000E-12	GC	E		II
0047.0+0319	PG 0044+030	00 47 05.9	03 19 55.0	0.6233	16.37	0.037	0.062	0.90	0.1171E-11	Q		q	
0047.3+1442	UGC 488	00 47 19.4	14 42 12.7	0.0393	15.28	0.000	0.003#	0.00	0.1668E-11	G	S	1	
0047.5-2517	NGC 0253	00 47 33.1	-25 17 17.6	0.0008	13.97	0.130	2.439	0.62	0.3943E-11	G	S	s	
	NGC 262	00 48 47.1	31 57 25.1	0.0150	14.59	0.000	0.244	-0.40	0.2425E-12	G	0	2	
	PMN J0049-2509	00 49 33.7	-25 09 34.8	1.4720	21.50	0.000	0.096#	0.00	0.9200E-13	Q		q	
0049.9-1847		00 49 37.0	-18 47 52.6	0.2898	17.20*	0.000	0.003#	0.00	0.1860E-12	G		q	
0050.0-5738	PKS 0047-579	00 49 59.5	-57 38 27.3	1.7970	18.50	0.000	2.480	0.70	0.8769E-12	Q		q	
	NVSSJ005040-...	00 50 40.9	-25 41 23.0	0.7800	18.77	0.000	0.057#	0.00	0.8008E-12	Q		q	
0051.2-2830	EDCC 485:004849	00 51 15.6	-28 31 33.1	0.1111	17.50*	0.000	0.032#	0.00	0.3010E-11	GC			
0051.5+2924	UGC 524	00 51 35.0	29 24 04.5	0.0359	14.50	0.000	0.011#	0.00	0.2294E-11	G	S	1	
0052.8+4336	NPM1G +43.0016	00 52 50.5	43 36 14.3	0.0590	17.70	0.000	0.004#	0.00	0.4027E-11	G		5	
0053.5+1241	UGC 545	00 53 34.9	12 41 36.2	0.0611	14.36*	0.002	0.009#	0.00	0.2094E-10	G	S	1	I
0054.6+0000	LBQS 0052-0015	00 54 41.2	00 01 10.7	0.6468	17.70	0.000	0.004#	0.00	0.1059E-11	Q		q	
	3C 28	00 55 50.3	26 24 34.4	0.1953	17.50	0.000	0.450	0.97	0.5989E-11	GC	E	w	I
	RBS 133	00 56 20.1	-09 36 31.1	0.1010	16.70	0.000	0.201#	0.00	0.8099E-11	G		z	
0057.5-0932	FBQS J0057-0932	00 57 29.1	-09 32 58.7	0.5590	18.30	0.000	0.004#	0.00	0.6089E-12	Q		q	
	3C 29	00 57 34.9	-01 23 27.9	0.0450	14.14	0.093	2.200	0.76	0.2500E-12	GC	E		I
0057.8+3021	NGC 0315	00 57 48.9	30 21 08.8	0.0164	12.50	0.590	0.914	0.33	0.1175E-11	GC	E	l	I
	NPM1G -02.0022	00 58 22.4	-02 41 41.6	0.0728	16.60	0.000	0.004#	0.00	0.2696E-11	G		1	
0058.9+2657	NGC 0326	00 58 22.7	26 51 55.0	0.0474	13.00	0.008	4.900&	1.00	0.1010E-12	GC		r	I
	PKS 0056-572	00 58 46.6	-56 59 11.5	0.0180	18.00*	0.000	1.070	0.10	0.2254E-11	Q		q	
0059.1+0006	LBQS 0056-0009	00 59 05.5	00 06 51.6	0.7190	17.33	1.370	1.393	0.36	0.8750E-12	Q		q	
	PKS B0057-338	01 00 09.4	-33 37 33.5	0.8740	20.20	0.000	0.130	0.00	0.1207E-12	Q		q	
	MCG -03-03-017	01 00 15.9	-15 17 57.5	0.0553	15.28*	0.000	0.034#	0.00	0.2168E-11	G			
0102.7-2152	MRC 0100-221	01 02 41.7	-21 52 55.8	0.0570	15.10	0.000	2.470&	1.72	0.1385E-10	GC	E	r	
0105.7-1416		01 05 38.8	-14 16 13.5	0.0666	15.70*	0.000	0.006#	0.00	0.2190E-10	G		1	
0106.7-1033	PMN J0106-1034	01 06 44.1	-10 34 09.8	0.4690	18.04	0.000	0.277#	0.00	0.1624E-11	Q		q	
	PKS 0104-408	01 06 45.1	-40 34 19.9	0.5840	18.20	0.000	0.850	-0.65	0.8420E-12	Q		q	
0107.4+3227	3C 31	01 07 24.9	32 24 45.2	0.0170	12.20	0.092	2.084	0.52	0.3182E-11	GC	0	w	I
	GSN 93	01 07 50.4	-36 43 23.6	0.1217	16.39	0.000	0.009#	0.00	0.1721E-11	GC			
	3C 32	01 08 16.9	-16 04 20.6	0.4000	20.00	0.000	1.169	1.10	<0.2200E-12	G			II
0108.6+0135	LBQS 0106+0119	01 08 38.8	01 35 00.3	2.0990	18.39	3.841	4.179	0.02	0.3964E-12	Q		q	
0109.0+1815	RBS 157	01 09 08.2	18 16 06.6	0.1450	16.20	0.082	0.000	0.00	0.8937E-11	Q		z	

Table A.3: *(continued)*

RXJ name (1)	Name (2)	RA(J2000) (3)	DEC(J2000) (4)	z (5)	m_V (6)	F_{5GHz}^{core} (7)	F_{5GHz} (8)	α_r (9)	$F_{0.1-2.4\ keV}$ (10)	Type (11)	Host (12)	Class. (13)	FR (14)
	HE 0106-3248	01 09 11.2	-32 32 43.0	0.2270	16.80	0.000	0.003#	0.00	0.2882E-11	G		q	
0109.4+3149	RGB J0109+318	01 09 27.8	31 49 56.0	1.7100	18.10	0.181	0.212	0.13	0.1445E-11	G		q	
0109.6+0059	FIRSTJ010939.0+.	01 09 39.0	00 59 50.3	0.0929	17.50	0.000	0.001#	0.00	0.1518E-11	G		1	
	3C 33.1	01 09 43.6	73 11 56.0	0.1810	19.50*	0.000	0.854	0.80	0.8286E-12	G	E	b	II
0110.0+1359	RGB J0110+139	01 10 03.2	13 58 41.4	0.0610	16.50*	0.016	0.119	0.65	0.1375E-11	GC			
0110.0+4149	RGB J0110+418	01 10 04.8	41 49 50.9	0.0960	17.60	0.018	0.040	0.00	0.2660E-11	G		z	
	RBS 159	01 10 35.1	-16 48 31.3	0.7800	15.60	0.000	0.106#	0.00	0.2985E-11	Q		q	
	RBS 161	01 10 49.9	-12 55 04.9	0.2340	17.90	0.000	0.017#	0.00	0.1317E-10	Q		z	
0110.7+3309	NGC 0410	01 10 58.9	+33 09 08.3	0.0177	12.50*	0.000	0.006#	0.00	0.3540E-11	GC	E	l	
	NPM1G -16.0043	01 11 14.2	-16 15 54.2	0.0518	16.00	0.000	0.002#	0.00	0.1951E-11	G		1	
	NGC 424	01 11 27.6	-38 05 00.5	0.0117	14.12	0.000	0.023#	0.00	0.7616E-12	G	S	2	
	NVSSJ011130+...	01 11 30.3	05 36 26.5	0.3460	19.90	0.000	0.016#	0.00	0.3768E-11	Q		z	
0112.1+2020	[HB89] 0109+200	01 12 10.1	20 20 21.0	0.7460	17.20	0.000	0.242#	0.55	0.9076E-12	Q		q	
0112.1+3522	B2 0109+35	01 12 12.9	35 22 19.3	0.4500	18.87	0.312	0.364	-0.09	0.1308E-11	Q		q	
0112.2+3819	GB6 J0112+3819	01 12 18.0	38 18 56.0	0.3330	17.30	0.113	0.000	0.09	0.1241E-11	Q		q	
0113.4+2958	4C +29.02	01 13 24.2	29 58 15.0	0.3630	17.00	0.077	0.341	0.71	0.1699E-11	Q		q	
0113.4+4948	S4 0110+49	01 13 27.0	49 48 24.0	0.3890	19.20	0.680	0.717	-0.22	0.2351E-11	Q		q	
	NGC 439	01 13 47.3	-31 44 49.7	0.0194	12.59*	0.000	0.022#	0.00	0.1860E-11	GC	0		
	MRK 1152	01 13 50.1	-14 50 44.1	0.0527	15.00	0.000	0.004#	0.00	0.1370E-10	G	S	5	
	UGC 774	01 13 51.0	13 16 18.2	0.0496	14.95	0.000	0.012#	0.00	0.6885E-12	G	S	1	
0115.2-0126	UM 310	01 15 17.1	-01 27 04.6	1.3650	17.50	0.000	1.100	-0.24	0.1243E-11	Q		q	
0116.2-1136	PKS 0113-118	01 16 12.5	-11 36 15.4	0.6700	19.00	0.000	1.879	-0.09	0.1591E-11	Q		q	
0116.9+2549	2MASXiJ0116540..	01 16 54.0	25 49 28.7	0.0990	16.70	0.000	0.014#	0.00	0.2300E-11	G		1	
0117.0+0000	RBS 0175	01 17 03.6	00 00 27.4	0.0456	15.90	0.000	0.001#	0.00	0.4364E-11	G		1	
0118.3+0257	3C 37	01 18 18.5	02 58 05.9	0.6720	18.82	0.269	0.614	1.30	0.1873E-11	Q		q	
0118.7-1849	PKS 0116-19	01 18 34.4	-18 49 14.8	0.2800	18.00*	0.000	1.171#	0.60	0.2550E-11	G	N		
	NVSS J011836-..	01 18 36.0	-18 43 32.2	0.4461	16.90	0.000	0.005#	0.00	0.1377E-11	G		q	
0118.9-0100	UGC 842	01 18 53.6	-01 00 07.3	0.0452	14.10	0.001#	0.004#	0.00	0.7848E-12	G	0	z	
	3C 38	01 20 27.1	-15 20 16.6	0.5650	20.00	0.000#	1.600	0.90	<0.3000E-12	G			II
	PKS 0118-272	01 20 31.7	-27 01 24.6	0.5590	15.56	0.000#	1.179	-0.33	0.1354E-11	QC		z	
	GIN 69	01 20 58.5	-13 51 00.5	0.0513	14.00*	0.000#	0.008#	0.00	0.6101E-11	GC	c		
0121.0+0344	3C 39	01 21 01.2	03 44 14.4	0.7650	18.09	0.026	0.297	0.89	0.1387E-11	Q		q	
0121.6-6309	PKS 0119-63	01 21 40.2	-63 09 00.1	0.8370	17.90	0.000	0.390	0.90	0.8440E-12	Q		q	
	PKS 0119+11	01 21 41.6	11 49 50.4	0.5700	19.70	0.000	0.970	0.20	0.9751E-12	Q		q	

Table A.3: *(continued)*

RXJ name (1)	Name (2)	RA(J2000) (3)	DEC(J2000) (4)	z (5)	m_V (6)	F_{5GHz}^{core} (7)	F_{5GHz} (8)	α_r (9)	$F_{0.1-2.4\ keV}$ (10)	Type (11)	Host (12)	Class. (13)	FR (14)
0121.9+0422	PKS 0119+041	01 21 56.9	04 22 24.7	0.6370	19.50	0.000	0.900	-0.16	0.7591E-12	Q		q	
0122.0-0004	MRK 1503	01 21 59.8	-01 02 24.1	0.0543	15.17	0.004#	0.005#	0.00	0.3704E-11	G	S	5	
0122.4-0421	4C -04.04	01 22 27.9	-04 21 27.5	1.9250	16.88	0.000#	0.670	0.70	0.1908E-11	Q		q	
	RBS 187	01 22 37.4	-26 46 46.0	0.4170	18.80	0.000#	0.004#	0.00	0.4376E-11	G		q	
0123.0+3420	RGB J0123+343	01 23 08.5	34 20 47.5	0.2720	18.46	0.040	0.000#	0.00	0.5082E-10	Q		z	
0123.0+3149	RGB J0123+318	01 23 08.8	31 49 13.0	0.0760	17.94	0.004	0.023	0.00	0.1763E-11	G		1	
	RBS 193	01 23 38.3	-23 10 59.4	0.4040	19.00	0.000	0.027#	0.00	0.9043E-11	G		z	
0123.6+3315	NGC 0507	01 23 40.0	33 15 20.0	0.0164	12.89	0.001	0.690&	0.00	0.8871E-11	GC	0		I
0123.6+2615	RGB J0123+262	01 23 43.0	26 15 22.4	0.8490	18.60	0.173	0.255	-0.18	0.7079E-12	G		q	
	NGC 526A	01 23 54.4	-35 03 55.6	0.0191	14.60	0.000	0.014#	0.00	0.2074E-11	G	p	9	
	[HB89] 0121+034	01 24 33.2	03 43 34.4	0.3360	18.50	0.000	0.003#	0.00	0.5235E-12	Q		q	
	NGC 521	01 24 33.8	01 43 53.0	0.0167	11.73	0.000	0.003#	0.00	0.1559E-12	GC	S		
	NGC 520	01 24 35.1	03 47 32.7	0.0076	11.42	0.000	0.087#	1.10	0.1470E-12	G	p		
	MS 0122.1+0903	01 24 44.5	09 18 50.0	0.3390	19.98	0.000	0.001	0.00	0.3470E-12	QC		z	
0124.8+0932	NGC 524	01 24 47.8	09 32 19.0	0.0079	10.25	0.000	0.003#	0.00	0.4312E-12	GC	0		
0124.7+3207	MRK 992	01 24 47.8	32 07 27.3	0.6540	17.80	0.082	0.171	0.43	0.1191E-11	Q		q	
	PMN J0125+0146	01 25 05.5	01 46 26.5	1.5590	19.86	0.000	0.079	0.60	0.3275E-12	Q		q	
0125.3-0018	UM 320	01 25 17.1	-00 18 28.9	2.2783	19.50	0.000	0.230	0.10	0.2144E-12	Q		q	
0125.4+0005	UM 321	01 25 28.8	-00 05 55.9	1.0800	16.70	0.000	1.290	0.23	0.1664E-11	QC		q	
0125.4+0146	NGC 533	01 25 31.4	01 45 32.8	0.0185	11.39	0.000	0.029#	0.00	0.5073E-11	GC	c		
0125.5+3208	UGC 987	01 25 31.5	32 08 11.4	0.0155	13.96	0.000	0.006#	0.00	0.2227E-11	G	S	5	
0125.9+3510	NVSSJ012555+...	01 25 55.9	35 10 36.7	0.3120	16.42	0.000	0.039#	0.00	0.1511E-11	Q		q	
	3C 40	01 25 59.8	-01 20 34.0	0.0180	13.34	0.100	1.879	0.91	0.4022E-12	GC	0	w	I
	NVSSJ012615-...	01 26 15.2	-05 01 21.1	0.4110	18.30	0.000	0.060#	0.00	0.6142E-12	Q		q	
0126.7+2558	[HB89] 0123+257	01 26 42.8	25 59 01.3	2.3580	17.50	0.777	1.302	0.13	0.1587E-11	Q		q	
	IC 115	01 26 54.4	19 12 52.9	0.0427	15.15*	0.000	0.580	1.46	0.1280E-12	GC	E		
0127.2-4112	[HB89] 0125-414	01 27 14.3	-41 12 42.0	1.0990	17.25	0.000	0.330	1.00	0.7353E-12	Q		q	
0127.5+1910	UGC 1032	01 27 32.5	19 10 43.8	0.0174	14.22	0.000	0.005#	0.00	0.1526E-10	G	S	!	
	RBS 0207	01 29 11.0	-21 41 56.8	0.0930	14.52	0.000	0.002#	0.00	0.1088E-10	G	S	1	
0132.5-0804	PKS 0130-083	01 32 41.1	-08 04 04.7	0.1485	16.50*	0.000	0.307#	0.00	0.4170E-11	G		q	
0133.0-5159	PKS 0131-522	01 33 05.8	-52 00 03.9	0.0200	20.30	0.000	1.179	0.80	0.1760E-11	Q		q	
0133.4+2427	PKS 0130+24	01 33 24.6	24 27 41.0	0.4570	17.40	0.049	0.262	0.52	0.1567E-11	Q		q	
0133.8+0113	UM 338	01 33 52.6	01 13 45.4	0.3081	18.10	0.000	0.069	0.00	0.1392E-11	Q			
	NGC 612	01 33 57.7	-36 29 35.7	0.0298	13.15	0.038	4.080	0.51	<0.1900E-12	GC	p		II

Table A.3: *(continued)*

RXJ name (1)	Name (2)	RA(J2000) (3)	DEC(J2000) (4)	z (5)	m_V (6)	F_{5GHz}^{core} (7)	F_{5GHz} (8)	α_r (9)	$F_{0.1-2.4\ keV}$ (10)	Type (11)	Host (12)	Class. (13)	FR (14)
	MCG -03-05-007	01 34 25.2	-15 49 08.8	0.0199	14.00	0.000	0.011#	0.00	0.8776E-12	G		s	
0135.3+0625	HS 0132+0610	01 35 21.1	06 25 47.0	0.1480	18.00	0.000	0.010#	0.00	0.1730E-11	G		a	
	RBS 219	01 35 27.0	-04 26 35.0	0.1547	16.20	0.000	0.008#	0.00	0.7738E-11	G		q	
	3C 47	01 36 24.4	20 57 27.0	0.4250	18.10	0.000	1.100	0.90	0.4435E-11	Q		q	
	MRC 0134-083	01 36 35.6	-08 06 06.8	0.1461	15.20	0.000	0.399#	0.74	0.1196E-11	G			
	[HB89] 0133+476	01 36 58.6	47 51 29.1	0.8590	19.50	0.000	1.811#	-0.27	0.2780E-11	Q		q	
	MRC 0134-094	01 37 15.4	-09 11 51.7	0.0412	15.00	0.053	0.180#	0.00	0.8203E-11	GC	S		
0137.6-2430	[HB89] 0135-247	01 37 38.3	-24 30 53.9	0.8370	17.33	0.000	1.649	-0.30	0.1874E-11	Q		q	
0137.6+3309	3C 48	01 37 41.3	33 09 35.1	0.3670	16.20	5.610	5.718	0.80	0.1567E-10	Q		g	
	NVSS J013756-..	01 37 56.0	-12 49 10.4	0.2125	19.20	0.000	0.021#	0.00	0.6751E-12	GC			
	KUG 0135-131	01 38 05.4	-12 52 11.1	0.0404	15.90	0.000	0.069#	0.00	0.1256E-12	G	S	2	
	GB6 J0138+0621	01 38 55.8	06 21 32.2	0.4500	18.70	0.000	0.045#	0.00	0.4989E-12	Q		q	
0139.7+1753	[HB89] 0136+176	01 39 41.9	17 53 07.5	2.7300	18.70	0.000	0.520	0.21	0.1011E-11	Q		q	
0139.9+0131	UM 355	01 39 57.2	01 31 46.2	0.2600	17.07	0.150	0.665	0.59	0.3048E-11	G		q	
	PMN J0140-1533	01 40 04.4	-15 32 55.3	0.8188	16.30	0.000	0.233#	0.00	0.1626E-11	G		q	
0140.0+1129	RX J0140.1+1129	01 40 05.1	+11 29 27.0	0.0650	16.20*	0.000	0.005#	0.00	0.3170E-11	G		!	
	UM 357	01 40 17.1	-00 50 03.0	0.3340	16.49	0.000	0.003#	0.00	0.5190E-11	Q		q	
	PKS 0139-09	01 41 25.8	-09 28 43.7	0.7330	16.55	0.000	1.189	-0.50	0.4416E-12	Q		z	II
0141.9+3923	RGB J0141+393	01 41 57.7	39 23 29.1	0.0800	16.01	0.080	0.080	0.31	0.1146E-11	G		1	
	NGC 660	01 43 02.3	13 38 44.4	0.0028	11.86	0.000	0.184	0.00	0.2376E-12	G	S	l	
0143.9+0220	UGC 1214	01 43 57.8	02 20 59.6	0.0173	14.07	0.000	0.025#	0.00	0.1323E-11	G	S	2	
	[HB89] 0142-278	01 45 03.4	-27 33 34.3	1.1550	18.30	0.000	0.900	-0.15	0.6820E-12	Q		q	
	MCG -01-05-031	01 45 25.5	-03 49 37.6	0.0182	14.00	0.000	0.014#	0.00	0.3284E-11	G	S	2	
	NPM1G-00.0070	01 46 44.8	-00 40 43.2	0.0827	16.00	0.000	0.009#	0.00	0.2728E-11	G		!	
	LEDA 094078	01 48 27.6	-04 07 46.9	0.0862	16.30*	0.000	0.012#	0.00	0.1862E-11	G			
	NGC 675	01 49 08.6	13 03 35.3	0.0178	15.50*	0.000	0.003#	0.00	0.2898E-11	G	S		
	PKS 0146+056	01 49 22.4	05 55 53.6	2.3450	20.10	0.000	0.730	-0.02	<0.2430E-12	Q		q	
	RGB J0150+362	01 50 51.2	36 16 32.9	0.0172	13.77*	0.017	0.019	0.00	0.1724E-11	GC	E		
0152.4-2319	RBS 247	01 52 27.1	-23 19 53.6	0.1130	15.60	0.000	0.005#	0.00	0.1261E-10	G	S	q	
0152.5+3350	[HB89] 0149+335	01 52 34.6	33 50 33.1	2.4310	18.20	0.470	0.611	0.13	0.7837E-12	Q		q	
0152.6-0143	FBQS J0152-0143	01 52 37.1	-01 43 58.6	0.8500	17.50	0.000	0.001#	0.00	0.4993E-12	Q		q	
0152.6+0147	RGB J0152+017	01 52 39.6	01 47 17.2	0.0800	16.60	0.065	0.000#	0.00	0.5866E-11	G		z	
	NGC 0708	01 52 46.5	36 09 06.6	0.0162	12.03	0.131#	0.067#	0.00	0.1473E-10	GC	E	2	I
	PKS 0150-334	01 53 10.1	-33 10 25.9	0.6100	18.60	0.000#	0.860	0.11	0.6300E-12	Q		q	

Table A.3: *(continued)*

RXJ name (1)	Name (2)	RA(J2000) (3)	DEC(J2000) (4)	z (5)	m_V (6)	F_{5GHz}^{core} (7)	F_{5GHz} (8)	α_r (9)	$F_{0.1-2.4\ keV}$ (10)	Type (11)	Host (12)	Class. (13)	FR (14)
0153.3+7115	RGB J0153+712	01 53 25.8	71 15 06.5	0.0220	15.50	0.291	0.643	0.47	0.1188E-11	G	E	z	
	PMN J0153-0117	01 53 34.3	-01 18 08.8	0.2458	19.00	0.000	0.106#	0.00	0.2563E-11	G		z	
0156.3+0537	NGC 0741	01 56 21.0	05 37 44.2	0.0185	12.82	0.000	0.280	1.56	0.1975E-11	GC	E	r	I
0156.3+2418	NVSS J015620+..	01 56 21.3	24 18 36.0	0.1550	17.00	0.000	0.003#	0.00	0.2104E-11	G		1	
	RGB J0157+413	01 57 05.0	41 20 30.4	0.0810	13.80	0.023	0.030	0.00	0.6933E-11	GC	E	q	
0157.3+3154	[HB89] 0154+316	01 57 15.3	31 54 17.7	0.3730	18.00	0.290	0.414	0.81	0.9125E-12	Q		q	
	[HB89] 0153+744	01 57 34.9	74 42 43.2	2.3380	16.50	0.000	1.548	0.00	0.6301E-11	Q		q	
0157.9-2101	PKS 0155-212	01 57 53.4	-21 02 17.1	0.1597	18.15*	0.074	0.220	1.00	0.5693E-12	G	E	r	
0159.8+0023	MRK 1014	01 59 50.2	00 23 40.6	0.1630	15.69	0.008	0.027#	0.00	0.3757E-11	G		q	
0200.2+3126	NGC 777	02 00 14.9	31 25 46.0	0.0166	11.45	0.000	0.007#	0.00	0.3797E-11	GC	E	2	
0200.4+0240	MRK 584	02 00 26.3	02 40 09.8	0.0788	15.30*	0.000	0.006#	0.00	0.7318E-11	G	E	8	
0201.1+0034	RBS 267	02 01 06.2	00 34 00.2	0.2984	17.96	0.000	0.013#	0.00	0.6366E-11	Q		z	
0201.3+0034	MS 0158.5+0019	02 01 06.2	+00 34 00.2	0.2990	18.00*	0.000	0.013#	0.00	0.6600E-11	Q		z	
	FIRSTJ020143.1+.	02 01 43.1	-02 11 47.6	0.1959	16.70*	0.000	0.012#	0.00	0.4780E-11	GC	c		
0201.7-0139	2MASXiJ0201456..	02 01 45.6	-01 40 13.4	0.2090	20.20	0.000	0.022#	0.00	0.1298E-11	G		a	
0201.9-1132	3C 57	02 01 57.1	-11 32 33.6	0.6690	16.40	0.000	1.350	0.60	0.2704E-11	Q		q	
0202.3-7619	[HB89] 0202-765	02 02 13.7	-76 20 03.0	0.3890	16.90	0.000	0.800	0.50	0.2650E-11	Q		q	
0202.9+1904	UGC 01518	02 02 18.9	+19 04 01.7	0.0650	16.00*	0.000	0.025#	0.00	0.7620E-11	GC		a	
0202.9-0223		02 02 52.3	-02 23 21.2	0.2600	19.10*	0.000	0.068#	0.00	0.1960E-11	?		z	
	RBS 273	02 03 00.7	-24 02 11.0	0.1781	16.50	0.000	0.002#	0.00	0.2677E-11	G		q	
	PKS 0201+113	02 03 46.6	11 34 45.4	3.6100	19.50	0.000	1.199	0.52	0.1033E-11	Q		g	
	KUG 0202-122	02 04 36.8	-11 59 43.4	0.0720	16.50	0.000	0.008#	0.00	0.1131E-11	G		1	
	4C +15.05	02 04 50.4	15 14 11.0	0.4050	21.00	0.000	2.299	0.30	0.5451E-12	Q		s	
0204.9-1701	PKS 0202-17	02 04 57.7	-17 01 19.8	1.7400	17.90	0.000	1.379	0.02	0.1000E-11	Q		q	
0206.9-0017	UGC 01597	02 06 15.9	-00 17 29.2	0.0424	14.30*	0.000	0.004#	0.00	0.6720E-11	G	0	5	
0207.0+2930	RBS 281	02 07 02.2	29 30 46.0	0.1096	16.80	0.066	0.681	1.43	0.5532E-11	G		8	
0208.5+3523	MS 0205.7+3509	02 08 38.2	35 23 12.7	0.3180	19.24	0.000	0.005#	0.00	0.6371E-11	Q		z	
0209.5-0438	FBQS J0209-0438	02 09 30.8	-04 38 26.7	1.1280	17.20	0.000	0.219#	0.00	0.6641E-12	Q		q	
	B2 0206+35	02 09 38.6	35 47 50.1	0.0377	13.00	0.106	4.559&	0.50	0.4230E+02*	GC	E		
	NGC 838	02 09 38.6	-10 08 49.1	0.0129	12.95	0.000	0.088#	0.00	0.2549E-12	GC	p	*	
	NGC 839	02 09 42.9	-10 11 02.7	0.0131	13.13	0.000	0.034#	0.00	0.7207E-13	GC	p	l	
	PMN J0209-1003	02 10 00.2	-10 03 53.9	1.9760	19.70	0.000	0.266#	0.00	0.1076E-12	Q		q	
	NGC 848	02 10 17.6	-10 19 17.2	0.0133	13.04	0.000	0.009#	0.00	0.3762E-13	GC	p	*	
	FBQS J0210-1015	02 10 28.3	-10 15 38.9	1.2100	18.75	0.000	0.003#	0.00	0.2133E-12	Q		q	

Table A.3: *(continued)*

RXJ name (1)	Name (2)	RA(J2000) (3)	DEC(J2000) (4)	z (5)	m_V (6)	F_{5GHz}^{core} (7)	F_{5GHz} (8)	α_r (9)	$F_{0.1-2.4\ keV}$ (10)	Type (11)	Host (12)	Class. (13)	FR (14)
0210.7-5100	[HB89] 0208-512	02 10 46.2	-51 01 01.9	0.9990	16.93	0.000	3.209	0.20	0.1316E-11	Q		z	
0212.1+3625	RGB J0212+364	02 12 09.7	36 26 18.1	0.4900	18.20	0.082	0.000	0.00	0.1611E-11	Q		q	
0212.3+0101	RGB J0212+010	02 12 25.6	01 00 56.1	0.5128	18.55	0.024	0.051	0.00	0.4733E-12	Q		q	
	RBS 292	02 12 30.5	-35 03 32.7	0.3930	18.70	0.000	0.019#	0.00	0.3004E-11	G		z	
0214.0+0042	NVSSJ021359+..	02 13 59.8	00 42 26.8	0.1921	18.00	0.004#	0.003#	0.00	0.2834E-11	G		1	
0214.6-0046	NGC 863	02 14 33.6	-00 46 00.1	0.0264	13.81	0.007#	0.017#	0.00	0.5464E-10	G	S	1	
	3C 62	02 15 37.5	-12 59 30.5	0.1470	18.50	0.024	1.800	0.74	<0.2500E-12	G	E		II
	UM 416	02 16 12.2	-01 05 18.9	1.4800	17.80	0.000	0.141#	0.00	0.3036E-12	Q		q	
0216.5+2314	RBS 298	02 16 32.1	23 14 47.0	0.2890	17.90	0.000	0.036#	0.00	0.1167E-10	Q		z	
0216.7-4749	PKS 0214-48	02 16 45.2	-47 49 09.8	0.0640	14.36*	0.000	0.790	0.60	0.2194E-11	GC	E		
0217.1+1104	PKS 0214+10	02 17 07.7	11 04 10.1	0.4080	16.46	0.000	0.460	0.84	0.7426E-11	Q		q	
0217.2+0837	ZS 0214+083	02 17 17.1	08 37 03.6	1.4000	17.90	0.296	0.462	0.06	0.1550E-11	Q		z	
0217.5+7349	S5 0212+73	02 17 30.8	73 49 32.6	2.3670	20.00	2.412	0.000	-0.13	0.2642E-11	Q		q	
	PKS 0215+015	02 17 48.9	01 44 49.7	1.7150	16.09	0.000	1.060	-0.60	0.9385E-12	Q		q	
	NVSS J021753-..	02 17 53.5	-19 58 19.0	0.4680	17.10	0.000	0.142#	0.00	0.2365E-11	G		q	
0217.9-1630	PKS 0215-16	02 17 57.2	-16 31 10.5	0.5157	19.10	0.000	0.360	0.21	0.1047E-11	Q		q	
	NVSSJ021905-...	02 19 05.5	-17 25 13.7	0.1280	17.25	0.000	0.062#	0.00	0.1327E-11	Q		z	
	S4 0218+35	02 21 05.5	35 56 13.7	0.6847	20.00	0.000	1.498	-0.02	0.7741E-12	G		z	
	PKS 0219-164	02 22 00.7	-16 15 16.5	0.7000	15.00	0.000	0.380	-0.10	0.5387E-12	Q		q	
	3C 61.1	02 22 36.0	86 19 08.0	0.1878	19.00	0.002	17.600&	0.77	0.8833E-12	GC		n	II
	3C 066A	02 22 39.6	43 02 07.8	0.4440	15.21	0.917	0.806	0.03	0.5836E-11	QC		z	
	3C 66B	02 23 11.4	42 59 31.5	0.0212	14.81	0.182	19.230&	1.04	0.9546E-12	G		1	I
0223.5+3935	B3 0220+393A	02 23 34.1	39 36 03.8	0.2200	19.80*	0.067	0.252	0.56	0.1197E-11	G		r	
0224.4+0659	[HB89] 0221+067	02 24 28.4	06 59 23.3	0.5110	20.70	0.000	0.770	0.04	0.1878E-11	Q		q	
	ESO 545- G 013	02 24 40.6	-19 08 31.3	0.0337	15.33	0.000	0.031#	0.00	0.4360E-11	G	S	5	
0225.0-2312	PKS 0222-23	02 25 02.7	-23 12 47.9	0.2300	18.50	0.000	0.780	0.65	0.6929E-11	Q		q	
	RBS 315	02 25 04.7	18 46 48.8	2.6900	18.90	0.000	0.580	0.21	0.7873E-11	Q		q	
0225.1+0035	PKS 0222-00	02 25 08.1	-00 35 31.4	0.6870	19.70	0.000	0.420	0.70	0.1358E-11	Q		q	
	PMN J0227-0847	02 27 32.1	-08 48 12.9	2.2280	17.30	0.000	0.066#	0.00	0.4026E-12	Q		q	
	NVSS J022739+..	02 27 39.6	44 09 57.2	0.1754	17.10	0.000	0.006#	0.00	0.3441E-11	G		q	
	PMN J0228-1038	02 27 59.2	-10 38 36.9	1.0380	19.34	0.000	0.132#	0.00	0.5092E-12	G		q	
0228.2+3118	NGC 931	02 28 14.5	31 18 41.9	0.0166	14.74	0.000	0.015#	0.00	0.1025E-10	G	S	1	
	VV 107a	02 29 01.1	38 05 54.5	0.0381	15.50*	0.000	0.010#	0.00	0.3001E-11	G			
0229.3-1027	[HB89] 0226-106	02 29 21.2	-10 27 48.0	0.6200	18.70	0.000	0.110#	0.00	0.4487E-12	Q		q	

Table A.3: *(continued)*

RXJ name (1)	Name (2)	RA(J2000) (3)	DEC(J2000) (4)	z (5)	m_V (6)	F_{5GHz}^{core} (7)	F_{5GHz} (8)	α_r (9)	$F_{0.1-2.4\ keV}$ (10)	Type (11)	Host (12)	Class. (13)	FR (14)
0230.0-0859	MRK 1044	02 30 05.4	-08 59 52.6	0.0164	14.29	0.001#	0.003#	0.00	0.4342E-10	G	S	1	
	IRAS 02295+3351	02 32 33.1	34 04 28.9	0.0788	16.30	0.000#	0.003#	0.00	0.3026E-11	G		1	
	NPM1G +06.0105	02 32 46.2	06 37 42.8	0.0708	17.73*	0.000#	0.008#	0.00	0.4245E-11	GC			
0232.8+2017	1ES 0229+200	02 32 48.5	20 17 16.2	0.1400	18.00	0.000#	0.045#	0.00	0.1455E-10	G		z	
0233.3+3442	RGB J0233+347	02 33 20.4	34 42 53.9	0.4580	20.80	0.123	0.179	0.22	0.8615E-12	Q		z	
0233.6-0454	PKS 0230-051	02 33 22.5	-04 55 05.4	0.7786	17.00*	0.000	0.212#	0.50	0.2000E-11	G		1	
0233.8+0229	[HB89] 0231+022	02 33 48.9	02 29 24.6	0.3210	17.30	0.000	0.110	0.70	0.3554E-11	Q		q	
	CGCG 388-052	02 33 51.6	01 08 13.8	0.0222	16.10*	0.000	0.005#	0.00	0.2514E-12	G			
	NGC 985	02 34 37.8	-08 47 15.4	0.0431	14.28	0.000	0.002#	0.00	0.2521E-10	G	S	5	
0235.1-0401	4C -04.06	02 35 07.4	-04 02 05.7	1.4500	16.46	0.000	0.620	0.49	0.2128E-11	Q		q	
	ESO 416- G 002	02 35 13.5	-29 36 17.2	0.0591	14.90	0.106	0.158#	0.00	0.5328E-11	GC	S	9	
	[HB89] 0234-301	02 36 31.2	-29 53 55.7	2.1020	18.30	0.000	0.530	0.00	0.3327E-12	Q		q	
	NGC 1004	02 37 41.8	01 58 31.1	0.0216	12.71	0.000	0.070	0.60	0.9824E-13	GC	E		
	PKS 0235-19	02 37 43.4	-19 32 33.3	0.6200	20.30	0.000	1.439	0.87	<0.4300E-12	G			II
0237.8+2848	B2 0234+28	02 37 52.4	28 48 08.9	1.2130	19.30	2.091	2.794	-0.20	0.1429E-11	Q		q	
	NGC 1016	02 38 19.6	02 07 09.3	0.0219	11.60	0.000	0.008#	0.00	0.3688E-12	GC	E		
0238.4+0154	NGC 1019	02 38 27.4	01 54 27.8	0.0242	14.95	0.000	0.008#	0.00	0.6578E-11	GC	S	5	
0238.4+0233	PC 0235+0220	02 38 32.7	02 33 48.8	0.2090	17.70	0.023	0.128	0.72	0.3523E-11	G		1	
	PKS 0235+164	02 38 38.9	16 36 59.3	0.9400	15.50	0.000	1.639	-0.20	0.2463E-11	Q		z	
	TXS 0236-131	02 38 49.3	-12 58 49.1	0.1951	17.60	0.000	0.077#	0.00	0.2134E-11	G		z	
	PKS 0237-027	02 39 45.5	-02 34 40.9	1.1160	19.90	0.000	1.159	-0.10	<0.4130E-12	Q		q	
	PKS 0237+040	02 39 51.3	04 16 21.4	0.9780	18.30	0.000	0.680	-0.09	<0.1070E-11	Q		q	
0240.1-2309	PKS 0237-23	02 40 08.2	-23 09 15.7	2.2230	16.63	0.000	1.510	-0.70	0.1696E-11	Q		g	
0241.0-0815	NGC 1052	02 41 04.8	-08 15 20.7	0.0049	11.24	0.000	1.399	-2.90	0.5640E-12	GC	E	l	
0242.2+0530	RBS 0345	02 42 14.6	+05 30 36.0	0.0685	15.90*	0.000	0.003#	0.00	0.1370E-10	G		1	
	PKS 0239+108	02 42 29.2	11 01 00.7	2.6940	20.00*	0.000	0.590	0.00	0.8240E-12	Q			
0242.6-2131	MRC 0240-217	02 42 35.9	-21 32 26.2	0.3140	17.00	0.000	0.820	0.27	0.4298E-11	G	N	q	
0242.6+0057	PHL 1443	02 42 40.3	00 57 27.2	0.5692	16.52	0.000	0.008#	0.00	0.3702E-11	Q		q	
0242.2+0057	E 0240+007	02 42 40.3	+00 57 27.2	0.5690	16.60*	0.000	0.008#	0.00	0.4250E-11	Q		a	
0242.6+0000	3C 071/NGC1068	02 42 40.7	-00 00 47.8	0.0038	10.83	2.307#	1.919	0.80	0.3573E-10	GC	S	2	
0244.9+6228	[HB89] 0241+622	02 44 57.7	62 28 06.5	0.0440	12.19	0.300	0.376	-0.36	0.5004E-10	G		q	
	4C +10.08	02 45 13.5	10 47 22.8	0.0700	16.50	0.000	0.211	0.00	0.1905E-11	G		z	
0246.3-3016	NGC 1097	02 46 18.9	-30 16 28.7	0.0043	9.75	0.126	0.150	0.00	0.2881E-11	G	S	1	
0248.6-0332	[CGH98] J0248-.	02 48 03.4	-03 31 45.0	0.1883	16.50*	0.000	0.041#	0.00	0.5920E-11	G			

Table A.3: *(continued)*

RXJ name (1)	Name (2)	RA(J2000) (3)	DEC(J2000) (4)	z (5)	m_V (6)	F_{5GHz}^{core} (7)	F_{5GHz} (8)	α_r (9)	$F_{0.1-2.4\ keV}$ (10)	Type (11)	Host (12)	Class. (13)	FR (14)
0249.3+1918	IC 1854	02 49 20.7	19 18 14.1	0.0310	14.81	0.000	0.004#	0.00	0.7954E-11	G	S	5	
	RBS 361	02 50 18.9	-21 29 37.7	0.4980	20.10	0.000	0.004#	0.00	0.4373E-11	G		z	
0250.6+1712	RGB J0250+172	02 50 37.9	17 12 08.5	1.1003	17.50	0.035	0.040	0.00	0.3965E-11	G		q	
	B3 0248+430	02 51 34.5	43 15 15.8	1.3100	17.60	0.000	1.413	-0.42	0.9861E-12	Q		g	
	PMN J0251-2052	02 51 54.9	-20 51 49.0	0.7610	18.50	0.000	0.053	0.00	0.2713E-12	Q		q	
0251.9-6718	[HB89] 0251-675	02 51 55.8	-67 18 00.1	1.0020	17.00	0.000	0.310	0.90	0.1549E-11	Q		q	
	PKS 0252-71	02 52 46.1	-71 04 32.3	0.5680	19.00*	0.000	1.580	1.14	<0.2400E-12	G		g	
	NGC 1132	02 52 51.8	-01 16 28.8	0.0232	12.26	0.000	0.008#	0.00	0.3933E-11	GC	E		
0253.4-5441	PKS 0252-549	02 53 29.2	-54 41 51.4	0.5390	17.80	0.000	0.800	-0.80	0.1350E-11	Q		q	
0253.9+3625	CGCG 0250.9+3613	02 54 00.0	36 25 52.0	0.0474	15.20	0.073	0.063	0.22	0.2293E-11	G	0		
0254.6+3931	RGB J0254+395	02 54 42.6	39 31 34.7	0.2890	16.30	0.273	0.352	-0.31	0.3229E-11	G		q	
	LEDA 097508	02 57 40.8	-16 30 46.0	0.0680	16.00	0.000	0.011#	0.00	0.3216E-11	G		5	
	PKS 0256+075	02 59 27.1	07 47 39.6	0.8930	19.00	0.000	0.980	-0.57	0.3150E-12	Q		q	
	RBS 377	02 59 30.5	-24 22 53.6	0.0350	16.20	0.000	0.004#	0.00	0.5761E-11	G	S	1	
	NVSS J030020+..	03 00 20.0	38 54 57.7	0.1897	16.10	0.000	0.009#	0.00	0.4435E-11	G		q	
	MS 0257.9+3429	03 01 03.8	34 41 00.9	0.2450	18.53	0.000	0.010	0.00	0.1618E-11	Q		z	
0301.6+0155	4C +01.06	03 01 38.5	01 55 16.5	0.1700	18.50	0.000	0.500#	0.96	0.6375E-11	GC	c		
	RGB J0301+358	03 01 51.5	35 50 30.0	0.0469	15.65*	0.003	0.230	1.29	0.6030E-11	GC			
0303.4-2407	RBS 0383	03 03 26.5	-24 07 11.0	0.2600	16.18	0.000	0.390	0.47	0.9774E-11	QC		z	
0303.0+0554	RBS 0384	03 03 30.1	+05 54 17.0	0.1960	17.90*	0.000	0.030#	0.00	0.1130E-10	Q		z	
0304.5-0054	FBQS J0304-0054	03 04 33.9	-00 54 04.2	0.3300	19.80	0.000	0.019#	0.00	0.1671E-11	Q		z	
	US 3621	03 04 58.9	00 02 35.7	0.5630	17.80	0.000	0.103#	0.00	0.7636E-12	Q		q	
	PMN J0305-2421	03 05 19.5	-24 21 34.5	0.2110	18.80	0.000	0.102#	0.00	0.2027E-12	G		n	
0306.3-3902	NGC 1217	03 06 06.0	-39 02 11.0	0.0210	13.60*	0.000	0.036#	0.00	0.3180E-11	GC	S	l	
0306.6+0003	NVSSJ030639+..	03 06 39.6	00 03 43.2	0.1073	17.87*	0.000	0.004#	0.00	0.2206E-11	G		*	
	PKS 0305-308	03 07 08.4	-30 37 29.6	1.1060	18.63	0.000	0.121#	0.00	0.9008E-12	Q		q	
0308.4+0406	3C 078	03 08 26.2	04 06 39.3	0.0286	13.90	0.964	3.649	0.64	0.6290E-11	G	0	1	I
0309.0+1029	PKS 0306+102	03 09 03.6	10 29 16.3	0.8630	18.40	0.000	0.700	-0.10	0.1253E-11	Q		q	
	3C 79	03 10 00.1	17 05 58.3	0.2559	18.75	0.010	14.000&	0.91	<0.2031E-12	G	N	2	II
0310.3+3911	RGB J0310+391	03 10 24.5	39 10 58.0	0.3700	18.60	0.015	0.090	0.13	0.3104E-11	Q		q	
0311.3-2046	RBS 392	03 11 18.8	-20 46 18.2	0.0660	16.47	0.000	0.005#	0.00	0.1597E-10	G		1	
0311.9-7651	LEDA 088074	03 11 55.2	-76 51 50.8	0.2230	16.10	0.000	0.590	-0.60	0.5928E-11	Q		q	
0312.4+3916	4C +39.11	03 12 26.5	39 16 30.4	0.1610	18.20	0.056	0.859	0.65	0.8022E-11	G		1	II
0312.8+3615	V ZW 326	03 12 50.3	36 15 19.5	0.0715	17.60	0.037	0.065	0.50	0.5148E-11	G		z	

Table A.3: *(continued)*

RXJ name (1)	Name (2)	RA(J2000) (3)	DEC(J2000) (4)	z (5)	m_V (6)	F_{5GHz}^{core} (7)	F_{5GHz} (8)	α_r (9)	$F_{0.1-2.4\ keV}$ (10)	Type (11)	Host (12)	Class. (13)	FR (14)
	S4 0309+41	03 13 01.9	41 20 01.2	0.1340	18.00	0.408	0.516	-0.08	0.7241E-11	G		1	
	V Zw 331	03 13 57.6	41 15 24.1	0.0294	17.00	0.048	0.000	0.00	0.9539E-12	G	E	z	
	RGB J0314+247	03 14 02.7	24 44 33.1	0.0542	18.30	0.006	0.044	0.00	0.1732E-11	G		a	
	4C -03.11	03 15 22.7	-03 16 46.0	1.0720	18.80	0.000	0.370	0.80	0.8824E-12	Q		q	
0316.0-0226	NGC 1266	03 16 00.7	-02 25 38.5	0.0073	14.00*	0.000	0.082#	0.00	0.5488E-12	G	S	s	
	IC 310	03 16 43.0	41 19 29.4	0.0189	12.74	0.000	0.258#	1.10	0.9979E-11	GC	0		
0317.9-4414	MRC 0316-444	03 17 57.7	-44 14 17.4	0.0759	13.90	0.000	0.620	0.45	0.1029E-10	GC	0		
	3C 83.1	03 18 15.9	41 51 27.8	0.0251	14.70*	0.040	3.529	0.54	0.1828E-12	GC	E	w	I
	NGC 1313	03 18 16.0	-66 29 53.7	0.0016	8.71	0.000	0.100	0.00	0.5145E-11	G	S	h	
	RBS 410	03 18 28.1	-21 22 08.0	0.1894	16.20	0.000	0.004#	0.00	0.4423E-11	G		q	
0319.8+4131	3C 084/PERSEUS A	03 19 48.2	41 30 42.1	0.0175	12.48	28.489	46.893	0.14	0.1981E-09	GC	c	5	I
0319.8+1845	LEDA 138616	03 19 51.8	18 45 34.2	0.1900	18.12	0.000	0.017	0.00	0.2273E-10	G		z	
0320.6+4305	RGB J0320+430	03 20 38.2	43 04 44.0	0.0517	16.10	0.010	0.406	0.00	0.1763E-11	GC	E		
0321.8+1221	PKS 0319+12	03 21 53.1	12 21 13.9	2.6620	18.30	1.620	0.000	0.34	0.1179E-11	Q		q	
	PMN J0322-1335	03 22 38.4	-13 35 17.7	1.4680	22.00	0.000	0.164	0.00	0.1142E-12	Q		q	
0322.7-3712	Fornax A	03 22 41.7	-37 12 29.6	0.0059	10.60	0.026	72.000	0.52	0.2324E-11	GC	S	l	I
0324.6+3410	RGB J0324+341	03 24 41.2	34 10 45.8	0.0610	15.72*	0.304	0.364	-0.08	0.9654E-11	G		1	
	PMN J0325-2140	03 25 00.8	-21 40 41.5	2.8280	17.80	0.000	0.100#	0.00	0.2279E-12	Q		q	
0325.2-0608	MRK 0609	03 25 25.3	-06 08 38.7	0.0341	15.10*	0.000	0.030#	0.00	0.1140E-10	G	p	8	
	RBS 421	03 25 41.1	-16 46 15.7	0.2910	16.70	0.000	0.027#	0.00	0.5418E-10	G		z	
0326.2+0225	RGB J0326+024	03 26 13.9	02 25 14.7	0.1470	16.55	0.068	0.047	0.00	0.3035E-10	G		z	
0327.9+0233	UGC 02748	03 27 54.2	02 33 41.8	0.0302	15.50	0.159	1.990	0.79	0.6406E-12	GC	E	n	II
0330.5+4102	4C +40.11	03 30 27.6	41 01 43.1	0.2010	18.50	0.548	1.700#	0.96	0.1083E-11	G			
0330.9+0538	RX J0330.8+0538	03 30 52.2	+05 38 25.6	0.0460	16.70*	0.000	0.004#	0.00	0.1040E-10	G		1	
	MS 0331.3-3629	03 33 12.2	-36 19 48.0	0.3080	18.00	0.000	0.009	0.00	0.1207E-11	Q		z	
0334.2-4007	PKS 0332-403	03 34 13.6	-40 08 25.4	1.4450	17.50	0.000	2.600	-0.46	0.1191E-11	Q		z	
0334.2-0111	3C 089	03 34 15.6	-01 10 56.4	0.1386	16.00	0.728	0.810	0.95	0.1719E-11	GC	0	r	I
0334.5-1513	IRAS 03321-152	03 34 24.5	-15 13 39.8	0.0348	15.40*	0.000	0.005#	0.00	0.9200E-11	G		5	
0335.6+1907		03 35 22.5	+19 07 28.0	0.1901	16.50*	0.000	0.005#	0.00	0.1280E-10	G		q	
0336.0+2235	RGB J0336+225B	03 36 04.8	22 35 35.0	0.5630	17.80	0.064	0.078	0.41	0.1063E-11	G		q	
0336.5+3218	B2 0333+32	03 36 30.1	32 18 29.3	1.2580	17.50	3.326	0.000	0.10	0.8603E-11	Q		q	
0338.1-2443	E 0336-248	03 38 12.5	-24 43 50.3	0.2509	19.10*	0.000	0.014#	0.00	0.1870E-11	G		z	
0338.1+0958	PGC 013424	03 38 40.5	+09 58 11.6	0.0346	16.00*	0.000	0.038#	0.00	0.1520E-09	GC	c	2	
0338.5-3535	NGC 1404	03 38 51.9	-35 35 39.8	0.0065	10.90*	0.000	0.004#	0.00	0.3960E-11	GC	E		

Table A.3: *(continued)*

RXJ name (1)	Name (2)	RA(J2000) (3)	DEC(J2000) (4)	z (5)	m_V (6)	F_{5GHz}^{core} (7)	F_{5GHz} (8)	α_r (9)	$F_{0.1-2.4\ keV}$ (10)	Type (11)	Host (12)	Class. (13)	FR (14)
0339.4-1735	APMBGC 548-090-	03 39 13.7	-17 36 00.8	0.0655	16.20*	0.000	0.171#	0.10	0.4340E-11	G	0		
0339.4-0145	PKS 0336-01	03 39 30.9	-01 46 35.8	0.8520	18.41	0.000	3.000	-0.05	0.1762E-11	Q		q	
	PKS 0338-214	03 40 35.6	-21 19 31.2	0.0480	17.10	0.000	0.940	-0.22	0.8513E-12	Q		z	
	MRC 0338-183	03 40 48.0	-18 14 00.3	0.1950	19.60	0.000	0.148	3.40	0.6687E-13	G		s	
0341.9+1524	III Zw 054 NED0	03 41 17.5	+15 23 51.0	0.0290	17.00*	0.000	0.021#	0.00	0.2360E-10	GC			
0342.8-2114	ESO 548- G 081	03 42 03.7	-21 14 39.7	0.0145	12.90*	0.000	0.004#	0.00	0.5170E-11	G	S	1	
	[HB89] 0340-372	03 42 05.4	-37 03 22.5	0.2840	18.60	0.000	0.710	0.31	0.1763E-11	Q		q	
0342.0+6339	RGB J0342+636	03 42 10.1	63 39 33.5	0.1280	18.50*	0.013	0.067	0.00	0.2177E-11	G		r	II
0343.0+1858	RX J0343.1+1858	03 43 08.3	+18 58 26.4	0.1090	16.70*	0.000	0.003#	0.00	0.8620E-11	G		1	
0347.6+0105	IRAS 03450+0055	03 47 40.2	01 05 14.0	0.0310	14.64	0.000	0.032#	0.00	0.1203E-11	G		5	
	PKS 0346-27	03 48 38.1	-27 49 13.6	0.9910	20.00	0.000	0.960	0.22	0.1448E-11	Q		q	
	1ES 0347-121	03 49 23.2	-11 59 27.0	0.1850	19.10	0.000	0.008	0.00	0.2661E-10	G		z	
	PKS 0347+05	03 49 46.5	05 51 42.3	0.3390	20.90	0.000	1.260	0.78	<0.3000E-12	G			II
0350.4-2217	HE 0348-2226	03 50 19.2	-22 17 22.0	0.1110	17.20*	0.000	0.019#	0.00	0.6350E-11	G		1	
0351.4-1429	3C 95	03 51 28.5	-14 29 08.7	0.6162	16.22	0.000	0.810	1.40	0.2423E-11	Q		q	
	PKS 0349-27	03 51 35.8	-27 44 34.7	0.0662	16.00	0.013	2.040	0.59	<0.2800E-12	G	E	n	II
	MS 0350.0-3712	03 51 53.8	-37 03 46.0	0.1650	18.50	0.000	0.017	0.00	0.5000E-12	Q		z	
	RGB J0352+214	03 52 41.0	21 26 09.8	0.1324	16.40	0.029	0.243	0.99	0.1951E-11	GC	E		
0352.9+1941	RX J0352.9+1941	03 52 58.9	+19 41 00.0	0.1080	18.30*	0.000	0.020#	0.00	0.1090E-10	GC	c		
0353.3+8256		03 53 08.4	+82 56 31.4	0.0694	16.00*	0.000	0.023#	0.00	0.4300E-11	G			
0353.7+1958	CGCG 0350.8+1949	03 53 46.3	19 58 26.4	0.0288	15.40	0.000	0.008#	0.00	0.5158E-11	G	S	1	
0354.1+0249	PGC 014064	03 54 09.5	+02 49 30.7	0.0360	16.30*	0.000	0.007#	0.00	0.1490E-10	G		1	
0354.5-1340		03 54 32.8	-13 40 07.8	0.0766	16.60*	0.000	0.016#	0.00	0.4650E-11	G		1	
	PKS 0356-421	03 57 36.8	-41 59 01.0	1.2710	20.90	0.000	0.118#	0.00	0.2031E-12	Q		q	
0357.9-0011	NPM1G -00.0144	03 57 58.7	-00 11 26.0	0.0140	16.40	0.000	0.005#	0.00	0.1409E-11	G	E	s	
	3C 98	03 58 54.4	10 26 03.0	0.0304	15.41	0.009	25.300&	0.10	0.3927E-13	G	E	n	II
	NVSS J040019+..	04 00 19.1	30 41 21.3	0.1135	17.20	0.000	0.013#	0.00	0.4113E-11	G		2	
0401.1+8153		04 01 32.5	+81 53 21.5	0.2149	19.60*	0.000	0.013#	0.00	0.5040E-11	G		z	
	PKS 0400-319	04 02 21.3	-31 47 25.9	1.2880	20.10	0.000	1.030	0.16	<0.1810E-12	Q		g	
	RBS 505	04 03 53.7	-36 05 01.9	1.4170	17.17	0.000	1.290	-0.47	0.2356E-11	Q		q	
0405.5-1308	PKS 0403-13	04 05 34.0	-13 08 13.7	0.5705	17.09	0.000	3.240	-0.05	0.1962E-11	Q		q	
0405.8+3803	4C +37.11	04 05 49.3	38 03 32.2	0.0550	18.50	0.621	1.020	0.57	0.1212E-10	G		s	
	PKS 0405-385	04 06 59.0	-38 26 28.0	1.2850	19.30	0.000	1.060	-0.06	0.4040E-12	Q		q	
	3C 105	04 07 16.5	03 42 25.7	0.0890	18.50	0.014	2.390	0.60	<0.3700E-12	G		n	II

Table A.3: *(continued)*

RXJ name (1)	Name (2)	RA(J2000) (3)	DEC(J2000) (4)	z (5)	m_V (6)	F_{5GHz}^{core} (7)	F_{5GHz} (8)	α_r (9)	$F_{0.1-2.4\ keV}$ (10)	Type (11)	Host (12)	Class. (13)	FR (14)
0407.6+0637	HS 0404+0629	04 07 37.9	06 38 04.6	0.3460	16.70	0.083	0.197	0.70	0.1363E-11	Q		q	
0407.8-1211	RBS 511	04 07 48.4	-12 11 36.6	0.5726	14.86	0.760	1.830	0.42	0.9277E-11	QC		q	
	PKS 0410-75	04 08 48.5	-75 07 19.3	0.6930	21.70	0.000	4.250	0.86	<0.4200E-12	GC		n	II
	PKS 0406+121	04 09 22.0	12 17 39.8	1.0200	20.20	0.000	1.620	-0.20	0.1934E-11	Q		z	
0412.0-6436	MRC 0411-647	04 11 59.4	-64 36 23.4	0.0570	16.50	0.000	0.380	0.80	0.1375E-11	G	E	r	
0413.3+2343	RGB J0413+237	04 13 22.5	23 43 35.3	0.3090	15.60	0.068	0.068	0.16	0.1640E-11	G		q	
0413.6+1112	3C 109	04 13 40.4	11 12 13.8	0.3056	18.01	0.219	1.391	0.85	0.4825E-11	G		b	II
0413.5-3805	ESO 303- G 005	04 13 58.9	-38 05 45.1	0.0498	15.10*	0.000	0.005#	0.00	0.7440E-11	G	c		
0415.1-2928	PKS 0413-296	04 15 08.7	-29 29 02.9	1.6300	17.50	0.000	0.300	1.10	0.6490E-12	Q		q	
0416.1-2056	[HB89] 0413-210	04 16 04.3	-20 56 27.5	0.8080	19.70	0.000	1.360	0.45	0.8162E-12	Q		q	
	PKS 0414-189	04 16 36.5	-18 51 08.3	1.5360	18.20	0.000	1.310	-0.17	<0.2500E-12	Q		q	
0416.8+0105	[HB89] 0414+009	04 16 52.5	01 05 23.5	0.2870	16.38	0.048	0.074	0.00	0.5785E-10	Q		z	
0417.2-0553	3C 110	04 17 16.7	-05 53 45.0	0.7750	15.94	0.000	0.320	0.50	0.2671E-11	Q		q	
0418.3+3801	3C 111	04 18 21.1	38 01 32.6	0.0485	18.05	1.139	5.168	0.95	0.1042E-10	G	N	b	II
	3C 114	04 20 21.0	17 53 47.0	0.8150	22.00*	0.000	0.330	0.51	0.2002E-12	G		r	
	RBS 537	04 21 32.8	-06 29 06.2	0.3907	18.70	0.000	0.016#	0.00	0.5340E-11	G		z	
	GB6 J0421+1433	04 21 33.1	14 33 54.4	0.0590	18.80	0.000	0.116#	0.00	0.1260E-12	G		z	
0421.8-1819	APMBGC 550-098-	04 21 57.7	-18 19 33.1	0.0954	16.20*	0.000	0.041#	0.00	0.2860E-11	G	0		
	MS 0419.3+1943	04 22 18.3	19 50 55.8	0.5120	20.26	0.000	0.009#	0.00	0.7625E-11	Q		z	
	PKS 0420+022	04 22 52.2	02 19 26.9	2.2770	19.50	0.000	0.670	-2.20	0.5000E-12	Q		q	
0423.2-0120	MRC 0420-014	04 23 15.8	-01 20 33.1	0.9140	17.00	0.000	4.150	-0.18	0.3632E-11	Q		q	
	[HB89] 0422-380	04 24 42.2	-37 56 20.8	0.7820	18.08	0.000	0.810	-2.10	0.1339E-11	Q		q	
0424.7+0036	[HB89] 0422+004	04 24 46.8	00 36 06.3	0.3100	16.98	1.100	0.000	-0.04	0.1636E-11	Q		z	
0427.0+0716	KUV 04244+0710	04 27 04.5	07 16 32.7	0.0900	16.50	0.000	0.003#	0.00	0.4570E-11	Q		1	
	PMN J0427-0756	04 27 14.2	-07 56 24.1	1.3750	21.00	0.000	0.075#	0.00	0.4193E-12	Q		q	
0428.6-3756	PKS 0426-380	04 28 40.4	-37 56 19.6	1.0300	19.00	0.000	1.139	-0.15	0.7453E-12	Q		z	
0433.1+0521	3C 120	04 33 11.1	05 21 15.6	0.0330	15.05	3.458	8.599	0.30	0.6461E-10	G	0	b	I
	PKS 0432-148	04 34 19.0	-14 42 55.3	1.8990	21.20	0.000	0.210	0.10	0.8661E-13	Q		q	
	IRAS 04288+7121	04 34 29.2	71 28 02.0	0.0248	16.50	0.000	0.008#	0.00	0.5999E-11	G		5	
0434.7+4014	IRAS 04312+4008	04 34 41.5	40 14 21.8	0.0207	15.20	0.000	0.018#	0.00	0.1156E-10	G	S	!	
	PMN J0435-0811	04 35 08.4	-08 11 03.5	0.7910	21.10	0.000	0.051#	0.00	0.3016E-12	Q			
	MRK 618	04 36 22.2	-10 22 33.8	0.0355	14.51	0.000	0.017#	0.00	0.1580E-10	G	S	1	
	MRC 0433+099	04 36 44.2	10 03 09.6	0.1590	18.50	0.029	0.046	-0.30	0.4115E-11	G			
	PKS 0434-188	04 37 01.5	-18 44 48.6	2.7020	18.50	0.000	1.189	-0.20	<0.3050E-12	Q		q	

Table A.3: *(continued)*

RXJ name (1)	Name (2)	RA(J2000) (3)	DEC(J2000) (4)	z (5)	m_V (6)	F_{5GHz}^{core} (7)	F_{5GHz} (8)	α_r (9)	$F_{0.1-2.4\ keV}$ (10)	Type (11)	Host (12)	Class. (13)	FR (14)
	3C 123	04 37 04.4	29 40 13.9	0.2177	21.70	6.599	134.259&	0.83	<0.6364E-13	G	c	w	II
0437.6-2954	PKS 0435-300	04 37 36.5	-29 54 03.0	1.3280	17.50	0.000	0.500	1.38	0.2106E-11	Q		q	
	PMN J0438-4728	04 38 47.0	-47 28 02.0	1.4450	20.50	0.000	0.130	0.00	0.2407E-11	Q		q	
0438.9+0520	RGB J0439+053	04 39 02.3	05 20 43.7	0.2080	16.10	0.139	0.149	0.00	0.6052E-11	G	c	q	
0440.3-4333	[HB89] 0438-436	04 40 17.2	-43 33 08.6	2.8630	19.50	0.000	7.000	-0.12	0.5692E-12	Q		q	
	RBS 570	04 40 18.3	-24 59 34.7	0.6000	18.60	0.000	0.013#	0.00	0.3765E-11	G		z	
0441.7-2708	IRAS 04392-271	04 41 22.6	-27 08 20.1	0.0835	16.50*	0.000	0.034#	0.00	0.1320E-10	G		1	
	UGC 3134	04 41 48.3	-01 18 06.6	0.0289	14.10	0.000	0.009#	0.00	0.2199E-11	G	S	2	
	[HB89] 0440-285	04 42 37.6	-28 25 30.8	1.9520	18.00	0.000	0.450	0.00	0.2772E-11	Q		q	
	PKS 0440-00	04 42 38.7	-00 17 43.4	0.8440	19.22	0.000	1.399	0.20	0.3771E-11	Q		g	
	IRAS 04416+1215	04 44 28.7	12 21 11.4	0.0889	16.15	0.000	0.014#	0.00	0.6933E-11	G		!	
0444.6-2810	MRC 0442-282	04 44 37.7	-28 09 54.3	0.1470	18.20	0.039	2.160	0.93	0.1344E-11	G	E	n	II
	NGC 1659	04 46 29.9	-04 47 19.6	0.0153	12.48	0.000	0.022#	0.00	0.7354E-13	G	S		
0447.2-2657	IRAS 04451-270	04 47 09.6	-26 57 34.0	0.1144	16.60*	0.000	0.027#	0.00	0.2500E-11	G		1	
	PMN J0447-0322	04 47 54.7	-03 22 42.0	0.7740	15.94	0.000	0.087#	0.00	0.2149E-11	Q		q	
	PKS 0446-212	04 48 17.4	-21 09 44.7	1.9710	18.60	0.000	0.280	0.40	0.1665E-12	Q		q	
0449.3+0728	RGB J0449+074	04 49 21.1	07 29 10.5	1.4620	16.90	0.057	0.042	-0.01	0.1539E-11	G		q	
	[HB89] 0448-392	04 49 42.2	-39 11 10.0	1.3020	16.46	0.000	0.890	0.10	0.1693E-11	Q		q	
	PKS 0454-81	04 50 05.4	-81 01 02.2	0.4440	19.70	0.000	1.280	0.30	0.1038E-11	Q		1	
	3C 129.1	04 50 06.7	45 03 05.8	0.0222	19.00*	0.004	0.195	0.94	0.7460E-11	GC	E		
0451.3-0348	MCG -01-13-025	04 51 41.5	-03 48 33.7	0.0159	15.00*	0.000	0.008#	0.00	0.7270E-11	G	S	1	
0452.0+4932	LEDA 168563	04 52 05.0	49 32 45.2	0.0290	17.10	0.000	0.015#	0.00	0.5415E-10	G		1	
0452.4-2953	[HB89] 0450-299	04 52 30.0	-29 53 35.0	0.2860	16.00*	0.000	0.010#	0.00	0.3200E-11	G		1	
	NGC 1684	04 52 31.1	-03 06 21.8	0.0148	13.00*	0.000	0.104#	0.00	0.3079E-12	G	E		
	IRAS 04502-0317	04 52 44.5	-03 12 57.3	0.0158	15.00	0.000	0.006#	0.00	0.1283E-12	G	S	2	
0452.7-2200	PKS 0450-220	04 52 44.7	-22 01 19.0	0.8980	18.10	0.000	0.260	0.90	0.1128E-11	Q		q	
	PKS 0451-28	04 53 14.6	-28 07 37.3	2.5590	18.20	0.000	2.500	-0.08	0.3790E-12	Q		q	
0453.5-5130	PKS 0452-515	04 53 36.5	-51 30 21.1	1.1570	17.60	0.000	0.260	0.70	0.1106E-11	Q		q	
	NGC 1691	04 54 38.3	03 16 04.7	0.0153	12.66	0.000	0.047#	0.00	0.2793E-12	G	S	*	
	NGC 1692	04 55 23.7	-20 34 16.2	0.0354	14.00	0.040	1.810	0.73	0.3500E-12	GC	E		I
0455.8-4616	PKS 0454-46	04 55 50.8	-46 15 58.7	0.8580	16.90	0.000	1.840	-0.10	0.1292E-11	Q		q	
0456.1-2159	MRC 0454-220	04 56 08.9	-21 59 09.0	0.5335	16.10	0.000	0.900	0.46	0.3779E-11	Q		q	
	PKS 0454-234	04 57 03.2	-23 24 52.0	1.0030	18.90	0.000	2.000	-0.21	0.5375E-12	Q		q	
	4C +46.09	04 58 26.7	46 24 31.8	0.1950	19.10	0.000	0.034	1.00	0.1006E-10	G	c		

Table A.3: *(continued)*

RXJ name (1)	Name (2)	RA(J2000) (3)	DEC(J2000) (4)	z (5)	m_V (6)	F_{5GHz}^{core} (7)	F_{5GHz} (8)	α_r (9)	$F_{0.1-2.4\ keV}$ (10)	Type (11)	Host (12)	Class. (13)	FR (14)
	UGC 3223	04 59 09.4	04 58 30.0	0.0156	14.41	0.000	0.020#	0.00	0.1369E-10	G	S	5	
	PKS 0457+024	04 59 52.0	02 29 31.2	2.3840	18.00	0.000	1.159	0.17	<0.3940E-12	Q		g	
0459.8-2439	MRC 0457-247	04 59 55.2	-24 39 39.7	0.1860	18.24*	0.035	0.250	0.50	0.7261E-12	GC	E		I
	4C -02.19	05 01 12.8	-01 59 14.2	2.2860	18.06	0.000	2.189	0.20	0.9592E-12	Q		q	
	LEDA 075258	05 02 09.0	03 31 50.0	0.0160	14.80	0.000	0.019#	0.00	0.6945E-11	G	E	1	
	3C 133	05 02 58.5	25 16 24.7	0.2775	20.00*	0.000	2.145	0.56	0.1345E-11	G			II
	MRC 0500+019	05 03 21.2	02 03 04.7	0.5846	21.20	0.000	2.040	0.47	0.3778E-12	Q		g	
0505.3+0459	PKS 0502+049	05 05 23.2	04 59 42.7	0.9540	18.90	0.747	1.014	-0.53	0.1520E-11	Q		q	
0505.5+0416	PMN J0505+0416	05 05 34.8	04 15 54.7	0.0272	17.60	0.090	0.112	0.00	0.8299E-11	G		z	
0506.7-6109	PKS 0506-61	05 06 43.9	-61 09 40.9	1.0930	16.85	0.000	1.459	0.80	0.1786E-11	Q		q	
	NVSS J050648-..	05 06 47.9	-19 36 50.9	0.0941	16.50	0.000	0.004#	0.00	0.2264E-11	G		5	
0507.7-3730	NGC 1808	05 07 42.3	-37 30 45.7	0.0033	12.55	0.000	0.220	-0.68	0.1064E-11	G	S	h	
0507.9+6737	RGB J0507+676	05 07 56.2	67 37 24.4	0.3140	18.50	0.021	0.027	0.00	0.3348E-10	Q		z	
0508.3+1721	RGB J0508+173	05 08 20.5	17 21 58.0	0.0182	15.40*	0.017	0.039	0.00	0.2958E-11	G		2	
	S5 0454+84	05 08 42.4	84 32 04.5	0.1120	16.50	0.000	1.409	0.00	0.1537E-12	Q		z	
0508.9+2113	NVSS J050855+..	05 08 55.1	21 13 02.4	0.1900	17.70	0.000	0.003#	0.00	0.3509E-11	G		1	
	1H 0506-039	05 09 38.1	-04 00 45.5	0.3040	19.50	0.000	0.071#	0.00	0.2502E-10	Q		z	
	PKS 0507+17	05 10 02.4	18 00 41.6	0.4160	20.00	0.000	1.040	-0.20	0.1367E-11	Q		g	
0513.8+0156	4C +01.13	05 13 52.5	01 57 10.4	0.0840	14.80	0.007	0.131	0.68	0.1083E-11	G	E	q	
0514.6-4903	FAIRALL 0790	05 14 39.4	-49 03 29.6	0.0910	17.00	0.000	0.280	0.40	0.2088E-11	G	E		
0515.7-4556	PKS 0514-459	05 15 45.3	-45 56 43.3	0.1940	17.50	0.000	0.790	0.50	0.2116E-11	Q		q	
	ARK 120	05 16 11.4	-00 08 59.4	0.0323	13.92	0.000	0.003	0.00	0.8284E-10	G	S	1	
	MCG -02-14-009	05 16 21.2	-10 33 41.4	0.0284	15.50	0.000	0.004#	0.00	0.8446E-11	G		1	
	MRC 0515+063	05 18 15.9	06 24 22.6	0.8910	19.00	0.000	0.239#	1.74	0.2649E-12	Q		q	
0519.8-4546	PICTOR A	05 19 49.7	-45 46 44.5	0.0350	15.77	1.000	15.369	1.07	0.1462E-10	GC	p	l	II
0521.1+1638	3C 138	05 21 09.9	16 38 22.0	0.7590	18.84	1.088	3.584	0.71	0.2197E-11	Q		g	
0521.1+6718		05 21 34.6	+67 18 07.9	0.0147	17.60*	0.000	0.004#	0.00	0.6120E-11	G		5	
	PMN J0522-0725	05 22 23.2	-07 25 13.4	0.1642	16.50	0.000	0.056#	0.00	0.6079E-11	G		1	
0522.9-3627	ESO 362- G 021	05 22 57.9	-36 27 30.8	0.0553	14.62	1.399	9.349	0.49	0.1876E-10	G	N	z	
	PKS 0524-460	05 25 31.4	-45 57 54.7	1.4790	18.00	0.000	0.990	1.20	0.8353E-12	Q		q	
0527.4+0412		05 27 10.9	+04 12 34.3	0.1537	17.30*	0.000	0.007#	0.00	0.8380E-11	G			
	RBS 653	05 28 53.0	-39 28 17.9	0.2839	19.10	0.000	0.005#	0.00	0.5372E-11	Q			
	IRAS 05262+4432	05 29 55.5	44 34 39.0	0.0318	13.60	0.000	0.023#	0.00	0.4276E-11	G	S	!	
	PKS 0528-250	05 30 07.9	-25 03 29.9	2.8130	17.34	0.000	1.129	0.25	<0.3390E-12	Q		g	

Table A.3: *(continued)*

RXJ name (1)	Name (2)	RA(J2000) (3)	DEC(J2000) (4)	z (5)	m_V (6)	F_{5GHz}^{core} (7)	F_{5GHz} (8)	α_r (9)	$F_{0.1-2.4\ keV}$ (10)	Type (11)	Host (12)	Class. (13)	FR (14)
0530.9+1332	PKS 0528+134	05 30 56.4	13 31 55.1	2.0600	20.00	4.299	0.000	0.07	0.3235E-11	Q		q	
	PMN J0535-0239	05 35 12.3	-02 39 07.3	1.0330	18.70	0.000	0.099	0.00	0.3941E-12	Q		q	
0535.3-3743	MRC 0533-377	05 35 22.4	-37 43 14.0	0.0964	16.00	0.000	0.160	0.70	0.2211E-12	GC	E	r	I
0538.8-4405	PKS 0537-441	05 38 50.4	-44 05 08.9	0.8940	16.48	0.000	3.799	0.19	0.3501E-11	Q		q	
	PKS 0537-344	05 39 05.4	-34 27 11.4	0.2630	19.90	0.000	0.236#	0.00	0.2635E-12	Q		1	
0539.5-1550	PKS 0537-158	05 39 32.0	-15 50 30.3	0.9470	17.30	0.000	0.610	0.05	0.1581E-11	Q		q	
0539.9-2839	PKS 0537-286	05 39 54.3	-28 39 55.9	3.1040	19.00	0.000	0.990	-0.47	0.1451E-11	Q		q	
	3C 147	05 42 36.1	49 51 07.2	0.5450	17.80	0.000	8.179	0.00	0.9800E-12	Q		g	
	PKS 0541-24	05 43 07.6	-24 21 02.9	0.5230	18.00	0.069	0.350	0.92	0.2920E-12	G	N	r	
	PMN J0544-2241	05 44 07.5	-22 41 09.0	1.5370	17.00	0.000	0.134#	0.00	0.7636E-12	Q		q	
	IRAS 05472-2426	05 49 14.9	-24 25 51.6	0.0448	17.80	0.000	0.003#	0.00	0.4742E-11	G			
0550.6-3216	PKS 0548-322	05 50 40.8	-32 16 17.8	0.0690	15.50	0.000	0.230	0.00	0.4593E-10	QC		z	
	IRAS 05480+5927	05 52 28.0	59 28 32.1	0.0585	15.80	0.000	0.004#	0.00	0.1552E-10	G		1	
	LEDA 165443	05 54 01.2	60 58 40.9	0.0910	16.30	0.000	0.009#	0.00	0.2144E-11	G		8	
	UGC 3374	05 54 53.6	46 26 21.6	0.0205	14.62	0.000	0.083#	0.90	0.8339E-10	G	0	5	
	[HB89] 0552+398	05 55 30.8	39 48 49.2	2.3650	18.30	0.000	5.424#	-1.00	0.2827E-11	Q		g	
	CTS 84	05 58 02.0	-38 20 04.7	0.0339	14.98	0.000	0.035#	0.00	0.2397E-11	G		1	
	GB6 J0558+5328	05 58 11.8	53 28 17.7	0.0360	14.00	0.000	0.238#	0.60	0.2472E-12	Q		z	
0559.6-1652	PKS 0557-16	05 59 40.7	-16 52 11.0	1.2400	18.27	0.000	0.150	0.98	0.1409E-11	Q		q	
	[HB89] 0558-504	05 59 47.4	-50 26 51.8	0.1370	14.97	0.000	0.113	0.80	0.1006E-09	Q		q	
	PKS 0558-396	06 00 31.4	-39 37 02.4	1.6610	18.60	0.000	0.300	-0.80	0.7066E-12	Q		q	
	PKS 0602-31	06 04 14.5	-31 55 58.0	0.4520	18.60	0.000	1.250	0.93	0.4319E-12	Q		q	
0607.9+6720	S4 0602+67	06 07 52.7	67 20 55.4	1.9700	20.60	0.495	0.581	-0.06	0.7913E-12	Q		q	
0607.9-0834	PKS 0605-08	06 07 59.7	-08 34 49.9	0.8720	17.60	0.000	3.390	0.40	0.8453E-12	Q		q	
0607.9+3058	RGB J0608+309	06 08 00.9	30 58 42.0	0.0730	17.30	0.059	0.076	0.00	0.9631E-11	G		1	
	PKS 0606-223	06 08 59.7	-22 20 20.9	1.9260	20.00	0.000	1.360	0.80	0.7711E-12	Q		q	
0609.6-1542	MRC 0607-157	06 09 40.9	-15 42 40.7	0.3240	18.00	0.000	1.770	-0.20	0.2352E-11	Q		q	
	MS 0607.9+7108	06 13 43.3	71 07 26.7	0.2670	18.50	0.000	0.024	0.00	0.6462E-12	Q		z	
0613.8+2604	3C 154	06 13 49.1	26 04 37.6	0.5800	18.00	0.000	2.020	0.69	0.1989E-11	Q			
	8C 0609+607	06 14 23.9	60 46 21.7	2.7020	18.60	0.921	1.058	0.00	0.4450E-12	Q		q	
0615.6+7102	MRK 0003	06 15 36.4	71 02 15.1	0.0135	13.35	0.361	0.363	1.05	0.1821E-11	G	0	2	
	NGC 2146	06 18 38.2	78 21 21.6	0.0029	10.59	0.000	1.020#	0.00	0.1298E-11	GC	S	h	
0621.6-5241	PKS 0620-52	06 21 43.2	-52 41 35.9	0.0511	15.50	0.260	1.250	0.87	0.3510E-11	GC			I
	IRAS 06205-2316	06 22 33.5	-23 17 41.7	0.0380	14.85	0.000	0.004#	0.00	0.5379E-11	G		1	

Table A.3: *(continued)*

RXJ name (1)	Name (2)	RA(J2000) (3)	DEC(J2000) (4)	z (5)	m_V (6)	F_{5GHz}^{core} (7)	F_{5GHz} (8)	α_r (9)	$F_{0.1-2.4\ keV}$ (10)	Type (11)	Host (12)	Class. (13)	FR (14)
0623.5-4413	MRC 0622-44	06 23 31.8	-44 13 02.5	0.6880	16.93	0.000	0.890	-0.24	0.1436E-11	Q		q	
	NVSS J062335+..	06 23 35.1	64 45 36.2	0.0860	17.20	0.000	0.004#	0.00	0.7989E-11	G		1	
	PMN J0624-3231	06 24 44.9	-32 30 53.6	0.2750	19.70	0.000	0.044#	0.00	0.1647E-11	Q		q	
0626.3-5342	MRC 0625-536	06 26 19.0	-53 41 32.0	0.0539	15.40	0.042	1.850	1.17	0.5283E-11	GC	p		I
0626.7-5432	MRC 0625-545	06 26 49.4	-54 32 34.6	0.0517	16.00	0.000	0.870	0.90	0.1627E-11	GC	E		
0627.1-3529	MRC 0625-354	06 27 06.7	-35 29 15.3	0.0546	17.60*	0.600	2.120	0.53	0.1257E-10	GC	E	r	I
0631.3+2500	3C 162	06 31 22.7	25 01 06.7	0.0830	16.80	0.039	0.381	0.81	0.1833E-10	GC	E		
0632.7+6340	UGC 3478	06 32 47.2	63 40 25.2	0.0128	12.90	0.000	0.013#	0.00	0.1129E-10	G	S	1	
	PMN J0633-2333	06 33 12.8	-23 33 09.0	2.9280	21.50	0.000	0.224#	0.00	0.1078E-12	Q		q	
0635.7-7516	MRC 0637-752	06 35 46.5	-75 16 16.8	0.6530	15.75	0.000	5.490	-0.10	0.7295E-11	Q		q	
	ESO 490-IG 026	06 40 11.7	-25 53 43.3	0.0248	15.00	0.000	0.039#	0.00	0.1025E-10	GC	p	1	
0643.3+4214	B3 0639+423	06 43 26.8	42 14 18.8	0.0893	17.00	0.033	0.038	0.00	0.3124E-10	G		z	
	B3 0642+449	06 46 32.0	44 51 16.6	3.3960	18.49	0.000	1.191	-0.56	0.7200E-12	Q		q	
	8C 0641+681	06 46 42.4	68 07 41.0	0.9270	19.70	0.000	0.074	0.50	0.2035E-12	Q		q	
	NGC 2258	06 47 45.8	74 28 54.0	0.0133	13.00*	0.000	0.010#	0.00	0.1796E-11	G	0		
	PKS 0646-437	06 48 13.4	-43 47 15.0	1.0290	18.30	0.000	0.126#	1.00	0.7503E-12	Q		q	
	PKS 0646-306	06 48 14.1	-30 44 19.6	0.4550	18.60	0.000	1.060	0.00	0.7367E-12	Q			
	S4 0646+60	06 50 31.2	60 01 44.5	0.4550	18.60	0.000	0.916	0.88	0.1289E-11	Q		g	
	8C 0646+699	06 51 54.6	69 55 26.4	1.3600	20.00	0.000	0.127	0.70	0.4369E-12	Q		q	
0652.1+7425	MRK 0006	06 52 12.2	74 25 37.5	0.0188	14.19	0.100	0.105	0.79	0.1777E-11	G	S	5	
0653.4+6919	4C +69.08	06 53 21.4	69 19 51.8	0.1100	15.20*	0.005	0.435	0.87	0.2148E-11	GC			
0654.6+4247	B3 0651+428	06 54 43.5	42 47 58.7	0.1260	17.00	0.134	0.190	0.44	0.8994E-12	G		z	
	3C 171	06 55 14.8	54 09 00.1	0.2384	19.08	0.002	8.400	0.90	<0.2708E-13	G	N	n	II
	UGC 3601	06 55 49.5	40 00 00.8	0.0171	14.80	0.000	0.005#	0.00	0.3913E-11	G	S	5	
0656.1+4236	4C +42.22	06 56 10.7	42 37 02.7	0.0590	16.90	0.138	0.480	0.56	0.3463E-11	G		z	
0659.5+5411	MRK 0374	06 59 38.1	+54 11 47.9	0.0435	15.00*	0.000	0.014#	0.00	0.2550E-10	G	S	1	
0702.9+6840	4C +68.07	07 02 54.2	68 41 16.5	0.1100	16.00	0.119	0.610	0.66	0.7265E-12	G		r	
0704.2+5412	CGCG 0700.2+5418	07 04 16.3	54 13 21.4	0.0368	15.00	0.013	0.028	0.00	0.8229E-12	G	E		
	KUG 0659+633	07 04 28.8	63 18 39.1	0.0949	17.40*	0.000	0.037#	3.00	0.9414E-11	GC			
	NVSS J070702+..	07 07 02.9	27 06 48.4	0.0623	16.40*	0.000	0.046#	0.00	0.6059E-11	G			
0707.0+6435	VII Zw 118	07 07 13.1	64 35 59.1	0.0797	14.61	0.000	0.003#	0.00	0.2204E-10	G		q	
0707.5+3822	[HB89] 0704+384	07 07 32.9	38 22 13.4	0.5790	17.50	0.061	0.321	0.80	0.1314E-11	Q		q	
	RGB J0709+486	07 09 08.0	48 36 55.5	0.0193	13.70*	0.069	0.259	0.30	0.3247E-11	GC	0		I
0710.0+5002	RGB J0710+500	07 10 06.8	50 02 46.0	0.1540	16.80	0.011	0.057	0.00	0.3768E-11	G		q	

Table A.3: *(continued)*

RXJ name (1)	Name (2)	RA(J2000) (3)	DEC(J2000) (4)	z (5)	m_V (6)	F_{5GHz}^{core} (7)	F_{5GHz} (8)	α_r (9)	$F_{0.1-2.4\ keV}$ (10)	Type (11)	Host (12)	Class. (13)	FR (14)
0710.4+5908	EXO 0706.1+5913	07 10 30.0	59 08 19.6	0.1250	18.40	0.034	0.080	0.00	0.2803E-10	G		z	
0711.7+3219	RGB J0711+323	07 11 47.7	32 18 35.9	0.0672	15.80	0.023	0.039	0.00	0.9520E-11	G	E	2	
0713.1+3655	B2 0709+37	07 13 09.5	36 56 06.8	0.4870	15.66	0.000	0.208	0.51	0.1550E-11	Q		q	
	B3 0710+439	07 13 38.2	43 49 17.2	0.5180	19.70	0.000	1.629	0.09	0.5833E-12	Q		g	
	IRAS F07102+3825	07 13 40.3	38 20 39.7	0.1230	16.30	0.000	0.011#	0.00	0.3329E-11	G		q	
	UGC 3752	07 14 03.9	35 16 45.4	0.0157	14.80	0.000	0.023#	0.00	0.2469E-12	G	S	2	
	B2 0711+35	07 14 24.8	35 34 39.8	1.6200	18.20	0.000	0.901	0.37	0.1828E-12	Q		g	
0714.5+7408	RGB J0714+741	07 14 36.1	74 08 10.1	0.3710	17.10	0.065	0.216	-0.50	0.3092E-11	Q		q	
0716.5+5323	4C +53.16	07 16 41.2	53 23 09.4	0.0642	14.00	0.015	0.649	0.76	0.2244E-11	GC			
	B3 0713+441	07 17 26.7	44 05 02.3	0.0652	16.60*	0.000	0.070	1.10	0.4704E-11	G			
0717.8+6430	RGB J0717+645	07 17 54.0	64 30 48.4	0.6330	17.70	0.008	0.018	0.00	0.1483E-11	G		q	
0718.0+4405	IRAS F07144+4410	07 18 00.6	44 05 27.1	0.0614	15.50	0.029	0.032	0.00	0.2060E-10	G		5	
	NVSS J071858+..	07 18 57.8	70 59 21.2	0.0660	17.40	0.000	0.003#	0.00	0.1881E-11	G		s	
0719.0+7124	8C 0713+714	07 18 59.6	71 24 18.0	1.4190	17.70	0.000	0.061#	0.00	0.1765E-12	G		q	
	GB2 0716+332	07 19 19.4	33 07 09.7	0.7790	17.05	0.000	0.358#	0.00	0.7551E-12	Q		q	
0720.3+2349	NVSS J072018+..	07 20 18.6	23 49 03.7	0.1660	17.20*	0.000	0.007#	0.00	0.5734E-11	G			
0720.7+3028	FIRSTJ072040.4..	07 20 40.5	30 28 48.4	0.1520	17.00	0.000	0.001#	0.00	0.3412E-11	G		1	
0720.7+6543	8C 0715+658	07 20 49.2	65 44 05.0	0.4830	19.66	0.130	0.335	0.80	0.9345E-12	G		1	
	ESO 428- G 023	07 22 09.4	-29 14 08.0	0.0101	13.41*	0.000	0.057#	0.00	0.3669E-12	GC	S		
0722.3+3030	HS 0719+3036	07 22 17.5	30 30 50.2	0.1000	16.20	0.000	0.006#	0.00	0.3987E-11	Q		1	
0723.8+6504	RGB J0723+650	07 23 54.8	65 04 54.6	0.2184	18.70	0.050	0.359	0.68	0.1477E-11	G		r	
	PMN J0724-0715	07 24 17.3	-07 15 19.7	0.2700	18.00	0.000	0.331#	0.00	0.3300E-11	Q		q	
0724.8+6659	4C +67.13	07 24 54.1	66 59 10.3	0.0872	17.60	0.248	1.425#	0.90	0.2362E-11	GC			
0725.0+6658	RGB J0724+669	07 24 56.3	66 59 09.1	0.0870	18.30	0.006	0.246	0.90	0.2362E-11	GC			
	PKS 0723-008	07 25 50.6	-00 54 56.5	0.1280	18.00	0.000	2.060	0.80	0.1273E-11	G		z	
	GB1 0723+488	07 27 03.1	48 44 10.1	2.4600	19.50	0.000	0.288	0.30	0.9077E-12	Q		q	
	3C 181	07 28 10.3	14 37 36.2	1.3820	18.92	0.006	0.660	1.00	<0.3385E-12	Q		q	II
	3C 179	07 28 11.6	67 48 47.5	0.8460	18.40	0.000	0.898	0.70	0.7858E-12	Q		q	
0729.5+2436	TXS 0726+247	07 29 27.8	24 36 23.6	0.1630	18.20	0.000	0.069#	2.20	0.4898E-11	G		2	
0729.9+3046	FBQS J0729+3046	07 29 52.3	30 46 45.1	0.1500	17.70	0.000	0.001#	0.00	0.5073E-12	Q			
0730.0+3307		07 30 26.0	+33 07 22.7	0.1130	17.00*	0.000	0.009#	0.00	0.3280E-11	Q		z	
0731.8+2804	2MASXiJ0731526..	07 31 52.7	28 04 32.6	0.2500	17.60	0.048	0.047	0.00	0.5165E-11	G		z	
	NGC 2300	07 32 20.5	85 42 31.9	0.0065	10.99	0.000	0.003#	0.00	0.1678E-11	GC	0		
	RGB J0733+394	07 33 00.7	39 25 06.3	0.1680	17.90*	0.020	0.035	1.40	0.1804E-11	GC		r	

Table A.3: *(continued)*

RXJ name (1)	Name (2)	RA(J2000) (3)	DEC(J2000) (4)	z (5)	m_V (6)	F_{5GHz}^{core} (7)	F_{5GHz} (8)	α_r (9)	$F_{0.1-2.4\ keV}$ (10)	Type (11)	Host (12)	Class. (13)	FR (14)
0733.2+3904	B3 0729+391	07 33 20.8	39 05 04.8	0.6600	18.20	0.000	0.120	0.30	0.1033E-11	Q		q	
0733.4+3515	RGB J0733+352	07 33 29.6	35 15 42.9	0.1769	17.70*	0.048	0.070	0.31	0.3450E-11	G		z	
0735.0+4750	S4 0731+47	07 35 02.3	47 50 08.4	0.7820	17.60	0.499	0.511	0.15	0.1788E-11	Q		q	
	FBS 0732+396	07 36 23.1	39 26 17.1	0.1180	16.00	0.000	0.004#	0.00	0.9521E-11	G		q	
0736.9+5846	MRK 9	07 36 56.9	58 46 13.4	0.0399	14.37	0.000	0.085#	0.00	0.3230E-11	G	p	5	
0737.0+2846	FIRST J073701.8+	07 37 01.9	28 46 45.9	0.2730	19.50	0.000	0.015#	0.00	0.1412E-11	Q		z	
0737.3+3518	GB6 J0737+3517	07 37 21.0	35 17 41.4	0.2130	18.90	0.016	0.019	0.00	0.2157E-11	Q		z	
0737.4+5941	CGCG 0733.1+5949	07 37 30.1	59 41 03.2	0.0405	15.17*	0.299	0.370	0.34	0.1561E-11	G	0	w	
0738.1+1742	MRC 0735+178	07 38 07.4	17 42 18.9	0.4240	16.22	1.290	1.812	0.02	0.1953E-11	Q		z	
0739.2+0136	PKS 0736+01	07 39 18.0	01 37 04.6	0.1910	16.47	1.754	1.891	0.40	0.5810E-11	Q		q	
0740.5+5525	UGC 03957	07 40 58.3	+55 25 37.6	0.0338	15.40*	0.000	0.053#	0.00	0.1400E-10	G	E	a	
	4C +74.13	07 41 44.5	74 14 39.5	0.2160	17.70*	0.000	0.023#	0.00	0.5201E-11	G	c		
	UGC 03973	07 42 32.8	49 48 34.7	0.0222	14.27	0.000	0.022#	0.00	0.6033E-10	G	S	1	
0742.6+5444	IVS B0738+548	07 42 39.8	54 44 24.7	0.7200	16.90	0.279	0.000#	-0.43	0.7246E-12	Q		q	
	3C 184.1	07 43 01.3	80 26 26.3	0.1182	17.00	0.006	7.599&	0.00	0.1645E-12	G	E	b	II
0743.5-6726	MRC 0743-673	07 43 31.6	-67 26 25.5	1.5100	16.37	0.000	1.510	0.30	0.2239E-11	Q		q	
0743.7+2329	[HB89] 0740+235	07 43 44.9	23 28 39.0	0.7700	19.30	0.127	0.196	1.00	0.6395E-12	Q		q	
	MS 0737.9+7441	07 44 05.3	74 33 57.6	0.3150	16.89	0.000	0.023#	0.00	0.1158E-10	Q		z	
	3C 186	07 44 17.4	37 53 17.1	1.0630	17.60	0.000	0.380	1.04	0.4232E-11	Q		g	
0745.6+3142	4C +31.30	07 45 41.7	31 42 56.6	0.4611	15.63	0.150	0.941	0.49	0.2973E-11	Q		q	
0745.8+2848	2MASXiJ0745482..	07 45 48.3	28 48 38.0	0.1580	17.50	0.000	0.001#	0.00	0.8338E-12	G			
	PKS 0743-006	07 45 54.1	-00 44 17.5	0.9940	18.10	0.000	1.310	-1.10	0.1715E-11	Q		g	
0745.9+3313	HS 0742+3320	07 45 59.3	33 13 34.5	0.6100	17.80	0.124	0.000	0.30	0.8493E-12	Q		q	
0746.8+5246	RGB J0746+527	07 46 57.1	52 46 19.9	0.5420	18.40	0.008	0.057	0.00	0.1024E-11	G		q	
0747.0+4132	UGC 04018	07 47 02.0	41 32 10.2	0.0290	10.30*	0.000	0.001#	0.00	0.2036E-11	G	0		
0747.4+6055	UGC 04013	07 47 29.1	60 56 00.6	0.0292	14.71	0.000	0.006#	0.00	0.1426E-10	G	S	1	
	MRC 0745-191	07 47 31.3	-19 17 39.9	0.1028	19.60*	0.000	0.410	0.99	0.7143E-10	GC	N		
0747.6+2456	NVSS J074737+..	07 47 38.4	24 56 37.6	0.1300	17.20	0.000	0.005#	0.00	0.6480E-12	G		1	
0748.6+2400	PKS 0745+241	07 48 36.1	24 00 24.1	0.4100	19.60	0.719	1.262	0.03	0.2532E-11	Q		q	
0749.0+4510	B3 0745+453	07 49 06.4	45 10 33.0	0.1900	16.60	0.051	0.113	0.28	0.2843E-11	Q		q	
0749.8+3454	FBQSJ074948.1..	07 49 48.2	34 54 43.8	0.1320	17.40*	0.000	0.001#	0.00	0.2484E-11	G		q	
0750.1+5522	CGCG 0746.1+5530	07 50 08.4	55 23 02.9	0.0193	14.07*	0.005	0.091	-1.00	0.7651E-12	G	E		
0750.8+4130	FBQS J075047.3+.	07 50 47.4	41 30 33.1	1.1840	17.59	0.000	0.002#	0.00	0.5610E-12	Q		q	
0750.9+0320	IRAS 07483+0328	07 51 00.7	03 20 40.9	0.0990	15.20	0.000	0.011#	0.00	0.1299E-10	G	S	q	

Table A.3: *(continued)*

RXJ name (1)	Name (2)	RA(J2000) (3)	DEC(J2000) (4)	z (5)	m_V (6)	F_{5GHz}^{core} (7)	F_{5GHz} (8)	α_r (9)	$F_{0.1-2.4\ keV}$ (10)	Type (11)	Host (12)	Class. (13)	FR (14)
	1RXSJ075122.1..	07 51 22.3	55 12 08.9	0.0640	17.00	0.002#	0.010#	0.00	0.3547E-11	G	c		
0751.3+1730		07 51 25.1	+17 30 51.1	0.1863	18.20*	0.000#	0.010#	0.00	0.3460E-11	GC		2	
	SBS 0748+499	07 51 51.9	49 48 51.6	0.0244	15.16	0.000#	0.004#	0.00	0.1732E-11	G		!	
0752.6+4556	RGB J0752+459	07 52 44.2	45 56 57.3	0.0600	16.20	0.061	0.286	0.66	0.4857E-11	G		9	
0752.6+4556	NPM1G +46.0092	07 52 44.2	+45 56 57.3	0.0517	16.20*	0.061	0.286	0.66	0.5760E-11	G		9	
0753.0+5352	4C +54.15	07 53 01.4	53 52 59.6	0.2000	18.50	0.907	0.964	-0.27	0.8330E-12	Q		z	
0753.4+3350	[HB89] 0750+339	07 53 28.1	33 50 51.0	2.0700	18.20	0.029	0.061	0.80	0.1015E-11	Q		q	
	NVSS J075407+..	07 54 07.9	43 16 10.0	0.3474	17.30	0.000	0.016#	0.00	0.3011E-11	G		q	
0754.6+3911	FIRST J075437.0+	07 54 37.1	39 10 47.6	0.0960	15.90	0.000	0.043#	0.00	0.9016E-12	Q		z	
0754.7+3033	GB6 J0754+3033	07 54 48.8	30 33 55.1	0.8000	18.07	0.108	0.114	-0.60	0.1657E-11	Q		q	
0755.9+3526	FIRSTJ075551.3..	07 55 51.3	35 26 35.2	0.1130	17.50*	0.000	0.001#	0.00	0.8254E-12	G		*	
0756.4+4102	2MASXiJ0756304..	07 56 30.4	41 02 10.5	0.0720	14.00*	0.011	0.016	0.00	0.7545E-12	G		a	
0757.1+0956	MRC 0754+100	07 57 06.6	09 56 34.8	0.6600	15.00	1.250	0.000	-0.13	0.2090E-11	Q		z	
	B3 0754+394	07 58 00.0	39 20 29.1	0.0960	14.36	0.000	0.011	0.00	0.2007E-11	G		q	
0758.3+4219	IRAS F07548+4227	07 58 19.6	42 19 35.0	0.2100	16.13	0.000	0.004#	0.00	0.3669E-11	Q		q	
0758.4+3747	3C 189	07 58 28.1	37 47 12.0	0.0428	14.10*	0.163	1.104	0.50	0.6791E-12	G	0		I
0759.7+4149	FIRSTJ075939.3..	07 59 39.4	41 50 23.6	0.1330	17.00*	0.000	0.001#	0.00	0.8035E-12	G			
0800.3+2636	IC 486	08 00 20.9	26 36 48.5	0.0269	13.20	0.000	0.012#	0.00	0.1442E-11	G	S	1	
	NPM1G +10.0129	08 00 26.9	10 13 08.9	0.0478	16.40	0.000	0.006#	0.00	0.3946E-11	G		5	
0801.0+6444	NVSSJ080102+...	08 01 02.5	64 44 48.3	0.2000	18.76	0.000	0.013#	0.00	0.1357E-11	Q		z	
0801.4+4736	RBS 688	08 01 31.9	47 36 15.0	0.1567	15.73	0.042	0.065	0.14	0.7672E-11	Q		q	
	3C 190	08 01 33.5	14 14 42.4	1.1950	20.30	0.000	0.820	1.00	0.5551E-12	Q		g	
0801.7+5633	NGC 2488	08 01 45.9	56 33 13.9	0.0287	13.40*	0.003	0.052	-1.10	0.2271E-11	G	0		
0802.7+6747	GB6 J0802+6747	08 02 49.0	67 47 43.1	0.2090	17.10	0.008	0.076	0.00	0.1965E-11	Q		q	
	CGCG 118-054	08 03 16.5	24 40 36.3	0.0446	15.70*	0.003	0.320&	0.00	0.7635E-12	G	E		I
0804.0+0506	MRK 1210	08 04 05.8	05 06 49.7	0.0135	13.70	0.057	0.059	1.26	0.6679E-12	G	S	2	
0804.4+6040	8C 0800+608	08 04 25.0	60 40 08.1	0.6890	18.50	0.078	0.244	0.53	0.8725E-12	Q		q	
0805.8+7534	RX J0805.4+7534	08 05 26.7	+75 34 23.8	0.1210	18.10*	0.000	0.053#	0.00	0.7570E-11	Q		z	
	3C 192	08 05 35.0	24 09 49.9	0.0598	17.10	0.008	12.199&	0.40	<0.3385E-13	G		n	II
0806.4+1725		08 06 24.9	+17 25 04.0	0.1038	16.90*	0.000	0.041#	0.00	0.1950E-11	G			
0806.6+7248	RGB J0806+728	08 06 38.9	72 48 20.6	0.0980	17.70	0.020	0.026	0.00	0.3019E-11	G		!	
0806.6+4841	RGB J0806+486	08 06 44.4	48 41 49.1	0.2700	18.50	0.081	0.344	0.58	0.2314E-11	G		a	
0807.9+3832	2MASXiJ0807522..	08 07 52.3	38 32 10.9	0.0670	15.80*	0.000	0.001#	0.00	0.1199E-11	G		*	
	OJ +508	08 08 39.7	49 50 36.5	1.4300	18.27	0.000	1.221	-0.25	0.6484E-12	Q		q	

Table A.3: *(continued)*

RXJ name (1)	Name (2)	RA(J2000) (3)	DEC(J2000) (4)	z (5)	m_V (6)	F_{5GHz}^{core} (7)	F_{5GHz} (8)	α_r (9)	$F_{0.1-2.4\ keV}$ (10)	Type (11)	Host (12)	Class. (13)	FR (14)
	3C 195	08 08 53.6	-10 27 40.2	0.1100	18.80	0.055	1.629	0.72	<0.7500E-12	G	N		II
0808.9+4052	B3 0805+410	08 08 56.6	40 52 44.9	1.4200	19.00	0.400	0.690	-0.42	0.1062E-11	Q		q	
	MG2 J080937+3455	08 09 38.9	34 55 37.2	0.0820	17.37	0.000	0.176	0.00	0.8013E-11	G		z	
0809.8+5218	RBS 692	08 09 49.1	52 18 58.7	0.1380	15.30	0.123	0.184	-0.07	0.1682E-10	Q		z	
0809.9+5025	RGB J0810+504	08 10 02.7	50 25 38.0	1.2000	16.96	0.012	0.023	0.00	0.6244E-12	G		q	
0810.0+7602	PG 0804+761	08 10 58.6	+76 02 42.0	0.1000	15.10*	0.000	0.004#	0.00	0.2930E-10	Q		q	
0810.9+5714	SBS 0806+573	08 11 00.6	57 14 12.5	0.6110	17.70	0.306	0.375	0.12	0.1567E-11	Q		q	
0811.1+5730	RGB J0811+575	08 11 10.2	57 30 10.0	0.0820	19.33	0.035	0.054	0.00	0.1327E-11	G		s	
	RGB J0811+700	08 11 12.4	70 02 30.6	0.2230	18.60*	0.004	0.032	-0.10	0.2981E-11	GC	c		
	PKS 0808+019	08 11 26.7	01 46 52.2	0.9300	17.20	0.000	0.590	-1.60	0.6672E-12	Q		z	
0811.6+4831	MS 0808.0+4840	08 11 37.2	48 31 33.9	0.7000	17.96	0.020	0.076	0.00	0.8639E-12	G		q	
	3C 196	08 13 36.0	48 13 02.6	0.8710	17.79	0.007	4.360	0.90	0.1354E-12	Q		q	II
0814.1+3236	B2 0810+32	08 14 09.2	32 37 31.9	0.8420	18.20	0.140	0.194	0.23	0.5498E-12	Q		q	
0814.4+2941	FIRSTJ081425.8..	08 14 25.9	29 41 15.8	0.3720	18.80	0.000	0.005#	0.00	0.1793E-11	G		q	
0814.4+5610	RGB J0814+561	08 14 32.1	56 09 56.8	0.5110	18.10	0.049	0.043	0.00	0.1295E-11	G		q	
0815.2+4604	KUG 0811+462	08 15 16.9	46 04 30.6	0.0409	15.20	0.000	0.008#	0.00	0.3379E-11	G	S	5	
0815.3+0155	PKS 0812+02	08 15 22.9	01 54 59.6	0.4020	17.10	0.196	0.845	0.90	0.3647E-11	Q		q	
	B2 0812+36	08 15 25.9	36 35 15.1	1.0250	19.00	0.000	0.980	0.04	0.4164E-12	Q		q	
0815.4-0308	3C 196.1	08 15 27.8	-03 08 26.7	0.1980	16.94	1.860#	0.480	1.10	0.5590E-11	GC		r	
0816.2+6600	RGB J0816+660	08 16 21.1	66 00 49.6	0.2510	18.95	0.012	0.058	0.00	0.7436E-12	G		1	
0818.0+0122		08 18 14.7	+01 22 27.1	0.0890	16.50*	0.000	0.021#	0.00	0.8530E-11	G		8	
0818.3+4222	S4 0814+42	08 18 15.9	42 22 45.4	0.2453	18.18	0.000	1.877#	-0.10	0.6358E-12	Q		z	
0819.2+2641	TXS 0816+268	08 19 16.7	26 42 01.1	0.5270	17.90	0.000	0.120#	0.83	0.6053E-12	Q			
0819.2+6429	MCG +11-10-073	08 19 17.6	64 29 40.2	0.0390	16.00	0.000	0.016#	0.00	0.3736E-11	G		1	
0819.4+6337	KOS NP6 038	08 19 25.7	63 37 28.0	0.1183	15.00	0.000	0.035#	0.00	0.4004E-11	GC	E		
082007.6..	IRAS F08168+3738	08 20 07.8	37 28 39.0	0.0810	21.60	0.000	0.001#	0.00	0.3993E-12	G		1	
0820.4+4853	RGB J0820+488	08 20 28.1	48 53 47.5	0.1300	17.50	0.000	0.090#	0.61	0.5763E-12	G		a	
	3C 197.1	08 21 33.7	47 02 36.9	0.1280	16.50	0.000	0.860	0.80	0.4656E-12	G	E		II
0822.1+4706	RGB J0822+470	08 22 09.6	47 05 53.0	0.1267	15.90	0.078	0.096	0.00	0.7519E-11	GC		q	
0822.2+2538	5C 07.194	08 22 14.4	25 38 32.6	1.7380	18.70	0.000	0.111	0.80	0.8048E-12	Q		q	
	4C +22.21	08 23 24.7	22 23 03.3	0.9510	19.50	0.000	1.590	0.40	0.4142E-12	Q		q	
0824.0+6136	RGB J0824+616	08 24 06.5	61 36 19.6	0.4010	18.18	0.007	0.018	0.00	0.1559E-11	G		q	
0824.7+5552	SBS 0820+560	08 24 47.2	55 52 42.7	1.4170	18.20	1.000	1.155	-0.14	0.1212E-11	Q		q	
0824.9+3916	4C +39.23	08 24 55.5	39 16 41.9	1.2160	17.71	0.880	1.030	-0.37	0.2035E-11	Q		q	

Table A.3: *(continued)*

RXJ name (1)	Name (2)	RA(J2000) (3)	DEC(J2000) (4)	z (5)	m_V (6)	F^{core}_{5GHz} (7)	F_{5GHz} (8)	α_r (9)	$F_{0.1-2.4\ keV}$ (10)	Type (11)	Host (12)	Class. (13)	FR (14)
0825.3+4436	4C +44.17	08 25 17.6	44 36 26.8	0.9040	17.60	0.012	0.236	1.07	0.1075E-11	QC		q	
0825.5+6157	[HB89] 0821+621	08 25 38.6	61 57 28.6	0.5420	17.70	0.464	0.619	0.11	0.1481E-11	Q		q	
0825.7+2703	[HB89] 0822+272	08 25 47.4	27 04 22.0	2.0600	18.70	0.133	0.150	0.00	0.1166E-11	Q		q	
0825.8+0309	MRC 0823+033	08 25 50.3	03 09 24.5	0.5060	16.80	0.000	0.940	-0.42	0.3118E-11	Q		z	
	PKS 0823-223	08 26 01.6	-22 30 27.2	0.9100	16.20	0.000	1.219	0.50	0.4617E-11	Q		z	
	PKS 0825-20	08 27 17.4	-20 26 24.0	0.8220	17.00	0.000	1.199	0.96	0.1216E-11	Q		q	
0828.1+4153	B3 0824+420	08 28 14.2	41 53 51.9	0.2230	18.90	0.007	0.047	0.00	0.2011E-11	Q		z	
0829.0+1755	RGB J0829+179	08 29 04.8	17 54 15.6	0.0894	13.90	0.120	0.210	0.11	0.2991E-11	G		z	
	PMN J0829+0858	08 29 30.3	08 58 21.0	0.8660	21.50	0.000	0.169	0.60	0.4101E-12	Q			
0830.8+2410	OJ +248	08 30 52.1	24 10 59.8	0.9390	17.26	1.661	0.000	0.00	0.2350E-11	Q		q	
0831.8+0430	[HB89] 0829+046	08 31 48.9	04 29 39.1	0.1800	16.40	1.000	1.913	-0.15	0.1052E-11	Q		z	
	[HB89] 0828+493	08 32 23.2	49 13 21.0	0.5480	18.82	0.000	0.349	0.50	0.3083E-12	Q		z	
0832.4+3707	RBS 0707	08 32 25.3	37 07 36.7	0.0906	16.61	0.000	0.012#	0.00	0.9125E-11	G		1	
0832.8+2853	FBQS J0832+2853	08 32 46.9	28 53 12.7	0.2260	17.80	0.000	0.001#	0.00	0.2172E-11	G		a	
0832.9+3300	RX J0832.8+3300	08 32 52.0	+33 00 11.0	0.6710	20.70*	0.000	0.004#	0.00	0.3380E-11	Q		z	
0833.8+4223	B3 0830+425	08 33 53.9	42 24 01.8	0.2530	18.60	0.310	0.390	-0.10	0.1357E-11	Q		z	
0834.8+3928	FIRSTJ083447.6..	08 34 47.6	39 28 17.7	0.1720	17.40*	0.000	0.003#	0.00	0.7113E-12	G			
0834.9+5534	4C +55.16	08 34 54.9	55 34 21.1	0.2420	18.50	5.599	5.740	0.74	0.2394E-11	GC		l	
0835.1-0405	NGC 2617	08 35 38.8	-04 05 17.6	0.0143	14.00*	0.000	0.029#	0.00	0.4650E-11	G		8	
0835.8+2957	IRAS F08328+3007	08 35 52.4	29 57 16.0	0.0770	14.70*	0.000	0.003#	0.00	0.1453E-11	G		*	
0836.4+2728	OJ +256	08 36 22.9	27 28 52.5	0.7650	19.10	0.000	0.301#	0.00	0.4280E-12	Q		q	
0836.5+4126	B3 0833+416	08 36 36.9	41 25 54.7	1.2980	18.11	0.269	0.385	0.35	0.1383E-11	Q		q	
	PKS 0834-223	08 36 50.8	-22 33 10.1	0.8370	18.00*	0.000	0.470	0.80	0.1536E-11	Q		q	
0836.3+4426	[HB89] 0833+446	08 36 58.8	+44 26 02.0	0.2550	15.60*	0.000	0.007#	0.00	0.9070E-11	Q		q	
	3C 204	08 37 44.9	65 13 34.9	1.1120	18.21	0.027	0.340	1.00	0.6202E-12	Q		q	II
0838.2+2454	NGC 2622	08 38 10.9	24 53 43.0	0.0286	14.12	0.063#	0.068	0.00	0.4529E-11	G	S	8	
	3C 205	08 39 06.4	57 54 17.1	1.5340	17.62	0.000#	0.670	0.90	0.3738E-12	Q		g	
	TXS 0836+182	08 39 30.7	18 02 47.1	0.2800	17.00	0.000#	0.350	0.10	0.8539E-12	Q		z	
	PKS 0837+035	08 39 49.2	03 19 53.8	1.5700	20.70	0.000#	0.580	0.25	0.7971E-12	Q		q	
0839.8-1214	3C 206	08 39 50.6	-12 14 33.9	0.1976	15.76	0.000#	0.720	0.70	0.1015E-10	QC		q	
0840.7+1312	3C 207	08 40 47.5	13 12 23.0	0.6808	18.15	0.657	1.244	0.44	0.1793E-11	Q		q	
0841.4+7053	4C +71.07	08 41 24.4	70 53 42.2	2.1720	17.30	3.742	0.000	0.34	0.1030E-10	Q		q	
0841.4-7540	MRC 0842-754	08 41 27.0	-75 40 27.9	0.5210	18.40	0.590	1.399	0.70	0.2956E-11	Q		q	
0841.7+2320	TXS 0838+235	08 41 53.9	23 19 55.1	1.1830	17.20	0.000	0.108	0.60	0.3081E-11	Q		q	

Table A.3: *(continued)*

RXJ name (1)	Name (2)	RA(J2000) (3)	DEC(J2000) (4)	z (5)	m_V (6)	F_{5GHz}^{core} (7)	F_{5GHz} (8)	α_r (9)	$F_{0.1-2.4\ keV}$ (10)	Type (11)	Host (12)	Class. (13)	FR (14)
0842.0+4018	RBS 0718	08 42 03.7	40 18 31.4	0.1520	16.20	0.015	0.042	0.00	0.4741E-11	Q		q	
	PKS 0839+18	08 42 05.1	18 35 40.9	1.2700	16.36	0.000	1.120	0.10	0.1015E-11	Q		q	
0842.6+0759	RX J0842.1+0759	08 42 05.6	+07 59 25.6	0.1339	17.70*	0.000	0.017#	0.00	0.9100E-11	G		5	
0842.9+2927	LEDA 139129	08 42 55.9	29 27 27.2	0.1980	17.00	0.000	0.020#	0.00	0.3150E-11	G	c		
0843.2+6129	4C +61.19	08 43 12.0	61 29 43.7	0.8620	17.85	0.052	0.238	0.94	0.6158E-12	Q		q	
	NGC 2639	08 43 38.1	50 12 20.0	0.0111	11.88	0.000	0.037	0.00	0.3274E-12	G	S	l	
0844.3-1402	IRAS 08417-135	08 44 06.5	-14 02 12.9	0.0278	15.00*	0.000	0.008#	0.00	0.9700E-11	G		5	
0845.0-0241		08 45 53.4	-02 41 00.5	0.4690	16.60*	0.000	0.055#	0.00	0.3420E-11	Q		q	
	HS 0843+0715	08 46 00.4	07 04 24.6	0.3400	17.60	0.000	0.250#	0.30	0.3840E-11	Q		q	
0846.6+0704	PMN J0846+0704	08 46 00.4	+07 04 24.6	0.3418	16.60*	0.000	0.336#	0.30	0.4490E-11	Q		q	
0846.5-1214	IRAS F08440-120	08 46 28.5	-12 14 10.4	0.1076	16.50*	0.000	0.016#	0.00	0.1260E-10	G		5	
0847.1+1133	RGB J0847+115	08 47 12.9	11 33 50.1	0.1990	16.90	0.022	0.032	0.00	0.2150E-10	G		z	
0847.3+3732	[HB89] 0844+377	08 47 16.0	37 32 17.8	0.4510	17.70	0.000	0.002#	0.00	0.1799E-11	Q		q	
0848.0+3147	IC 2402	08 47 59.1	31 47 08.2	0.0673	14.99*	0.035	0.328	0.70	0.8596E-12	GC			II
	IC 2401	08 48 10.3	37 45 19.2	0.0406	14.82*	0.000	0.002#	0.00	0.5405E-13	G	0		
0850.4+3746	4C +37.25	08 50 24.7	37 47 09.5	0.4070	19.50	0.224	0.391	0.24	0.3433E-12	G		r	II
0850.5+3455	RGB J0850+349	08 50 36.2	34 55 22.8	0.1490	17.50	0.028	0.000	0.00	0.1157E-11	Q		z	
0851.5+5228	RX J0851.8+5228	08 51 51.4	+52 28 25.0	0.0640	17.50*	0.000	0.005#	0.00	0.2520E-11	G		5	
	3C 208	08 53 08.8	13 52 55.5	1.1100	17.42	0.090	0.545	1.10	0.6269E-12	Q		q	II
0854.9+1741	MRK 1220	08 54 39.2	+17 41 21.8	0.0649	16.50*	0.000	0.006#	0.00	0.4150E-11	G		1	
0854.6+5757	4C +58.17	08 54 41.9	57 57 29.9	1.3220	18.30	0.900	1.183	0.22	0.4948E-12	Q		q	
0854.8+2006	OJ +287	08 54 48.9	20 06 30.6	0.3060	15.43	2.299	2.907	-0.30	0.3150E-11	Q		z	
0856.0+5418	RGB J0856+543	08 56 08.2	54 18 56.2	0.2539	15.00*	0.014	0.026	0.00	0.2120E-11	G			
0857.6+3404	3C 211	08 57 40.6	34 04 06.6	0.7500	22.00	0.000	0.549	0.93	0.6915E-12	G			II
0857.7-7719	PKS 0858-77	08 57 42.5	-77 19 31.9	0.4900	17.57	0.000	0.330	0.40	0.1905E-11	Q		q	
	3C 212	08 58 41.5	14 09 43.9	1.0480	19.06	0.150	0.890	1.00	0.7447E-12	Q		q	II
0859.3+0047	CGCG 0856.8+0059	08 59 19.2	00 47 51.9	0.0131	15.40*	0.000	0.050	0.00	0.4899E-11	G			
0859.1+7455	RX J0859.5+7455	08 59 31.0	+74 54 52.0	0.2520	16.80*	0.000	0.006#	0.00	0.2440E-11	Q		q	
	PMN J0900-2818	09 00 15.3	-28 17 59.2	0.8940	18.90	0.000	0.512#	0.00	0.8491E-12	Q		q	
	PKS 0859-25	09 01 47.5	-25 55 18.7	0.3050	18.50	0.000	1.740	1.08	<0.3400E-12	G			II
0902.2-1415	PKS 0859-14	09 02 16.8	-14 15 30.9	1.3330	16.59	0.000	2.290	0.40	0.1418E-11	Q		q	
0903.0+4650	B3 0859+470	09 03 03.9	46 51 04.1	1.4620	19.20	1.645	0.000	0.25	0.5140E-12	Q		q	
0903.2+4056	RBS 739	09 03 14.7	40 55 59.7	0.1882	18.70	0.000	0.026#	0.00	0.4053E-11	Q		z	
0904.6-1957	PKS 0902-19	09 04 40.7	-19 57 26.9	0.7580	18.20	0.000	0.180	0.77	0.8325E-12	Q		q	

Table A.3: *(continued)*

RXJ name (1)	Name (2)	RA(J2000) (3)	DEC(J2000) (4)	z (5)	m_V (6)	F_{5GHz}^{core} (7)	F_{5GHz} (8)	α_r (9)	$F_{0.1-2.4\ keV}$ (10)	Type (11)	Host (12)	Class. (13)	FR (14)
	B2 0902+34	09 05 30.1	34 07 56.9	3.3909	24.00	0.000	0.100	0.90	0.2146E-13	G		r	
0905.4+1840	RX J0905.5+1840	09 05 33.6	+18 40 02.7	0.1228	16.20*	0.000	0.019#	0.00	0.3050E-11	GC		1	
0906.0+1941	[HB89] 0903+198	09 06 03.6	19 41 42.0	1.2060	16.42	0.079	0.000#	0.00	0.2349E-11	Q		q	
0906.5+1646	3C 215	09 06 31.9	16 46 11.4	0.4121	18.27	0.026	0.378	1.00	0.3532E-11	QC		q	
0908.1-0959	NPM1G -09.0307	09 08 02.2	-09 59 37.6	0.0533	15.00*	0.000	0.652#	0.20	0.3220E-11	GC	E		
	TXS 0904+507	09 08 16.7	50 31 06.2	0.9170	20.80	0.000	0.085#	0.60	0.1247E-12	Q		q	
0908.5+3026	FIRSTJ090829.5..	09 08 29.5	30 26 39.5	0.1120	15.80*	0.000	0.002#	0.00	0.6852E-12	G			
0908.5+4150	B3 0905+420	09 08 35.9	41 50 46.2	0.7325	19.40	0.114	0.222	0.21	0.9197E-12	Q		q	
0908.7+3235	IC 2439	09 08 38.4	32 35 34.4	0.0143	14.80*	0.000	0.002#	0.00	0.5503E-12	G	0		
0908.9+2311	RGB J0909+231	09 09 00.6	23 11 12.0	0.2230	16.20	0.000	0.032	0.00	0.9041E-12	Q		z	
0909.1+0121	PKS 0906+01	09 09 10.1	01 21 35.6	1.0200	17.79	1.002	0.000	-0.03	0.1237E-11	Q		q	
0909.2+0354	RGB J0909+039	09 09 15.9	03 54 42.9	3.2000	19.30	0.078	0.111	-0.42	0.9767E-12	Q			
0909.3+5216	RGB J0909+522	09 09 24.6	52 16 32.0	0.4110	18.60	0.033	0.048	0.00	0.8621E-12	G		q	
	3C 216	09 09 33.5	42 53 46.1	0.6700	18.10	0.000	1.810	0.70	0.5277E-12	Q		g	
0909.8+3105	B2 0906+31	09 09 53.4	31 05 59.0	0.2740	17.80	0.078	0.096	0.70	0.5808E-11	Q		z	
	MRC 0908-103	09 10 35.9	-10 34 56.8	0.0921	15.50*	0.000	0.120	0.20	0.2927E-11	GC		r	
	TON 1015	09 10 37.1	33 29 24.5	0.3540	16.50	0.000	0.102	0.00	0.2311E-11	Q		z	
0911.5+4423	B3 0908+445	09 11 33.9	44 22 50.9	0.2976	17.20	0.031	0.157	0.65	0.1533E-11	Q		q	
0912.5+6834	RGB J0912+685	09 12 36.6	68 34 25.1	1.0800	18.80	0.104	0.126	0.00	0.4572E-12	G		q	
0913.2+3658	FIRSTJ091313.7..	09 13 13.7	36 58 17.3	0.1070	16.60	0.000	0.001#	0.00	0.1694E-11	G		!	
0913.0+4056	IRAS 09104+410	09 13 45.4	+40 56 28.0	0.4420	18.00*	0.000	0.017#	0.00	0.1140E-11	GC		2	
0913.4+4742		09 13 45.4	+47 42 06.2	0.0511	16.10*	0.000	0.017#	0.00	0.2050E-11	G			
0914.0+0507	[HB89] 0911+053	09 14 01.8	05 07 50.5	0.3030	17.43	0.054	0.217	0.12	0.2659E-11	Q		q	
	NGC 2782	09 14 05.1	40 06 49.2	0.0085	13.45	0.000	0.047	0.00	0.1072E-12	G	S	*	
0916.8+3854	4C +38.28	09 16 48.9	38 54 28.1	1.2500	20.00	0.620	0.000	0.28	0.3084E-12	Q		q	
0916.8+5238	RBS 760	09 16 52.0	52 38 27.9	0.1900	19.50	0.046	0.069	0.00	0.5954E-11	Q		z	
0918.1-1205	3C 218/Hyd A	09 18 05.7	-12 05 43.9	0.0538	14.80	0.217	13.779	0.90	0.5950E-10	GC	S	l	I
0918.2+1618	MRK 0704	09 18 26.0	+16 18 19.2	0.0299	15.40*	0.000	0.007#	0.00	0.1760E-10	G	S	5	
0918.9+2325	RGB J0918+234	09 18 58.1	23 25 55.4	0.6880	17.70	0.045	0.000#	0.00	0.6415E-12	Q		q	
0919.4+3347	IRAS 09164+3400	09 19 27.3	33 47 27.2	0.0194	13.20*	0.000	0.002#	0.00	0.4069E-12	GC			
0920.9+4441	[HB89] 0917+449	09 20 58.4	44 41 53.9	2.1800	19.20	1.310	0.000#	-0.30	0.1599E-11	Q		q	
0921.1+4538	3C 219	09 21 08.6	45 38 57.4	0.1744	17.44	0.005	1.998	1.08	0.1675E-11	GC		b	II
0921.3+7136	8C 0916+718	09 21 23.9	71 36 12.4	0.5940	18.70	0.200	0.295	0.15	0.6118E-12	Q		q	
	S4 0917+62	09 21 36.2	62 15 52.2	1.4460	19.50	0.000	1.322	-0.06	0.3600E-12	Q		q	

Table A.3: *(continued)*

RXJ name (1)	Name (2)	RA(J2000) (3)	DEC(J2000) (4)	z (5)	m_V (6)	F_{5GHz}^{core} (7)	F_{5GHz} (8)	α_r (9)	$F_{0.1-2.4\ keV}$ (10)	Type (11)	Host (12)	Class. (13)	FR (14)
	GB6 J0922+7109	09 22 30.0	71 09 36.0	2.4320	18.30	0.000	0.086	0.00	0.5587E-13	Q		q	
	PKS 0920-39	09 22 46.4	-39 59 35.1	0.5910	18.40	0.000	1.510	-0.40	0.1239E-11	Q		q	
0923.8-2135	NPM1G -21.0236	09 23 38.9	-21 35 47.1	0.0530	16.50*	0.000	0.268#	0.38	0.1110E-10	G		r	
0923.7+2254	CGCG 121-075	09 23 43.0	22 54 32.6	0.0323	14.80	0.000	0.005#	0.00	0.3455E-10	G		1	
	RGB J0924+141B	09 24 05.3	14 10 21.1	0.1364	16.90	0.034	0.475#	-0.20	0.7932E-11	GC			
0925.2+5217	MRK 110	09 25 12.9	52 17 10.5	0.0353	15.37	0.000	0.010#	0.00	0.2054E-10	G	S	5	
0925.9+4004	FBQS J092554.7+.	09 25 54.7	40 04 14.2	0.4700	17.93	0.000	0.009#	0.00	0.2497E-11	Q		q	
0927.0+3902	[HB89] 0923+392	09 27 03.0	39 02 20.8	0.6948	17.86	2.681	6.913	-0.82	0.3376E-11	Q		q	
0927.8+5327		09 27 10.6	+53 27 31.6	0.2082	17.80*	0.000	0.005#	0.00	0.1800E-11	G			
0927.8-2034	PKS 0925-203	09 27 51.8	-20 34 51.2	0.3480	16.40	0.000	0.700	0.24	0.4600E-11	Q		q	
0928.0+7447	8C 0923+750	09 28 02.9	74 47 19.1	0.6380	19.74	0.005	0.057	0.00	0.1941E-11	QC		z	
0928.0+2031	RGB J0928+205	09 28 04.5	20 31 45.3	0.1921	18.20*	0.013	0.035	0.00	0.1581E-11	G			
0928.5+6025	RGB J0928+604	09 28 37.9	60 25 21.0	0.2960	16.72	0.013	0.118	0.00	0.1706E-11	GC		q	
0929.1+2537	RGB J0929+256C	09 29 15.5	25 36 58.1	0.5390	18.70	0.113	0.121	0.43	0.7753E-12	Q		q	
0930.5+4644	B3 0927+469	09 30 35.1	46 44 08.6	2.0320	18.10	0.150	0.202	0.40	0.6797E-12	Q		q	
0930.6+4950	RBS 782	09 30 37.6	49 50 25.5	0.1880	17.20	0.015	0.022	0.00	0.4553E-10	Q		z	
0930.9+3933	FIRST J093056.8+	09 30 56.8	39 33 35.9	0.6380	21.00	0.000	0.009#	0.00	0.1402E-11	Q		z	
0931.8+2937	2MASXiJ0931477..	09 31 47.8	29 37 42.5	0.1400	17.40	0.000	0.001#	0.00	0.4823E-12	G		s	
0932.0+5534	SBS 0928+559B	09 32 00.1	55 33 47.5	0.2660	16.70	0.007	0.053	0.00	0.7849E-12	Q		q	
	NGC 2903	09 32 10.1	21 30 03.0	0.0019	9.01	0.000	0.136	0.66	0.2007E-12	G	S	h	
	3C 220.1	09 32 39.6	79 06 31.5	0.6100	20.50*	0.025	7.200&	0.93	0.4024E-12	GC		n	II
0933.2-1714		09 33 18.1	-17 14 40.8	0.3132	16.70*	0.000	0.020#	0.00	0.6700E-11	G		q	
0934.2-1721		09 34 30.3	-17 21 23.7	0.2500	18.10*	0.000	0.054#	0.00	0.8020E-11	G		z	
0935.4+2617	RX J0935.4+2617	09 35 27.1	+26 17 09.7	0.1220	17.80*	0.000	0.003#	0.00	0.2720E-11	G		1	
0937.0+3615	IRAS F09339+3629	09 37 03.0	36 15 37.3	0.1796	17.70*	0.000	0.004#	0.00	0.1346E-11	G		1	
0937.1+5008	RGB J0937+501	09 37 12.3	50 08 52.1	0.2750	18.00	0.217	0.315	-0.38	0.1357E-11	Q		q	
	3C 220.3	09 39 22.5	83 15 24.5	0.6800	20.50*	0.000	0.640	1.19	<0.6161E-13	G		n	II
	3C 223	09 39 52.7	35 53 58.2	0.1368	17.06	0.009	5.299&	0.78	<0.1219E-12	G	E	n	II
	MG2 J094013+2604	09 40 14.7	26 03 29.9	0.4980	20.90	0.000	0.322&	0.20	0.5821E-12	Q		z	
0940.7+6148	RX J0940.3+6148	09 40 22.4	+61 48 26.2	0.2106	18.00*	0.000	0.013#	0.00	0.2490E-11	G		z	
0941.0+3853	[HB89] 0937+391	09 41 03.9	38 53 50.8	0.6180	18.00	0.005	0.212	1.00	0.1541E-11	Q		q	
0942.0+2341	CGCG 122-055	09 42 04.8	+23 41 06.5	0.0214	15.30*	0.000	0.006#	0.00	0.2250E-11	G			
0943.3+3615	NGC 2965	09 43 19.1	36 14 52.3	0.0224	14.70	0.237	0.081	-0.06	0.5222E-12	GC	0	a	
0943.4+2835	FBQS J094324.3+.	09 43 24.3	28 35 40.2	0.4610	18.50	0.000	0.001#	0.00	0.4820E-12	Q		q	

Table A.3: *(continued)*

RXJ name (1)	Name (2)	RA(J2000) (3)	DEC(J2000) (4)	z (5)	m_V (6)	F_{5GHz}^{core} (7)	F_{5GHz} (8)	α_r (9)	$F_{0.1-2.4\ keV}$ (10)	Type (11)	Host (12)	Class. (13)	FR (14)
0945.9-1419	NGC 2992	09 45 42.0	-14 19 34.9	0.0077	13.10*	0.000	0.227#	0.00	0.8470E-11	G	S	2	
0945.9+4238	IRAS F09427+425	09 45 54.4	+42 38 39.9	0.0740	16.30*	0.000	0.003#	0.00	0.1260E-11	G		2	
0946.0+1320	MS 0944.1+1333	09 46 51.9	+13 20 26.1	0.1310	16.00*	0.000	0.008#	0.00	0.5900E-11	G		1	
0947.7+4721	IRAS F09438+473	09 47 04.5	+47 21 43.0	0.5410	18.10*	0.000	0.003#	0.00	0.1490E-11	G		q	
	RBS 797	09 47 12.5	76 23 12.5	0.3540	19.20	0.000	0.022#	0.00	0.4519E-11	G		l	
0947.2+1005	RX J0947.5+1005	09 47 33.2	+10 05 09.0	0.1392	16.00*	0.000	0.004#	0.00	0.5770E-11	G		1	
	3C 227	09 47 45.1	07 25 20.6	0.0862	16.33	0.032	2.640	0.82	0.4445E+02*	G	N	b	II
0948.9+4039	4C +40.24	09 48 55.3	40 39 44.6	1.2520	18.37	1.227	1.800	-0.24	0.4123E-12	Q		q	
0948.8+0022	RGB J0948+003	09 48 57.3	00 22 25.5	0.5837	18.67	0.127	0.295	-0.24	0.1010E-11	Q		1	
0949.0-1957	MRC 0946-197	09 49 05.8	-19 57 11.0	0.5190	17.60	0.000	0.116	0.00	0.1283E-11	QC		q	
	4C +73.08	09 49 45.9	73 14 23.1	0.0581	16.00*	0.000	0.994	0.00	<0.1496E-12	G		n	II
0951.9-0649	NGC 3035	09 51 55.0	-06 49 22.5	0.0145	13.50*	0.000	0.006#	0.00	0.6950E-11	G	S	1	
0952.4+7502	1RXSJ095225.8..	09 52 24.3	75 02 13.5	0.1813	19.90	0.000	0.012#	0.00	0.4174E-11	G		z	
0953.5+2539	RX J0953.5+2539	09 53 31.3	+25 39 42.0	0.0441	17.10*	0.000	0.004#	0.00	0.1920E-11	G		a	
0953.4+0141		09 53 41.4	+01 42 02.3	0.0983	17.10*	0.000	0.010#	0.00	0.2690E-11	G			
0954.1+2122	4C +21.26	09 54 07.0	21 22 36.0	0.2954	20.00	0.033	0.336	0.51	0.1958E-11	Q		1	
	MS 0950.9+4929	09 54 09.8	49 14 59.4	0.2070	19.30	0.000	0.003	0.00	0.2075E-11	Q		z	
0954.9+0930	[HB89] 0952+097	09 54 56.8	09 29 55.2	0.2980	17.24	0.007	0.139	0.78	0.1798E-11	Q		q	
0955.6+4532	B3 0952+457	09 55 39.8	45 32 16.0	0.2590	16.70	0.000	0.029	0.00	0.1502E-11	Q		q	
0955.8+6940	M 82	09 55 52.2	69 40 46.9	0.0007	9.20*	0.042	3.795	0.72	0.2054E-10	GC		*	
0956.2-0957		09 56 28.2	-09 57 19.3	0.1585	17.60*	0.000	0.094#	0.00	0.4240E-11	GC			
0956.8+2515	[HB89] 0953+254	09 56 49.9	25 15 16.0	0.7120	17.21	1.439	0.000#	-0.07	0.9050E-12	Q		q	
0957.1+2433	2MASXiJ0957072..	09 57 07.2	24 33 16.1	0.0820	15.80	0.001#	0.006#	0.00	0.2776E-11	G		!	
0957.6+5523	[HB89] 0954+556	09 57 38.2	55 22 57.8	0.9090	17.40	2.568	0.000#	0.39	0.7875E-12	Q		q	
0957.7+4745	87GB 095433.0+..	09 57 46.6	47 45 49.9	0.4180	20.40	0.026	0.024#	0.00	0.2060E-12	G		s	
0958.2+4608	B3 0955+464	09 58 17.5	46 08 39.1	0.6480	20.10	0.006	0.032	0.00	0.1091E-11	Q		q	
0958.3+4725	B3 0955+476	09 58 19.7	47 25 07.8	1.8730	18.65	0.700	1.004	0.00	0.7290E-12	Q		q	
0958.3+3223	4C +32.33	09 58 20.9	32 24 02.2	0.5305	15.78	1.100	0.000	0.26	0.2289E-12	Q		q	
0958.7+6533	S4 0954+65	09 58 47.2	65 33 54.8	0.3680	16.81	0.480	1.125	0.09	0.1225E-11	Q		z	
0959.4+2123	87GB 095643.1..	09 59 29.9	21 23 20.0	0.3646	17.40	0.033	0.035	0.00	0.7786E-11	G		z	
0959.1-3113	RX J0959.7-3113	09 59 42.6	-31 12 58.4	0.0370	10.90*	0.000	0.008#	0.00	0.2120E-10	G		1	
0959.7+2223	RGB J0959+224	09 59 46.9	22 24 08.4	0.2449	18.40*	0.008	0.025	0.00	0.2477E-11	GC			
0959.4+1302	NGC 3080	09 59 55.8	+13 02 37.8	0.0354	14.30*	0.000	0.003#	0.00	0.4900E-11	G	S	1	
1000.3+0005	4C +00.34	10 00 17.7	00 05 23.7	0.9053	17.57	0.077	0.345	0.80	0.1080E-11	Q		q	

Table A.3: *(continued)*

RXJ name (1)	Name (2)	RA(J2000) (3)	DEC(J2000) (4)	z (5)	m_V (6)	F_{5GHz}^{core} (7)	F_{5GHz} (8)	α_r (9)	$F_{0.1-2.4\ keV}$ (10)	Type (11)	Host (12)	Class. (13)	FR (14)
1000.3+2233	[HB89] 0957+227	10 00 21.9	22 33 18.7	0.4190	18.00	0.000	0.390	0.80	0.9172E-12	Q		q	
1000.9+4409	RX J1000.5+4409	10 00 28.9	+44 09 10.0	0.1530	19.10*	0.000	0.004#	0.00	0.2270E-11	GC			
1001.3+5553	SBS 0957+561	10 01 20.9	55 53 56.5	1.4141	16.70	0.017	0.208	0.80	0.1324E-11	Q			
	MS 0958.9+2102	10 01 42.4	20 48 17.8	0.3460	19.84	0.000	0.002	0.00	0.6632E-12	Q		z	
	3C 234	10 01 49.5	28 47 09.3	0.1848	17.27	0.000	1.540	0.90	0.4667E-12	G	N	n	II
1002.0+5541	NGC 3079	10 01 57.8	55 40 47.1	0.0038	12.18	0.065	0.320	0.00	0.4935E-12	G	S	2	
1001.9-4437	PKS 0959-443	10 01 59.9	-44 38 00.6	0.8370	15.10	0.000	0.830	0.30	0.1316E-11	Q		q	
1002.3-0809	IRAS 09595-075	10 02 00.0	-08 09 41.6	0.0152	15.20*	0.000	0.013#	0.00	0.6510E-11	G		1	
1002.5+3242	NGC 3099	10 02 36.5	32 42 24.2	0.0506	15.40*	0.000	0.008#	0.00	0.2560E-11	GC			
	7C 1001+3258	10 03 57.6	32 44 03.5	1.6820	19.30	0.000	0.316#	0.40	0.8224E-13	Q		q	
1004.8+2224	PKS 1002+22	10 04 45.7	22 25 19.4	0.9740	18.10	0.000	0.180	0.90	0.1144E-11	Q		q	
1005.1+3414	FBQS J100507.9+.	10 05 07.9	34 14 24.1	0.1620	16.86	0.000	0.003#	0.00	0.1615E-11	Q		q	
1005.3+4058	FBQS J100522.9+.	10 05 22.9	40 58 34.5	0.3170	18.08	0.000	0.001#	0.00	0.7909E-12	Q		q	
1005.7+4332	IRAS 10026+4347	10 05 41.9	43 32 40.5	0.1782	16.39	0.000	0.003#	0.00	0.7486E-11	G	S	!	
	3C 236	10 06 01.7	34 54 10.4	0.1005	17.91	0.084	6.139	0.60	<0.5281E-13	G		w	
1006.0+3236	7C 1003+3251	10 06 07.5	32 36 26.9	1.0200	18.10	0.058	0.231	0.67	0.7071E-12	Q		q	
	PMN J1006+0509	10 06 37.6	05 09 53.9	1.2160	21.70	0.000	0.181	0.00	0.2563E-12	Q		q	
1006.7+2554	B2 1003+26	10 06 38.9	25 54 44.0	0.1165	15.50*	0.000	0.050#	1.90	0.3573E-11	GC	E	r	
1006.6+2701	7C 1003+2716	10 06 42.6	27 01 15.3	0.5490	17.70	0.018	0.021	0.00	0.6325E-12	Q		q	
1007.9+3039	FIRSTJ100753.2..	10 07 53.3	30 40 02.3	0.1300	17.70*	0.000	0.001#	0.00	0.7730E-12	G			
1008.5+4705	RX J1008.1+4705	10 08 11.3	+47 05 20.0	0.3430	19.00*	0.000	0.005#	0.00	0.1080E-10	Q		z	
1008.1+0030	PKSJ 1008+0029	10 08 11.4	00 29 59.9	0.0977	16.90*	0.073	0.194	0.51	0.1004E-11	GC	N	r	
1008.8-0954	NPM1G -09.0361	10 08 48.6	-09 54 51.2	0.0575	15.90*	0.000	0.003#	0.00	0.6650E-11	G		1	
1010.0+3003	TON 0488	10 10 00.7	30 03 21.5	0.2600	17.39	0.000	0.001#	0.00	0.2176E-11	Q		q	
1010.4+4132	4C +41.21	10 10 27.5	41 32 38.9	0.6123	15.97	0.200	0.854	0.70	0.2981E-11	Q		q	
	PKS B1008-041	10 11 30.2	-04 23 27.7	1.5880	20.00	0.000	0.210	-0.20	0.1273E-12	Q		q	
1011.5+7124	4C +71.09	10 11 32.5	71 24 41.0	1.1920	17.60	0.669	0.753	1.07	0.5537E-12	Q		q	
1012.6+4229	B3 1009+427	10 12 44.3	42 29 57.0	0.3640	18.27	0.029	0.046	0.44	0.7636E-11	Q		z	
1012.9+3932	RGB J1012+395	10 12 58.4	39 32 38.9	0.1710	17.77*	0.019	0.026	0.00	0.8075E-12	G			
1013.5-2831	[HB89] 1011-282	10 13 29.6	-28 31 25.7	0.2530	16.88	0.000	0.290	0.70	0.3624E-11	Q		q	
1013.8+2449	TON 0490	10 13 53.4	24 49 16.4	1.6360	16.57	0.800	0.937	-0.37	0.1074E-11	Q		q	
1014.7+2301	[HB89] 1012+232	10 14 47.0	23 01 16.6	0.5650	17.80	1.300	0.000	0.20	0.9103E-12	Q		q	
1015.0+4926	[HB89] 1011+496	10 15 04.1	49 26 00.7	0.2000	16.15	0.242	0.299	0.27	0.1899E-10	QC	E	z	
1015.9+0109	LBQS 1013+0124	10 15 57.1	01 09 13.7	0.7790	17.20	0.173	0.174	-0.21	0.1808E-11	Q		q	

Table A.3: *(continued)*

RXJ name (1)	Name (2)	RA(J2000) (3)	DEC(J2000) (4)	z (5)	m_V (6)	F_{5GHz}^{core} (7)	F_{5GHz} (8)	α_r (9)	$F_{0.1-2.4\ keV}$ (10)	Type (11)	Host (12)	Class. (13)	FR (14)
	4C +48.28	10 15 57.6	48 38 00.4	0.3850	19.40	0.000	0.159	0.70	0.2710E-12	Q		q	
1016.3+4108	RBS 0844	10 16 16.8	41 08 12.2	0.2700	17.30	0.000	0.015#	0.00	0.5657E-11	Q		z	
1016.9+7323	NGC 3147	10 16 53.6	73 24 02.6	0.0094	12.65	0.009	0.040	0.00	0.4497E-11	G	S	2	
1017.3+2914	IRAS F10144+2929	10 17 18.2	29 14 33.8	0.0476	15.70	0.000	0.002#	0.00	0.7007E-11	G		!	
1017.8+2732	3C 240	10 17 49.3	27 32 04.0	0.4690	18.90	0.014	0.494	0.90	0.1716E-11	Q		q	
1018.1+3542	B2 1015+35B	10 18 10.9	35 42 39.4	1.2260	18.64	0.900	0.000	-0.14	0.4433E-12	Q		q	
1018.4+3805	B2 1015+38	10 18 25.4	38 05 32.6	0.3800	17.93	0.016	0.117	0.66	0.1202E-11	Q		q	
1019.0+3752	RBS 852	10 19 00.4	37 52 40.4	0.1330	17.20	0.000	0.003#	0.00	0.1009E-10	Q		1	
1019.2+6358	MRK 141	10 19 12.5	63 58 02.8	0.0417	15.09	0.000	0.004#	0.00	0.6221E-11	GC	S	1	
	PKS 1018-42	10 20 03.9	-42 51 30.7	1.2800	18.80	0.000	1.199	-0.90	0.8429E-12	Q		q	
1021.1+4523	RGB J1021+453	10 21 05.8	45 23 20.7	0.3640	18.16	0.023	0.082	0.00	0.7813E-12	G		q	
	3C 241	10 21 54.5	21 59 30.1	1.6170	23.50*	0.003	6.299	1.20	<0.1015E-12	G		n	II
1022.5+5124	MS 1019.0+5139	10 22 12.6	+51 24 00.3	0.1410	18.10*	0.000	0.005#	0.00	0.5110E-11	G		z	
1022.5-1037	RBS 0862	10 22 32.8	-10 37 44.2	0.1970	16.11	0.000	0.490	0.43	0.5670E-11	Q	E	q	
1022.5+3932	B3 1019+397	10 22 37.4	39 31 50.5	0.6050	17.04	0.041	0.048	0.00	0.5337E-12	Q		q	
	GB1 1020+481	10 23 10.4	47 51 46.1	0.5800	18.60*	0.000	0.169	0.80	0.1382E-12	QC		q	
1023.1+3948	S4 1020+40	10 23 11.5	39 48 15.0	1.2540	18.17	0.574	0.789	-0.43	0.8002E-12	Q		q	
1023.5+1952	NGC 3227	10 23 30.6	19 51 53.9	0.0039	11.79	0.032	0.048	0.00	0.1612E-11	G	S	5	
1024.7+1912	[HB89] 1022+194	10 24 44.8	19 12 20.4	0.8280	17.49	0.581	0.765	-0.21	0.1116E-11	Q		q	
1025.8+4013	HS 1022+4027	10 25 53.6	40 12 43.5	0.4100	17.18	0.000	0.001#	0.00	0.7605E-12	Q		q	
	IVS B1023+131	10 25 56.3	12 53 49.0	0.6630	18.20	0.000	0.655#	0.00	0.6225E-12	Q		q	
1026.5+6746	8C 1022+680	10 26 33.5	67 46 11.1	1.1780	15.00*	0.000	0.130#	0.38	0.5720E-13	Q		q	
1026.5-1749		10 26 58.5	-17 48 58.5	0.1142	16.60*	0.000	0.011#	0.00	0.5700E-11	G		z	
1027.4+4817	4C +48.30	10 27 33.6	48 17 18.5	0.2800	21.70*	0.010	0.327	0.78	0.3572E-12	G			
1027.8-4354	NGC 3256	10 27 51.8	-43 54 08.7	0.0091	11.51	0.000	0.250	-0.34	0.2111E-11	GC	p	h	
1027.9-2311	MRC 1025-229	10 27 54.9	-23 12 02.0	0.3090	20.10	0.000	0.170	1.10	0.1508E-11	Q		1	
1028.2+0130	LBQS 1025+0145	10 28 15.9	01 30 05.8	1.0550	18.20	0.032	0.032	0.00	0.7821E-12	Q		q	
1028.7+3844	4C +39.32	10 28 44.3	38 44 36.7	0.3610	18.40	0.332	0.659#	0.56	0.4594E-12	G		r	II
1029.4+2729		10 29 01.6	+27 28 51.6	0.0384	16.50*	0.000	0.005#	0.00	0.3110E-11	G		1	
1030.3+5516	SBS 1027+555	10 30 24.9	55 16 22.7	0.4354	17.80	0.007	0.080	0.60	0.1971E-11	Q		q	
1030.5+5132	RGB J1030+515	10 30 35.1	51 32 32.3	0.5180	18.40	0.103	0.128	0.19	0.7518E-12	G		q	
1030.9+3103	RBS 0875	10 30 59.1	31 02 55.7	0.1782	16.71	0.091	0.161	0.39	0.7122E-11	GC		q	
1031.3+5053	RBS 877	10 31 18.5	50 53 36.4	0.3610	17.00	0.023	0.034	0.09	0.5327E-10	Q		z	
1031.3+7442	LEDA 100167	10 31 22.0	74 41 58.3	0.1230	17.20	0.124	0.250	0.28	0.1935E-11	G		5	

Table A.3: *(continued)*

RXJ name (1)	Name (2)	RA(J2000) (3)	DEC(J2000) (4)	z (5)	m_V (6)	F_{5GHz}^{core} (7)	F_{5GHz} (8)	α_r (9)	$F_{0.1-2.4\ keV}$ (10)	Type (11)	Host (12)	Class. (13)	FR (14)
1031.6-1846	IRAS 10295-183	10 31 57.3	-18 46 33.9	0.0403	15.60*	0.000	0.010#	0.00	0.4360E-11	G	S	1	
	FIRSTJ103213.9+.	10 32 13.9	40 16 16.4	0.0776	13.90	0.000	0.005#	0.00	0.1714E-11	GC	c		
1032.1+2756	7C 1029+2813	10 32 14.0	27 56 01.6	0.0854	16.00*	0.024	0.037	0.00	0.4918E-12	G			
1032.1+2121	IRAS 10298+213	10 32 38.0	+21 21 48.0	0.1114	17.30*	0.000	0.004#	0.00	0.1940E-11	?		2	
1034.0+3555	IRAS 10311+3610	10 33 59.5	35 55 09.5	0.1690	16.76	0.000	0.002#	0.00	0.6932E-12	Q		q	
1034.1+7345	NGC 3252	10 34 23.1	+73 45 53.9	0.0039	14.10*	0.000	0.004#	0.00	0.4130E-11	G	S		
1034.6+3938	KUG 1031+398	10 34 38.6	39 38 28.2	0.0424	15.60	0.000	0.024#	0.00	0.3529E-10	G	S	!	
1034.9+3041	LEDA 093943	10 35 00.2	30 41 38.2	0.1373	17.07*	0.000	0.007#	0.00	0.3612E-11	GC			
	PKS 1032-199	10 35 02.1	-20 11 34.3	2.1980	18.20	0.000	1.149	-0.07	<0.4180E-12	Q		q	
	7C 1031+5708	10 35 06.2	56 52 57.9	0.5770	19.80	0.000	0.222	0.50	0.4789E-13	Q		q	
1035.1+3406	MG2 J103513+3406	10 35 11.7	34 06 25.1	0.6800	18.30	0.058	0.090	0.40	0.3860E-12	Q		q	
	[HB89] 1034-293	10 37 16.1	-29 34 02.8	0.3120	16.46	0.000	1.510	-0.21	0.1595E-11	Q		q	
1038.7+5330	NGC 3310	10 38 45.9	53 30 11.7	0.0033	12.15	0.149	0.290#	0.63	0.1625E-11	G	S	h	
1039.7+2422	7C 1036+2438	10 39 41.9	24 22 40.3	1.1730	19.00	0.000	0.098#	0.00	0.5534E-12	Q		q	
1039.0-0840	MCG -01-27-030	10 39 43.4	-08 41 13.1	0.0649	15.40*	0.000	0.003#	0.00	0.5310E-11	GC	c		
	IRAS F10378+4012	10 40 44.5	39 57 11.1	0.1386	17.98	0.000	0.024#	0.00	0.7405E-11	GC		2	
1041.8+3901	B3 1038+392	10 41 49.1	39 01 19.9	0.2082	15.80	0.023	0.019	0.00	0.1621E-11	G		z	
	3C 245	10 42 44.6	12 03 31.2	1.0290	17.29	0.910	1.389	0.60	0.1124E-11	Q		q	II
1043.0+0054	[HB89] 1040+011	10 43 03.8	+00 54 20.5	0.7300	19.20*	0.000	0.033#	0.00	0.6280E-11	QC		q	
1043.0+2408	RGB J1043+241	10 43 09.0	24 08 35.4	0.5600	17.69	0.609	0.000#	-0.55	0.1257E-11	Q		z	
1044.1+5322	TXS 1041+536	10 44 10.7	53 22 20.5	1.8970	20.10	0.308	0.437	0.04	0.4760E-12	Q		q	
	S5 1039+81	10 44 23.1	80 54 39.4	1.2600	17.90	0.000	0.733#	-0.40	0.1288E-11	Q		q	
1044.5+2718	1RXSJ104427.6+..	10 44 27.7	27 18 05.4	0.0760	16.20*	0.000	0.001#	0.00	0.3734E-11	G		1	
1044.6+3845	CGCG 212-045	10 44 39.2	38 45 34.5	0.0358	14.90	0.000	0.003#	0.00	0.4865E-11	G	S	5	
1045.6+5251	RGB J1045+528A	10 45 42.2	52 51 12.6	1.0500	18.10	0.043	0.105	0.50	0.7154E-12	G		q	
	GB6 J1046+5354	10 46 24.0	53 54 26.2	1.7040	19.20	0.000	0.264	0.00	0.1812E-12	Q		q	
1046.3+5449	7C 1043+5505	10 46 28.8	54 49 44.5	0.2490	15.50	0.049	0.077	0.05	0.2265E-12	G			
1047.1+3515	MS 1044.2+3531	10 47 03.3	35 15 21.0	0.3700	19.27	0.000	0.001#	0.00	0.7071E-12	G		1	
1048.1-1909	MRC 1045-188	10 48 06.6	-19 09 35.7	0.5950	18.20	0.000	1.110	-0.27	0.1359E-11	Q		q	
1048.6-4114	PKS 1046-409	10 48 38.3	-41 13 59.6	0.6200	18.20	0.000	1.040	0.84	0.1527E-11	Q		q	
1050.7-1250	NGC 3411	10 50 26.1	-12 50 42.3	0.0153	13.10	0.000	0.033#	0.00	0.1650E-10	G	E		
1050.1+8012	IRAS F10460+802	10 50 35.6	+80 11 50.7	0.1183	16.10*	0.000	0.006#	0.00	0.4030E-11	Q		q	
	NVSS J105036-..	10 50 36.5	-02 36 16.2	0.1400	16.80	0.000	0.014#	0.00	0.3512E-11	G		q	
	B2 1048+34	10 50 58.1	34 30 10.9	2.5200	19.40	0.000	0.291#	0.30	0.1747E-12	Q		q	

Table A.3: *(continued)*

RXJ name (1)	Name (2)	RA(J2000) (3)	DEC(J2000) (4)	z (5)	m_V (6)	F_{5GHz}^{core} (7)	F_{5GHz} (8)	α_r (9)	$F_{0.1-2.4\ keV}$ (10)	Type (11)	Host (12)	Class. (13)	FR (14)
	PKS 1048-313	10 51 04.8	-31 38 14.3	1.4290	19.40	0.000	0.730	0.15	<0.2090E-12	Q		q	
1051.4-0918	PG 1048-090	10 51 29.9	-09 18 10.0	0.3440	16.79	0.000	0.700	0.90	0.5253E-11	QC		q	
1051.8+2119	4C +21.28	10 51 48.8	21 19 52.3	1.3000	19.00	0.900	1.076	-0.08	0.5551E-12	Q		q	
1051.8+5733	7C 1048+5749	10 51 48.8	57 32 48.4	0.9900	22.90	0.000	0.154#	0.00	0.1838E-13	G		a	
1052.5+6125	4C +61.20	10 52 32.7	61 25 21.0	0.4220	16.48	0.132	0.363	0.78	0.3421E-11	Q		q	
	7C 1049+5746	10 52 37.4	57 31 04.1	0.7080	20.90	0.000	0.059#	0.00	0.6454E-14	G		a	
	RGB J1053+494	10 53 44.1	49 29 56.1	0.1400	16.90	0.029	0.059	0.07	0.1322E-11	G		z	
1054.0+6949	RX J1054.5+6949	10 54 30.4	+69 49 20.8	0.0920	17.00*	0.000	0.004#	0.00	0.1600E-11	G			
1054.4+3855	GB6 J1054+3855	10 54 31.9	38 55 21.7	1.3630	16.93	0.048	0.056	0.08	0.1162E-11	Q		z	
1056.0+0252	RBS 0921	10 56 06.6	+02 52 13.0	0.2363	18.30*	0.000	0.004#	0.00	0.1480E-10	G		z	
1057.0+3119	RGB J1057+313B	10 57 05.2	31 19 07.8	1.3320	18.70	0.016	0.044	0.00	0.5376E-12	Q		q	
	PKS 1056-771	10 57 33.4	-77 24 29.0	0.1810	21.00	0.000	0.400	0.40	0.1772E-12	Q		z	
1057.7-2753	RX J1057.8-2753	10 57 50.8	-27 54 10.8	0.0920	17.80*	0.000	0.064#	0.00	0.4550E-11	G		z	
1058.2+2029	MRK 0634	10 58 01.2	+20 29 13.9	0.0662	15.90*	0.000	0.003#	0.00	0.2490E-11	G		1	
	S5 1053+81	10 58 11.5	81 14 32.7	0.7060	20.00	0.341#	0.770	0.36	0.5075E-12	G		q	
1058.2+1951	[HB89] 1055+201	10 58 17.9	19 51 50.9	1.1100	17.07	0.768	1.504	0.48	0.2096E-11	Q		q	
1058.5+0134	4C +01.28	10 58 29.6	01 33 58.8	0.8880	18.28	2.641	3.403	-0.03	0.1969E-11	Q		q	
1058.5+5628	RBS 926	10 58 37.7	56 28 11.2	0.1440	15.80	0.178	0.247	-0.05	0.4333E-11	Q		z	
	3C 247	10 58 58.8	43 01 23.1	0.7489	21.50*	0.003	6.919	0.70	<0.1354E-13	G		n	II
	PMN J1100+0949	11 00 20.2	09 49 35.1	1.3170	17.20	0.000	0.161	0.80	0.1080E-11	Q		q	
1100.7+1046	PKS 1058+110	11 00 47.8	10 46 13.2	0.4230	17.10	0.000	0.260	1.01	0.1297E-11	Q		q	
1101.7+7225	[HB89] 1058+726	11 01 48.8	72 25 37.1	1.4600	17.88	0.530	0.858	0.23	0.1054E-11	Q		q	
1101.8+6241	4C +62.15	11 01 53.4	62 41 50.6	0.6630	17.70	0.285	0.700	-0.13	0.7110E-12	Q		q	
1103.1+4141	CGCG 1100.3+4158	11 03 11.0	41 42 18.9	0.0308	15.10*	0.000	0.007#	0.00	0.1435E-11	G			
1103.2+3014	B2 1100+30B	11 03 13.3	30 14 42.7	0.3800	18.00	0.106	0.202	-0.33	0.9839E-12	G		q	II
1103.5-3251	MRC 1101-325	11 03 31.5	-32 51 16.7	0.3554	16.30	0.000	0.730	0.39	0.4532E-11	G		q	
1103.6-2329	PMN J1103-2329	11 03 37.6	-23 29 30.2	0.1860	16.55	0.000	0.066	0.00	0.4447E-10	Q		z	
	3C 249.1	11 04 13.7	76 58 58.0	0.3115	15.72	0.000	0.775	0.00	0.7272E-11	Q		q	
1104.4+3812	MRK 0421	11 04 27.3	38 12 31.8	0.0300	12.90	0.600	0.723	0.07	0.9303E-10	G		z	
1104.5+2124	RGB J1104+214	11 04 36.2	21 24 18.0	0.1876	16.40	0.021	0.036	0.00	0.1499E-11	G		q	
1104.8+6038	7C 1101+6054	11 04 53.7	60 38 55.3	1.3630	19.20	0.000	0.198	0.00	0.1647E-12	Q		q	
1105.6+0202	PMN J1105+0202	11 05 38.9	02 02 57.5	0.1066	17.98*	0.000	0.316	0.00	0.1325E-11	G		1	
1106.5+7234	NGC 3516	11 06 47.5	+72 34 06.9	0.0088	12.50*	0.000	0.032#	0.00	0.3310E-11	G	0	5	
	PKS 1104-445	11 07 08.7	-44 49 07.6	1.5980	18.60	0.000	2.029	1.00	0.7884E-12	Q		q	

Table A.3: *(continued)*

RXJ name (1)	Name (2)	RA(J2000) (3)	DEC(J2000) (4)	z (5)	m_V (6)	F_{5GHz}^{core} (7)	F_{5GHz} (8)	α_r (9)	$F_{0.1-2.4\ keV}$ (10)	Type (11)	Host (12)	Class. (13)	FR (14)
	PKS 1105-680	11 07 12.7	-68 20 50.7	0.5880	19.20	0.000	1.370	0.10	0.2029E-11	Q		q	
1107.2+1628	4C +16.30	11 07 15.0	16 28 02.2	0.6320	15.70	0.388	0.561	0.29	0.4614E-11	Q		q	
1107.4+3616	4C +36.18	11 07 26.9	36 16 11.7	0.3930	18.00	0.012	0.216	0.80	0.1424E-11	G		q	II
	MRC 1105-304	11 07 43.9	-30 43 36.8	0.7400	20.20	0.000	0.260	0.00	0.1057E-11	Q		q	
1107.2+1502	87GB 110510.0+1	11 07 48.0	+15 02 10.0	0.2594	18.00*	0.030	0.037	0.00	0.5940E-11	Q		z	
1108.7+0202	PKSJ 1108+0202	11 08 45.5	02 02 40.6	0.1570	18.01	0.674	0.490	0.46	0.9792E-12	G	N	1	
1108.0-0149		11 08 58.4	-01 49 31.9	0.1056	18.00*	0.000	0.082#	0.00	0.3500E-11	G		z	
	NGC 3557	11 09 57.6	-37 32 21.0	0.0102	10.91	0.000	0.270	0.40	0.3496E-12	GC	E	r	I
1110.1-2830	ESO 438- G 009	11 10 48.0	-28 30 03.8	0.0245	14.20*	0.000	0.015#	0.00	0.7840E-11	GC		1	
1111.5+3452	RBS 946	11 11 30.9	34 52 03.4	0.2120	19.50	0.000	0.005#	0.00	0.7162E-11	Q		z	
1111.6+4050	RGB J1111+408	11 11 39.8	40 50 24.2	0.0737	17.00*	0.036	0.264	1.30	0.4361E-11	GC			
	GB6 J1112+2601	11 12 20.7	26 01 13.0	0.7280	18.26	0.000	0.028	0.00	0.4908E-12	Q		q	
1113.5+0935	IC 2637	11 13 49.7	+09 35 10.7	0.0292	14.00*	0.000	0.044#	0.00	0.4770E-11	G	E	5	
1113.9+1442	[HB89] 1111+149	11 13 58.7	14 42 26.9	0.8690	17.90	0.436	0.495	0.30	0.1502E-11	Q		q	
1114.2+5823	RGB J1114+583	11 14 21.9	58 23 19.0	0.2060	14.00	0.003	0.016	0.70	0.2393E-11	GC	c		
1114.6+4037	3C 254	11 14 38.5	40 37 20.3	0.7340	17.98	0.000	0.790	1.10	0.1167E-11	Q		q	
	B2 1113+29	11 16 34.8	29 15 08.0	0.0490	14.90	0.041	4.950&	0.50	0.6200E-13	GC	d		
1118.0+4506	LEDA 139560	11 18 03.3	45 06 46.8	0.1060	16.50	0.000	0.016#	0.00	0.4004E-11	G		1	
1118.4-4634	[HB89] 1116-462	11 18 26.9	-46 34 15.0	0.7130	17.00	0.000	1.300	0.44	0.2601E-11	Q		q	
1118.9+1234	4C +12.39	11 18 57.3	12 34 41.7	2.1180	19.25	1.887	0.000	0.06	0.7645E-12	Q		q	
	RBS 0964	11 19 07.1	41 30 14.6	0.0951	18.00	0.000	0.002#	0.00	0.3153E-11	G		1	
1119.1+2119	PG 1116+215	11 19 08.6	+21 19 18.0	0.1765	15.20*	0.000	0.006#	0.00	0.1200E-10	Q	E	1	
1119.4+2226	RBS 966	11 19 30.3	22 26 49.3	0.4220	17.31	0.104	0.138	0.00	0.2903E-11	Q		q	
1120.1-2507	MRC 1117-248	11 20 09.1	-25 08 07.6	0.4660	17.07	0.000	0.730	0.80	0.9889E-12	Q		g	
1120.2+1259	NGC 3627	11 20 15.0	12 59 29.5	0.0024	11.94	0.005	0.147	0.62	0.2105E-11	GC	S	l	
1120.7+4212	RBS 970	11 20 48.1	42 12 12.4	0.1240	17.30	0.019	0.030	-0.18	0.1363E-10	Q		z	
1121.1+5351	1RXSJ112109.9+..	11 21 08.7	53 51 16.9	0.1027	16.00	0.000	0.003#	0.00	0.2878E-11	G		1	
1121.5+1236	PKS 1118+128	11 21 29.8	12 36 17.4	0.6850	19.30	0.007	0.122	0.90	0.6806E-12	Q		q	
1121.3+1144	PG 1119+120	11 21 47.1	+11 44 18.3	0.0502	15.10*	0.000	0.003#	0.00	0.8070E-11	G		1	
1122.4+1805	[HB89] 1119+183	11 22 29.7	18 05 26.3	1.0400	18.30	0.700	0.744	0.00	0.4560E-12	Q		q	
1124.0-2404	PMN J1124-2405	11 24 03.9	-24 05 20.1	0.6750	19.10	0.000	0.200	0.90	0.7209E-12	Q		q	
1124.9+0612	CGCG 039-167	11 24 08.7	+06 12 53.3	0.0372	14.90*	0.000	0.015#	0.00	0.1060E-10	G	S	1	
1125.6-0742		11 25 51.9	-07 42 21.1	0.2786	19.00*	0.000	0.039#	0.00	0.5120E-11	G		z	
1126.8+4516	B3 1124+455	11 26 57.6	45 16 06.3	1.8110	17.70	0.355	0.330	0.38	0.6555E-12	G		q	

Table A.3: *(continued)*

RXJ name (1)	Name (2)	RA(J2000) (3)	DEC(J2000) (4)	z (5)	m_V (6)	F^{core}_{5GHz} (7)	F_{5GHz} (8)	α_r (9)	$F_{0.1-2.4\ keV}$ (10)	Type (11)	Host (12)	Class. (13)	FR (14)
	PKS 1124-186	11 27 04.4	-18 57 17.4	1.0500	18.65	0.000	0.840	-1.70	0.1073E-10	Q		q	
1127.6+1909		11 27 16.3	+19 09 20.2	0.1055	16.10*	0.000	0.007#	0.00	0.1530E-11	G		8	
1128.5+5833	MRK 0171	11 28 32.2	58 33 44.0	0.0104	12.86	0.000	0.678#	0.95	0.1198E-11	G	S	h	
1130.1+4116	KUV 11274+4133	11 30 04.7	41 16 19.0	1.5300	16.75	0.000	0.002#	0.00	0.5750E-12	Q		q	
1130.1-1449	PKS 1127-14	11 30 07.0	-14 49 27.4	1.1840	16.90	0.000	5.459	0.14	0.2676E-11	Q		g	
1130.7+3031	B2 1128+30A	11 30 42.4	30 31 35.4	0.7400	18.30	0.000	0.378	0.20	0.8082E-12	Q		q	
1130.8+3815	B2 1128+38	11 30 53.3	38 15 18.5	1.7330	19.46	0.869	0.000	-0.22	0.6238E-12	Q		q	
1131.1+2632	FBQSJ113109.2..	11 31 09.2	26 32 08.4	0.2440	17.00	0.000	0.003#	0.00	0.2016E-11	G		q	
1131.1+3114	TON 580	11 31 09.5	31 14 05.5	0.2890	16.80	0.084	0.311	-0.04	0.8999E-11	Q		q	
1131.3+3334	FIRSTJ113120.9..	11 31 20.9	33 34 46.9	0.2203	17.50	0.000	0.007#	0.00	0.1834E-11	G		z	
	[HB89] 1130+106	11 32 59.5	10 23 42.5	0.5400	17.49	0.000	0.400	0.70	0.1431E-11	Q		q	
	TXS 1130+504	11 33 13.2	50 08 39.7	0.3100	21.30*	0.000	0.303	0.60	0.1054E-11	G			
1133.2+2813	US 2599	11 33 14.8	28 11 59.6	0.5130	17.60	0.019	0.034	0.00	0.9289E-12	Q		q	
1134.4+4147	CSO 1195	11 34 27.8	41 47 21.7	0.8180	17.50	0.000	0.003#	0.00	0.1161E-11	Q		q	
1135.3+3153	7C 1132+3210	11 35 26.7	31 53 33.1	0.2310	19.60*	0.019	0.024	0.20	0.1127E-11	G			
	MS 1133.7+1618	11 36 17.5	16 01 53.1	0.4600	20.04	0.000	0.009	0.00	0.6486E-12	Q		z	
1136.5+7009	MRK 180	11 36 26.4	70 09 27.3	0.0453	14.49	0.139	0.267	0.38	0.5647E-10	G		z	
1136.4+2135	NGC 3758	11 36 29.1	+21 35 46.0	0.0299	15.20*	0.000	0.011#	0.00	0.7420E-11	G	S	1	
1136.5+6737	RBS 1004	11 36 30.1	67 37 04.0	0.1350	17.30	0.040	0.047	-0.02	0.2454E-10	Q		z	
1137.4+1039		11 37 38.0	+10 39 30.1	0.1745	16.60*	0.000	0.003#	0.00	0.2630E-11	G		1	
1139.6-3744	NGC 3783	11 39 01.7	-37 44 18.9	0.0097	12.60*	0.000	0.045#	0.00	0.5480E-10	G	S	1	
1139.1-1350	PKS 1136-13	11 39 10.7	-13 50 43.6	0.5580	16.17	0.000	2.220	0.35	0.3079E-11	Q		q	
1139.7+3154	NGC 3786	11 39 42.5	31 54 29.1	0.0089	13.74	0.000	0.011#	0.00	0.5776E-12	G	p	8	
1139.9+6547	3C 263	11 39 57.0	65 47 49.4	0.6460	16.32	0.162	1.139	0.79	0.3242E-11	QC		q	
1140.0+4115	IRAS F11374+4131	11 40 03.4	41 15 03.3	0.0710	13.80	0.000	0.001#	0.00	0.1040E-11	G		q	
1140.5+1528		11 40 23.5	+15 28 09.8	0.2447	17.40*	0.000	0.070#	0.00	0.8370E-11	GC			
1141.1+0241	RX J1141.1+0241	11 41 05.7	+02 41 16.3	0.0928	16.90*	0.000	0.002#	0.00	0.2120E-11	G		1	
1141.2+2156	PG 1138+222	11 41 16.1	+21 56 21.0	0.0632	14.90*	0.000	0.005#	0.00	0.2620E-10	G		1	
1142.4+5831	RGB J1142+585	11 42 24.7	58 32 05.7	0.3229	19.00	0.006	0.039	0.00	0.1084E-11	GC			
1143.0+1843	RGB J1143+187	11 43 05.9	18 43 43.0	0.3739	16.40	0.043	0.053	0.00	0.2030E-11	G		q	
1143.3+0211	LBQS 1140+0228	11 43 19.6	02 11 45.7	0.4520	19.30	0.000	0.060	0.00	0.8464E-12	Q		q	
	3C 263.1	11 43 25.1	22 06 55.9	0.8240	20.00*	0.003	0.780	1.10	0.2166E-12	G	E	n	II
1143.5+2314	RGB J1143+232	11 43 37.9	23 15 02.5	0.8370	17.80	0.100	0.146	0.00	0.5596E-12	Q		q	
1144.9+3653	KUG 1141+371	11 44 29.8	+36 53 08.3	0.0400	16.50*	0.000	0.003#	0.00	0.2040E-10	G	S	1	

Table A.3: *(continued)*

RXJ name (1)	Name (2)	RA(J2000) (3)	DEC(J2000) (4)	z (5)	m_V (6)	F_{5GHz}^{core} (7)	F_{5GHz} (8)	α_r (9)	$F_{0.1-2.4\ keV}$ (10)	Type (11)	Host (12)	Class. (13)	FR (14)
1144.7+6724	RGB J1144+674	11 44 36.8	67 24 20.8	0.1158	12.80	0.019	0.087	1.10	0.5062E-11	GC			
	3C 264	11 45 05.0	19 36 22.7	0.0217	13.97	0.200	15.500&	0.20	0.3290E-11	GC	E	w	I
1145.1+3047	[HB89] 1142+310	11 45 10.3	30 47 17.4	0.0596	16.00	0.000	0.003#	0.00	0.6845E-11	G		5	
1145.1+0110	RGB J1145+011	11 45 10.4	01 10 56.3	0.6261	21.10*	0.015	0.049	0.00	0.4517E-12	Q		q	
	MCG +03-30-100	11 45 22.2	15 29 43.6	0.0679	17.00*	0.000	0.187	0.50	0.2964E-11	GC			
1145.8-0339	LCRS B114301.7-	11 45 35.1	-03 40 01.7	0.1675	17.20*	0.000	0.020#	0.00	0.7320E-11	G		a	
1145.5-1827	IRAS F11431-181	11 45 40.5	-18 27 15.5	0.0330	14.70*	0.000	0.010#	0.00	0.7580E-10	G	p	1	
	3C 266	11 45 43.4	49 46 08.2	1.2750	22.00*	0.000	0.320	1.20	<0.2708E-13	G		g	II
	PKS 1143-245	11 46 08.1	-24 47 32.9	1.9400	18.00	0.000	1.179	0.18	<0.2410E-12	Q		g	
	MRC 1144-379	11 47 01.4	-38 12 11.0	1.0480	16.20	0.000	0.900	-1.18	0.3582E-11	Q		q	
1147.3+3500	B2 1144+35B	11 47 22.1	35 01 07.5	0.0630	16.60	0.363	0.669	0.27	0.6667E-12	G		2	I
	PKS 1145-071	11 47 51.5	-07 24 41.1	1.3420	18.70	0.000	1.209	-0.17	0.3430E-12	Q		q	
1147.9+2715	US 2964	11 47 58.6	27 15 00.0	0.3630	16.30	0.000	0.024	0.00	0.2577E-11	Q		q	
1147.9+2635	7C 1145+2652	11 47 59.8	26 35 42.3	0.8670	17.70	0.329	0.420	-0.20	0.8025E-12	G		q	
1148.3+3154	B2 1145+32	11 48 18.9	31 54 09.8	0.5490	17.30	0.096	0.000	0.00	0.1138E-11	Q		q	
1148.9-0404	PKS 1146-037	11 48 55.9	-04 04 09.6	0.3400	16.90	0.000	0.340	0.30	0.2128E-11	Q		q	
1149.9+2119	NGC 3910	11 49 59.3	21 20 01.1	0.0261	13.83*	0.000	0.029	0.00	0.4647E-12	G	0		
	PMN J1150+0156	11 50 24.8	01 56 16.4	1.5020	19.50	0.000	0.090	0.60	0.3044E-12	Q		q	
1150.5+4154	RBS 1040	11 50 34.8	41 54 40.1	1.0180	17.50	0.000	0.022#	0.00	0.3516E-11	Q		q	
1150.7+3411	2MASXiJ1150439..	11 50 43.8	34 11 17.1	0.0710	14.90*	0.000	0.001#	0.00	0.8212E-12	G		*	
	LBQS 1148-0007	11 50 43.9	-00 23 54.2	1.9828	17.60	0.000	1.899	0.44	0.9015E-12	Q		q	
1151.1+4729	B3 1148+477	11 51 09.3	47 28 55.7	0.8670	18.00	0.000	0.147	1.27	0.7186E-12	Q		q	
1152.9-1122	PG 1149-110	11 52 03.5	-11 22 24.3	0.0490	15.50*	0.000	0.011#	0.00	0.1410E-10	G		1	
1152.3+3209	RBS 1045	11 52 27.5	32 09 59.3	0.3740	17.50	0.046	0.036	0.00	0.3308E-11	G		q	
1152.2-0512	MCG -01-30-041	11 52 38.2	-05 12 25.2	0.0192	14.70*	0.000	0.012#	0.00	0.1930E-11	G	S	8	
1152.9+3307	7C 1150+3324	11 52 51.9	33 07 18.8	1.4000	16.30	0.000	0.161#	0.00	0.5017E-12	Q		q	
	[HB89] 1150+812	11 53 12.5	80 58 29.1	1.2500	19.40	0.000	1.343#	0.09	0.7186E-12	Q		q	
1153.3+5831	RGB J1153+585	11 53 23.9	58 31 38.5	0.2023	17.30	0.000	0.109	0.00	0.1664E-11	Q		q	
1153.4+4931	SBS 1150+497	11 53 24.5	49 31 08.8	0.3340	17.10	0.500	0.717	-0.31	0.6100E-11	Q		q	
1153.4+3617	RGB J1153+362	11 53 26.7	36 17 26.2	1.3360	17.90	0.049	0.060	0.00	0.1389E-11	Q		q	
	PKS 1151-34	11 54 21.8	-35 05 29.1	0.2580	17.84	0.000	2.779	0.69	<0.7200E-12	Q		g	
1155.2+6538	[HB89] 1152+659	11 55 17.7	65 39 17.0	1.1990	18.10	0.000	0.167	1.03	0.8469E-12	Q		q	
1155.3+2324	MCG +04-28-097	11 55 18.0	23 24 18.2	0.1429	18.00*	0.000	0.001#	0.00	0.1176E-10	GC			
1155.2+1939	RGB J1155+196	11 55 18.3	19 39 42.2	1.0189	16.90	0.070	0.076	0.50	0.1297E-11	Q		q	

Table A.3: *(continued)*

RXJ name (1)	Name (2)	RA(J2000) (3)	DEC(J2000) (4)	z (5)	m_V (6)	F_{5GHz}^{core} (7)	F_{5GHz} (8)	α_r (9)	$F_{0.1-2.4\ keV}$ (10)	Type (11)	Host (12)	Class. (13)	FR (14)
1156.6+2415	RX J1157.0+2415	11 56 55.6	+24 15 37.0	0.1419	16.00*	0.000	0.005#	0.00	0.2630E-11	G			
1157.1+2821	FBQSJ1157+2822	11 57 09.5	28 22 00.8	0.3010	19.80*	0.000	0.026#	0.00	0.9940E-12	G			
1157.9+5527	NGC 3998	11 57 56.1	55 27 12.7	0.0035	12.10	0.053	0.088	0.12	0.6832E-11	G	0	l	
1158.6+6254	[HB89] 1156+631	11 58 39.8	62 54 27.0	0.5940	17.79	0.013	0.269	0.89	0.9242E-12	Q		q	
	7C 1156+2123	11 59 26.2	21 06 55.0	0.3490	16.90	0.000	0.081	0.60	0.1131E-11	Q		q	
1159.5+2914	FBQS J1159+2914	11 59 31.8	29 14 43.8	0.7290	14.41	1.457	1.461	0.30	0.1302E-11	Q		q	
1159.4-1959	IRAS F11571-194	11 59 41.0	-19 59 24.0	0.4500	16.20*	0.000	0.010#	0.00	0.6930E-11	Q		q	
1200.5-0046		12 00 14.1	-00 46 38.7	0.1791	17.50*	0.000	0.040#	0.00	0.2680E-11	G		1	
1201.6-0006		12 01 06.2	-00 07 01.6	0.1651	18.70*	0.000	0.071#	0.00	0.1710E-11	G		z	
1201.3-0340	MRK 1310	12 01 14.4	-03 40 41.4	0.0194	14.50*	0.000	0.004#	0.00	0.1520E-10	G	E	1	
1201.9+5802	RGB J1202+580	12 02 03.8	58 02 09.3	0.1028	15.40	0.007	0.258	-0.40	0.8050E-12	GC			
1202.9-0129	IRAS 11598-011	12 02 26.8	-01 29 15.4	0.1510	17.90*	0.000	0.015#	0.00	0.2440E-11	G		1	
1202.5+2756	7C 1159+2813	12 02 34.0	27 56 26.0	0.6720	18.90	0.156	0.000#	0.00	0.8669E-12	Q		q	
1202.5-0528	RBS 1059	12 02 34.2	-05 28 02.5	0.3810	17.30	0.000	0.460	0.14	0.5319E-11	Q		q	
1202.6+2631	RGB J1202+265	12 02 40.7	26 31 38.6	0.4780	17.70	0.070	0.082	0.00	0.1680E-11	Q		q	
1202.7+3735	B3 1200+378	12 02 43.5	37 35 51.7	1.1940	18.20	0.000	0.049	0.60	0.4877E-12	Q		q	
1202.0-0347	LCRS B120011.5-	12 02 45.3	-03 47 21.3	0.0645	16.40*	0.000	0.003#	0.00	0.1900E-11	G		1	
1203.0+6031	SBS 1200+608	12 03 03.5	60 31 19.1	0.0656	17.00	0.146	0.182	0.05	0.1228E-11	G		l	
1203.1+4432	NGC 4051	12 03 09.6	44 31 52.8	0.0023	12.92	0.032	0.170&	0.00	0.4963E-10	G	S	!	
1203.4+4803	RGB J1203+480	12 03 29.9	48 03 13.6	0.8133	16.40	0.232	0.164	-1.03	0.1755E-11	G		q	
1203.5+4511	RGB J1203+451	12 03 35.4	45 10 50.0	1.0700	17.20	0.053	0.043	-0.08	0.6637E-12	G		q	
1203.7+2836	1RXSJ120343.3+..	12 03 43.2	28 35 55.0	0.3730	17.79	0.000	0.002#	0.00	0.3688E-11	GC		q	
1203.8+3711	FBQS J120354.7+.	12 03 54.8	37 11 37.4	0.4010	18.57	0.000	0.004#	0.00	0.1077E-11	Q		q	
1204.4+0153	RGB J1204+018	12 04 27.9	01 53 44.0	0.0198	13.21*	0.000	0.073	0.00	0.1424E-10	GC	E		
1204.5+4856	SBS 1202+492	12 04 36.2	48 56 54.0	0.4460	18.19	0.040	0.111	0.70	0.1352E-11	Q		q	
1204.6+3110	UGC 07064	12 04 43.3	31 10 38.2	0.0250	14.01	0.000	0.005#	0.00	0.3509E-12	G	S	9	
1205.5-2633	PKS 1203-26	12 05 33.2	-26 34 04.5	0.7890	19.50	0.000	0.990	0.49	0.1341E-11	Q		q	
1205.8+3510	MRK 0646	12 05 49.8	35 10 45.7	0.0537	15.28	0.000	0.001#	0.00	0.2728E-11	G		5	
	GB6 J1206+2823	12 06 19.6	28 22 54.6	0.7080	19.50	0.000	0.030#	0.00	0.1928E-12	Q		q	
	3C 268.3	12 06 24.7	64 13 36.8	0.3710	20.00	0.000	1.090	0.80	<0.4739E-13	G		g	II
1207.4+2755	B2 1204+28	12 07 27.9	27 54 58.8	2.1770	18.43	0.440	0.457	0.10	0.4125E-12	Q		q	
1207.8+2802	FIRSTJ120754.8..	12 07 54.7	28 02 59.9	0.3540	17.33	0.000	0.001#	0.00	0.1033E-11	GC		q	
1208.0+2514	CGCG 1205.5+2531	12 08 05.6	25 14 14.1	0.0226	14.36*	0.044	0.185	1.10	0.5040E-12	G	E		I
1208.3+5240	EXO 1205.8+5256	12 08 22.4	52 40 13.5	0.4350	16.91	0.019	0.028	0.00	0.9139E-12	G		q	

Table A.3: *(continued)*

RXJ name (1)	Name (2)	RA(J2000) (3)	DEC(J2000) (4)	z (5)	m_V (6)	F_{5GHz}^{core} (7)	F_{5GHz} (8)	α_r (9)	$F_{0.1-2.4\ keV}$ (10)	Type (11)	Host (12)	Class. (13)	FR (14)
	PKS J1209-2406	12 09 02.4	-24 06 20.7	1.2990	18.00	0.000	0.710	1.30	0.5466E-12	Q		z	
	3C 268.4	12 09 13.5	43 39 18.4	1.4000	18.42	0.050	0.600	0.90	0.5349E-12	Q		q	II
1209.7+3217	RBS 1071	12 09 45.2	32 17 00.9	0.1450	17.70	0.000	0.002#	0.00	0.7756E-11	G		!	
1209.9+0628	IRAS F12073+064	12 09 54.6	+06 28 13.3	0.0796	16.80*	0.000	0.004#	0.00	0.2030E-11	G		1	
1210.4+3929	[HB89] 1207+397	12 10 26.7	39 29 09.0	0.6150	20.30	0.000	0.015#	0.00	0.4382E-11	QC		z	
1210.5+3924	NGC 4151	12 10 32.6	39 24 20.6	0.0033	11.85	0.125	0.139	0.88	0.3755E-11	G	S	5	
1210.6+3157	[HB89] 1208+322	12 10 37.6	31 57 06.0	0.3880	16.68	0.000	0.160	1.59	0.1378E-11	Q		q	
1211.0+3520	7C 1208+3536	12 11 08.3	35 19 59.3	0.1400	17.40*	0.000	0.034	2.60	0.1498E-11	G			
	MG2 J121300+3247	12 13 03.8	32 47 36.9	2.5020	19.90	0.000	0.063	0.70	0.1834E-12	Q		q	
	GB6 J1213+1444	12 13 14.9	14 44 00.0	0.7180	21.00	0.000	0.065	0.70	0.3829E-12	Q			
1213.6-2618	RBS 1080	12 13 23.0	-26 18 07.0	0.2780	19.00*	0.000	0.007#	0.00	0.1060E-10	Q		z	
1213.2+3637	NGC 4190	12 13 44.7	+36 38 02.9	0.0008	13.90*	0.000	0.007#	0.00	0.1900E-11	G	p		
1213.7+0001	RGB J1213+000	12 13 47.5	00 01 30.0	0.9610	18.20*	0.050	0.103	0.00	0.6236E-12	Q		q	
1215.0+3311	NGC 4203	12 15 05.0	33 11 50.0	0.0036	11.99	0.000	0.007#	0.00	0.6273E-11	G	0	l	
1215.1+0732	RGB J1215+075	12 15 10.9	07 32 03.8	0.1300	16.00	0.084	0.117	0.55	0.4955E-11	G		z	
1216.6-0243		12 16 03.3	-02 43 05.7	0.1690	18.00*	0.000	0.011#	0.00	0.2200E-11	G		z	
1216.0+0929	RGB J1216+094	12 16 06.2	09 29 09.4	0.0935	13.20	0.074	0.157	0.29	0.1681E-11	G		z	
1216.8+3754	IRAS F12144+3811	12 16 51.8	37 54 37.9	0.0620	16.68	0.000	0.001#	0.00	0.4888E-12	G		2	
	WGA J1217.1+2925	12 17 08.2	29 25 33.5	0.9740	19.90	0.000	0.037#	0.00	0.1821E-12	Q		q	
1217.0+0711	NGC 4235	12 17 09.9	+07 11 29.1	0.0080	12.60*	0.000	0.015#	0.00	0.1390E-11	G	S	1	
1217.3+3056	RBS 1090	12 17 21.4	30 56 30.6	0.3074	17.00	0.000	0.008#	0.00	0.2979E-11	Q		q	
1217.6+0339	PGC 039445	12 17 41.1	+03 39 21.9	0.0759	14.90*	0.000	1.117#	0.00	0.2110E-10	G	E		
1217.8+3007	7C 1215+3023	12 17 52.1	30 07 00.6	0.1300	15.62	0.353	0.478	0.15	0.3921E-10	Q		z	
	PKS 1215-45	12 18 06.2	-46 00 29.0	0.5290	20.30	0.000	1.990	-0.50	0.1213E-11	Q		a	
1218.4+2948	NGC 4253	12 18 26.5	29 48 46.3	0.0129	13.57	0.000	0.038#	0.00	0.6893E-10	G	S	5	
	RGB J1218+052	12 18 52.1	05 14 43.3	0.0752	17.11	0.010	0.271	0.30	0.5700E-12	GC			
1219.0+4717	MESSIER 106	12 18 57.5	47 18 14.2	0.0015	11.65	0.792#	0.305	0.00	0.2344E-11	G	S	2	
1219.4+0549	3C 270	12 19 23.2	05 49 30.8	0.0074	12.87	0.285	4.043	0.86	0.1199E-11	GC	E	l	I
1220.0+2916	NGC 4278	12 20 06.8	29 16 50.7	0.0022	10.87	0.283	0.372	0.62	0.5862E-12	G	E	l	
1220.1+0203	MRC 1217+023	12 20 11.9	02 03 42.2	0.2390	16.53	0.257	0.572	0.36	0.4919E-11	Q		q	
1220.5+3343	3C 270.1	12 20 33.8	33 43 10.0	1.5190	18.61	0.174	0.842	0.88	0.6782E-12	Q		q	
1221.9+4742	RX J1221.1+4742	12 21 07.8	+47 42 28.6	0.2099	19.00*	0.000	0.042#	0.00	0.1450E-11	G			
1221.3+3010	PG 1218+304	12 21 21.9	30 10 37.1	0.1820	15.85	0.060	0.000#	0.00	0.2302E-10	Q		z	
1221.5+2813	B2 1219+28	12 21 31.7	28 13 58.5	0.1020	16.11	0.940	1.084	0.14	0.2238E-11	Q		z	

Table A.3: *(continued)*

RXJ name (1)	Name (2)	RA(J2000) (3)	DEC(J2000) (4)	z (5)	m_V (6)	F_{5GHz}^{core} (7)	F_{5GHz} (8)	α_r (9)	$F_{0.1-2.4\ keV}$ (10)	Type (11)	Host (12)	Class. (13)	FR (14)
1221.4+0821	MG1 J122131+0821	12 21 32.1	08 21 43.8	0.1320	17.10	0.030	0.058	0.00	0.1804E-11	G		z	
1221.4+7518	[HB89] 1219+755	12 21 44.0	+75 18 38.5	0.0709	14.50*	0.000	0.008#	0.00	0.1740E-10	G	S	1	
1221.9+0429	NGC 4303	12 21 54.9	04 28 25.1	0.0052	12.60	0.153	0.365#	1.46	0.6530E-12	GC	S	2	
1222.3+0413	PKS 1219+04	12 22 22.5	04 13 15.8	0.9650	17.98	0.665	1.351	-0.10	0.1446E-11	Q		q	
	GB6 J1222+2934	12 22 43.2	29 34 41.5	0.7870	18.70	0.000	0.063	0.00	0.2454E-12	Q		q	
	NGC 4335	12 23 01.9	58 26 40.7	0.0154	13.70*	0.000	0.082	1.10	0.2941E-13	G	E		I
1223.1+3706	B2 1220+37	12 23 11.2	37 07 01.9	0.4890	18.35	0.014	0.153	0.82	0.1018E-11	Q		q	
1223.1+5409	RGB J1223+541	12 23 13.2	54 09 06.0	0.1570	18.50	0.042	0.140	0.00	0.2643E-11	G		q	
1223.2+0922	LBQS 1220+0939	12 23 17.8	09 23 07.2	0.6810	17.30	0.000	0.024	0.00	0.6255E-12	Q		q	
	PMN J1223+0650	12 23 54.6	06 50 02.6	1.1890	21.20	0.000	0.285	0.00	0.2582E-12	Q		q	
1224.4+2436	RGB J1224+246	12 24 24.2	24 36 23.5	0.2180	17.37	0.025	0.027	0.00	0.2592E-11	Q		z	
1224.3+4015	CSO 1316	12 24 24.2	40 15 10.7	0.4150	17.79	0.031	0.037	0.00	0.4709E-12	Q		q	
	4C +26.37	12 24 33.5	26 13 15.6	0.6870	21.30	0.000	0.270	1.44	0.2186E-12	G			
1224.7+3832	RGB J1224+385	12 24 50.2	38 32 48.5	0.0750	19.65	0.047	0.033	0.00	0.8352E-12	G		l	
1224.8+0330	4C +03.23	12 24 52.4	03 30 50.3	0.9570	18.79	1.000	1.221	-0.10	0.9481E-12	Q		q	
1224.9+2122	PG 1222+216	12 24 54.4	21 22 46.4	0.4350	17.50	0.480	1.153	-0.20	0.3334E-11	Q		q	
	M 84	12 25 03.8	12 53 13.1	0.0035	12.31	0.000	2.839	0.50	0.1868E-11	GC	E	w	I
1225.1+3213	RGB J1225+322	12 25 13.1	32 14 01.7	0.0610	13.00	0.072	0.047	0.00	0.2354E-11	G		q	
1225.5+7214		12 25 14.1	+72 14 48.1	0.1138	16.30*	0.000	0.005#	0.00	0.1370E-11	G		z	
1225.2+3146	B2 1222+32B	12 25 16.3	31 45 25.3	1.2840	17.30	0.026	0.034	0.80	0.4178E-12	Q		q	
	GB6 J1225+0715	12 25 31.2	07 15 52.0	1.1200	21.30	0.000	0.055	0.00	0.1459E-12	Q		q	
1225.6+2458	TON 0616	12 25 39.5	24 58 36.4	0.2680	17.12	0.004	0.137	0.75	0.2180E-11	Q		q	
	NGC 4388	12 25 46.7	12 39 43.5	0.0084	13.90	0.000	0.090	0.00	0.5845E-12	G	S	2	
1226.3+3244	RBS 1112	12 26 24.2	32 44 29.4	0.2420	17.01	0.000	0.001#	0.00	0.4864E-11	G		q	
1226.4+3113	NGC 4414	12 26 27.1	31 13 24.3	0.0024	10.96*	0.075	0.226#	0.00	0.4356E-12	GC	S		
1227.1+0841	RX J1227.7+0841	12 27 44.8	+08 41 49.8	0.0852	16.80*	0.000	0.004#	0.00	0.4840E-11	G		1	
1227.8+3214	FBQS J122749.1+.	12 27 49.1	32 14 59.0	0.1370	17.20	0.000	0.006#	0.00	0.9112E-12	Q			
1227.8+6323	RGB J1227+633	12 27 51.2	63 23 05.3	0.1453	15.50*	0.005	0.071	3.00	0.2111E-11	GC			
1228.4+3128	B2 1225+31	12 28 24.9	31 28 37.6	2.2190	15.87	0.305	0.345	0.00	0.2883E-12	Q		q	
1228.7+3706	CJ2 1226+373	12 28 47.4	37 06 12.1	1.5150	18.40	0.608	0.856	0.02	0.3106E-12	G		q	
1229.1+0203	3C 273	12 29 06.7	02 03 08.6	0.1583	12.85	26.399	43.572	-0.05	0.1024E-09	Q		q	
	MG2 J122932+2711	12 29 34.2	27 11 56.4	0.4900	19.20	0.000	0.152	0.20	0.2080E-12	G		n	
1229.7+0759	NGC 4472	12 29 46.8	08 00 01.5	0.0033	9.37*	0.012	0.086	0.85	0.1453E-10	GC	E	2	
1230.1+1145	[OLK95]1227+120W	12 30 11.6	11 44 38.8	0.0873	17.18	0.019	0.184	0.00	0.6534E-12	GC	E		

Table A.3: *(continued)*

RXJ name (1)	Name (2)	RA(J2000) (3)	DEC(J2000) (4)	z (5)	m_V (6)	F_{5GHz}^{core} (7)	F_{5GHz} (8)	α_r (9)	$F_{0.1-2.4\ keV}$ (10)	Type (11)	Host (12)	Class. (13)	FR (14)
1230.2+2517	RBS 1121	12 30 14.1	25 18 07.1	0.1350	15.60	0.351	0.000	0.00	0.3429E-11	Q		z	
	RGB J1231+006	12 31 08.4	00 36 49.4	0.0231	14.90*	0.000	0.081	0.00	0.5806E-12	G			
	GB6 J1231+1421	12 31 23.9	14 21 24.4	0.2600	17.70	0.000	0.058	0.00	0.3101E-11	G		z	
1231.5+6414	[HB89] 1229+645	12 31 31.4	64 14 18.3	0.1700	16.90	0.034	0.036	0.40	0.4409E-11	Q		z	
1231.6+4017	B3 1229+405	12 31 40.4	40 17 32.9	0.6490	20.00	0.052	0.109	0.90	0.5288E-12	Q		q	
1231.6+2847	RGB J1231+287	12 31 43.6	28 47 49.7	1.0000	16.40	0.060	0.114	0.55	0.2114E-11	Q		q	
1231.9+3530	CSO 0900	12 31 55.9	35 30 15.1	0.1310	15.24	0.000	0.003#	0.00	0.9630E-12	Q		q	
	PKS 1229-02	12 32 00.0	-02 24 05.3	1.0450	16.75	0.000	0.900	0.38	<0.5250E-12	Q		q	
1232.0+2009	MRK 771	12 32 03.6	20 09 29.2	0.0630	15.30	0.000	0.003#	0.00	0.1162E-10	G	S	1	
	NGC 4535	12 34 20.3	08 11 51.9	0.0065	9.96	0.000	0.038#	0.00	0.2995E-12	GC	S		
1234.6+2350	NGP9F378-0239966	12 34 38.6	23 50 13.0	0.1320	19.30*	0.000	0.015#	0.00	0.2368E-11	G			
1235.6+1233	NGC 4552	12 35 39.8	12 33 22.6	0.0011	11.20	0.081	0.067	0.00	0.1948E-11	GC	E	2	
1236.3+2559	NGC 4565	12 36 20.8	25 59 15.7	0.0043	12.43	0.007	0.024	0.00	0.5226E-12	G	S	9	
1236.3+1632	4C +16.33	12 36 27.8	16 32 04.5	0.0684	17.30	0.640	0.710	3.10	0.2762E-11	GC	d		
1236.8+4539	CGCG 244-033	12 36 51.2	45 39 04.1	0.0305	16.00	0.000	0.004#	0.00	0.6826E-11	G		5	
1236.8+2507	7C 1234+2524	12 36 51.6	25 07 50.7	0.5460	17.60	0.015	0.109	0.00	0.1500E-11	G		q	
1236.9+6311	ABELL1576[HHP90]	12 36 58.7	63 11 13.6	0.3019	21.50*	0.000	0.020#	0.00	0.1501E-11	GC			
1237.0+3020	RBS 1133	12 37 05.6	30 20 05.2	0.7000	21.10	0.000	0.003#	0.00	0.6649E-11	Q		z	
1237.6+6258	[HB89] 1235+632	12 37 38.8	62 58 43.1	0.2970	18.52	0.000	0.007	0.00	0.3658E-11	Q		z	
	M 58	12 37 43.6	11 49 05.1	0.0051	11.72	0.000	0.054	0.00	0.6793E-11	G	S	l	
1238.0+5326	RGB J1238+534	12 38 07.7	53 25 55.0	0.3473	18.30	0.037	0.056	0.00	0.2921E-11	G		q	
1239.2+4049	GB6 J1239+4050	12 39 15.0	40 49 56.0	1.3100	18.90	0.000	0.074	0.00	0.2649E-12	Q		q	
1239.4+0730	[HB89] 1236+077	12 39 24.6	07 30 17.2	0.4000	19.18	0.700	0.000	-0.10	0.7128E-12	Q			
1239.6-0520	NGC 4593	12 39 39.4	-05 20 39.3	0.0090	11.70*	0.000	0.005#	0.00	0.6000E-10	G	S	1	
1239.8-1137	MESSIER 104	12 39 59.4	-11 37 22.9	0.0036	9.00*	0.000	0.094#	0.00	0.2700E-11	G	S	l	
1240.1+2425	RGB J1240+244	12 40 09.1	24 25 31.1	0.8290	17.30	0.077	0.000#	0.00	0.6945E-12	Q		q	
1240.2+3502	B2 1237+35	12 40 21.1	35 02 58.8	1.1940	17.24	0.063	0.065	0.90	0.5499E-12	Q		q	
1240.8-3334	ESO 381- G 007	12 40 47.0	-33 34 10.8	0.0500	15.90*	0.000	0.003#	0.00	0.1380E-10	GC	0	5	
1241.2+5141	SBS 1238+519	12 41 16.4	51 41 29.0	0.8180	18.30	0.000	0.081#	0.00	0.1011E-11	G		q	
1241.4+3132	FBQSJ124121.7..	12 41 21.7	31 32 03.6	0.0720	18.17	0.000	0.003#	0.00	0.7547E-12	G		s	
1241.5+4934	RGB J1241+495	12 41 39.7	49 34 05.0	0.4600	17.70	0.007	0.040	0.00	0.1147E-11	G		q	
1241.7+3503	NGC 4619	12 41 44.6	35 03 43.6	0.0231	13.50	0.000	0.001#	0.00	0.2886E-11	G	S	1	
1241.8+3202	MCG +05-30-060	12 41 45.7	32 02 56.3	0.0530	17.08	0.000	0.002#	0.00	0.5943E-12	G		1	
1241.3+0636	RX J1241.8+0636	12 41 48.3	+06 36 01.0	0.1500	19.40*	0.000	0.016#	0.00	0.1630E-11	Q		z	

Table A.3: *(continued)*

RXJ name (1)	Name (2)	RA(J2000) (3)	DEC(J2000) (4)	z (5)	m_V (6)	F_{5GHz}^{core} (7)	F_{5GHz} (8)	α_r (9)	$F_{0.1-2.4\ keV}$ (10)	Type (11)	Host (12)	Class. (13)	FR (14)
1242.1+3317	CG 1043	12 42 10.6	33 17 02.2	0.0439	15.40	0.000	0.006#	0.00	0.1097E-10	G	S	!	
1242.7+0241	NGC 4636	12 42 49.9	+02 41 16.0	0.0037	10.40*	0.000	0.079#	0.00	0.1370E-10	G	E	l	
1242.5+1315	NGC 4639	12 42 52.4	+13 15 26.9	0.0034	12.20*	0.000	0.009#	0.00	0.2870E-11	G	S	8	
1243.6+1133	NGC 4649	12 43 39.7	11 33 09.4	0.0037	10.30*	0.016	0.037	0.00	0.6303E-11	GC	0		
1243.7+7442	RGB J1243+747	12 43 45.0	74 42 37.1	0.7820	19.20*	0.158	0.279	0.15	0.5381E-12	Q		q	
1243.9+1623	3C 275.1	12 43 57.7	16 22 53.2	0.5551	19.00	0.095	1.022	1.00	0.7512E-12	QC		q	
1245.2+3356	CSO 0919	12 45 11.3	33 56 10.2	0.7170	17.52	0.000	0.002#	0.00	0.3232E-12	Q		q	
1246.0-0730	MRC 1243-072	12 46 04.2	-07 30 46.6	1.2860	18.90	0.000	1.110	-0.55	0.7244E-12	Q		q	
1246.2+4108	IRAS 12438+4124	12 46 12.1	41 08 12.7	0.0667	17.61	0.000	0.005#	0.00	0.4597E-12	G		5	
1246.7-2548	PKS 1244-255	12 46 46.8	-25 47 49.3	0.6330	17.41	0.000	1.550	-0.24	0.2915E-11	Q		q	
1247.3+3208	4C +32.41	12 47 20.7	32 08 59.3	0.9490	17.54	0.000	0.183	0.90	0.9896E-12	Q		q	
1248.1+1838	[HB89] 1245+189	12 48 06.9	18 38 12.6	0.7230	17.80	0.016	0.130	0.46	0.6843E-12	Q		q	
1248.1+3624	RGB J1248+364	12 48 13.9	36 24 23.9	0.2060	18.61	0.006	0.035	0.00	0.8149E-12	Q		1	
1248.7-4118	NGC 4696	12 48 49.3	-41 18 40.0	0.0099	11.75*	0.000	1.330	0.85	0.1025E-09	GC	S		I
1249.3+4444	4C +45.26	12 49 23.4	44 44 50.0	0.7990	17.70	0.000	0.205	0.93	0.1013E-11	Q		q	
1250.8+4107	NGC 4736	12 50 53.1	41 07 13.6	0.0010	10.85	0.004	0.106	0.63	0.3392E-11	G	S	s	
1252.5-1324	NGC 4748	12 52 12.5	-13 24 53.0	0.0146	14.30*	0.000	0.014#	0.00	0.2300E-10	G	S	1	
1252.3+6451	RGB J1252+648	12 52 23.7	64 51 38.0	0.3130	17.70	0.026	0.025	0.00	0.1696E-11	G		q	
1252.4+5634	SBS 1250+568	12 52 26.3	56 34 19.7	0.3210	17.93	0.700	0.819	0.96	0.2492E-11	Q		g	
	PKS 1250-330	12 52 58.4	-33 19 59.3	0.8590	21.50	0.000	0.490	0.10	0.1132E-11	Q		z	
1253.0+3826	RBS 1176	12 53 00.9	38 26 25.9	0.3720	19.40	0.000	0.005#	0.00	0.5483E-11	G		z	
1253.0-0912	NGC 4761	12 53 09.9	-09 11 54.7	0.0142	13.50*	0.000	0.005#	0.00	0.2510E-11	G	E		
1253.4+5055	RGB J1253+509	12 53 26.2	50 54 28.2	0.1210	17.70*	0.007	0.040	0.00	0.5303E-12	G		r	
	3C 277.2	12 53 33.0	15 42 29.2	0.7660	22.00	0.000	0.580	1.00	<0.1327E-13	G		n	II
1253.3+0326	CGCG 043-056	12 53 46.9	+03 26 30.1	0.0654	15.70*	0.000	0.107#	0.00	0.2860E-11	G		z	
	MRC 1251-287	12 54 22.2	-29 00 47.0	0.0541	14.53*	0.000	0.333#	0.68	0.9051E-11	GC	0		
	3C 278	12 54 36.1	-12 33 48.0	0.0150	13.00*	0.088	2.500	0.93	0.5700E-12	G			I
1254.6-1233	NGC 4783	12 54 36.6	-12 33 28.2	0.0154	12.36	0.000	14.699&	1.00	0.1491E-11	G	p		
1254.6+1141	MRC 1252+119	12 54 38.2	11 41 05.9	0.8710	16.64	0.641	0.724	0.20	0.1153E-11	Q		q	
1254.6-2913	MRC 1251-289	12 54 41.0	-29 13 39.2	0.0574	14.20*	0.000	0.240	1.31	0.1105E-10	GC	S		
1256.5-0809	MCG -01-33-054	12 56 10.1	-08 09 04.8	0.0129	14.50*	0.000	0.003#	0.00	0.3150E-11	G	S		
1256.1-0547	3C 279	12 56 11.2	-05 47 21.5	0.5362	17.75	0.000	13.000	-0.13	0.3393E-10	Q		q	
1256.7+2141	NGC 4826	12 56 43.8	21 40 51.9	0.0014	12.14	0.017	0.055	0.00	0.7513E-12	G	S	s	
	3C 280	12 56 57.1	47 20 19.6	0.9960	22.00	0.001	12.199&	0.80	0.1151E-13	G		n	II

Table A.3: *(continued)*

RXJ name (1)	Name (2)	RA(J2000) (3)	DEC(J2000) (4)	z (5)	m_V (6)	F_{5GHz}^{core} (7)	F_{5GHz} (8)	α_r (9)	$F_{0.1-2.4\ keV}$ (10)	Type (11)	Host (12)	Class. (13)	FR (14)
1257.6-1339	NGC 4825	12 57 12.2	-13 39 53.4	0.0149	12.60*	0.000	0.013#	0.00	0.3150E-11	GC	S		
1257.3+3647	[BLS68] 142	12 57 16.6	36 47 15.2	0.2800	17.84	0.000	0.065#	0.00	0.7247E-12	Q			
1257.3-3334	PKS 1254-333	12 57 20.7	-33 34 46.2	0.1900	18.60	0.000	0.540	0.47	0.1720E-11	Q		1	
1257.5+6930	ZwCl 1255.4+694	12 57 21.6	+69 30 19.1	0.2770	19.00*	0.000	0.003#	0.00	0.1520E-11	GC	c		
1257.7+2412	RX J1257.5+2412	12 57 31.9	+24 12 40.1	0.1410	15.40*	0.000	0.015#	0.00	0.1160E-10	G		z	
	PKS 1255-316	12 57 59.1	-31 55 16.8	1.9240	18.30	0.000	1.679	-0.19	<0.5060E-12	Q		q	
1258.4+6521	RGB J1258+653	12 58 25.0	65 21 38.4	0.2339	19.70	0.005	0.020	0.00	0.8779E-12	GC			
	MS 1256.3+0151	12 58 52.4	01 34 57.0	0.1620	20.00	0.000	0.008	0.00	0.4479E-12	Q		z	
	PKS B1256-229	12 59 08.5	-23 10 38.6	1.3650	16.72	0.000	0.540	-0.12	0.1504E-11	Q		q	
	NGC 4874	12 59 35.7	27 57 33.8	0.0241	13.62	0.001	0.500&	1.90	0.4097E+02*	GC	c		I
1259.6+3848	IC 4003	12 59 39.3	38 48 55.8	0.0335	15.40*	0.000	0.001#	0.00	0.2838E-12	GC			
1259.8+3423	BSO 201	12 59 48.8	34 23 22.6	1.3750	16.79	0.000	0.010#	0.00	0.6261E-12	Q		q	
	PKS 1257-326	13 00 42.4	-32 53 12.0	1.2560	18.70	0.000	0.238#	0.00	0.4536E-12	Q		q	
1300.9-2312	MRC 1258-229	13 00 58.5	-23 12 14.5	0.1300	17.50*	0.000	0.390	0.60	0.3835E-11	G	E	r	
1301.4+7120	RGB J1301+713	13 01 30.3	71 20 13.0	0.2750	16.40	0.030	0.027	0.00	0.1023E-11	G		q	
1301.9+3915	B3 1259+395	13 02 01.2	39 15 25.6	0.5770	20.60	0.018	0.023	0.00	0.3078E-12	Q			
1302.2+4819	RGB J1302+483	13 02 17.2	48 19 17.6	0.8771	18.20	0.090	0.218	0.00	0.5236E-12	G		q	
1302.6+5056	RX J1302.9+5056	13 02 55.5	+50 56 17.0	0.6880	20.20*	0.000	0.003#	0.00	0.6000E-11	Q		z	
1302.8+1624	MRK 0783	13 02 58.8	+16 24 27.5	0.0672	16.00*	0.000	0.033#	0.00	0.4570E-11	G		5	
1304.8+2454	HS 1302+2510	13 04 51.4	24 54 45.9	0.6050	18.00	0.000	0.048#	0.00	0.2005E-11	Q		q	
1305.0-0332	LCRS B130235.1-	13 05 09.9	-03 32 09.5	0.0837	16.40*	0.000	0.005#	0.00	0.3100E-11	G		5	
1305.4-4928	NGC 4945	13 05 27.5	-49 28 05.6	0.0019	14.40	0.000	2.839	0.80	0.3639E-11	G	S	s	
	PG 1302-102	13 05 33.0	-10 33 19.4	0.2784	15.23	0.000	1.000	0.20	0.7501E-11	Q	E	q	
1305.2-1033	PG 1302-102	13 05 33.0	-10 33 19.4	0.2784	14.90*	0.000	0.712#	-0.19	0.8140E-11	Q		q	
1305.8+3054	MCG +05-31-128	13 05 50.7	30 54 19.0	0.1816	18.00*	0.000	0.049#	-1.30	0.2665E-11	GC			
1306.0+5529	RGB J1306+554	13 06 03.3	55 29 43.9	1.6000	17.90	0.282	0.249	-0.38	0.2672E-12	G		q	
1307.8+0642	3C 281	13 07 54.0	06 42 14.3	0.6020	17.02	0.000	0.340	0.95	0.1087E-11	QC		q	
1308.3+3546	5C 12.291	13 08 23.7	35 46 37.2	1.0550	21.50	0.449	0.461	-0.68	0.3295E-12	Q		q	
	PKS 1306-09	13 08 39.1	-09 50 32.5	0.4640	20.50	0.000	1.899	0.65	<0.5100E-12	G		g	
	[HB89] 1306+274	13 08 56.8	27 08 11.5	1.5370	18.34	0.000	0.151	0.70	0.3923E-12	Q		q	
1309.0+5557	SBS 1307+562	13 09 09.7	55 57 38.2	1.6290	18.20	0.256	0.423	0.05	0.8123E-12	Q		q	
1310.4-1157		13 10 12.2	-11 57 48.9	0.1397	16.50*	0.000	0.083#	0.00	0.2300E-11	G		z	
1310.1-0727	MCG -01-34-008	13 10 17.1	-07 27 15.5	0.0224	14.50*	0.000	0.009#	0.00	0.2580E-11	G	S	2	
1310.4+3220	7C 1308+3236	13 10 28.7	32 20 43.8	0.9960	15.24	1.970	0.000#	-0.71	0.7882E-12	Q		q	

Table A.3: *(continued)*

RXJ name (1)	Name (2)	RA(J2000) (3)	DEC(J2000) (4)	z (5)	m_V (6)	F_{5GHz}^{core} (7)	F_{5GHz} (8)	α_r (9)	$F_{0.1-2.4\ keV}$ (10)	Type (11)	Host (12)	Class. (13)	FR (14)
1310.9+3703	NGC 5005	13 10 56.2	37 03 33.1	0.0032	13.67	0.017	0.055	0.00	0.7268E-12	G	S	l	
	JVAS J1310+3233	13 10 59.4	32 33 34.4	1.6500	20.96	0.000	0.684	0.00	0.1649E-12	Q		q	
	3C 284	13 11 04.7	27 28 07.7	0.2394	18.00*	0.003	5.030	0.90	<0.6770E-13	GC	E	n	II
1312.1+4809	RGB J1312+481	13 12 11.1	48 09 25.0	0.7160	17.60	0.062	0.085	0.00	0.8518E-12	G		q	
1312.2+4449	CGCG 1310.0+4507	13 12 16.9	44 50 21.3	0.0356	15.50*	0.032	0.106	0.23	0.2807E-12	G	E		
1312.2+3515	PG 1309+355	13 12 17.8	35 15 21.2	0.1840	15.64	0.032	0.036	0.23	0.1559E-11	Q	S	q	
	PKS 1309-216	13 12 31.5	-21 56 24.4	1.4910	18.90	0.000	0.198	0.30	0.1141E-11	Q		z	
1313.2+3753	FBQS J131314.2+.	13 13 14.3	37 53 57.2	0.6560	17.70	0.000	0.002#	0.00	0.5715E-12	Q		q	
	7C 1311+3211	13 13 27.3	31 55 23.2	0.3030	18.86	0.000	0.053#	0.20	0.2517E-12	G		5	
1313.4+3635	NGC 5033	13 13 27.5	36 35 38.1	0.0029	12.03	0.014	0.079	0.36	0.3718E-11	G	S	9	
	FIRSTJ131344.1+.	13 13 44.2	31 18 29.9	0.7887	19.26	0.000	0.002#	0.00	0.2041E-12	G		q	
1315.0-4236	MS 1312.1-4221	13 15 03.4	-42 36 49.7	0.1080	17.00	0.000	0.018	0.00	0.2161E-10	Q		z	
1315.8-1623	NGC 5044	13 15 23.9	-16 23 07.9	0.0090	11.80*	0.000	0.036#	0.00	0.5230E-10	GC	E		
1315.8+4201	MESSIER 63	13 15 49.2	42 01 49.3	0.0017	9.70*	0.000	0.083	0.00	0.7685E-12	G	S	l	
	PKS 1313-333	13 16 07.9	-33 38 59.2	1.2100	18.70	0.000	1.320	-0.45	<0.4530E-12	Q		q	
1317.2+3925	4C +39.38	13 17 18.6	39 25 28.0	1.5600	18.50	0.277	0.227	0.39	0.2645E-12	G		q	
1317.6+3425	[HB89] 1315+346	13 17 36.5	34 25 15.9	1.0500	18.70	0.350	0.000	0.11	0.4835E-12	Q		q	
1317.4+6010	RX J1317.8+6010	13 17 50.4	+60 10 40.9	0.1372	18.40*	0.000	0.003#	0.00	0.2650E-11	G		5	
1319.4+1405	RBS 1248	13 19 31.8	14 05 33.0	0.5720	17.80	0.052	0.057	0.00	0.9171E-11	Q		z	
1319.7+5148	S4 1317+52	13 19 46.2	51 48 05.8	1.0600	16.79	0.000	0.655	0.57	0.6048E-12	Q		q	
1319.9+5235	1RXSJ131957.2+..	13 19 57.1	52 35 34.0	0.0920	17.30	0.000	0.004#	0.00	0.7982E-11	G		1	
	PKS 1317+019	13 20 26.8	01 40 36.8	1.2350	20.20	0.000	0.590	0.00	0.3390E-12	G	N	q	
	NGC 5090	13 21 12.8	-43 42 16.4	0.0114	11.51	0.580	1.750	0.96	0.1800E-11	GC	E		I
1322.8+5455	1RXSJ132248.5+..	13 22 49.2	54 55 28.1	0.0640	15.56	0.000	0.010#	0.00	0.2963E-11	G		5	
1323.6+3816	FIRSTJ132336.4..	13 23 36.4	38 16 41.3	0.2150	18.20	0.000	0.001#	0.00	0.4528E-12	G		1	
1324.0+5739	RGB J1324+576	13 24 00.9	57 39 16.5	0.1150	17.30	0.025	0.042	0.00	0.2370E-11	G		z	
	PKS B1321-105	13 24 25.8	-10 49 23.1	0.8720	18.50	0.000	0.640	0.00	0.1218E-11	Q		q	
	NGC 5141	13 24 51.4	36 22 41.7	0.0174	13.90*	0.150	1.710&	0.60	<0.4091E+02*	G	0		I
1325.5-4301	NGC 5128/CenA	13 25 27.6	-43 01 08.8	0.0018	6.98	6.984	62.829	1.20	0.1359E-10	GC	0	2	I
1325.8+3413	FIRSTJ132547.6..	13 25 47.6	34 13 20.9	1.9340	17.80	0.000	0.004#	0.00	0.2859E-12	G		q	
1326.2+2933	RBS 1265	13 26 15.0	29 33 30.0	0.4310	19.80	0.000	0.035#	1.10	0.3732E-11	Q		z	
1327.7-2451	GSC 6717 00254	13 27 12.7	-24 51 40.7	0.0410	15.40*	0.000	0.004#	0.00	0.4430E-11	G		1	
	PKS 1324-300	13 27 44.7	-30 18 16.7	0.2000	18.00	0.000	0.330	0.00	0.7454E-12	G	E		
1328.6-2719	IRAS F13253-270	13 28 09.9	-27 19 54.9	0.0418	15.00*	0.000	0.016#	0.00	0.3120E-11	GC	S		

Table A.3: *(continued)*

RXJ name (1)	Name (2)	RA(J2000) (3)	DEC(J2000) (4)	z (5)	m_V (6)	F_{5GHz}^{core} (7)	F_{5GHz} (8)	α_r (9)	$F_{0.1-2.4\ keV}$ (10)	Type (11)	Host (12)	Class. (13)	FR (14)
1329.0+2531	MS 1326.6+2546	13 29 03.2	25 31 09.6	0.9860	18.50	0.000	0.046#	0.00	0.5243E-12	Q		q	II
	IVS B1327+504	13 29 05.8	50 09 26.4	2.6540	18.10	0.000	0.140#	0.00	0.2524E-12	Q		q	
1329.8+4711	NGC 5194/M51a	13 29 52.7	47 11 42.6	0.0015	13.47	0.015	0.210	0.00	0.1827E-11	G	S	2	
1330.1-2141	[HB89] 1327-214	13 30 07.1	-21 42 01.0	0.5240	16.74	0.000	0.900	1.12	0.2578E-11	Q		q	
1330.6+2508	3C 287	13 30 37.7	25 09 10.9	1.0550	17.67	2.998	3.289	0.60	0.4497E-12	Q		g	
1331.1+3030	3C 286	13 31 08.3	30 30 32.9	0.8490	17.25	7.541	0.000	0.60	0.3228E-12	Q		g	
1331.6-2524	ESO 509- G 038	13 31 13.9	-25 24 10.0	0.0260	14.70*	0.000	0.013#	0.00	0.2200E-10	GC	S	1	
1331.5-1736	OP -148	13 31 36.1	-17 36 35.0	0.3290	17.70	0.000	0.150	0.70	0.1861E-11	Q		q	
1332.5-2559	PKS 1329-25	13 32 32.0	-25 59 49.4	0.1900	18.00	0.103	0.480	1.57	0.1016E-11	G		r	
1332.6+4722	B3 1330+476	13 32 45.2	47 22 22.7	0.6680	19.30	0.312	0.333	-0.26	0.4655E-12	Q		q	
1332.8+0200	3C 287.1	13 32 53.3	02 00 45.6	0.2156	18.27	0.000	1.429	0.55	0.3683E-11	G	N	b	II
1333.7+4141	FBQS J133345.4+.	13 33 45.5	41 41 28.2	0.2250	18.30	0.000	0.002#	0.00	0.5967E-12	Q		1	
1334.4+3044	MG2 J133418+3043	13 34 22.5	30 44 12.4	1.3520	18.90	0.000	0.073#	0.00	0.3159E-12	Q		q	
1334.4+3441	NGC 5223	13 34 25.2	34 41 25.8	0.0240	14.40*	0.000	0.001#	0.00	0.9221E-12	GC	E		
1334.5+5631	RGB J1334+565	13 34 37.5	56 31 47.9	0.3430	17.90	0.036	0.107	0.00	0.6258E-12	G		q	
	FIRSTJ133438.5+.	13 34 38.5	38 06 27.1	0.2350	17.74	0.000	0.015#	0.00	0.7595E-14	G		n	
	1WGA J1334.9+380	13 34 58.4	38 04 30.3	2.0070	20.91	0.000	0.001#	0.00	0.6945E-14	Q		q	
1335.2+4100	RGB J1335+409	13 35 20.1	41 00 03.8	0.2278	17.70*	0.017	0.225	0.97	0.4154E-11	GC			
	RBS 1291	13 35 29.7	-29 50 39.0	0.2500	19.10	0.000	0.011	0.00	0.6524E-11	Q		z	
1336.0+2727	87GB 133344.0+..	13 36 02.8	27 27 46.6	1.1170	19.40	0.000	0.037	0.00	0.3215E-12	Q		q	
	IC 4296	13 36 39.0	-33 57 57.2	0.0125	10.57	0.297	6.299	0.79	0.1290E-11	GC	E		
1336.8+6541	RGB J1336+656	13 36 55.5	65 41 16.1	0.4360	18.20	0.006	0.069	0.00	0.8458E-12	G		q	
1337.0-2952	M83/NGC 5236	13 37 00.8	-29 51 58.6	0.0017	7.89	0.000	0.760	0.00	0.5875E-11	G	S	*	
1337.3+2423	RGB J1337+243	13 37 18.7	24 23 03.3	0.1076	15.00	0.006	0.018	0.00	0.2892E-10	G		q	
1337.6-1257	PKS 1335-127	13 37 39.8	-12 57 24.7	0.5390	19.00	0.000	2.180	-0.13	0.3465E-11	Q		q	
	PKS 1335-06	13 38 08.0	-06 27 10.9	0.6250	17.68	0.000	0.980	0.90	0.5295E-12	Q		q	
1338.8+3851	3C 288	13 38 49.9	38 51 09.2	0.2460	18.30*	0.034	0.942	1.11	0.5743E-12	GC		w	I
1339.4+2920	CGCG 161-108	13 39 31.5	29 21 27.5	0.0372	15.70*	0.000	0.002#	0.00	0.6934E-12	G	E		
	B3 1338+402	13 41 04.9	39 59 35.2	0.1630	18.50	0.034	0.034	0.00	0.7622E-11	Q		z	
1341.5-1438	CTS 0023	13 41 12.9	-14 38 40.6	0.0418	16.00*	0.000	0.006#	0.00	0.9480E-11	G		1	
	RGB J1341+263	13 41 49.7	26 22 20.0	0.0757	15.30*	0.006	0.106	1.51	0.7656E-11	GC		r	
1341.9+3707	7C 1339+3723	13 41 59.9	37 07 10.2	1.1060	16.89	0.024	0.032	0.00	0.9109E-12	Q		q	
	NGC 5273	13 42 08.3	35 39 15.2	0.0035	13.12	0.000	0.003#	0.00	0.2499E-12	G	0	9	
1342.1+2709	[HB89] 1339+274	13 42 08.4	27 09 30.6	1.1850	18.13	0.280	0.247	0.00	0.5092E-12	Q		q	

Table A.3: *(continued)*

RXJ name (1)	Name (2)	RA(J2000) (3)	DEC(J2000) (4)	z (5)	m_V (6)	F_{5GHz}^{core} (7)	F_{5GHz} (8)	α_r (9)	$F_{0.1-2.4\ keV}$ (10)	Type (11)	Host (12)	Class. (13)	FR (14)
1342.7+0504	4C +05.57	13 42 43.6	05 04 32.0	0.1360	17.80	0.000	0.780	0.50	0.8022E-12	G	N	1	
1343.0+2844	B2 1340+29	13 43 00.2	28 44 07.5	0.9050	17.07	0.141	0.174	-0.01	0.1054E-11	Q		q	
1344.3+3907	7C 1342+3921	13 44 19.2	39 06 39.1	0.2950	18.40*	0.000	0.001#	0.00	0.5172E-12	G			
1345.3+4142	NGC 5290	13 45 19.1	41 42 44.4	0.0086	13.14	0.000	0.005#	0.00	0.1041E-11	G	S		
	3C 289	13 45 26.4	49 46 32.6	0.9674	23.00*	0.000	0.600	1.00	<0.2099E-13	G		n	II
1345.7+5332	RGB J1345+535	13 45 45.4	53 32 52.3	0.1600	17.80*	0.070	0.223	0.00	0.2943E-11	G		1	
1346.2+6220	RGB J1346+623	13 46 17.6	62 20 45.5	0.1170	17.90	0.007	0.068	4.50	0.1250E-11	G		b	
1347.6+3012	FBQS J1347+3012	13 47 37.4	30 12 52.2	0.1200	16.23	0.000	0.015#	0.00	0.4304E-12	Q		q	
1348.8+2635	4C +26.42	13 48 52.4	26 35 33.9	0.0632	15.50	0.043	0.250	1.20	0.4543E-10	GC	c	l	I
1348.9+3958	NGC 5311	13 48 56.1	39 59 06.4	0.0090	13.70*	0.051	0.120&	0.24	0.1292E-12	GC	S		
	NGC 5322	13 49 15.2	60 11 25.5	0.0059	10.23	0.000	0.048&	0.50	0.1510E-12	G	E	l	
1349.0-3018	IC 4329A	13 49 19.3	-30 18 34.0	0.0161	14.00*	0.000	0.067#	0.00	0.8050E-10	GC	S	1	
1349.5+5341	8C 1347+539	13 49 34.6	53 41 17.0	0.9800	17.39	0.900	0.000#	0.30	0.5525E-12	Q		q	
1350.3+0940	RBS 1322	13 50 22.1	09 40 10.6	0.1325	18.10	0.000	0.472#	-0.40	0.6104E-11	G		9	
1350.7+2331	7C 1348+2346	13 50 45.7	23 31 45.1	0.5289	16.60	0.076	0.141	0.27	0.1498E-11	Q		q	
	3C 293	13 52 17.8	31 26 46.5	0.4550	15.60*	0.100	1.870	0.70	<0.4468E-13	G		w	
	PKS 1349-439	13 52 56.5	-44 12 40.4	0.0520	16.37	0.000	0.760	0.10	0.5282E-11	Q		z	
1353.8+6918	UGC 08823	13 53 03.4	+69 18 29.6	0.0294	14.60*	0.000	0.024#	0.00	0.4150E-10	G	0	5	
1353.2+3741	RGB J1353+376	13 53 14.1	37 41 13.7	0.2160	18.30	0.024	0.027	0.00	0.8765E-12	G		z	
1353.5+4016	NGC 5353	13 53 26.7	40 16 58.9	0.0077	11.80*	0.000	0.033	0.00	0.5211E-12	GC	0	a	
1353.2+5601	RX J1353.4+5601	13 53 28.0	+56 00 55.0	0.3700	18.80*	0.000	0.015#	0.00	0.2990E-11	Q		z	
1353.6+2631	RBS 1328	13 53 35.9	26 31 47.5	0.3100	17.18	0.025	0.085	0.67	0.2819E-11	Q		q	
1354.3+3255	UGC 08829	13 54 19.9	32 55 47.9	0.0260	15.40	0.000	0.001#	0.00	0.1027E-10	G	S	1	
1354.7-1040	[HB89] 1352-104	13 54 46.5	-10 41 03.1	0.3320	18.40	0.000	0.980	-0.35	0.3520E-11	Q		q	
1355.2+5612	1RXSJ135515.9+..	13 55 16.5	56 12 44.6	0.1220	17.10	0.000	0.006#	0.00	0.6397E-11	G	S	!	
1355.8+3834	MRK 0464	13 55 53.5	38 34 28.5	0.0510	17.95	0.000	0.014#	0.00	0.2412E-11	G		5	
1356.0-3420	MRC 1353-341	13 56 05.4	-34 21 10.9	0.2230	18.50	0.000	0.670	-0.07	0.1625E-11	G		r	
1356.0+4136	RGB J1356+416	13 56 07.4	41 36 15.3	0.6970	16.69	0.047	0.040	-0.33	0.9837E-12	G		q	
1356.4+2831	VV 158b	13 56 25.3	28 31 34.6	0.0348	15.70	0.000	0.001#	0.00	0.7426E-12	GC	S	s	
1357.0+1919	PKS 1354+19	13 57 04.4	19 19 07.4	0.7200	16.03	1.308	2.617	0.37	0.2000E-11	Q		q	
	PKS 1354-17	13 57 06.0	-17 44 02.2	3.1470	18.40	0.000	0.970	0.45	<0.5590E-12	Q		g	
	PKS 1354-152	13 57 11.2	-15 27 28.8	1.8900	18.10	0.000	1.209	1.20	<0.6220E-12	Q		q	
1358.2+5752	4C +58.29	13 58 17.6	57 52 04.9	1.3710	17.37	0.039	0.136	1.12	0.5755E-12	Q		q	
1358.7+3904	B3 1356+393	13 58 47.9	39 04 03.3	0.8000	19.40	0.063	0.094	0.90	0.3848E-12	Q		q	

Table A.3: *(continued)*

RXJ name (1)	Name (2)	RA(J2000) (3)	DEC(J2000) (4)	z (5)	m_V (6)	F_{5GHz}^{core} (7)	F_{5GHz} (8)	α_r (9)	$F_{0.1-2.4\ keV}$ (10)	Type (11)	Host (12)	Class. (13)	FR (14)
1358.8+2511	RBS 1334	13 58 51.9	25 11 39.9	0.0886	17.00	0.000	0.003#	0.00	0.2795E-11	G		!	
	PKS 1355-41	13 59 00.2	-41 52 52.6	0.3130	15.86	0.037	1.439	0.93	0.4879E-11	Q		q	
1359.4+0159	MRC 1356+022	13 59 27.1	01 59 54.6	1.3290	18.27	0.000	0.680	0.00	0.7830E-12	Q		q	
	IVS B1357+404	13 59 38.1	40 11 38.2	0.4070	19.20	0.000	0.279	0.00	0.1621E-12	Q			
1400.0+3910	B3 1357+394B	14 00 03.1	39 10 55.8	0.8040	19.60	0.000	0.084	0.80	0.2172E-12	Q		q	
	PMN J1400+0425	14 00 48.4	04 25 30.9	2.5500	21.30	0.000	0.288	0.40	0.1436E-12	Q		q	
1401.0-1107	GSC 5557 00266	14 01 36.4	-11 07 43.4	0.0691	14.60*	0.000	0.005#	0.00	0.1020E-10	GC			
	MCG +03-36-031	14 02 44.5	15 59 58.3	0.2442	16.74	0.000	0.470	0.60	0.4340E-12	Q		z	
1404.1+0937	[HB89] 1401+098	14 04 10.6	09 37 45.0	0.4410	17.22	0.019	0.027	0.00	0.1002E-11	QC		q	
	7C 1402+3427	14 04 16.7	34 13 16.0	0.9370	18.60	0.000	0.061	0.70	0.1288E-12	Q		q	
1404.6+2701	RGB J1404+270	14 04 36.9	27 01 40.0	0.1360	18.40*	0.012	0.031	0.00	0.3659E-12	Q		z	
1404.8+0402	RBS 1342	14 04 50.9	04 02 02.3	0.2000	16.61	0.000	0.021	0.00	0.3725E-11	Q		z	
1404.2+6554	RX J1404.8+6554	14 04 51.6	+65 54 35.0	0.3640	19.40*	0.000	0.015#	0.00	0.2850E-11	Q		z	
1405.0+2925	MCG +05-33-047	14 05 12.9	29 25 03.1	0.0639	15.00*	0.000	0.097	0.00	0.3735E-12	G	S		
1406.3+2223	PG 1404+226	14 06 21.8	22 23 46.0	0.0980	15.82	0.000	0.002#	0.00	0.7243E-11	G		q	
	3C 294	14 06 44.0	34 11 25.1	1.7790	22.00	0.000	0.280	1.30	<0.2234E-13	G		n	II
	GB2 1404+347	14 06 53.8	34 33 37.3	2.5560	18.20	0.000	0.211	0.00	0.1642E-12	Q		q	
1408.9+2409	RX J1408.4+2409	14 08 27.8	+24 09 24.4	0.1310	16.60*	0.000	0.004#	0.00	0.3680E-11	G		1	
	PKS 1406-076	14 08 56.5	-07 52 26.7	1.4940	19.60	0.000	1.050	-0.15	<0.2350E-12	Q		q	
1409.3+5939	MS 1407.9+5954	14 09 23.4	59 39 40.8	0.4950	19.67	0.000	0.016	0.00	0.1687E-11	QC		z	
1409.4+2618	PG 1407+265	14 09 23.9	26 18 21.0	0.9400	15.74	0.000	0.006	0.00	0.2197E-11	Q		q	
	NGC 5490	14 09 57.3	17 32 43.7	0.0162	11.92	0.000	0.620	0.00	0.3294E-12	GC	E		I
1410.6+6100	RX J1410.5+6100	14 10 31.7	+61 00 10.0	0.3840	20.10*	0.000	0.011#	0.00	0.2740E-11	Q		z	
1411.3+5212	3C 295	14 11 20.6	52 12 09.0	0.4641	20.20	0.010	6.764	1.14	0.1027E-11	GC	E	1	II
1411.9+4239	B3 1409+429	14 11 59.7	42 39 50.4	0.8880	17.40	0.046	0.050	0.49	0.8295E-12	G		q	
1412.6+3918	NGC 5515	14 12 38.2	39 18 36.9	0.0253	13.70	0.015	0.024	0.00	0.3624E-12	G	S	9	
1413.1-6520	Circinus Gal	14 13 09.3	-65 20 20.6	0.0015	9.84	0.000	0.610	0.40	0.6554E-11	G	S	2	
1413.2-0312	NGC 5506	14 13 14.9	-03 12 26.9	0.0062	13.40*	0.000	0.339#	0.00	0.2730E-11	G	S	9	
1413.7+4339	RGB J1413+436	14 13 43.7	43 39 45.1	0.0890	18.03	0.034	0.039	0.18	0.4661E-11	G	c	b	
1414.2+3430	FBQS J141409.2+.	14 14 09.3	34 30 57.7	0.2750	19.42	0.000	0.003#	0.00	0.5866E-12	Q		z	
1415.7+0903	[HB89] 1413+092	14 15 44.2	09 03 21.5	0.2000	19.30	0.000	0.096#	0.00	0.6519E-12	Q		a	
	[HB89] 1413+135	14 15 58.8	13 20 23.7	0.2467	20.50	0.000	0.640	0.50	0.5303E-13	Q		z	
1416.4+3721	B3 1414+375	14 16 30.7	37 21 37.1	0.9210	18.80	0.041	0.045	0.00	0.6125E-12	Q		q	
1416.6-1158	LCRS B141408.4-	14 16 50.0	-11 58 58.4	0.0986	15.70*	0.000	0.003#	0.00	0.5720E-11	G			

Table A.3: *(continued)*

RXJ name (1)	Name (2)	RA(J2000) (3)	DEC(J2000) (4)	z (5)	m_V (6)	F_{5GHz}^{core} (7)	F_{5GHz} (8)	α_r (9)	$F_{0.1-2.4\ keV}$ (10)	Type (11)	Host (12)	Class. (13)	FR (14)
	3C 296	14 16 53.2	10 48 11.0	0.0237	12.19*	0.077	6.799	0.10	0.3913E-12	GC	E		I
1417.1+4606	[HB89] 1415+463	14 17 08.2	46 07 05.4	1.5520	18.15	0.000	0.910	0.32	0.2980E-12	Q		q	
	[WB92] 1415+2659	14 17 30.4	26 44 57.0	1.4550	21.90	0.000	0.074	0.00	0.8295E-13	Q		q	
1417.6+3818	B3 1415+385	14 17 40.4	38 18 21.0	0.4510	17.90	0.181	0.000	-0.48	0.3450E-12	Q		q	
1417.9+2543	RBS 1366	14 17 56.7	25 43 24.7	0.2370	17.20	0.040	0.045	0.00	0.2410E-10	QC	E	z	
1417.9+2508	NGC 5548	14 17 59.5	25 08 12.4	0.0171	13.30*	0.000	0.011#	0.00	0.7062E-10	G	S	5	
1419.1+0628	3C 298	14 19 08.2	06 28 34.8	1.4360	16.79	1.700	2.075	1.10	0.5415E-11	Q		g	
	PMN J1419+0603	14 19 09.3	06 03 30.0	2.3890	20.50	0.000	0.326	0.00	0.1566E-12	Q		q	
1419.3+3202	PB 03578	14 19 16.7	32 03 03.0	0.3770	16.30	0.000	0.007#	0.00	0.2492E-12	Q		q	
1419.5-2638	ESO 511- G 030	14 19 22.4	-26 38 41.0	0.0224	13.30*	0.000	0.013#	0.00	0.3510E-10	GC	S	1	
1419.8+3822	[HB89] 1417+385	14 19 46.6	38 21 48.5	1.8320	19.30	0.719	0.871	-0.17	0.3156E-12	Q		q	
1419.7+5423	S4 1418+54	14 19 46.6	54 23 14.8	0.1510	15.65	1.399	0.000	-0.10	0.1253E-11	Q		z	
1419.8-1928	MRC 1417-192	14 19 49.7	-19 28 26.8	0.1200	16.66	0.000	0.830	0.46	0.1115E-10	G	N	5	II
	MRC 1418+070	14 20 40.9	06 50 59.4	0.2360	17.50	0.000	0.207	0.00	0.5470E-12	G			
	3C 299	14 21 05.6	41 44 48.5	0.3670	19.40	0.050	7.700&	0.80	<0.1151E-13	GC		n	II
1421.0+3855	TXS 1419+391	14 21 06.0	38 55 23.0	0.4900	18.74	0.099	0.103	-0.73	0.4784E-12	Q		q	
1421.6+4933	MCG +08-26-021	14 21 35.8	49 33 05.0	0.0710	16.00*	0.000	0.004#	0.00	0.5071E-11	GC	c		
1421.6+3717	2MASXiJ1421405..	14 21 40.5	37 17 30.7	0.1600	17.20*	0.000	0.002#	0.00	0.3385E-11	GC	c		
1422.3+2942	2MASXiJ1422201..	14 22 20.2	29 42 55.0	0.0533	15.85	0.000	0.002#	0.00	0.1357E-11	G	S	1	
1422.5+3223	B2 1420+32	14 22 30.4	32 23 10.4	0.6850	17.50	0.368	0.000#	0.48	0.8352E-12	Q		q	
1422.6+5801	RBS 1383	14 22 38.9	58 01 55.5	0.6380	19.00	0.006	0.095	0.00	0.2544E-10	Q		z	
1422.9+3251	UGC 09214	14 22 55.4	32 51 02.7	0.0342	14.42	0.000	0.002#	0.00	0.3333E-12	G	S	8	
1423.0+2615	NGC 5594	14 23 10.3	+26 15 56.5	0.0375	15.10*	0.000	0.015#	0.00	0.1560E-11	G			
1423.1+5055	RGB J1423+509	14 23 14.2	50 55 37.3	0.2740	16.70	0.128	0.232	0.36	0.5388E-11	G		q	
	TXS 1421+487	14 23 18.1	48 30 15.9	0.5690	19.40	0.000	0.102	0.60	0.3297E-12	Q		q	
1423.8+4015	2MASXiJ1423515..	14 23 51.5	40 15 31.9	0.0820	13.60*	0.000	0.008#	0.00	0.2240E-11	GC			
1424.2+5952		14 24 24.1	+59 53 00.7	0.1348	16.50*	0.000	0.002#	0.00	0.2410E-11	G		1	
1424.4+3858	2MASXiJ1424253..	14 24 25.4	38 58 46.9	0.1890	18.00*	0.000	0.003#	0.00	0.2138E-12	G			
1424.6+2255	CLASS J1424+2256	14 24 38.1	22 56 00.6	3.6200	16.50	0.305	0.548	0.20	0.4882E-12	Q		q	
	PKS 1422+26	14 24 40.5	26 37 30.3	0.0371	15.62	0.013	0.367	1.09	0.4107E+02*	GC	E		I
1425.8+2404	PKS 1423+24	14 25 50.7	24 04 03.9	0.6490	17.93	0.059	0.520	0.90	0.1323E-11	Q		q	
1426.0+4024	RGB J1426+404	14 26 06.2	40 24 32.0	0.6640	18.80	0.019	0.057	0.00	0.7254E-12	G		q	
1427.1+3553	LEDA 214269	14 27 04.5	35 54 09.4	0.0295	13.10*	0.000	0.003#	0.00	0.1998E-12	G			
1427.4+5409	RGB J1427+541	14 27 30.3	54 09 23.5	0.1050	17.40	0.024	0.026	0.00	0.5944E-12	G		z	

Table A.3: *(continued)*

RXJ name (1)	Name (2)	RA(J2000) (3)	DEC(J2000) (4)	z (5)	m_V (6)	F_{5GHz}^{core} (7)	F_{5GHz} (8)	α_r (9)	$F_{0.1-2.4\ keV}$ (10)	Type (11)	Host (12)	Class. (13)	FR (14)
1427.6-1203	PKS 1424-11	14 27 38.1	-12 03 50.0	0.8060	16.49	0.000	0.330	1.00	0.1758E-11	Q		q	
	PKS 1424-41	14 27 56.3	-42 06 19.4	1.5220	18.90	0.000	2.120	0.85	0.5284E-11	Q		q	
	WGA J1427.9+3247	14 27 58.7	32 47 41.6	0.5680	18.10	0.000	0.017#	0.00	0.8241E-12	Q		q	
1428.5+4240	RBS 1399	14 28 32.7	42 40 20.6	0.1290	16.45	0.021	0.031	0.00	0.5453E-10	Q		z	
1429.7+0117	PG 1426+015	14 29 06.6	+01 17 06.5	0.0865	17.50*	0.000	0.004#	0.00	0.2060E-10	G		1	
1430.3+4203	B3 1428+422	14 30 23.7	42 04 36.5	4.7150	20.90	0.132	0.337	0.35	0.5986E-12	Q		q	
1431.0+2817	MRK 684	14 31 04.8	28 17 14.1	0.0461	14.68	0.000	0.004#	0.00	0.7811E-11	G	S	!	
1431.1+2538	2MASXiJ1431068..	14 31 06.8	25 38 01.3	0.0964	16.30*	0.000	0.007#	0.00	0.4353E-11	GC	c		
1431.4+2442	MG2 J143127+2441	14 31 25.9	24 42 20.5	0.4080	17.90	0.000	0.164#	0.00	0.7461E-12	Q		q	
1432.0+3416	FBQS J143157.9+.	14 31 57.9	34 16 50.3	0.7040	16.84	0.000	0.001#	0.00	0.4880E-12	Q		q	
1432.1+3135	CGCG 163-074	14 32 08.9	31 35 04.8	0.0551	15.50	0.000	0.001#	0.00	0.9371E-12	G		5	
1432.5+3138	1RXSJ143236.0+..	14 32 37.9	31 38 49.0	0.1313	16.06*	0.000	0.007#	0.00	0.2293E-11	GC			
1435.4+5507	RGB J1435+551	14 35 28.5	55 07 52.1	0.1402	15.20*	0.015	0.148	0.40	0.1735E-11	GC			
1435.9+1729	[HB89] 1433+177	14 35 56.7	17 29 32.3	1.2030	18.20	0.000	0.540	0.03	0.7528E-12	Q		q	
1436.2+5847	UGC 09412	14 36 22.1	+58 47 39.4	0.0315	14.50*	0.000	0.012#	0.00	0.1380E-11	G	S	5	
1436.6-1613	EC 14340-1600	14 36 49.6	-16 13 41.0	0.1440	15.80*	0.000	0.100#	0.00	0.2080E-10	Q		q	
1437.4+5045	RGB J1437+507	14 37 26.2	50 45 55.9	0.7850	17.66	0.008	0.023	0.00	0.7176E-12	G		q	
1437.8+2439	B2 1435+24	14 37 48.6	24 39 05.8	1.0100	20.40	0.000	0.165	0.73	0.4424E-12	Q		q	
1439.7+5827	RGB J1439+584	14 39 42.9	58 27 59.1	0.4250	18.26	0.016	0.045	0.00	0.6370E-12	G		q	
1440.6+6156	IRAS F14390+620	14 40 12.7	+61 56 33.0	0.2760	16.40*	0.000	0.004#	0.00	0.2640E-11	G		1	
1442.1+3526	MRK 0478	14 42 07.5	35 26 22.9	0.0790	14.58	0.000	0.004#	0.00	0.6283E-10	G	S	q	
1442.2+2218	UGC09480	14 42 19.4	22 18 13.1	0.0968	17.32	0.000	0.007#	-0.07	0.5859E-11	G	S		
	TXS 1440+528	14 42 19.6	52 36 21.0	1.8000	19.30	0.000	0.110#	0.60	0.2239E-12	Q		q	
1442.6+2920	IRAS F14405+2933	14 42 39.6	29 20 48.0	0.0739	15.51	0.002#	0.034	0.00	0.3772E-12	G	S		
1442.8+1200	RBS 1420	14 42 48.2	12 00 40.4	0.1620	17.10	0.045	0.053	0.00	0.1232E-10	Q		z	
1443.0+5201	3C 303	14 43 02.8	52 01 37.3	0.1410	17.29	0.065	1.070	0.49	0.4738E-11	G	N	b	II
	TXS 1442+637	14 43 58.6	63 32 26.4	1.3800	17.90	0.000	0.448	0.33	0.3159E-12	G		q	
	RGB J1444+193	14 44 33.7	19 21 21.4	0.1906	16.00	0.026	0.126	-0.30	0.9095E-12	GC			
1444.5+6336	MS 1443.5+6349	14 44 34.9	63 36 05.6	0.2990	19.65	0.000	0.012	0.00	0.2128E-11	Q		z	
1444.9-0311	MRC 1442-029	14 44 56.7	-03 12 01.3	0.1059	17.60*	0.000	0.160	-0.20	0.1329E-11	G	E		
	PKS 1442+101	14 45 16.5	09 58 36.1	3.5220	17.78	0.000	1.149	0.50	0.6000E-12	Q		g	
	B3 1445+410	14 47 12.7	40 47 45.7	0.1800	17.90	0.000	0.155	1.30	0.9410E-13	G		g	
	RBS 1430	14 47 33.0	34 55 06.8	0.6590	18.20	0.000	0.014#	0.00	0.2943E-11	Q		q	
	RBS 1433	14 48 25.1	35 59 47.2	0.1130	16.06	0.000	0.001#	0.00	0.4161E-11	Q		q	

Table A.3: *(continued)*

RXJ name (1)	Name (2)	RA(J2000) (3)	DEC(J2000) (4)	z (5)	m_V (6)	F_{5GHz}^{core} (7)	F_{5GHz} (8)	α_r (9)	$F_{0.1-2.4\ keV}$ (10)	Type (11)	Host (12)	Class. (13)	FR (14)
	3C 305	14 49 21.7	63 16 14.0	0.0416	13.74	0.029	7.200&	0.80	0.4165E+02*	G	E		I
1449.3+2746	RBS 1434	14 49 32.7	+27 46 20.0	0.2250	19.10*	0.000	0.091#	0.00	0.6840E-11	Q		z	
1450.5+4635	CBS 0287	14 50 05.1	+46 35 21.0	0.2920	18.00*	0.000	0.004#	0.00	0.1840E-11	G			
1450.0-0714		14 50 54.0	-07 14 12.7	0.0722	16.60*	0.000	0.004#	0.00	0.4290E-11	G		5	
1451.0+5333	RGB J1451+535	14 51 06.4	53 33 53.0	0.4330	19.47	0.006	0.022	0.00	0.8574E-12	G		b	
1451.1+2709	PG 1448+273	14 51 08.8	27 09 26.7	0.0650	15.01	0.000	0.003#	0.00	0.1553E-10	G	S	q	
1451.5+6354	RX J1451.4+6354	14 51 27.8	+63 54 26.2	0.6500	19.60*	0.000	0.010#	0.00	0.2670E-11	Q		q	
1451.5+3402	FIRSTJ145131.9..	14 51 31.9	34 02 32.0	0.4840	18.00	0.000	0.025#	0.00	0.2291E-12	G		q	
1452.3+4522	RGB J1452+453	14 52 24.7	45 22 23.7	0.4690	17.80	0.124	0.219	0.34	0.2287E-11	G		q	
1452.7+4736	PC 1451+4747	14 52 47.4	47 35 29.1	1.1610	19.20	0.016	0.031	0.00	0.5097E-12	Q		q	
1454.4-3747	MRC 1451-375	14 54 27.4	-37 47 33.1	0.3210	16.69	0.000	1.840	-0.20	0.7530E-11	Q		q	
1454.5+2955	[HB89] 1452+301	14 54 32.3	29 55 58.5	0.5800	19.03	0.202	0.406	0.60	0.7104E-12	Q		q	
1456.0+5048	RBS 1444	14 56 08.1	50 48 36.3	0.4800	19.30	0.212	0.232	0.08	0.2160E-10	Q		z	
1458.3+4832	RX J1458.4+4832	14 58 27.3	+48 32 46.2	0.5390	20.20*	0.000	0.003#	0.00	0.6110E-11	Q		z	
1458.9+0416	4C +04.49	14 58 59.3	04 16 13.8	0.3940	20.15	0.493	0.615	0.16	0.1434E-11	Q		q	
1459.1+7140	3C 309.1	14 59 07.6	71 40 19.9	0.9050	16.78	0.804	3.567	0.68	0.1316E-11	Q		g	
1459.9+3336	RGB J1459+336	14 59 58.5	33 37 01.6	0.6440	17.60	0.105	0.048	0.00	0.1558E-11	G		q	
1500.3+2122	LEDA 140447	15 00 19.5	21 22 09.7	0.1532	15.60*	0.000	0.027#	0.00	0.8878E-11	GC	0		
1501.0+2238	RBS 1452	15 01 01.8	22 38 06.5	0.2350	16.79	0.000	0.030	0.00	0.7341E-11	Q		z	
1501.6+0141	NGC 5813	15 01 11.3	+01 42 07.1	0.0064	11.40*	0.000	0.016#	0.00	0.1430E-10	GC	E		
1504.4-0248	LCRS B150131.5-	15 04 07.5	-02 48 16.5	0.2169	16.40*	0.000	0.062#	0.00	0.3060E-10	G		a	
1504.1+6856	[HB89] 1503+691	15 04 12.7	68 56 12.0	0.3180	17.10	0.069	0.227	0.65	0.4411E-11	Q		q	
	PKS 1502+106	15 04 24.9	10 29 39.2	1.8390	18.56	0.000	2.040	-0.20	0.2779E-12	Q		q	
1504.8+5649	RGB J1504+568	15 04 55.5	56 49 20.0	0.3600	17.00	0.006	0.061	0.00	0.4399E-12	G		q	
	3C 310	15 04 57.1	26 00 58.3	0.0538	15.24*	0.080	23.399&	0.20	0.1896E-12	G	E		I
1506.3+0136	NGC 5846	15 06 29.3	+01 36 20.7	0.0061	11.10*	0.000	0.022#	0.00	0.1240E-10	GC	E	l	
	PKS 1504-167	15 07 04.8	-16 52 30.3	0.8760	18.50	0.000	1.960	0.26	0.2819E-11	Q		q	
1507.7+5127	MRK 845	15 07 45.0	51 27 10.3	0.0460	14.86	0.000	0.004#	0.00	0.3558E-11	G	S	1	
	8C 1506+624	15 07 57.3	62 13 34.3	1.4780	18.50	0.000	0.213#	0.70	0.2620E-12	Q		q	
1509.6+5718	RGB J1509+573	15 09 40.7	57 18 11.9	0.8140	18.50*	0.010	0.046	0.00	0.4273E-12	G		q	
	RBS 1469	15 10 41.2	33 35 04.5	0.1148	17.70	0.000	0.003#	0.00	0.3936E-11	Q		z	
	PKS 1508-05	15 10 53.6	-05 43 07.5	1.1850	17.21	0.000	2.330	0.36	<0.1130E-11	Q		q	
1510.9+0544	4C +06.53	15 10 56.1	05 44 41.2	0.0779	15.40*	0.084	3.740&	0.61	0.6626E-10	GC	c		
	RGB J1511+063	15 11 26.5	06 20 54.8	0.0809	15.50	0.006	0.202	-0.42	0.1062E-10	GC			

Table A.3: *(continued)*

RXJ name (1)	Name (2)	RA(J2000) (3)	DEC(J2000) (4)	z (5)	m_V (6)	F_{5GHz}^{core} (7)	F_{5GHz} (8)	α_r (9)	$F_{0.1-2.4\ keV}$ (10)	Type (11)	Host (12)	Class. (13)	FR (14)
	PMN J1511+0518	15 11 41.3	05 18 09.3	0.0840	19.00	0.000	0.496	0.00	0.1911E-12	G		1	
1511.4-2119	IRAS 15091-210	15 11 59.8	-21 19 01.7	0.0446	15.50*	0.000	0.047#	0.00	0.1350E-10	G		!	
1512.2+0203	PKS 1509+022	15 12 15.7	02 03 17.0	0.2190	18.50	0.130	0.510	0.40	0.1542E-11	G		r	
	PKS 1510-08	15 12 50.5	-09 05 59.8	0.3600	16.54	1.613	3.240	-0.13	0.3151E-11	Q		q	
	PKS 1511-100	15 13 44.9	-10 12 00.3	1.5130	18.80	0.000	0.700	-0.36	<0.1040E-11	Q		q	
1514.3+4244	IRAS F15125+4255	15 14 20.5	42 44 44.0	0.1520	18.00	0.000	0.001#	0.00	0.2022E-11	G		s	
1514.7+3650	PG 1512+370	15 14 43.0	36 50 50.4	0.3707	16.27	0.068	0.351	0.87	0.3357E-11	Q		q	
1515.1+4754	TXS 1513+481	15 15 12.2	47 55 09.2	0.9140	17.40	0.000	0.068	0.90	0.3512E-12	G		a	
1515.3+5530	NGC 5905	15 15 23.3	+55 31 01.8	0.0113	12.50*	0.000	0.021#	0.00	0.4060E-11	G	S	1	
1516.6+0014	4C +00.56	15 16 40.2	00 15 01.9	0.0525	15.80	0.762	1.585	0.90	0.1928E-11	GC		l	
1516.6+2917	RGB J1516+293	15 16 41.6	29 18 09.5	0.1300	18.20	0.034	0.082	0.77	0.2101E-11	G	E	z	
1516.7+0700	3C 317	15 16 44.5	07 01 16.6	0.0344	14.17	0.256	0.947	0.84	0.4879E-10	GC	c	2	I
	PKS 1514+197	15 16 56.8	19 32 12.9	1.0700	18.70	0.000	0.460	-0.20	0.8654E-12	Q		z	
1517.5+2856	FBQS J1517+2856	15 17 28.5	28 56 15.9	0.2080	18.65	0.000	0.001#	0.00	0.4082E-12	Q			
1517.6-2422	AP LIBRAE	15 17 41.8	-24 22 19.5	0.0486	14.80	0.000	1.940	0.05	0.2642E-11	GC	N	z	
1517.7+6525	RBS 1481	15 17 47.6	65 25 23.9	0.7020	17.77	0.000	0.035	0.16	0.1877E-10	Q		z	
1517.8+0506	CGCG 049-106	15 17 51.7	+05 06 27.8	0.0387	15.60*	0.000	0.013#	0.00	0.2450E-11	G		a	
1518.4+4832	RGB J1518+485	15 18 30.9	48 32 14.4	0.5760	18.40	0.005	0.034	0.00	0.9876E-12	G		q	
1518.5+4045	RGB J1518+407	15 18 38.9	40 45 00.1	0.0650	17.54	0.029	0.044	0.01	0.8520E-12	G		1	
1518.7+0613	PMN J1518+0613	15 18 45.7	06 13 55.8	0.1021	15.20*	0.000	0.223	1.40	0.1110E-10	GC		a	
1519.6+2838	FBQS J1519+2838	15 19 36.1	28 38 27.9	0.2700	17.22	0.000	0.002#	0.00	0.7420E-12	Q		q	
	3C 318	15 20 05.4	20 16 05.8	1.5740	20.90	0.000	0.750	1.00	<0.3724E-12	G	N	g	II
1520.7+7224	4C +72.20	15 20 47.7	72 25 05.3	0.7990	16.50	0.000	0.514	0.96	0.1326E-11	Q		q	
1520.7+4840	MCG +08-28-020	15 20 52.2	+48 39 38.2	0.0738	16.00*	0.000	0.082#	0.00	0.5860E-11	GC			
	3C 318.1	15 21 51.9	07 42 31.9	0.0453	15.50*	0.000	0.126#	1.38	0.3314E-10	GC	c	n	II
1522.1-0644	[HB89] 1519-065	15 22 28.7	-06 44 40.9	0.0830	14.90*	0.000	0.015#	0.00	0.5340E-11	G		1	
	PKS 1519-273	15 22 37.7	-27 30 10.8	0.0710	17.70	0.000	2.279	0.66	0.4209E-11	Q		g	
1522.9+6645	4C +66.16	15 22 59.6	66 45 06.9	0.6290	17.70	0.000	0.218	0.65	0.1170E-11	G		q	
1523.6+6339	RGB J1523+636	15 23 45.8	63 39 24.0	0.2040	16.80	0.014	0.236	1.17	0.5718E-11	G		q	
1524.6+1521	[HB89] 1522+155	15 24 41.6	15 21 21.0	0.6280	17.50	0.258	0.350	0.10	0.1239E-11	Q		q	
1525.0+1107	OR +139	15 25 02.9	11 07 44.1	0.3310	18.30	0.246	0.286	0.40	0.3207E-11	Q		q	
	NGC 5929	15 26 06.2	41 40 14.4	0.0083	14.00	0.000	0.065#	0.00	0.2125E-12	G	p	l	
	4C +10.43	15 26 46.3	09 59 10.0	1.3580	18.40	0.000	0.341#	0.60	0.4809E-12	Q		q	
1529.1+5616	IRAS F15279+5626	15 29 07.4	56 16 06.0	0.0990	16.08	0.000	0.005#	0.00	0.9326E-11	G	S	5	

Table A.3: *(continued)*

RXJ name (1)	Name (2)	RA(J2000) (3)	DEC(J2000) (4)	z (5)	m_V (6)	F_{5GHz}^{core} (7)	F_{5GHz} (8)	α_r (9)	$F_{0.1-2.4\ keV}$ (10)	Type (11)	Host (12)	Class. (13)	FR (14)
1530.9+4356	RGB J1531+439	15 31 02.4	43 56 37.0	0.4520	16.80	0.021	0.027	0.66	0.7442E-12	G		q	
1531.2+0727	NGC 5940	15 31 18.1	+07 27 27.9	0.0337	14.30*	0.000	0.009#	0.00	0.6270E-11	G	S	1	
	3C 320	15 31 25.4	35 33 39.9	0.3420	18.00*	0.555	0.500	0.78	0.4851E-12	G			II
	3C 321	15 31 43.4	24 04 19.1	0.0961	16.00	0.030	7.099&	1.14	0.2600E-12	G	p	n	II
1531.9+3016	RBS 1508	15 32 02.2	30 16 28.9	0.0640	15.60	0.047	0.042	0.00	0.6152E-11	G		z	
1532.8+3020	RBS 1509	15 32 53.8	30 20 59.5	0.3611	19.10	0.008	0.020	0.00	0.3918E-11	G		l	
1533.2+1332	[HB89] 1530+137	15 33 15.1	13 32 23.9	0.7110	18.74	0.000	0.380	0.90	0.1356E-11	Q		q	
1534.7+3716	RGB J1534+372	15 34 47.2	37 15 54.8	0.1430	18.30	0.020	0.024	0.00	0.3833E-12	Q		z	
1534.9+0130	PKS 1532+01	15 34 52.4	01 31 04.2	1.4350	20.20	0.800	1.284	0.17	0.7095E-12	Q		q	
1534.9+5839	SBS 1533+588	15 34 57.2	58 39 23.5	1.8950	18.30	0.150	0.000	0.00	0.2523E-12	Q		q	
1535.1+5320	RX J1535.0+5320	15 35 00.8	+53 20 35.0	0.8900	17.60*	0.000	0.018#	0.00	0.1750E-10	Q		z	
1535.4+3922	FBQS J153529.0+.	15 35 29.0	39 22 46.7	0.2570	18.46	0.000	0.019#	0.00	0.2268E-11	Q		z	
1535.8+5754	MRK 290	15 35 52.4	57 54 09.2	0.0296	14.96	0.000	0.005#	0.00	0.1535E-10	G	E	5	
1536.7+0137	RBS 1517	15 36 46.7	01 37 59.5	0.3120	18.70	0.035	0.045	-0.48	0.1036E-10	Q		z	
1538.0-1026		15 38 46.7	-10 26 21.3	0.1958	16.70*	0.000	0.004#	0.00	0.5470E-11	G		1	
1539.5+4735	[HB89] 1538+477	15 39 34.8	47 35 31.0	0.7721	15.81	0.015	0.032	0.66	0.1170E-11	Q		q	
1539.8+3043	LEDA 140531	15 39 50.8	30 43 03.9	0.0968	18.10*	0.000	0.006#	0.00	0.7696E-11	GC			
1539.8+4143	FIRST J153951.3+	15 39 51.4	41 43 25.5	0.1200	17.32	0.000	0.019#	0.00	0.3304E-12	Q		z	
1539.8+3349	FIRSTJ153952.2..	15 39 52.2	33 49 30.0	0.3300	16.80	0.000	0.002#	0.00	0.7664E-12	G		q	
1540.8+1447	MRC 1538+149	15 40 49.5	14 47 45.9	0.6050	17.30	0.716	1.209	0.40	0.1493E-11	Q		q	
	NVSS J154126+	15 41 26.5	04 43 56.0	0.1102	16.60*	0.000	0.027#	0.00	0.2424E-11	GC			
1543.5+0452	CGCG 1541.1+0501	15 43 33.9	04 52 19.2	0.0399	15.10	0.154	0.293	0.03	0.1186E-11	G	E		
	MG1 J154345+1847	15 43 43.8	18 47 19.8	1.3960	19.50	0.000	0.294	0.40	0.2374E-12	Q		q	
1543.8+4013	FBQS J154348.5+.	15 43 48.6	40 13 24.9	0.3180	17.91	0.000	0.003#	0.00	0.2294E-11	Q		q	
1545.0+0406	4C +04.53	15 44 59.4	04 07 46.3	2.1820	18.90	0.358	0.387	0.24	0.5518E-12	Q		q	
1545.7+4846	PG 1543+489	15 45 30.2	+48 46 09.0	0.4000	16.00*	0.000	0.004#	0.00	0.1490E-11	Q		q	
1547.3+1024		15 47 32.2	+10 24 51.2	0.1390	16.60*	0.000	0.003#	0.00	0.1490E-11	G		1	
1547.7+2051	PG 1545+210	15 47 43.5	20 52 16.7	0.2643	16.69	0.039	0.870	0.81	0.7182E-11	QC		q	
1547.7+0255	MS 1545.3+0305	15 47 51.9	+02 55 50.8	0.0980	16.80*	0.000	0.004#	0.00	0.3560E-11	G		1	
1548.3+3511	[HB89] 1546+353	15 48 17.9	35 11 28.3	0.4800	18.26	0.060	0.107	0.50	0.8441E-12	Q		q	
1548.9-1345	NGC 5995	15 48 24.9	-13 45 27.9	0.0252	14.50*	0.000	0.031#	0.00	0.9690E-11	G		2	
1548.3-3207	ESO 450-PN?016	15 48 43.1	-32 07 12.0	0.0489	14.50*	0.000	0.012#	0.00	0.1150E-10	G			
1549.2+5038	S4 1547+50	15 49 17.5	50 38 05.8	2.1690	18.40	0.934	0.000#	-0.38	0.6588E-12	Q		q	
1549.4+0236	[HB89] 1546+027	15 49 29.4	02 37 01.2	0.4130	17.79	1.147	0.000#	0.50	0.2761E-11	Q		q	

Table A.3: *(continued)*

RXJ name (1)	Name (2)	RA(J2000) (3)	DEC(J2000) (4)	z (5)	m_V (6)	F^{core}_{5GHz} (7)	F_{5GHz} (8)	α_r (9)	$F_{0.1-2.4\ keV}$ (10)	Type (11)	Host (12)	Class. (13)	FR (14)
	3C 324	15 49 48.9	21 25 38.1	1.2063	21.70	0.000	0.610	1.00	<0.4468E-13	GC		n	II
	3C 325	15 49 58.6	62 41 20.6	0.8600	19.00	0.001	10.000&	0.90	0.1422E-12	G	N	q	II
	PKS 1548+056	15 50 35.3	05 27 10.4	1.4220	19.50	0.000	2.180	-0.28	0.5000E-12	Q		q	
1550.7+1120	PKS 1548+114	15 50 43.6	11 20 47.4	0.4360	17.23	0.176	0.543	0.57	0.9003E-12	Q		q	
1551.6+3548	2MASXiJ1551356..	15 51 35.6	35 48 51.6	0.0930	16.50*	0.000	0.005#	0.00	0.8570E-12	G		*	
1551.9+5806	RGB J1551+581	15 51 58.2	58 06 44.5	1.3240	16.73	0.263	0.348	0.08	0.5460E-12	G	E	q	
	3C 326	15 52 09.1	20 05 23.7	0.0895	17.00*	0.013	9.640&	0.00	0.2437E-13	G		w	II
	PKS 1550-269	15 54 02.5	-27 04 40.2	2.1450	19.60	0.000	1.139	0.27	<0.2390E-12	Q		q	
1554.2+3238	CG 1329	15 54 17.4	32 38 37.8	0.0475	15.70*	0.000	0.002#	0.00	0.1710E-11	G		a	
1554.4+2011	RGB J1554+201	15 54 24.1	20 11 25.4	0.2220	17.70	0.020	0.051	-1.41	0.6350E-11	G		z	
	[HB89] 1552+199	15 54 39.2	19 47 19.1	1.3400	20.10	0.000	0.540	0.80	0.4912E-12	Q		q	
	PKS 1547-79	15 55 21.6	-79 40 36.3	0.4830	19.90	0.000	1.379	0.85	<0.5900E-12	G			
1555.7+1111	[HB89] 1553+113	15 55 43.0	11 11 24.4	0.3600	15.00	0.398	0.510	-0.11	0.3339E-10	Q		z	
1556.0+2426	CGCG 1554.0+2435	15 56 03.9	24 26 52.9	0.0426	15.42*	0.056	0.109	0.20	0.3238E-12	G	E		I
1556.4+0903	MRK 0863	15 56 25.9	+09 03 18.8	0.0423	15.30*	0.000	0.005#	0.00	0.2750E-11	G		*	
	7C 1555+3538	15 57 42.1	35 30 24.7	0.1579	14.70	0.000	0.078#	0.70	0.2992E-11	G			
	PKS 1555+001	15 57 51.4	-00 01 50.4	1.7700	20.70	0.000	1.010	-0.21	<0.2200E-12	Q		q	
1558.3+2551	MRK 864	15 58 18.8	25 51 24.4	0.0719	17.10	0.000	0.002#	0.00	0.4164E-11	G	E	5	
1558.4-1410	PKS 1555-140	15 58 21.9	-14 09 59.0	0.0970	17.30*	0.000	0.461#	0.20	0.2320E-10	G			
1558.9+3323	[HB89] 1556+335	15 58 55.1	33 23 18.8	1.6460	17.00	0.000	0.086#	0.00	0.4394E-12	Q		q	
1559.1+3501	UGC 10120	15 59 09.6	35 01 47.5	0.0313	15.06	0.000	0.003#	0.00	0.8410E-11	G	S	!	
	MCG +09-26-046	16 01 28.4	53 54 14.9	0.0684	16.00*	0.000	0.043	0.00	0.2546E-11	G			
1601.7+1754	TXS 1559+180	16 01 48.2	17 54 03.8	0.6590	18.40*	0.000	0.080	0.70	0.8500E-12	G		a	
1602.3+1558	UGC 10143	16 02 17.0	+15 58 28.4	0.0347	14.20*	0.000	0.011#	0.00	0.1090E-10	GC	c		
	3C 327	16 02 27.3	01 57 56.2	0.1048	16.31	0.028	2.870	0.95	<0.2000E-12	G	0		II
1603.0+3039	FBQS J1602+3038	16 02 57.4	30 38 51.9	0.8100	18.05	0.000	0.001#	0.00	0.5734E-12	Q		q	
1603.2+0900	PMN J1603+0900	16 03 17.7	09 00 37.7	0.4880	17.30	0.000	0.103#	0.67	0.1685E-11	G		q	
	GIN 463	16 03 38.1	15 54 02.4	0.1095	15.50	0.000	0.269#	-0.96	0.7519E-11	G	E		
1603.9+5730	SBS 1602+576	16 03 55.9	57 30 54.4	2.8500	17.20	0.265	0.365	0.36	0.4550E-12	Q		g	
1604.5+5714	7C 1603+5722	16 04 37.3	57 14 36.7	0.7200	18.00	0.384	0.000	0.09	0.5234E-12	Q		q	
	3C 327.1	16 04 45.3	01 17 51.0	0.4620	20.30	0.065	1.129	1.07	0.8100E-12	G		b	II
1604.9+2355	NGC 6051	16 04 56.8	23 55 56.4	0.0319	14.90*	0.212	0.200	1.02	0.1264E-10	GC	c		
1605.2+3239	FBQSJ160508.8..	16 05 08.9	32 39 22.4	0.0910	18.20*	0.000	0.001#	0.00	0.5380E-12	G		h	
1605.5+3239	CGCG 195-013	16 05 34.6	32 39 40.9	0.0296	15.60*	0.000	5.980#	0.00	0.5380E-12	G			

Table A.3: *(continued)*

RXJ name (1)	Name (2)	RA(J2000) (3)	DEC(J2000) (4)	z (5)	m_V (6)	F_{5GHz}^{core} (7)	F_{5GHz} (8)	α_r (9)	$F_{0.1-2.4\ keV}$ (10)	Type (11)	Host (12)	Class. (13)	FR (14)
	[HB89] 1603+179	16 06 01.3	17 47 40.6	1.8130	20.00	0.000	0.031#	0.00	0.9875E-13	Q		q	
	MG2 J160607+2031	16 06 05.7	20 32 09.3	0.3830	18.30	0.000	0.178#	0.40	0.1254E-12	Q		q	
1606.3+5405	RGB J1606+540	16 06 23.5	54 05 55.5	0.8780	17.10	0.061	0.089	0.65	0.3170E-12	G		1	
	PKS 1604+159	16 07 06.4	15 51 34.5	0.3570	18.00	0.000	0.510	0.30	0.1059E-11	Q		z	
1607.8+3450	2MASXiJ1607459..	16 07 46.0	34 50 48.8	0.0540	16.30*	0.000	0.002#	0.00	0.4253E-12	G		*	
1608.3+6018	2MASXiJ1608205..	16 08 20.5	60 18 28.0	0.1780	16.00	0.000	0.079#	0.00	0.1759E-11	G		q	
1608.7+1028	4C +10.45	16 08 46.2	10 29 07.8	1.2260	18.70	1.347	1.411	0.05	0.1035E-11	Q		q	
1609.1+1756	PKS 1606+180	16 09 11.2	17 56 16.0	0.3460	18.00	0.015	0.238	0.56	0.6730E-12	Q		q	
	3C 330	16 09 36.6	65 56 43.6	0.5500	21.00	0.001	2.350	0.80	<0.8801E-13	GC		n	II
1609.9+6710	7C 1609+6718	16 10 02.6	67 10 29.8	0.0670	18.40	0.013	0.036	0.00	0.4245E-11	G		z	
1610.7+3303	RX J1610.7+3303	16 10 47.7	+33 03 37.7	0.0970	16.70*	0.000	0.005#	0.00	0.3420E-11	G		1	
1611.8+5851	SBS 1610+589	16 11 24.6	+58 51 01.6	0.0321	15.80*	0.000	0.004#	0.00	0.3620E-11	G		5	
1611.7+3812	2MASXiJ1611392..	16 11 39.2	38 12 41.7	0.0647	14.20*	0.000	0.007#	0.00	0.4810E-12	G			
	NGC 6086	16 12 35.6	29 29 04.3	0.0318	14.80*	0.006	0.000#	0.00	0.4156E+02*	GC	c		I
1613.0+6543	PG 1613+658	16 13 57.2	+65 43 09.6	0.1290	15.20*	0.000	0.004#	0.00	0.1800E-10	G		1	
1614.0+2604	PG 1612+261	16 14 13.2	+26 04 16.4	0.1310	15.40*	0.000	0.018#	0.00	0.1100E-10	Q		q	
1614.8+3745	FBQS J161446.9+.	16 14 46.9	37 46 07.3	1.5320	16.87	0.000	0.049#	0.26	0.3156E-12	Q		q	
1616.6+0459	[HB89] 1614+051	16 16 37.5	04 59 32.7	3.1970	19.60	0.711	0.916	0.06	0.7917E-12	Q		g	
1616.8+3621	EF B1615+3628	16 16 55.6	36 21 34.5	2.2590	18.60	0.269	0.286	-0.01	0.1775E-12	Q		q	
1617.0+4106	B3 1615+412	16 17 06.3	41 06 47.0	0.2670	16.20*	0.081	0.124	-0.08	0.2106E-11	Q		z	
1617.6+3501	NGC 6109	16 17 40.6	35 00 15.4	0.0295	14.90*	0.028	0.470	0.78	0.8124E-13	G	E		I
	3C 332	16 17 42.5	32 22 34.8	0.1515	16.00	0.010	0.830	0.74	0.2136E-12	G	E	q	II
1617.7+0603	RX J1617.7+0603	16 17 45.6	+06 03 53.4	0.0380	16.50*	0.000	0.006#	0.00	0.1630E-10	G		1	
	PKS 1610-77	16 17 49.3	-77 17 18.5	1.7100	19.20	0.000	5.549	0.00	0.1342E-11	Q		q	
1618.2+3619	RX J1618.1+3619	16 18 09.4	+36 19 57.9	0.0340	16.90*	0.000	0.003#	0.00	0.1020E-10	G		!	
1618.9+3031	FBQS J1619+3030	16 19 02.5	30 30 51.5	1.2860	17.24	0.038	0.044	0.65	0.5232E-12	Q		q	
1620.3+1736	3C 334	16 20 21.9	17 36 24.0	0.5551	16.41	0.195	0.584	0.80	0.1433E-11	QC		q	
1620.4+6904	GB6 J1620+6905	16 20 26.3	69 04 47.6	1.4900	16.51	0.000	0.051	0.36	0.2170E-12	Q		q	
1620.5+2953	LEDA 140601	16 20 31.1	29 53 27.6	0.0954	18.10*	0.000	0.004#	0.00	0.6051E-11	GC	c		
1621.1+3745	4C +37.46	16 21 11.3	37 46 04.9	0.3400	17.28	0.155	0.201	0.88	0.1549E-11	G		q	
1621.2+5427	SBS 1620+545	16 21 45.1	+54 27 23.7	0.0501	18.80*	0.000	0.005#	0.00	0.2320E-11	G		2	
1622.4+4006	RGB J1622+401	16 22 29.3	40 06 43.4	0.6870	18.30*	0.030	0.058	0.43	0.4930E-12	G		q	
1623.0+3755	NGC 6137	16 23 03.1	37 55 20.4	0.0310	14.10*	0.174	1.090&	0.82	0.9927E-12	GC	E		
1623.0+6624	RGB J1623+664	16 23 04.5	66 24 01.1	0.2010	18.60	0.243	0.481	0.20	0.5863E-12	Q		g	

Table A.3: *(continued)*

RXJ name (1)	Name (2)	RA(J2000) (3)	DEC(J2000) (4)	z (5)	m_V (6)	F_{5GHz}^{core} (7)	F_{5GHz} (8)	α_r (9)	$F_{0.1-2.4\ keV}$ (10)	Type (11)	Host (12)	Class. (13)	FR (14)
1623.1+3909	B3 1621+392	16 23 07.6	39 09 32.4	1.9800	15.91	0.292	0.000	0.15	0.5634E-12	Q		q	
1623.3+4022	KUV 16216+4030	16 23 18.9	40 22 58.3	0.9000	17.80	0.000	0.008#	0.00	0.2664E-12	Q		q	
1623.3+4116	KUV 16217+4124	16 23 19.9	41 17 02.8	1.6200	16.66	0.000	0.003#	0.00	0.3271E-12	Q		q	
1623.5+3559	[HB89] 1621+361	16 23 30.6	35 59 33.1	0.8700	17.91	0.000	0.146#	0.70	0.2374E-12	Q		q	
	MRK 699	16 23 45.9	41 04 56.7	0.0342	15.11	0.000	0.001#	0.00	0.3663E-12	G	E	5	
1624.7+2604	IRAS F16221+261	16 24 09.2	+26 04 32.8	0.0400	16.80*	0.000	0.004#	0.00	0.6210E-11	G		1	
	7C 1623+5748	16 24 24.8	57 41 16.3	0.7890	18.86	0.714	0.590	-0.13	0.1127E-12	G		q	
1624.7+3726	B3 1622+375	16 24 43.3	37 26 42.4	0.2000	18.20	0.014	0.031	0.26	0.4110E-12	Q		z	
1625.2+2650	4C +26.48	16 25 14.3	26 50 27.7	0.7790	17.50	0.032	0.233	1.11	0.6142E-12	Q		q	
1625.4+2705	MS 1623.4+2712	16 25 30.7	27 05 46.0	0.5250	18.41	0.031	0.210	0.78	0.1477E-11	G		q	
	PKS 1622-253	16 25 46.9	-25 27 38.3	0.7860	20.60	0.000	2.029	0.19	0.1900E-11	Q		q	
	4C +41.32	16 25 57.7	41 34 40.6	2.5500	22.00	0.000	1.362	0.17	0.1411E-12	Q		q	
	PKS 1622-29	16 26 06.0	-29 51 26.9	0.8150	19.50	0.000	1.860	0.00	0.1830E-11	Q		q	
1626.1+3359	FIRSTJ162607.0..	16 26 07.2	33 59 15.0	0.2040	15.80	0.000	0.003#	0.00	0.1693E-11	G		q	
1626.1+5120	RGB J1626+513	16 26 11.6	51 20 38.3	0.1780	19.50	0.014	0.035	0.29	0.1904E-11	G		b	
1626.4+3513	EF B1624+3520	16 26 25.8	35 13 41.5	0.5000	19.20	0.014	0.019	0.41	0.1419E-11	Q		z	
	7C 1625+5815	16 26 37.2	58 09 17.7	0.7480	16.37	0.000	0.328	0.43	0.4698E-12	G	S	q	
1627.4+3507	FBQSJ162726.6..	16 27 26.6	35 08 15.8	0.1900	19.04	0.000	0.001#	0.00	0.3173E-12	G		s	
1627.6+4055	NGC 6160	16 27 41.1	40 55 37.0	0.0317	14.80*	0.000	0.001#	0.00	0.7563E-12	GC	c		
1627.8+5419	87GB 162642.7+..	16 27 52.1	54 19 12.0	0.3150	17.00	0.000	0.036#	0.00	0.6177E-12	Q		q	
	3C 338	16 28 38.5	39 33 05.6	0.0303	12.61	0.106	0.463	1.75	0.1185E-12	GC	E	n	I
1628.7+5629	RGB J1628+564	16 28 50.3	56 29 29.0	0.4000	17.40	0.018	0.068	0.00	0.5581E-12	G		q	
1629.0+4007	EXO 1627.3+4014	16 29 01.3	40 07 59.6	0.2720	18.30	0.021	0.020	0.00	0.8094E-11	G		!	
1629.1+7431	7C 1630+7437	16 29 07.9	74 30 57.5	0.7000	20.70	0.000	0.174	0.00	0.6653E-12	Q		q	
1629.7+4048	NGC 6173	16 29 44.9	40 48 41.8	0.0293	14.00*	0.000	0.007#	0.00	0.4145E-12	GC	c		
	MG2 J162944+2117	16 29 47.6	21 17 17.7	0.8330	21.50	0.000	0.105#	0.80	0.3130E-12	Q		q	
1629.8+2426	MRK 0883	16 29 52.8	24 26 38.2	0.0375	14.43	0.007	0.021	0.00	0.9420E-12	G	0	9	
1630.3+3756	FBQS J163020.7+.	16 30 20.8	37 56 56.5	0.3940	16.59	0.000	0.020#	0.00	0.5482E-12	Q		q	
163057.7..	RIXOS F212_025	16 30 58.0	37 07 33.4	0.8020	19.60	0.000	0.003#	0.00	0.1877E-12	G		q	
1631.7+4216	RX J1631.4+4217	16 31 24.7	+42 17 03.0	0.4680	19.80*	0.000	0.007#	0.00	0.5680E-11	Q		z	
1631.7+1157	4C +12.59	16 31 45.3	11 56 02.9	1.7950	18.40	0.359	0.864	0.69	0.2029E-11	Q		g	
	NGC 6251	16 32 31.9	82 32 16.5	0.0249	14.00	0.000	0.802#	0.13	0.2702E-11	G	E	w	I
1632.7+0534	RGB J1632+055	16 32 46.9	05 34 32.6	0.1511	17.10*	0.010	0.065	1.70	0.2479E-10	GC			
1633.0+3924	RGB J1633+394	16 33 02.1	39 24 27.6	1.0230	16.00	0.021	0.035	0.49	0.3616E-12	Q		q	

Table A.3: *(continued)*

RXJ name (1)	Name (2)	RA(J2000) (3)	DEC(J2000) (4)	z (5)	m_V (6)	F_{5GHz}^{core} (7)	F_{5GHz} (8)	α_r (9)	$F_{0.1-2.4\ keV}$ (10)	Type (11)	Host (12)	Class. (13)	FR (14)
1633.3+3520	NGC 6185	16 33 17.8	35 20 32.4	0.0343	14.50*	0.000	0.060#	0.00	0.2222E-12	G	S		
1633.3+4718	RGB J1633+473	16 33 23.5	47 19 00.1	0.1163	16.90	0.030	0.035	1.19	0.2605E-11	G		!	
	3C 343	16 34 33.8	62 45 35.8	0.9880	20.61	0.105	1.490	0.70	<0.3114E-13	Q		g	
1635.6+1831	[HB89] 1633+186	16 35 39.1	18 31 03.7	1.0900	18.20	0.000	0.146	0.19	0.7490E-12	Q		q	
1635.8+7128	RGB J1635+714	16 35 52.1	71 28 53.7	0.1710	15.84	0.109	0.193	0.66	0.1005E-11	G		q	
1636.6+2648	3C 342	16 36 36.4	26 48 09.2	0.5610	17.75	0.000	0.340	1.12	0.9897E-12	Q		q	
1637.1+4140	KUV 16355+4146	16 37 09.3	41 40 30.6	0.7650	16.60	0.000	0.007#	0.00	0.7372E-12	Q		q	
	[HB89] 1636+473	16 37 45.1	47 17 33.8	0.7400	18.73	0.599	1.330	-0.27	0.2300E-12	Q		q	
1637.8+1150	[HB89] 1635+119	16 37 46.5	11 49 49.7	0.1460	16.50	0.011	0.062	0.00	0.3556E-11	Q		1	
1638.2+5720	7C 1637+5726	16 38 13.4	57 20 23.9	0.7506	16.90	1.233	1.750	-0.13	0.1733E-11	Q		q	
	3C 343.1	16 38 28.2	62 34 44.2	0.7500	20.70	0.000	1.199	0.90	<0.8395E-13	G		g	II
1639.6+5347	4C +53.37	16 39 30.1	53 46 45.0	0.1103	14.90	0.013	0.223	-1.80	0.6180E-12	GC			
1639.5+3908	FBQS J163931.8+.	16 39 31.8	39 08 45.4	0.1430	18.36	0.000	0.001#	0.00	0.7420E-12	Q		1	
1640.3+4642	RGB J1640+467	16 40 22.1	46 42 46.2	0.2344	17.00*	0.009	0.084	1.10	0.8259E-11	GC			
	B3 1638+398	16 40 29.6	39 46 46.0	1.6600	19.37	0.000	1.284	-0.54	0.2800E-12	Q		q	
1641.7+3934	[HB89] 1640+396	16 41 47.5	39 35 03.4	0.5400	18.30	0.047	0.052	0.00	0.4950E-12	Q		q	
1642.1+6856	8C 1642+690	16 42 07.8	68 56 39.7	0.7510	20.50	0.999	1.526	0.08	0.6161E-12	Q		q	
1642.7+2522	TXS 1640+254	16 42 40.4	25 23 07.7	1.7250	18.20	0.000	0.480	-0.01	0.3782E-12	Q		q	
1642.9+3948	3C 345	16 42 58.8	39 48 36.9	0.5928	15.96	8.500	8.718	0.24	0.3429E-11	Q		q	
	3C 346	16 43 48.6	17 15 49.0	0.1620	17.20	1.389	1.619	0.52	0.1719E-11	G	E	n	I
1644.2-7715	MRC 1637-771	16 44 16.1	-77 15 48.4	0.0427	15.50	0.184	2.609	0.62	0.2082E-11	G		r	II
1644.2+4546	B3 1642+458	16 44 19.9	45 46 44.5	0.2230	17.60	0.064	0.109	0.38	0.2644E-11	Q		z	
1644.6+2619	RGB J1644+263	16 44 42.5	26 19 13.2	0.1450	17.10	0.092	0.099	-0.57	0.2521E-11	G		!	
1646.3-1124	IRAS 16433-111	16 46 10.1	-11 23 59.1	0.0750	15.90*	0.000	0.040#	0.00	0.9760E-11	G		1	
1646.2+6939	RX J1646.2+6939	16 46 12.2	+69 39 59.2	0.2150	16.60*	0.000	0.003#	0.00	0.3010E-11	G		1	
1647.5+4950	SBS 1646+499	16 47 34.9	49 50 00.6	0.0475	17.00	0.178	0.191	-0.21	0.1526E-11	G		1	
	B3 1646+411	16 48 29.2	41 04 05.5	0.8508	20.40	0.000	0.189	0.36	0.8491E-12	Q		q	
1648.9+3954	FIRST J164855.9+	16 48 55.9	39 54 37.0	0.0700	17.51	0.000	0.004#	0.00	0.2715E-12	Q		z	
1650.0+4140	RGB J1650+416	16 50 05.5	41 40 32.6	0.5860	17.30	0.101	0.136	0.44	0.1002E-11	G		q	
1651.1+0459	3C 348/HerA	16 51 08.1	04 59 33.3	0.1540	18.25	0.010	12.740	1.16	0.4353E+02*	GC	c	w	I
1651.9+6231	87GB 165132.6+..	16 52 01.5	62 32 09.0	1.6322	19.29	0.000	0.097	0.00	0.1292E-11	Q		q	
1652.9+4009	FIRST J165253.2+	16 52 53.3	40 09 12.9	0.1475	17.00*	0.000	0.030#	0.00	0.1572E-11	Q		q	
1652.9+3123	FBQS J165255.9+.	16 52 55.9	31 23 43.9	0.5900	17.79	0.000	0.001#	0.00	0.3831E-12	Q		q	
1652.9+0223	NGC 6240	16 52 58.9	02 24 03.4	0.0245	16.30	0.042	0.164	0.45	0.2277E-11	G	p	l	

Table A.3: *(continued)*

RXJ name (1)	Name (2)	RA(J2000) (3)	DEC(J2000) (4)	z (5)	m_V (6)	F_{5GHz}^{core} (7)	F_{5GHz} (8)	α_r (9)	$F_{0.1-2.4\ keV}$ (10)	Type (11)	Host (12)	Class. (13)	FR (14)
1653.8+3945	MRK 0501	16 53 52.2	39 45 36.6	0.0336	13.78	0.450	1.375	0.18	0.6071E-10	G		z	
1655.0+3030	FBQS J165500.2+.	16 55 00.2	30 30 40.6	0.4050	18.21	0.000	0.003#	0.00	0.6890E-12	Q		q	
1655.9+5430	7C 1654+5434	16 55 59.2	54 30 04.4	1.0400	19.11	0.207	0.000#	0.14	0.5384E-12	Q		q	
	IVS B1655+534	16 56 39.6	53 21 48.8	1.5530	19.20	0.000	0.170#	0.00	0.2662E-12	Q		q	
1656.7+6012	RGB J1656+602	16 56 48.2	60 12 16.4	0.6230	19.00	0.213	0.000#	0.00	0.5329E-12	Q	E	q	
1657.3+5705	4C +57.28	16 57 20.7	57 05 53.5	1.2810	18.28	0.425	0.764	0.17	0.5300E-12	Q		q	
1658.0+2751	NGC 6269	16 57 58.1	27 51 15.6	0.0348	13.73	0.000	0.014#	0.00	0.2053E-11	GC	c		
1658.0+4737	S4 1656+47	16 58 02.8	47 37 49.2	1.6220	17.60	1.199	1.244	0.09	0.5037E-12	Q		q	
	PKS 1655+077	16 58 09.0	07 41 27.5	0.6210	20.00	0.000	1.600	-0.39	<0.3280E-12	Q		q	
1658.5+0515	PKS 1656+053	16 58 33.4	05 15 16.4	0.8790	16.54	1.300	1.381	0.18	0.3399E-11	Q		q	
	3C 349	16 59 29.5	47 02 44.1	0.2050	19.00	0.025	8.599&	0.85	0.1633E-12	G			II
1659.5+3735	FBQS J165931.9+.	16 59 31.9	37 35 28.9	0.7750	17.45	0.000	0.018#	0.00	0.3873E-12	Q		q	
1659.7+3236	4C +32.52C	16 59 43.9	32 36 54.9	0.0984	16.50*	0.000	0.015#	0.00	0.3770E-11	GC			
1700.1+6830	RGB J1700+685	17 00 09.3	68 30 06.9	0.3010	17.00	0.313	0.380	0.16	0.3063E-12	G	E	q	
	4C +32.52E	17 00 11.2	32 35 14.9	0.1020	16.10	0.002	0.600&	0.00	0.2789E-13	GC	E	r	
1700.6+3553	2MASXiJ1700332..	17 00 33.3	35 52 56.5	0.1420	16.00	0.000	0.001#	0.00	0.1711E-11	G		q	
1700.7+2919	NPM1G +29.0397	17 00 46.8	29 19 26.5	0.0680	15.00*	0.000	0.002#	0.00	0.2315E-11	G		a	
1700.9+3403	RGB J1701+340	17 01 02.3	34 03 59.0	0.0900	19.40	0.000	0.024	0.00	0.3195E-11	G		5	
1702.5+3247	RBS 1618	17 02 31.0	32 47 19.6	0.1640	16.30	0.000	0.002#	0.00	0.9987E-11	G		q	
1702.7+3403	FIRSTJ170242.5..	17 02 41.9	34 03 47.1	0.0974	19.40	0.000	0.002#	0.00	0.1671E-10	GC	c		
1702.5+7253	UGC 10697	17 02 44.2	+72 53 29.5	0.0530	15.70*	0.000	0.004#	0.00	0.1040E-10	G	S	1	
1703.3+3737	RBS 1622	17 03 20.2	37 37 24.8	0.0650	16.60	0.000	0.002#	0.00	0.3607E-11	G		1	
1703.4+3604	MCG +06-37-023	17 03 27.8	36 04 19.9	0.0628	15.00	0.000	0.004#	0.00	0.8869E-12	G		a	
1703.5+4540	B3 1702+457	17 03 30.4	45 40 47.3	0.0604	15.10	0.026	0.190&	0.00	0.1546E-10	G		!	
1704.6+6044	3C 351	17 04 41.4	60 44 30.5	0.3719	15.28	0.008	1.219	0.88	0.6731E-12	Q		q	
1705.2-0132	UGC 10683 NOTES	17 05 00.4	-01 32 28.6	0.0308	15.60*	0.000	0.004#	0.00	0.4610E-11	G	S	1	
	MS 1704.9+6046	17 05 34.8	60 42 15.8	0.2800	19.40	0.000	0.002	0.00	0.1705E-11	Q		z	
1706.5+3615	RGB J1706+362	17 06 34.2	36 15 08.0	0.9170	18.20	0.015	0.027	0.00	0.5080E-12	G		q	
1706.7+3214	RGB J1706+322	17 06 48.1	32 14 22.7	1.0700	17.10	0.020	0.062	0.00	0.5840E-12	G		q	
1707.2+4535	[HB89] 1705+456	17 07 17.7	45 36 10.5	0.6480	17.30	0.650	0.000	0.43	0.4609E-12	Q		q	
1708.0+3910	IRAS F17063+3914	17 07 59.7	39 10 29.2	0.1270	16.82	0.000	0.002#	0.00	0.3767E-12	G		h	
1708.4+4123	FBQS J170823.1+.	17 08 23.1	41 23 09.5	0.8370	17.36	0.000	0.001#	0.00	0.2997E-12	Q		q	
1709.5+3425	4C +34.45	17 09 38.4	34 25 53.8	0.0808	15.30*	0.005	0.201	1.10	0.2576E-11	GC	E		
1710.2+3344	FBQSJ171013.4..	17 10 13.4	33 44 02.8	0.2080	15.82	0.000	0.004#	0.00	0.2597E-11	G		q	

Table A.3: *(continued)*

RXJ name (1)	Name (2)	RA(J2000) (3)	DEC(J2000) (4)	z (5)	m_V (6)	F_{5GHz}^{core} (7)	F_{5GHz} (8)	α_r (9)	$F_{0.1-2.4\ keV}$ (10)	Type (11)	Host (12)	Class. (13)	FR (14)
1711.5+3941	NPM1G +39.0436	17 10 56.3	+39 41 30.9	0.0623	16.50*	0.000	0.497#	1.50	0.3210E-11	GC		a	
1711.5+3335	EXO 1709.6+3339	17 11 31.3	33 35 43.0	0.4710	17.50	0.000	0.013	0.00	0.1391E-11	G		q	
	B3 1710+442	17 12 02.8	44 13 36.9	0.8740	18.78	0.000	0.082	1.14	0.4658E-12	Q		q	
1712.6+3801	IC 1245	17 12 36.6	38 01 13.3	0.0373	14.72*	0.000	0.003#	0.00	0.8331E-12	G	0		
1713.1+3523	RBS 1631	17 13 04.5	35 23 33.4	0.0830	16.84	0.000	0.011#	0.00	0.1967E-10	Q		1	
1713.3+3256	FBQSJ171322.6..	17 13 20.9	32 56 32.0	0.1020	16.50	0.025	0.050	0.90	0.3510E-11	G		b	
1715.0+3619	MG2 J171511+3619	17 15 08.4	36 19 50.1	0.5549	18.40	0.039	0.093	0.66	0.3879E-12	Q		q	
1715.3+5725	NGC 6338	17 15 22.9	57 24 40.3	0.0274	14.20*	0.000	0.038	0.40	0.1296E-10	GC	c		
1716.0+3623	UGC 10782	17 15 58.8	36 23 23.0	0.0379	15.60*	0.000	0.001#	0.00	0.1004E-11	G	S	a	
1715.9+3112	RBS 1633	17 16 01.9	31 12 13.8	0.1110	16.00	0.000	0.003#	0.00	0.5926E-11	G		q	
1716.0+6836	HS 1716+6839	17 16 13.9	68 36 38.7	0.7770	18.50	0.520	0.838	-0.19	0.2723E-11	Q		q	
1717.2+4226	LEDA 093954	17 17 19.2	42 27 00.0	0.1829	14.80*	0.089	0.125	0.06	0.3333E-11	GC		a	
1718.8+3041	FBQS J171850.3+.	17 18 50.3	30 42 01.3	0.2800	18.70	0.000	0.001#	0.00	0.7516E-12	Q		1	
1718.9+6930	RGB J1719+694	17 19 13.4	69 29 37.2	0.2830	18.34	0.010	0.020	0.00	0.3013E-12	G		1	
1719.2+4858	CGCG 1717.9+4901	17 19 14.5	48 58 49.5	0.0242	14.81	0.139	0.164	-0.57	0.9769E-12	GC	E	l	
1719.5+2510	FBQSJ171934.1..	17 19 34.2	25 10 58.5	0.5790	16.80	0.000	0.013#	0.00	0.9604E-12	G		q	
1719.6+4804	[HB89] 1718+481	17 19 38.2	48 04 12.0	1.0840	14.60	0.104	0.109	-0.38	0.1994E-11	Q		q	
1720.1+2637	RGB J1720+266	17 20 09.9	26 37 31.1	0.1605	17.30*	0.007	0.021	0.00	0.1280E-10	GC			
	3C 353	17 20 28.1	-00 58 46.8	0.0304	15.36*	0.117	20.539	0.84	0.2080E-11	G		n	II
1721.1+3542	[HB89] 1719+357	17 21 09.5	35 42 16.0	0.2630	19.12	0.361	0.784	0.47	0.1294E-11	Q		q	
1721.5+2111	RGB J1721+211	17 21 33.2	21 11 02.0	0.6280	18.60	0.042	0.103	0.71	0.6657E-12	G		q	
1722.2+3042	CGCG 170-018	17 22 15.4	30 42 39.7	0.0467	15.60*	0.000	0.005#	0.00	0.1620E-11	GC			
1722.4+3207	2MASXiJ1722271..	17 22 27.1	32 07 58.0	0.2240	19.20*	0.000	0.003#	0.00	0.7876E-11	GC	c		
1722.6+3052	MRK 0506	17 22 39.9	30 52 53.0	0.0430	14.68	0.000	0.007#	0.00	0.3195E-10	G	S	5	
1722.6+2436	[HB89] 1720+246	17 22 41.2	24 36 19.4	0.1750	16.38	0.028	0.035	0.00	0.3366E-11	G		q	
1723.3+3417	4C +34.47	17 23 20.8	34 17 57.9	0.2060	15.46	0.370	0.493	1.07	0.2061E-10	Q		q	
1723.3+3630	RBS 1645	17 23 23.2	36 30 10.2	0.0400	17.08	0.000	0.003#	0.00	0.4705E-11	G		5	
1723.9+3748	FBQS J172354.2+.	17 23 54.3	37 48 41.6	0.8280	17.72	0.000	0.002#	0.00	0.7500E-12	Q		q	
1724.2+3303	[HB89] 1722+330	17 24 14.2	33 03 03.9	1.8700	20.80	0.000	0.432#	-0.43	0.4269E-12	Q		q	
	3C 356	17 24 19.0	50 57 40.3	1.0790	21.50	0.000	0.377	1.20	0.2324E-13	G		n	II
1725.0+1152	RGB J1725+118	17 25 04.4	11 52 15.2	0.0180	15.77	0.088	0.144	0.00	0.2892E-10	G		z	
1726.5+3957	[HB89] 1724+399	17 26 32.7	39 57 02.2	0.6600	18.40	0.274	0.296	0.38	0.8216E-12	Q		q	
	B3 1726+455	17 27 27.6	45 30 39.7	0.7170	18.10	0.897	1.066	-0.74	0.4632E-12	Q		q	
1728.2+5013	PGC 060348	17 28 18.6	50 13 10.5	0.0554	15.97	0.168	0.000	0.15	0.3741E-10	Q		z	

Table A.3: *(continued)*

RXJ name (1)	Name (2)	RA(J2000) (3)	DEC(J2000) (4)	z (5)	m_V (6)	F_{5GHz}^{core} (7)	F_{5GHz} (8)	α_r (9)	$F_{0.1-2.4\ keV}$ (10)	Type (11)	Host (12)	Class. (13)	FR (14)
1728.4+0426	[HB89] 1725+044	17 28 24.9	04 27 04.9	0.2960	16.99	0.980	0.000	0.40	0.1457E-11	Q		q	
1728.9+3838	[HB89] 1727+386	17 28 59.1	38 38 26.4	1.3900	17.19	0.172	0.219	0.23	0.7866E-12	Q		q	
1731.0+5007	[HB89] 1729+501	17 31 03.6	50 07 34.0	1.1070	17.50	0.038	0.414	0.81	0.1023E-11	Q		q	
1731.2+3232	RBS 1652	17 31 14.5	32 32 48.0	0.3750	17.80	0.037	0.224	0.00	0.4423E-11	Q		q	
1732.2+7123	MCG +12-16-046	17 32 33.0	71 24 10.4	0.0590	16.00*	0.004	0.187	-0.02	0.2495E-12	G		r	I
	FIRSTJ173300.4+.	17 33 00.5	40 36 43.4	0.1361	16.60*	0.000	0.020#	0.00	0.3031E-11	GC			
1733.0-1304	[HB89] 1730-130	17 33 02.7	-13 04 49.5	0.9020	19.50	0.000	4.099	-0.35	0.5891E-11	Q		q	
	B3 1732+389	17 34 20.6	38 57 51.4	0.9700	20.60	0.000	0.555	0.27	0.3365E-12	Q		q	
	4C +16.49	17 34 42.6	16 00 31.2	1.8800	19.60	0.016	0.320	1.20	0.3250E-12	Q		q	II
1737.5+1107	CGCG 1735.2+1110	17 37 33.4	11 07 18.3	0.0216	14.25*	0.043	0.066	0.00	0.1427E-11	G	E		
	PKS 1733-56	17 37 35.8	-56 34 03.1	0.0980	17.00	0.680	3.370	0.73	0.1460E-11	G		b	II
	S4 1738+47	17 39 57.1	47 37 58.4	0.3160	17.50	0.000	0.815	-0.27	0.3985E-12	Q		z	
1740.5+5211	4C +51.37	17 40 36.9	52 11 43.4	1.3750	18.70	0.000	1.899	-0.17	0.1070E-11	Q		q	
1741.1+0348	IRAS F17389+035	17 41 28.3	+03 48 52.9	0.0300	15.30*	0.000	0.014#	0.00	0.3250E-10	G		l	
1742.1+1827	PKS 1739+184	17 42 06.9	18 27 20.7	0.1860	17.50	0.025	0.333	0.10	0.5888E-11	Q		q	
1742.7+6146	4C +61.34	17 42 51.5	61 45 54.0	0.5230	18.50	0.000	0.531	0.85	0.2642E-12	Q		q	
	7C 1743+6344	17 43 23.1	63 42 58.6	0.3240	21.50	0.000	0.062	1.30	0.8238E-12	GC		l	
1743.9+2751	B2 1741+27	17 43 56.5	27 52 49.9	0.3720	17.70	0.000	0.329	0.74	0.1926E-11	Q		q	
1743.8+1935	NPM1G +19.0510	17 43 57.8	19 35 09.0	0.0840	16.80	0.157	0.353	0.45	0.9474E-11	G		z	
1743.9-034	MRC 1741-038	17 43 58.8	-03 50 04.6	1.0540	20.40	0.000	2.299	-0.30	0.3730E-11	Q		q	
1744.1+3259	RGB J1744+329	17 44 14.5	32 59 29.4	0.0757	13.50*	0.070	0.077	0.42	0.1701E-10	GC			
1744.9+5542	NGC 6454	17 44 56.6	55 42 17.1	0.0304	14.60*	0.292	0.562	0.31	0.9472E-12	GC	S	a	
1745.5+3951	B3 1743+398B	17 45 37.6	39 51 31.7	0.2670	18.30	0.118	0.249	0.69	0.1449E-11	G		z	
1746.1+6226	4C +62.29	17 46 14.0	62 26 54.7	3.8890	18.80	0.452	0.589	0.07	0.6782E-12	Q		q	
1748.5+7005	[HB89] 1749+701	17 48 32.8	70 05 50.8	0.7700	17.01	0.610	0.715	0.07	0.1407E-11	Q		z	
1750.0+4700	B3 1748+470	17 50 05.0	47 00 43.4	0.1600	19.00	0.010	0.046	0.00	0.3878E-11	G		z	
1750.2+3504	RGB J1750+350	17 50 16.8	35 04 58.7	0.1705	11.60*	0.027	0.032	0.00	0.4651E-11	GC			
1751.3+5045	IRAS 17500+504	17 51 16.6	+50 45 37.3	0.2997	15.40*	0.000	0.011#	0.00	0.9360E-11	G		l	
1751.4+4713	RGB J1751+472	17 51 31.6	47 13 22.0	1.4800	17.10	0.034	0.049	-0.01	0.1520E-11	G		q	
1751.5+0938	4C +09.57	17 51 32.8	09 39 00.7	0.3220	16.78	1.695	2.455	-0.58	0.2950E-11	Q		q	
	7C 1751+6455	17 51 52.8	64 54 33.3	0.2940	17.00	0.000	0.058	0.60	0.1993E-13	G		l	
1752.7+1733	[HB89] 1750+175	17 52 46.0	17 34 20.3	0.5040	16.60	0.364	0.437	-0.17	0.2083E-11	Q		q	
1753.3+4409	B3 1751+441	17 53 22.6	44 09 45.7	0.8710	19.68	0.900	1.000	-0.04	0.6246E-12	Q		q	
	RGB J1753+580	17 53 58.9	58 05 08.1	0.2276	18.90*	0.004	0.066	0.90	0.1382E-11	GC			

Table A.3: *(continued)*

RXJ name (1)	Name (2)	RA(J2000) (3)	DEC(J2000) (4)	z (5)	m_V (6)	F_{5GHz}^{core} (7)	F_{5GHz} (8)	α_r (9)	$F_{0.1-2.4\ keV}$ (10)	Type (11)	Host (12)	Class. (13)	FR (14)
	7C 1754+6737	17 54 22.3	67 37 35.8	3.6000	19.80	0.000	0.032	0.00	0.1814E-12	Q			
	IRAS 17550+6520	17 55 05.6	65 19 54.8	0.0803	15.50*	0.000	0.001#	0.00	0.2107E-11	G	S	1	
1755.1+3351	RGB J1755+338	17 55 11.2	33 50 59.8	0.2420	17.90	0.158	0.139	-0.05	0.1329E-11	G		q	
	NGC 6521	17 55 48.4	62 36 44.1	0.0275	13.90	0.000	0.189	0.28	0.1403E-11	GC	c	9	
	WN B1756+6531	17 56 40.1	65 31 46.2	2.7900	22.00*	0.000	0.047	0.00	0.3367E-13	Q		q	
	RGB J1757+538	17 57 06.7	53 51 37.7	0.1190	13.40*	0.031	0.042	0.29	0.2616E-11	GC	c		
1757.2+7033	MS 1757.7+7034	17 57 13.2	70 33 37.4	0.4070	18.27	0.000	0.007	0.00	0.8061E-11	Q		z	
1757.4+5522	RGB J1757+553	17 57 28.3	55 23 12.1	0.0650	13.70*	0.040	0.073	0.07	0.1660E-12	G		a	
1800.1+6636	NGC 6552	18 00 07.3	66 36 54.3	0.0265	14.60	0.000	0.040	0.00	0.1137E-12	G	S	2	
1800.3+3848	B3 1758+388B	18 00 24.8	38 48 30.7	2.0920	17.98	0.800	0.000	-0.66	0.1195E-11	Q		q	
1800.7+7828	[HB89] 1803+784	18 00 45.7	78 28 04.0	0.6800	15.90	0.000	2.222#	-0.28	0.1484E-11	Q		q	
	8C 1801+690	18 01 14.6	69 02 44.0	1.2710	19.70	0.000	0.132#	0.60	0.1384E-12	Q		q	
1801.5+4404	[HB89] 1800+440	18 01 32.3	44 04 21.9	0.6630	17.90	0.600	1.193	-0.14	0.1335E-11	Q		q	
1804.0+0042	RGB J1804+007	18 04 09.0	00 42 22.1	0.0700	13.90*	0.158	0.155	0.02	0.1627E-10	G	E		
	TXS 1802+179	18 04 42.5	17 55 59.0	0.4350	19.40	0.000	0.090	-0.77	0.2873E-12	Q		1	
1804.8+5224	RGB J1804+524	18 04 52.7	52 24 29.4	0.5160	17.00	0.007	0.024	0.00	0.6752E-12	G		q	
1807.0+6949	UGC 11130	18 06 50.6	69 49 28.1	0.0510	14.22	0.950	2.121	-0.02	0.3698E-11	GC		z	
1807.9+4349	B3 1806+438	18 07 59.8	43 50 36.0	0.8150	17.10	0.000	0.054	0.00	0.5391E-12	G		q	
1808.7+6634	EF B1808+6633	18 08 49.5	66 34 29.0	0.6970	17.50	0.006	0.021	1.35	0.5281E-12	G		q	
1811.0+4954	NGC 6582 NED01	18 11 01.8	+49 54 42.8	0.0481	16.00*	0.000	0.018#	0.00	0.6640E-11	G	E		
1813.5+3144	EXO 1811.7+3143	18 13 35.2	31 44 17.7	0.1170	17.40	0.074	0.127	0.24	0.1244E-11	G		z	
1814.5+4057	RGB J1814+409B	18 14 34.5	40 57 46.4	0.9710	19.00	0.007	0.022	0.00	0.5251E-12	G		q	
1815.3+6806	4C +68.20	18 15 24.8	68 06 32.0	0.2300	17.80	0.053	0.187	0.39	0.5637E-12	G		1	
	PKS 1814-63	18 19 35.0	-63 45 48.2	0.0627	16.00	0.000	4.370	0.92	<0.7600E-12	G		g	
1819.6+6708	RGB J1819+671	18 19 44.4	67 08 47.2	0.2200	17.54	0.102	0.162	0.80	0.1005E-12	G	E	g	
1821.8+6419	RGB J1821+643	18 21 57.3	64 20 36.4	0.2970	14.24	0.007	0.070	0.00	0.2412E-10	GC		q	
1823.1+3324	RGB J1823+334	18 23 09.8	33 24 39.1	0.1080	14.90*	0.003	0.051	1.10	0.2163E-11	G		a	
1824.0+1044	[HB89] 1821+107	18 24 02.8	10 44 23.8	1.3600	17.27	1.300	0.000	-0.30	0.1170E-11	Q		q	
1824.1+5650	S4 1823+56	18 24 07.1	56 51 01.5	0.6640	19.30	1.120	1.262	-0.23	0.2310E-11	QC		q	
	NVSSJ182608-...	18 26 08.1	-36 50 49.0	0.8880	18.80	0.000	0.514#	0.00	0.5918E-12	Q		q	
1826.5+6706	7C 1826+6704	18 26 37.5	67 06 45.0	0.2870	17.70	0.013	0.071	0.00	0.5666E-12	G	E	q	
	PKS 1823-455	18 27 10.2	-45 33 09.5	1.2440	18.10	0.000	0.470	0.40	0.6896E-12	Q		q	
1829.4+4843	3C 380	18 29 31.8	48 44 46.6	0.6920	16.18	4.500	5.519	0.58	0.4868E-11	Q		g	
1832.1+6848	87GB 183253.8+6	18 32 35.5	+68 48 07.1	0.2050	15.70*	0.000	0.150#	0.00	0.5170E-11	GC	E	z	

Table A.3: *(continued)*

RXJ name (1)	Name (2)	RA(J2000) (3)	DEC(J2000) (4)	z (5)	m_V (6)	F_{5GHz}^{core} (7)	F_{5GHz} (8)	α_r (9)	$F_{0.1-2.4\ keV}$ (10)	Type (11)	Host (12)	Class. (13)	FR (14)
1832.8+2833	B2 1830+28A	18 32 50.2	28 33 35.9	0.5940	17.16	0.496	0.984	0.28	0.2319E-11	Q		q	
1833.6-2103	PKS 1830-21	18 33 39.9	-21 03 39.8	2.5070	18.70	0.000	8.880	0.30	0.2532E-11	Q		q	
1833.6+6521	4C +65.23	18 33 43.3	65 21 37.9	0.1610	17.00	0.044	0.767	0.87	0.6002E-12	G	E		
1835.0+3241	3C 382	18 35 03.4	32 41 46.8	0.0578	15.39	0.146	2.193	0.26	0.5845E-10	G		b	II
	PKS 1831-711	18 37 28.7	-71 08 43.5	1.3560	17.40	0.000	1.149	0.90	0.1440E-11	Q		q	
	3C 386	18 38 26.2	17 11 49.7	0.0169	12.93*	0.000	2.580	1.06	0.4295E+02*	G	E		I
	IVS B1839+548	18 40 57.4	54 52 15.9	0.6460	19.40	0.000	0.257	0.00	0.4813E-12	Q		g	
1841.2+5906	RGB J1841+591	18 41 20.3	59 06 08.2	0.5300	19.70	0.006	0.019	0.00	0.6113E-12	G		z	
1842.1+7946	3C 390.3	18 42 08.9	79 46 17.1	0.0561	15.38	0.340	4.448	0.75	0.1052E-10	G		b	II
1842.4+6809	8C 1842+681	18 42 33.6	68 09 25.2	0.4720	18.10	0.700	0.925	-0.12	0.1418E-11	Q		q	
1842.9+3150	MG2 J184303+3150	18 43 03.0	31 50 26.0	0.4477	18.20	0.042	0.142	0.78	0.1642E-11	Q		q	
	PKS 1839-48	18 43 14.6	-48 36 23.1	0.1112	17.50	0.163	1.280	0.75	<0.1650E-11	G			I
1844.0+4532	3C 388	18 44 02.4	45 33 29.7	0.0910	15.56	0.062	1.770	0.82	0.3508E-11	GC		w	II
1844.4+5441	RGB J1844+546	18 44 30.8	54 41 44.0	0.2340	17.20	0.032	0.034	0.00	0.7641E-12	G		q	
1854.8+7351	S5 1856+73	18 54 57.3	73 51 19.9	0.4610	16.80	0.600	0.000	0.16	0.1994E-11	Q		q	
	PMN J1911-2102	19 11 53.9	-21 02 43.1	1.4200	17.00	0.000	0.620#	0.00	0.7052E-12	Q		q	
1916.9+7014	RGB J1917+702	19 17 01.0	70 14 16.9	0.1000	15.45	0.007	0.084	0.50	0.8899E-12	G	E		
	MRC 1914-455	19 17 39.6	-45 30 31.1	0.3640	16.80	0.000	0.180	0.86	0.1964E-11	Q		q	
1922.1+6910	RGB J1922+691	19 22 14.6	69 11 12.4	0.0970	17.00	0.020	0.322	0.70	0.2174E-11	G		1	
1924.8-2914	[HB89] 1921-293	19 24 51.0	-29 14 30.1	0.3520	18.21	0.000	10.599	0.00	0.5747E-11	Q		q	
	4C +50.47	19 26 06.3	50 52 57.0	1.0980	17.90	0.000	0.356	0.50	0.7715E-12	Q		q	
1927.7+6533	WN B1927+6527	19 27 19.5	+65 33 54.2	0.0170	15.40*	0.000	0.040#	0.00	0.4480E-10	G	S	2	
	[HB89] 1928+738	19 27 48.5	73 58 01.6	0.3021	16.06	0.000	3.927#	0.07	0.8479E-11	Q		q	
1931.6-3354	MRC 1928-340	19 31 38.6	-33 54 43.4	0.0980	17.00*	0.000	0.190	0.85	0.7960E-11	GC	E	r	
1932.7-4536	PKS 1929-457	19 32 44.9	-45 36 37.9	0.6520	18.40	0.000	0.680	-0.50	0.1019E-11	Q		g	
	PKS 1932-46	19 35 56.5	-46 20 40.6	0.2310	18.50	0.000	3.470	1.03	0.2100E-12	G			II
1937.2-3958	MRC 1933-400	19 37 16.2	-39 58 01.5	0.9650	19.00	0.000	1.439	-0.30	0.1816E-11	Q		q	
	PKS 1934-63	19 39 25.0	-63 42 45.6	0.1830	18.40	0.000	6.450	0.88	<0.1140E-11	G		g	
	PKS 1936-15	19 39 26.6	-15 25 43.0	1.6570	20.30	0.000	1.639	1.00	0.1200E-11	Q		q	
1939.9-1002	PKS 1937-101	19 39 57.2	-10 02 41.5	3.7870	17.00	0.000	0.660	0.10	0.1224E-11	Q		q	
	3C 401	19 40 25.1	60 41 34.9	0.2011	18.00	1.542	1.360	0.71	0.6814E-12	GC	E	s	II
	PKS 1938-15	19 41 15.1	-15 24 31.3	0.4520	20.00	0.000	2.339	0.82	0.4600E-12	Q		1	
1942.3-1019	NGC 6814	19 42 40.6	-10 19 24.6	0.0052	12.10*	0.000	0.052#	0.00	0.1670E-10	G	S	5	
1946.5-5700	[HB89] 1942-571	19 46 34.4	-57 00 27.5	0.5270	16.93	0.000	0.140	0.90	0.3148E-11	Q		q	

Table A.3: *(continued)*

RXJ name (1)	Name (2)	RA(J2000) (3)	DEC(J2000) (4)	z (5)	m_V (6)	F_{5GHz}^{core} (7)	F_{5GHz} (8)	α_r (9)	$F_{0.1-2.4\ keV}$ (10)	Type (11)	Host (12)	Class. (13)	FR (14)
	3C 403	19 52 15.8	02 30 24.5	0.0590	16.50	0.010	2.390	0.73	0.3667E-12	G	E	n	II
	[HB89] 1951+498	19 52 35.8	49 58 13.9	0.4660	18.40	0.000	0.206	0.52	0.2035E-11	Q		q	
1955.6+5131	[HB89] 1954+513	19 55 42.7	51 31 48.5	1.2200	18.50	1.100	1.675	-0.12	0.1548E-11	Q		q	
	PKS 1954-388	19 57 59.8	-38 45 06.3	0.6300	17.07	0.000	2.000	0.00	0.1461E-11	Q		q	
	PKS 1954-55	19 58 29.1	-55 09 12.5	0.0584	16.50*	0.050	2.310	0.78	0.1470E-11	GC	0		I
	Cygnus A	19 59 28.3	40 44 01.9	0.0561	15.10	0.776	415.000	0.74	0.6245E-10	GC	E	n	II
	TXS 1959+650	19 59 59.8	65 08 54.6	0.0470	12.80	0.000	0.246	0.00	0.9478E-10	G	E	z	
	[HB89] 1958-179	20 00 57.1	-17 48 57.7	0.6500	18.60	0.000	1.169	-1.50	0.3443E-11	Q		q	
	PKS 2000-330	20 03 24.1	-32 51 45.1	3.7730	17.30	0.000	1.199	-0.85	0.3500E-12	Q		g	
2003.5-0857		20 03 54.4	-08 56 42.9	0.0572	16.50*	0.000	0.009#	0.00	0.5790E-11	G		z	
2005.2-1821	[HB89] 2002-185	20 05 17.3	-18 22 03.3	0.8680	19.20	0.000	0.480	0.47	0.9578E-12	Q		q	
	S5 2007+77	20 05 30.9	77 52 43.1	0.3420	16.70	0.000	1.950	0.00	0.1084E-11	Q		z	
2006.1-3433	ESO 399-IG 020	20 06 57.9	-34 32 54.7	0.0250	17.00*	0.000	0.009#	0.00	0.1320E-10	G		1	
2009.4-4849	[HB89] 2005-489	20 09 25.4	-48 49 53.7	0.0710	12.81	0.000	1.189	-0.20	0.6653E-10	Q		z	
	PKS 2008-159	20 11 15.7	-15 46 40.2	1.1800	18.30	0.000	1.350	-0.40	0.3631E-11	Q		q	
2016.4-3035	PKS 2013-307	20 16 29.8	-30 35 18.5	0.9780	20.10	0.000	0.340	0.00	0.8836E-12	Q		q	
2017.1+7440	4C +74.25	20 17 13.1	74 40 47.9	2.1870	18.10	0.273	0.535	0.06	0.9723E-12	Q		q	
2020.1+2942	3C 410	20 20 06.5	29 42 14.2	0.2485	19.50	3.827	3.790	0.81	0.4320E-11	G		r	II
2022.1+1001	3C 411	20 22 08.4	10 01 11.7	0.4670	19.40	1.006	0.920	0.82	0.1706E-11	G	N	q	
2024.3-5723	IRAS F20203-5733	20 24 20.6	-57 23 43.5	0.3520	18.50	0.000	1.050	0.70	0.1387E-11	G			
	PKS 2022+031	20 25 09.6	03 16 44.5	2.2100	19.40	0.000	0.310	-0.40	0.9470E-12	Q		q	
2027.0-2136	MRC 2024-217	20 27 04.3	-21 36 19.2	0.4630	19.60	0.000	0.430	1.13	0.1912E-11	Q			
	PKS 2029+121	20 31 54.9	12 19 41.3	1.2150	19.20	0.000	1.290	0.00	0.1388E-11	Q		q	
2033.2-2253	MRC 2030-230	20 33 16.6	-22 53 17.1	0.1319	18.00	0.000	0.950	0.39	0.2042E-11	G	N	b	II
2034.1-3037	PGC 064989	20 34 31.3	-30 37 28.8	0.0190	13.30*	0.000	0.003#	0.00	0.5020E-11	G		1	
	PKS 2032+107	20 35 22.3	10 56 06.8	0.6010	16.37	0.000	0.770	0.20	0.9042E-12	Q		q	
	PMN J2038-2011	20 38 27.7	-20 11 07.0	0.5200	17.70	0.000	0.374	1.59	0.2634E-11	Q		q	
	3C 418	20 38 37.0	51 19 12.7	1.6860	21.00	0.000	3.810	0.40	0.4685E-12	Q		q	
2039.2-3018	RBS 1688	20 39 27.0	-30 18 53.0	0.0800	16.00*	0.000	0.006#	0.00	0.1260E-10	G		!	
	PKS 2037-253	20 40 08.8	-25 07 46.7	1.5740	20.30	0.000	1.169	-0.37	<0.2260E-12	Q		q	
2040.1-0247	4C -03.72	20 40 08.9	-02 47 38.8	0.1920	18.50	0.000	0.240	0.50	0.9535E-12	G		r	
	4C +74.26	20 42 37.3	75 08 02.4	0.1040	15.13	0.000	0.363	1.15	0.2245E-10	Q		q	
	MRC 2040-219	20 43 14.6	-21 44 34.1	0.2040	17.20*	0.000	0.098	1.20	0.3951E-11	G		r	
2044.9-1043	MRK 0509	20 44 09.7	-10 43 24.5	0.0344	13.00*	0.000	0.019#	0.00	0.9800E-10	G		1	

Table A.3: *(continued)*

RXJ name (1)	Name (2)	RA(J2000) (3)	DEC(J2000) (4)	z (5)	m_V (6)	F_{5GHz}^{core} (7)	F_{5GHz} (8)	α_r (9)	$F_{0.1-2.4\ keV}$ (10)	Type (11)	Host (12)	Class. (13)	FR (14)
2045.7-6133	[HB89] 2041-617	20 45 44.5	-61 33 04.6	0.2740	18.30	0.000	0.382#	0.00	0.3540E-11	Q		1	
	3C 422	20 47 10.3	-02 36 22.2	0.9420	20.30	0.000	0.830	0.90	0.2100E-12	Q		g	
2056.0-1956	MRC 2053-201	20 56 04.3	-19 56 35.5	0.1560	19.00*	0.000	0.990	0.54	0.2539E-11	G	E	r	II
2056.2-4714	PKS 2052-47	20 56 16.3	-47 14 47.6	1.4890	18.10	0.000	2.450	0.70	0.1129E-11	Q		q	
	PKS 2058-28	21 01 37.7	-28 01 54.9	0.0397	15.60	0.063	2.000	0.74	<0.8400E-12	GC	E		I
2101.6+0341	[HB89] 2059+034	21 01 38.8	03 41 31.3	1.0130	17.78	0.500	1.362	-0.29	0.1212E-11	Q		q	
2102.4-2432	QW 2059-247	21 02 09.8	-24 32 01.0	0.1899	16.50*	0.000	0.069#	0.00	0.6140E-11	G			
2102.7+1058	CGCG 425-034	21 02 21.6	+10 58 16.0	0.0287	15.40*	0.000	0.007#	0.00	0.7070E-11	G		5	
	NGC 7018	21 07 25.3	-25 25 39.9	0.0388	16.80	0.058	4.309	0.89	0.1270E-11	GC			II
2109.1-0940	H 2106-099	21 09 09.9	-09 40 14.7	0.0268	14.30*	0.000	0.006#	0.00	0.5180E-10	G		l	
2109.5-4110	PKS 2106-413	21 09 33.2	-41 10 20.6	1.0580	20.30	0.000	2.310	-0.13	0.1008E-11	Q		q	
	S5 2116+81	21 14 01.2	82 04 48.3	0.0840	15.70	0.155	0.376	0.22	0.1420E-10	G		1	I
	B2 2113+29B	21 15 29.4	29 33 38.4	1.5140	20.60	0.000	1.165	-0.21	0.4625E-12	Q		q	
2118.1-3019	PKS 2115-30	21 18 10.6	-30 19 11.6	0.9790	16.47	0.000	0.860	0.60	0.1719E-11	Q		q	
2118.7-0636	FBQS J2118-0636	21 18 43.2	-06 36 19.1	0.3280	17.00	0.000	0.075#	0.00	0.3132E-11	G		q	
2121.3-2629	MRC 2118-266	21 21 18.4	-26 28 54.3	0.3430	18.90	0.051	0.280#	0.86	0.9341E-12	G			
2123.4-1036	PMN J2123-1036	21 23 07.2	-10 36 49.4	0.0227	17.56*	0.000	0.119#	0.00	0.1370E-10	G		z	
2123.2+1008	PKS 2120+09	21 23 13.3	10 07 54.9	0.9320	19.30	0.301	0.527	0.43	0.6658E-12	Q		q	
2123.2+0646	RGB J2123+067	21 23 19.3	06 46 22.9	0.1860	18.00	0.011	0.071	0.00	0.9652E-12	G		b	
2123.6-0139	FBQS J2123-0139	21 23 36.0	-01 39 47.4	0.4940	19.36	0.000	0.001#	0.00	0.1657E-11	Q		q	
	PKS 2121+053	21 23 44.5	05 35 22.1	1.8780	20.40	0.000	3.160	-1.08	0.9779E-12	Q		q	
	3C 433	21 23 44.5	25 04 11.9	0.1016	15.70*	0.005	28.000&	1.11	<0.8801E-13	GC			II
	PMN J2125-2338	21 25 52.1	-23 38 15.3	1.7740	18.10	0.000	0.553#	0.00	0.1712E-11	Q		q	
	[HB89] 2126-158	21 29 12.2	-15 38 41.0	3.2680	17.00	0.000	1.240	0.51	0.3023E-11	Q		g	
2129.7+0035	FBQS J2129+0035	21 29 40.7	00 35 27.9	0.4250	20.00	0.000	0.006#	0.00	0.9730E-12	Q		z	
2130.0+0307	PKS J2130+0308	21 30 02.2	03 07 48.9	0.0877	17.00	0.000	0.140	0.62	0.2245E-11	G	E		
2131.4-3121	MRC 2128-315	21 31 23.2	-31 21 12.6	0.9900	19.20	0.000	0.480	0.25	0.6909E-12	Q		q	
2131.5-1207	RBS 1753	21 31 35.3	-12 07 04.8	0.5010	16.11	0.000	2.000	-0.08	0.5523E-11	Q		q	
	[HB89] 2131-021	21 34 10.3	-01 53 17.2	1.2850	19.00	0.000	2.669	-0.07	0.3841E-12	Q		q	
2136.6+0042	PHL 61	21 36 38.6	00 41 54.2	1.9320	16.79	4.817	10.938	0.12	0.1943E-11	Q		g	
	PHL 1657	21 37 45.2	-14 32 55.8	0.2003	15.53	0.121	1.379	0.80	0.1116E-10	Q	E	q	
	PKS 2135-209	21 37 49.9	-20 42 31.9	0.6350	19.80	0.000	1.530	0.63	<0.1600E-12	G		g	
2138.0+3205	CGCG 493-002	21 38 33.4	+32 05 05.8	0.0248	15.60*	0.000	0.007#	0.00	0.8560E-11	G		5	
	PKS 2136+141	21 39 01.3	14 23 35.9	2.4270	18.90	0.000	1.110	-0.10	0.7200E-12	Q		q	

Table A.3: *(continued)*

RXJ name (1)	Name (2)	RA(J2000) (3)	DEC(J2000) (4)	z (5)	m_V (6)	F_{5GHz}^{core} (7)	F_{5GHz} (8)	α_r (9)	$F_{0.1-2.4\ keV}$ (10)	Type (11)	Host (12)	Class. (13)	FR (14)
2141.8-3729	PKS 2138-377	21 41 52.4	-37 29 11.9	0.4250	18.06	0.000	0.350	0.20	0.5605E-12	Q		q	
2142.6-0437	MRC 2139-048	21 42 36.9	-04 37 43.5	0.3440	18.00	0.000	0.600	0.40	0.3042E-11	Q		q	
2143.6+1743	MRC 2141+174	21 43 35.5	17 43 48.0	0.2111	15.73	0.386	1.006	-0.21	0.1544E-11	Q		q	
	MRC 2140-568	21 43 59.2	-56 37 20.8	0.0815	15.40*	0.000	0.039	0.00	0.9180E-11	G		r	
2145.3+1115	[HB89] 2142+110	21 45 18.8	11 15 27.3	0.5500	18.80	0.367	0.414	-0.10	0.1584E-11	Q		q	
2145.6-0434	NPM1G -04.0578	21 45 33.4	-04 34 39.1	0.0697	16.20*	0.000	0.068#	0.00	0.3740E-11	G		z	
2145.8+0719	RGB J2145+073	21 45 52.3	07 19 27.2	0.2370	18.04	0.037	0.066	0.00	0.9331E-11	G		z	
2146.3-1525	MRC 2143-156	21 46 22.9	-15 25 43.9	0.7010	17.27	0.000	0.820	0.49	0.1003E-11	Q		g	
2146.8+0920	RGB J2146+093	21 46 54.1	09 20 48.9	0.9810	17.10	0.050	0.070	0.00	0.1821E-11	G		q	
2147.0-1019		21 47 00.4	-10 19 11.9	0.0797	16.10*	0.000	0.020#	0.00	0.4300E-11	G		z	
	PKS 2144+092	21 47 10.2	09 29 46.7	1.1130	18.54	0.000	1.010	-0.10	<0.2690E-12	Q		q	
	PKS 2142-75	21 47 12.7	-75 36 13.2	1.1390	17.30	0.000	1.280	-0.60	0.1410E-11	Q		q	
2148.0+0657	MRC 2145+067	21 48 05.4	06 57 38.6	0.9900	16.47	2.656	4.134	-0.64	0.2851E-11	Q		q	
2148.5-1723	PKS 2145-17	21 48 36.8	-17 23 44.0	2.1300	19.50	0.000	0.790	0.06	0.4491E-12	Q		q	
	MRC 2147-192	21 49 58.1	-18 59 23.8	0.1581	17.90	0.000	0.245	0.00	0.1069E-10	G		1	
2150.6-1410	RBS 1787	21 50 15.5	-14 10 50.1	0.2290	18.50*	0.000	0.068#	0.00	0.1510E-10	Q		z	
	PKS 2148-427	21 51 21.8	-42 33 34.7	0.0610	16.10	0.000	0.220	0.50	0.4976E-13	G	E	n	
	PKS 2149+069	21 51 31.4	07 09 26.8	1.3640	18.80	0.000	0.940	-0.09	<0.4190E-12	Q		q	
	PKS 2149+056	21 51 37.9	05 52 12.9	0.7400	19.50	0.000	1.189	-0.27	<0.4130E-12	Q		g	
2151.9-3027	PKS 2149-306	21 51 55.5	-30 27 53.7	2.3450	17.90	0.000	1.149	0.22	0.7618E-11	Q		g	
	PKS 2151-153	21 54 07.5	-15 01 31.0	1.2080	16.50	0.000	0.310	1.20	0.7580E-12	Q		q	
2155.6+1231	4C +12.76	21 55 42.3	12 31 27.0	0.1924	19.00*	0.153	0.684#	1.00	0.4528E-11	GC	E		
2155.8+3759	3C 438	21 55 52.3	38 00 29.6	0.2900	19.34	1.692	1.540	1.25	0.3877E-11	GC		r	II
2156.3+3318	RGB J2156+333	21 56 23.0	33 18 35.9	0.0790	16.20*	0.005	0.027	0.10	0.1814E-10	G			
2157.2+1014	[HB89] 2154+100	21 57 12.9	10 14 24.8	0.7610	17.70	0.363	0.000	0.00	0.7815E-12	Q		q	
2158.1-1500	PKS 2155-152	21 58 06.3	-15 01 09.3	0.6720	18.30	0.000	1.580	0.09	0.1526E-11	Q		q	
2158.5-2006	APMBGC 601+092+	21 58 22.5	-20 06 14.6	0.0578	15.50*	0.000	0.035#	0.00	0.2420E-11	G	E		
2158.3+2652	4C +26.59	21 58 25.4	26 52 37.5	0.7130	17.40	0.148	0.500#	0.69	0.1454E-11	G		a	
	RBS 1807	21 58 52.1	-30 13 32.1	0.1160	13.09	0.000	0.310	0.00	0.8039E-10	Q		z	
2159.4+0113	IRAS F21568+0058	21 59 24.0	01 13 05.3	1.0000	16.60	0.000	0.001#	0.00	0.1410E-11	G		q	
2201.1-0053	FBQS J2201-0052	22 01 03.1	-00 52 59.6	0.2130	16.70	0.000	0.001#	0.00	0.3782E-11	G		q	
2201.0+0504	PMN J2201+0504	22 01 07.5	05 04 43.4	0.2330	17.90*	0.000	0.134#	0.37	0.1666E-11	G		b	
2201.0-1706		22 01 55.8	-17 07 00.3	0.1686	16.70*	0.000	0.005#	0.00	0.4330E-11	G		z	
2202.7+4216	BL LACERTAE	22 02 43.3	42 16 39.9	0.0686	14.72	2.307	2.940	-0.13	0.5545E-11	Q		z	

Table A.3: *(continued)*

RXJ name (1)	Name (2)	RA(J2000) (3)	DEC(J2000) (4)	z (5)	m_V (6)	F^{core}_{5GHz} (7)	F_{5GHz} (8)	α_r (9)	$F_{0.1-2.4\ keV}$ (10)	Type (11)	Host (12)	Class. (13)	FR (14)
2203.2+3145	4C +31.63	22 03 14.9	31 45 38.3	0.2950	15.58	1.399	2.806	0.11	0.8588E-11	Q		q	
	PKS 2201+171	22 03 26.9	17 25 48.2	1.0750	19.50	0.000	0.590	0.15	0.5000E-12	Q		q	
2204.6-0857		22 04 07.5	-08 57 11.2	0.1154	16.10*	0.000	0.003#	0.00	0.3730E-11	G		8	
2204.2+0439	4C +04.77	22 04 17.6	04 40 02.0	0.0270	15.20	0.264	0.653	0.84	0.1532E-11	G	E	z	
	PKS 2203-18	22 06 10.4	-18 35 38.7	0.6200	18.50	0.000	4.280	0.33	0.1600E-12	Q		q	
2206.3-3005	RX J2206.1-3005	22 06 11.0	-30 05 06.5	0.1650	19.10*	0.000	0.011#	0.00	0.1480E-11	G		1	
	LBQS 2203-2134	22 06 41.3	-21 19 40.0	0.5760	18.70	0.000	0.240	-0.60	0.1434E-11	Q		q	
	PMN J2207+0042	22 07 19.8	00 41 56.9	1.8800	20.20	0.000	0.143	0.00	0.6115E-12	Q		q	
2207.6-5346	MRC 2204-540	22 07 43.7	-53 46 33.8	1.2060	18.40	0.000	1.320	0.50	0.9150E-12	Q		q	
2209.9-2748	NGC 7214	22 09 07.7	-27 48 34.1	0.0231	13.10*	0.000	0.029#	0.00	0.1010E-10	GC	S	1	
2209.4-2453	MRC 2206-251	22 09 22.9	-24 53 33.0	0.1580	18.00	0.015	0.270	0.70	0.7753E-12	G	N	r	
	MRC 2208-137	22 11 24.1	-13 28 09.7	0.3920	17.00	0.000	0.530	0.50	0.2944E-11	Q		q	
2211.5-3707	CTS 0377	22 11 50.5	-37 07 04.0	0.3200	16.10*	0.000	0.187#	0.00	0.1160E-11	Q		q	
2211.9+1841	RGB J2211+186	22 11 53.7	18 41 51.4	0.0700	15.44	0.117	0.134	-0.22	0.6037E-11	G		1	
2212.0+0819	PKS 2209+08	22 12 01.6	08 19 16.0	0.4840	19.10	0.225	0.742	0.50	0.1636E-11	Q		q	
2213.5-1710		22 13 00.3	-17 10 17.7	0.1460	16.70*	0.000	0.003#	0.00	0.7870E-11	G		1	
	PKS 2210-25	22 13 02.5	-25 29 30.1	1.8330	19.00	0.000	1.020	-0.10	<0.3360E-12	Q		q	
2214.4-1701	3C 444	22 14 25.7	-17 01 35.9	0.1530	17.80*	0.002	2.140	0.88	0.2334E-11	G		n	II
2214.8+1351	3C 442A	22 14 46.9	13 50 24.0	0.0263	14.30	0.040	0.333	0.85	<0.1015E-12	GC	0		I
2215.5+2902	4C +28.53	22 15 36.8	29 02 36.1	0.2288	16.60	0.103	0.177	0.74	0.3286E-11	Q		q	
2216.0-2803	PKS 2213-283	22 15 59.9	-28 03 29.8	0.9480	18.00	0.000	0.290	0.90	0.1748E-11	Q		q	
2217.1+2239	RGB J2217+226	22 17 10.9	22 39 46.8	0.4050	17.80	0.019	0.072	0.83	0.1145E-11	G		q	
	PKS 2215+02	22 17 48.2	+02 20 10.7	3.5720	21.10	0.000	0.630	0.00	<0.4700E-12	Q		q	
2218.1+0802	RX J2218.6+0802	22 18 38.5	+08 02 15.8	0.1200	16.60*	0.000	0.004#	0.00	0.3770E-11	G		1	
2218.9-0335	MRC 2216-038	22 18 52.0	-03 35 36.9	0.9010	16.38	0.000	3.629	-0.36	0.1656E-11	Q		q	
2219.2+2259	RGB J2219+229	22 19 21.0	22 59 22.7	1.2600	19.00	0.010	0.023	0.00	0.7854E-12	G		q	
2219.7+2120	RGB J2219+213	22 19 44.2	21 20 53.3	0.2000	18.70	0.098	0.123	-0.03	0.2045E-11	G		z	
2219.8+2613	RGB J2219+262	22 19 49.7	26 13 27.9	0.0850	17.00	0.230	0.810	0.46	0.2470E-11	G		b	
2220.5+3948	4C +39.66	22 20 31.4	39 48 47.1	0.6550	17.90	0.105	0.686	0.69	0.1389E-11	Q		q	
2223.1-3455	PKS 2220-351	22 23 05.9	-34 55 47.3	0.2980	16.60	0.000	0.360	0.00	0.1048E-11	G		q	
2223.8-0206	3C 445	22 23 49.6	-02 06 12.3	0.0562	15.77	0.086	2.279	0.70	0.4708E-12	G	N	b	II
2225.6+2118	[HB89] 2223+210	22 25 38.0	21 18 06.4	1.9590	17.50	1.766	0.000	0.56	0.3101E-11	Q		g	
2225.8-0457	3C 446	22 25 47.2	-04 57 01.4	1.4040	18.39	0.000	5.519	0.14	0.1775E-11	Q		q	
2226.0+1722	4C +17.89	22 26 03.4	17 22 09.0	0.1070	15.10*	0.000	0.034	0.00	0.4433E-11	GC			

Table A.3: *(continued)*

RXJ name (1)	Name (2)	RA(J2000) (3)	DEC(J2000) (4)	z (5)	m_V (6)	F_{5GHz}^{core} (7)	F_{5GHz} (8)	α_r (9)	$F_{0.1-2.4\ keV}$ (10)	Type (11)	Host (12)	Class. (13)	FR (14)
2226.0+2549	87GB 222433.6+2	22 26 57.0	+25 49 46.0	0.1678	18.50*	0.000	0.077#	0.00	0.3070E-11	R			
2227.0+0355	PMN J2227+0356	22 27 05.1	03 55 55.2	1.2490	17.76	0.000	0.126#	0.50	0.1460E-11	Q		q	
2227.7+2420	RGB J2227+243	22 27 47.9	24 21 12.4	0.3190	19.00	0.022	0.060	0.00	0.5671E-12	G		n	
2228.4+1647	NGC 7291	22 28 29.5	16 46 59.3	0.0344	14.12*	0.004	0.032	0.00	0.8941E-12	G	0		
2228.3+3335		22 28 46.3	+33 35 08.7	0.0897	16.40*	0.000	0.004#	0.00	0.4660E-11	G		1	
2228.9-0753	FBQS J2228-0753	22 28 52.6	-07 53 46.5	0.6390	18.50	0.000	0.132#	0.00	0.9285E-12	G		q	
2229.5+3057	RGB J2229+309	22 29 34.1	30 57 12.1	0.3196	16.80	0.059	0.143	0.31	0.2165E-11	Q		q	
	PKS 2227-08	22 29 40.1	-08 32 54.4	1.5620	18.10	0.000	1.409	0.09	0.5000E-12	Q		q	
	RBS 1867	22 30 40.3	-39 42 52.1	0.3230	17.80	0.000	1.020	1.00	0.6748E-11	Q		q	
	3C 449	22 31 20.9	39 21 48.0	0.0171	13.15*	0.037	6.450&	1.58	0.1083E-12	G	E		I
2232.5+1143	CTA 102	22 32 36.4	11 43 50.9	1.0370	17.33	6.468	0.000&	0.40	0.2513E-11	Q		g	
2233.0+1335	87GB 223033.7+	22 33 01.1	13 36 01.0	0.2140	18.58	0.000	0.033&	0.00	0.5768E-11	Q		z	
2235.2-4835	PKS 2232-488	22 35 13.2	-48 35 58.8	0.5100	18.10	0.000	0.870	-0.50	0.2035E-11	Q		q	
	[HB89] 2233+399	22 35 17.4	40 10 07.9	2.0900	19.50	0.000	0.128	0.84	0.5511E-12	Q		q	
2235.0-2603	NGC 7314	22 35 46.2	-26 03 00.9	0.0047	11.90*	0.000	0.034#	0.00	0.3090E-11	G	S	9	
	B2 2234+28A	22 36 22.5	28 28 57.4	0.7950	19.00	0.000	1.478#	-0.63	0.6382E-12	Q		q	
	PKS 2233-148	22 36 34.1	-14 33 22.2	0.3250	19.00	0.000	0.610	-0.32	0.1322E-11	Q		z	
2236.3-1232	MRK 0915	22 36 46.5	-12 32 42.6	0.0241	14.80*	0.000	0.071#	0.00	0.3560E-11	G	S	1	
2236.5-2213	ESO 602- G 031	22 36 55.9	-22 13 14.8	0.0337	14.90*	0.000	0.007#	0.00	0.7100E-11	G	S	8	
2237.0+3425	NGC 7331	22 37 04.1	34 24 56.3	0.0027	10.35	0.000	0.080#	1.60	0.1731E-11	G	S	l	
	UGC 12127	22 38 29.5	35 19 40.7	0.0276	15.00*	0.008	0.770&	0.54	0.4150E+02*	GC	E		I
2240.7+0803	UGC 12138	22 40 17.0	+08 03 14.1	0.0246	14.20*	0.000	0.016#	0.00	0.1640E-10	G	S	8	
2240.9+2732	RGB J2241+275	22 41 02.0	27 32 59.0	0.4930	17.60	0.035	0.046	0.00	0.1959E-11	G		q	
2241.5+0453	RGB J2241+048	22 41 34.2	04 53 10.2	0.0680	16.80*	0.041	0.114	0.46	0.1251E-11	G		r	
2242.6+2943	ARK 564	22 42 39.3	29 43 31.3	0.0247	14.16	0.000	0.029#	0.00	0.1097E-09	G	S	!	
	PKS 2240-260	22 43 26.4	-25 44 30.7	0.7740	18.40	0.000	1.000	0.12	0.7217E-12	Q		q	
	PKS B2242+03	22 45 28.3	03 24 08.9	1.3400	18.00	0.000	0.320	-0.90	0.5087E-12	Q		q	
	3C 452	22 45 48.8	39 41 15.7	0.0811	16.56	0.130	28.199&	0.94	0.4363E+02*	G	E	n	II
2246.3-1206	[HB89] 2243-123	22 46 18.2	-12 06 51.3	0.6320	16.45	0.000	2.379	0.23	0.2749E-11	Q		g	
2246.2+3142	RGB J2246+317	22 46 21.7	31 42 07.9	0.1470	17.10	0.013	0.147	0.46	0.4465E-11	G		1	
2248.1-1728	IRAS 22453-174	22 48 04.1	-17 28 29.8	0.1173	15.90*	0.000	0.016#	0.00	0.3590E-11	G		8	
2248.3-1015	FBQS J2248-1015	22 48 17.5	-10 15 47.0	0.2910	17.00	0.000	0.018#	0.00	0.3068E-11	G		q	
	PKS 2245-328	22 48 38.7	-32 35 52.2	2.2680	19.10	0.000	1.800	0.18	<0.2380E-12	Q		q	
2250.0+3824	B3 2247+381	22 50 05.8	38 24 37.1	0.1187	16.00	0.060	0.112	0.14	0.7076E-11	G		z	

Table A.3: *(continued)*

RXJ name (1)	Name (2)	RA(J2000) (3)	DEC(J2000) (4)	z (5)	m_V (6)	F_{5GHz}^{core} (7)	F_{5GHz} (8)	α_r (9)	$F_{0.1-2.4\ keV}$ (10)	Type (11)	Host (12)	Class. (13)	FR (14)
	PKS 2247+14	22 50 25.4	14 19 50.1	0.2370	16.93	0.000	1.110	0.50	0.1500E-12	Q	E	q	
2251.5-3827	LCRS B224829.3-	22 51 19.0	-38 27 06.8	0.1348	16.60*	0.000	0.060#	0.00	0.4390E-11	G		1	
	3C 454	22 51 34.7	18 48 40.1	1.7570	18.40	0.000	0.790	0.61	<0.1354E-12	Q		g	II
2252.7+1454	IRAS F22496+143	22 52 08.1	+14 54 49.6	0.1300	16.30*	0.000	0.002#	0.00	0.4530E-11	Q		q	
2252.6+2642	IRAS 22497+262	22 52 09.4	+26 42 41.3	0.0670	18.20*	0.000	0.002#	0.00	0.4070E-11	G		!	
2253.0+1942	MG1 J225308+1942	22 53 07.4	19 42 34.6	0.2840	18.00	0.254	0.357	-0.10	0.1031E-11	Q		q	
2253.9+1608	3C 454.3	22 53 57.7	16 08 53.6	0.8590	16.10	12.189	14.468	0.17	0.1755E-10	Q		q	
2254.7-1734	[HB89] 2251-178	22 54 05.8	-17 34 55.0	0.0680	14.40*	0.000	0.017#	0.00	0.2030E-10	G		1	
2254.1+2445	B2 2251+24	22 54 09.3	24 45 23.4	2.3280	18.50	0.800	0.869	0.40	0.1385E-11	Q		q	
2254.1+1136	PG 2251+113	22 54 10.4	11 36 38.3	0.3255	15.82	0.021	0.572	0.86	0.4732E-12	Q		q	
	3C 455	22 55 03.8	13 13 34.2	0.5430	19.50	0.000	2.899	0.90	<0.1354E-12	Q		g	II
	B3 2253+417	22 55 36.7	42 02 52.5	1.4760	19.40	0.000	1.120	0.19	0.1024E-11	Q		q	
2256.5+2618	RGB J2256+263	22 56 39.2	26 18 43.8	0.1210	19.10	0.040	0.046	0.00	0.1420E-11	G		b	
2257.1-3627	MRC 2254-367	22 57 10.6	-36 27 44.0	0.0056	11.85	0.000	0.720	0.21	0.1386E-11	GC	E	l	
	PKS 2254+074	22 57 17.3	07 43 12.3	0.1900	16.36	0.000	0.480	1.40	0.7903E-12	Q		z	
2258.9-0115		22 58 10.0	-01 15 15.5	0.1167	16.30*	0.000	0.003#	0.00	0.3950E-11	G		1	
2258.8-0707		22 58 18.6	-07 07 08.3	0.2150	15.80*	0.000	0.006#	0.00	0.2720E-11	G		q	
2258.8-2609		22 58 45.3	-26 09 15.0	0.0760	16.10*	0.000	0.003#	0.00	0.1090E-10	G		1	
2259.2+1857	RGB J2259+189	22 59 19.1	18 57 30.6	0.1320	17.60*	0.017	0.025	0.00	0.1234E-11	G		a	
2259.9+2455	PGC 070195	22 59 32.9	+24 55 05.6	0.0345	15.90*	0.000	0.004#	0.00	0.1570E-10	G	S	!	
2259.7+3125	RGB J2259+314	22 59 50.8	31 24 52.1	1.1400	18.60	0.013	0.023	0.00	0.5783E-12	G		q	
2300.1-1255	NGC 7450	23 00 47.8	-12 55 06.7	0.0106	14.00*	0.000	0.006#	0.00	0.8220E-11	G	S	5	
2303.0-1841	MRC 2300-189	23 03 02.9	-18 41 26.0	0.1283	17.82	0.000	0.890	0.16	0.8842E-11	G	N	1	
2303.2+0852	NGC 7469	23 03 15.6	08 52 26.4	0.0163	13.04	0.018	0.070	0.00	0.4704E-10	G	S	5	
2303.7-6807	[HB89] 2300-683	23 03 43.6	-68 07 37.5	0.5120	16.38	0.000	0.340	0.10	0.2018E-11	Q		q	
2304.8+2237	MRK 0315	23 04 02.6	+22 37 27.5	0.0389	14.80*	0.000	0.023#	0.00	0.4160E-11	G	p	5	
2304.8-0841	MRK 0926	23 04 43.4	-08 41 08.0	0.0473	15.00*	0.000	0.034#	0.00	0.4030E-10	G		5	
	PKS 2302-713	23 05 41.2	-71 03 10.4	0.3840	17.50	0.000	0.150	0.80	0.2563E-11	Q		q	
2306.2-0459	[HB89] 2303-052	23 06 15.3	-04 59 48.3	1.1390	19.70	0.000	0.450	0.30	0.7481E-12	Q		q	
2307.4+0406	4C +03.56	23 07 26.3	04 06 25.7	0.1531	18.00	0.083	0.187	1.91	0.9039E-12	G	E		
2307.7+1901	4C +18.68	23 07 45.6	19 01 20.6	0.3130	17.50	0.081	0.394	0.74	0.8731E-12	G		q	
2308.1+2008	RGB J2308+201	23 08 11.6	20 08 42.2	0.2342	17.60	0.177	0.163	0.07	0.1814E-11	G		q	
2308.7-2219	MS 2306.1-2236	23 08 46.8	-22 19 49.0	0.1370	17.50*	0.000	0.006#	0.00	0.6960E-11	Q		z	
2310.1+1047	RGB J2310+107	23 10 09.7	10 47 24.3	0.4360	17.90	0.012	0.045	0.11	0.1557E-11	G		q	

Table A.3: *(continued)*

RXJ name (1)	Name (2)	RA(J2000) (3)	DEC(J2000) (4)	z (5)	m_V (6)	F_{5GHz}^{core} (7)	F_{5GHz} (8)	α_r (9)	$F_{0.1-2.4\ keV}$ (10)	Type (11)	Host (12)	Class. (13)	FR (14)
	B2 2308+34	23 11 05.3	34 25 10.9	1.8170	19.50	0.000	1.016	-0.10	0.6584E-12	Q		q	
2311.3+1008	PG 2308+098	23 11 17.7	10 08 15.5	0.4333	16.00	0.093	0.291	0.70	0.4757E-11	Q		q	
2311.7+3535	RGB J2311+355	23 11 48.9	35 35 41.0	1.3900	17.60	0.018	0.023	0.00	0.6657E-12	Q		q	
2312.3+1436	NGC 7509	23 12 21.4	14 36 33.6	0.0163	15.00*	0.013	0.028	0.00	0.4816E-12	G			
2313.7-3158	[HB89] 2310-322	23 13 10.1	-31 57 48.6	0.3370	16.60*	0.000	0.817#	0.00	0.4660E-11	G		q	
2313.0+1401	NGC 7525	23 13 40.4	+14 01 22.7	0.0409	15.20*	0.000	0.007#	0.00	0.2950E-11	G		5	
2313.8+4712	4C +46.47	23 13 48.1	47 12 15.2	0.7420	18.20	0.353	0.798	0.84	0.1718E-11	Q		g	
2313.8+1019	RGB J2313+103	23 13 55.7	10 19 09.8	0.4560	17.90	0.035	0.083	0.00	0.5352E-12	G		q	
2313.9-4243	MRC 2311-429	23 13 58.7	-42 43 38.0	0.0564	14.60	0.000	0.049	0.00	0.3038E-10	GC	0		
	PKS 2311-452	23 14 09.4	-44 55 49.2	2.8840	19.60	0.000	1.429	-0.60	<0.2170E-12	Q		q	
2314.0+2243	IRAS F23124+222	23 14 55.7	+22 43 25.0	0.1692	16.30*	0.000	0.019#	0.00	0.3530E-11	Q		a	
2315.4-0222	NGC 7556	23 15 44.5	-02 22 53.4	0.0250	13.80*	0.000	0.004#	0.00	0.5700E-11	GC	0		
	3C 459	23 16 35.2	04 05 18.1	0.2199	16.68	1.129	1.330	0.97	<0.2300E-12	G	N	b	II
2317.6-1004	FBQS J2317-1005	23 17 33.2	-10 05 04.1	0.5900	19.30	0.000	0.003#	0.00	0.4358E-12	Q		q	
	MRC 2315-425	23 17 56.4	-42 13 33.4	0.0560	15.65*	0.000	0.115#	0.00	0.4413E-13	GC	0	r	
2318.5+3048	RGB J2318+308	23 18 36.9	30 48 36.7	0.1030	16.73	0.022	0.021	0.00	0.2272E-11	G		b	
2318.4+4257	UGC 12491	23 18 38.2	+42 57 28.9	0.0169	14.90*	0.000	0.004#	0.00	0.1100E-10	G	E		
2318.8+0014	NGC 7603	23 18 56.6	+00 14 38.2	0.0295	14.00*	0.000	0.025#	0.00	0.1060E-10	G	S	5	
	NGC 7618	23 19 47.2	42 51 09.5	0.0173	14.02*	0.000	0.040#	0.00	0.4774E-11	G	E		
2320.2+4147	RGB J2320+417	23 20 12.2	41 46 05.3	0.1520	18.50	0.007	0.046	0.00	0.6118E-11	Q		z	
2320.5+0810	NGC 7619	23 20 14.5	+08 12 22.5	0.0127	12.10*	0.000	0.021#	0.00	0.3780E-11	GC	E		
	PMN J2320+0031	23 20 38.0	00 31 39.0	1.8940	18.90	0.000	0.076#	0.00	0.2960E-12	Q		q	
	NGC 7626	23 20 42.3	08 13 02.5	0.0113	12.80*	0.000	0.210	0.80	0.4145E+02*	GC	E		I
2320.7+0513	[HB89] 2318+049	23 20 44.8	05 13 49.9	0.6220	19.00	0.728	1.048	0.04	0.1217E-11	Q		q	
2320.7+0829	RGB J2320+084	23 20 50.2	08 29 30.6	0.1240	19.90	0.006	0.062	0.00	0.5790E-12	G			
	4C +27.50	23 21 59.9	27 32 46.4	1.2530	19.00	0.000	1.016	0.07	0.1015E-11	QC	E	q	
	TXS 2319+209	23 22 02.5	21 13 56.0	0.7070	16.96	0.000	0.095	0.17	0.2815E-12	Q		q	
2322.3-1037	FBQS J2322-1037	23 22 14.7	-10 37 24.1	0.7450	17.70	0.000	0.001#	0.00	0.1821E-11	G		q	
2322.6+3436	RGB J2322+346	23 22 44.0	34 36 14.0	0.0980	18.15	0.030	0.078	0.05	0.2560E-11	G		z	
2322.1-1738		23 22 45.2	-17 38 55.6	0.1674	16.60*	0.000	0.238#	0.00	0.4690E-11	G		5	
2323.3+2035	PKS J2323+2035	23 23 20.3	20 35 23.5	0.0380	15.50	0.114	0.346	0.58	0.5143E-12	GC	E	w	
2323.2+4210	H 2321+419	23 23 52.1	+42 10 58.7	0.0590	17.00*	0.000	0.011#	0.00	0.8480E-11	Q		z	
2325.2-3236	PMN J2325-3236	23 25 11.8	-32 36 34.0	0.2160	17.00*	0.000	0.253#	0.00	0.6630E-11	G		1	
2325.4-1207	NPM1G -12.0625	23 25 19.8	-12 07 26.4	0.0822	15.40*	0.000	1.875#	1.30	0.2350E-10	GC	E		

Table A.3: *(continued)*

RXJ name (1)	Name (2)	RA(J2000) (3)	DEC(J2000) (4)	z (5)	m_V (6)	F_{5GHz}^{core} (7)	F_{5GHz} (8)	α_r (9)	$F_{0.1-2.4\ keV}$ (10)	Type (11)	Host (12)	Class. (13)	FR (14)
2325.6-3826	LCRS B232242.2-	23 25 24.2	-38 26 49.2	0.0359	14.90*	0.000	0.004#	0.00	0.1770E-10	G		1	
2325.6+2153	RBS 2005	23 25 54.2	+21 53 14.0	0.1202	15.90*	0.000	0.006#	0.00	0.1600E-10	G		1	
2327.3+1524	TXS 2324+151	23 27 21.9	15 24 37.3	0.0400	12.60	0.000	0.276#	0.00	0.1804E-11	G		q	
	NGC 7674	23 27 56.7	08 46 44.5	0.0289	14.38	0.000	0.086#	1.78	0.5414E-12	G	S	2	
2328.1+2937	4C +29.68	23 28 10.6	29 37 09.0	1.0150	17.30	0.000	0.427#	1.00	0.1693E-11	Q		q	
	PMN J2329+0834	23 29 05.8	08 34 15.8	0.9480	20.50	0.000	0.311#	0.00	0.1162E-12	Q		q	
2329.2-4730	RBS 2010	23 29 17.7	-47 30 19.1	1.2990	16.79	0.000	2.459	0.20	0.2959E-11	Q		q	
	PKS 2327-376	23 30 35.8	-37 24 38.1	0.2790	16.60	0.000	0.229	-0.20	0.4507E-12	G		z	
	PKS 2328+10	23 30 40.8	11 00 18.7	1.4890	18.50	0.000	0.960	-0.10	0.6455E-12	Q		q	
	PKS 2329-16	23 31 38.6	-15 56 57.0	1.1530	20.00	0.000	1.030	-0.08	0.2690E-12	Q		q	
	FBQS J2333-0131	23 33 16.7	-01 31 07.4	1.0620	19.60	0.000	0.290	-0.50	0.2956E-12	Q		q	
2333.9-2343	MRC 2331-240	23 33 55.2	-23 43 40.6	0.0477	16.50	0.000	1.060	-0.03	0.6401E-11	G	E	s	
2335.0+2722	PGC 071807	23 35 01.5	+27 22 20.5	0.0613	13.50*	0.000	0.078#	0.00	0.3170E-11	GC	c		
2336.2+0209	NGC 7714	23 36 14.1	02 09 18.6	0.0093	14.36	0.000	0.039#	0.00	0.5307E-12	G	S	h	
2337.9-1752	PKS 2335-18	23 37 56.6	-17 52 20.4	1.4460	17.34	0.000	0.590	0.25	0.7196E-12	Q		q	
	3C 465	23 38 29.5	27 01 55.9	0.0302	13.30	0.270	20.199&	0.98	0.5342E-11	GC		w	I
2338.8+2124	RBS 2031	23 38 56.4	21 24 41.4	0.2910	17.00	0.020	0.036	0.00	0.6825E-11	Q		z	
	MS 2336.5+0517	23 39 06.7	05 34 04.0	0.7400	20.30	0.000	0.005	0.00	0.8088E-12	Q		z	
	PKS 2337-334	23 39 54.5	-33 10 17.0	1.8020	22.50	0.000	1.169	0.24	<0.3380E-12	Q		q	
2340.8-2848	MRC 2338-290	23 40 51.0	-28 48 42.0	0.4460	19.00	0.000	0.240	0.00	0.1611E-11	Q		q	
2341.5+0938	NPM1G +09.0618	23 41 06.6	+09 38 09.4	0.0421	16.20*	0.000	0.005#	0.00	0.6440E-11	G		1	
2341.1+0018	PKS 2338+000	23 41 06.9	00 18 33.4	0.2769	19.00	0.277	0.310	0.30	0.2489E-11	GC	E	r	
	[HB89] 2340-036	23 42 56.5	-03 22 26.0	0.8960	16.02	0.000	0.220	0.30	0.4013E-11	Q		q	
2343.3-3638	RBS 2040	23 43 13.5	-36 37 54.0	0.6220	16.00*	0.000	0.010#	0.00	0.2740E-11	G		1	
2344.7-0032	FBQS J2344-0032	23 44 40.0	-00 32 31.7	0.5027	17.50	0.000	0.017#	0.00	0.7574E-12	Q		q	
	1ES 2343-151	23 45 38.4	-14 49 28.7	0.2240	19.20	0.000	0.008	0.00	0.1263E-11	Q		z	
2346.5+0930	PG 2344+092	23 46 36.8	09 30 45.5	0.6770	15.97	0.000	1.419	0.19	0.2318E-11	Q		q	
	TXS 2344+514	23 47 04.8	51 42 17.9	0.0440	15.50	0.000	0.224	0.20	0.2519E-10	Q		z	
	PMN J2347+0853	23 47 38.1	08 52 46.8	0.2920	17.10	0.000	0.052	0.00	0.1193E-11	G	E	q	
2347.2-2808	IC 5358	23 47 45.0	-28 08 26.7	0.0288	13.60*	0.000	0.090#	0.00	0.2910E-10	GC	c		
2348.0-1631	[HB89] 2345-167	23 48 02.6	-16 31 12.0	0.6000	18.41	0.000	3.470	0.26	0.2040E-11	Q		g	
2349.7-3311	CTS 0120	23 49 07.5	-33 11 44.0	0.1350	16.90*	0.000	0.005#	0.00	0.4910E-11	G		1	
	MS 2347.4+1924	23 50 00.7	19 41 36.0	0.5150	19.93	0.000	0.003	0.00	0.7388E-12	Q		z	
2350.0-0559	RBS 2051	23 50 17.9	-05 59 28.0	0.5150	19.50*	0.000	0.025#	0.00	0.6700E-11	Q		z	

Table A.3: *(continued)*

RXJ name (1)	Name (2)	RA(J2000) (3)	DEC(J2000) (4)	z (5)	m_V (6)	F_{5GHz}^{core} (7)	F_{5GHz} (8)	α_r (9)	$F_{0.1-2.4\ keV}$ (10)	Type (11)	Host (12)	Class. (13)	FR (14)
2350.6-2435	[CM98] R843053	23 50 22.9	-24 35 50.0	0.1930	16.80*	0.000	0.007#	0.00	0.1940E-11	GC	c		
	MG3 J235037+3622	23 50 36.7	36 22 10.9	0.3170	19.60	0.000	0.149#	0.32	0.2905E-12	Q		z	
2350.3+0609	MCG +01-60-039	23 50 50.5	+06 08 58.5	0.0561	15.00*	0.000	0.056#	4.40	0.1230E-10	GC			
2351.9-0109	4C -01.61	23 51 56.1	-01 09 13.4	0.1740	15.33	0.000	0.680	0.84	0.1161E-10	G	N	q	II
2354.4-1513	PKS 2351-154	23 54 30.2	-15 13 11.2	2.6680	18.80	0.000	0.930	0.24	0.8058E-12	Q		q	
	[HB89] 2352-342	23 55 25.5	-33 57 57.3	0.7020	16.40	0.000	0.390	0.00	0.1673E-11	Q		q	
	PKS 2353-68	23 56 00.7	-68 20 03.5	1.7160	17.00	0.000	1.070	-0.10	0.6841E-12	Q		q	
	S5 2353+81	23 56 22.8	81 52 52.2	1.3440	20.30	0.000	0.521#	0.00	0.1251E-11	Q		q	
2357.0-3445	ESO 349- G 010	23 57 00.7	-34 45 33.1	0.0491	13.90*	0.000	1.286#	1.70	0.2510E-10	GC	c		
2357.1-1718		23 57 29.7	-17 18 05.3	0.3899	17.40*	0.000	0.044#	0.00	0.2130E-10	G		z	
	PKS 2354-11	23 57 31.2	-11 25 39.2	0.9600	18.50	0.000	1.389	0.20	0.5480E-12	Q		q	
2358.1-0759	MRC 2355-082	23 58 09.6	-08 00 04.0	0.2110	17.50	0.000	0.220	0.70	0.8876E-12	Q		q	
	PKS 2356-61	23 59 04.4	-60 54 59.3	0.0963	16.00*	0.035	4.559	1.36	0.3900E-12	GC	E		II
	RBS 2070	23 59 07.8	-30 37 40.0	0.1650	17.00	0.000	0.065#	0.00	0.6636E-10	Q		z	
2359.6-0407	IC 1524	23 59 10.7	-04 07 37.2	0.0193	13.90*	0.000	0.004#	0.00	0.9040E-11	G	S	1	
	MRC 2356-210	23 59 19.5	-20 47 56.1	0.0960	17.97*	0.000	0.256#	0.48	0.1539E-11	G		r	